

The
University
Of
Sheffield.

**Evolution and development of epithelial
appendages in the jawed vertebrates**

By

Rory Cooper

A thesis submitted in partial fulfilment for the degree of Doctor of

Philosophy

The University of Sheffield

Faculty of Science

Department of Animal and Plant Sciences

December 2019

Summary

Epithelial appendages of the integument comprise a remarkably diverse group of structures that have facilitated the evolutionary adaptation of animal life to wide-ranging ecological niches. They include numerous appendages adorning the skin, such as scales, spines, feathers, hair and teeth. In many cases, for example with feathers and hair, they constitute clade-defining characteristics. This thesis aims to examine how alterations to the shared developmental mechanisms underpinning the formation of these structures can explain how their incredible evolutionary diversity has arisen.

Previous research into epithelial appendage development has broadly concerned the appendages of two classic vertebrate models: feathers of the chicken embryo and hair of the mouse embryo. I aim to compliment this research through developmental comparisons with the epithelial appendages of an emerging model cartilaginous fish, the small-spotted catshark (*Scyliorhinus canicula*). Sharks have epithelial appendages known as dermal denticles which cover the body. These units are structurally homologous to vertebrate teeth. Denticle-like structures have been observed in the fossil record from as long as 450 million years ago. They facilitate a plethora of functions, including the provision of drag reduction and protective armour. Here, I compare aspects of shark denticle patterning, initiation and morphogenesis to avian epithelial appendage development. This enables conclusions to be drawn regarding both the conservation and divergence of different aspects of epithelial appendage development throughout the gnathostomes (jawed vertebrates). Overall, I demonstrate that small alterations to broadly conserved developmental systems and genetic circuitry contribute to the incredible diversity of epithelial appendages we observe in nature.

Acknowledgements

First, I would like to thank my lead supervisor Dr. Gareth Fraser, who ignited my interest in evolutionary developmental biology as an undergraduate student, and enabled me to pursue a research career in this field. Gareth's supervisory approach, support and positivity has allowed me to develop into a productive, independent researcher. It has been a pleasure to be both a member of Gareth's lab and his friend. I would also like to thank Dr. Nicola Nadeau, who kindly adopted me after Gareth's departure to The University of Florida. Having support from both her and her group has been invaluable.

Without the help of past and present members of The Fraser lab, this work would not have been possible. Dr Alex Thiery has generously provided me with abundant scientific guidance and friendship throughout the course of my PhD and onwards, and I am truly grateful to have met him. Furthermore, Dr Kyle Martin's broad knowledge was essential in shaping the beginning of my research project. I would also like to extend my gratitude to Vicky Lloyd, for providing me with frequent scientific discussions, and kindly me helping with animal husbandry duties so that I could go on holiday. Additionally, I would like to thank all the collaborators who have helped me throughout my project, including Andy Parnell, Mike Hayle, Nicolas Di-Poï and Alex Fletcher. Their combined friendliness and willingness to support my projects has been inspirational.

Staff from The Department of Animal and Plant Sciences have provided a welcoming and supportive environment in which to undertake research. In particular, I would like to thank members of the animal facility for helping with the care of my shark embryos, and members of the molecular ecology lab for technical support throughout the project. I would also like to thank everyone in the department for going to the pub on Fridays.

Having the support of my partner Rachael Durham has been invaluable. Her provision of emotional aid, entertainment and relentless grammar knowledge has made my postgraduate life in Sheffield both incredibly fun and productive. I would also like to thank all of my friends. In particular, Dom Burns, Will Buswell and Jennie Crawley, who have been with me from the very beginning as undergraduates. John Jackson and Martin Garlovsky have provided both scientific support and entertainment in and out of work for the last few years, and I feel truly grateful to have met them. I'd also like to thank Astrid, Becca, Harriet, Jordan and Beth. Without you guys it would have been much more boring, and I feel profoundly lucky to have found such a likeminded group of friends. Although it's incredible that we are all going on to do new and exciting things, I'll always wish we could live in the same place again.

I'd also like to extend my deepest gratitude to my family. I've learnt that having such exceptionally supportive parents is rare, and you truly made me who I am today. Knowing that I'm only ever a phone call or train ride away from advice and assurance has provided with a safety net that has immeasurably improved my quality of life. Finally, I'd like to thank my brother and sister for their continual support. In particular, having a sister doing a PhD at the same time as myself has provided me with another understanding and compassionate person to talk to, whenever the need arises. I consider myself exceptionally lucky to have had, and continue to have such incredible support.

Statement of intellectual contribution

Chapter 2: Developing an ancient epithelial appendage: FGF signalling regulates early tail denticle formation in sharks

This chapter is published in *EvoDevo* (Cooper et al., 2017), and is presented here in its published format. This project was designed by myself, Kyle Martin and Gareth Fraser. Liam Rasch undertook section in situ hybridization (Fig. 8A-I). I undertook all other data collection. Part of the data collection was undertaken during my Masters project (Fig. 1B, C, D, E, H, Fig. 2, Fig. 4A-N (not including sections), Fig. 5A-N (not including sections) and Fig. 9). Myself, Kyle Martin and Gareth Fraser analysed and interpreted the results. I wrote the manuscript, which was read, edited and approved by all authors.

Chapter 3: An ancient Turing-like patterning mechanism regulates skin denticle development in sharks

This chapter is published in *Science Advances* (Cooper et al., 2018), and is presented here in its published format. The project was designed by myself and Gareth Fraser. Daniel Delbarre and I undertook the initial reaction-diffusion (RD) modelling, which was refined by Alex Fletcher, who wrote the Python RD script presented. Liam Rasch undertook section in situ hybridization (Fig. 3P-T) and Alex Thiery generated the gene trees shown in Supplementary Figure 1. I undertook all other data collection and experimental work, and wrote the manuscript, which was read, edited and approved by all authors.

Chapter 4: Conserved gene signalling and a derived patterning mechanism underlie the development of avian footpad scales

This chapter is published in *EvoDevo* (Cooper et al., 2019), and is presented here in its published format. This research was designed by myself and Gareth Fraser. In situ

hybridization was undertaken with help from Victoria Lloyd. All other data collection was undertaken by myself, except for Fig. 5G-J, which was provided by Nicolas Di-Poi. Paul Barrett provided interesting discussion points regarding the evolutionary implications of our findings. RD modelling was undertaken by myself, using the script presented in Chapter 3. I wrote the manuscript, which was read, edited and approved by all authors.

Chapter 5: Exogenous sonic hedgehog protein can trigger mineralised tissue deposition in the developing shark embryo

This research was designed by myself and Gareth Fraser. Victoria Lloyd helped to undertake in situ hybridization for chicken samples shown in Fig. 2K-R. I undertook all other data collection, interpreted results and wrote the manuscript.

Certified approval of major contributory co-authors

Victoria Lloyd

Date: 09/12/19



Dr. Gareth Fraser

Date: 04/12/19



Table of Contents

1.0	Chapter 1: General Introduction	14
1.1	Introduction	14
1.1.1	What is an epithelial appendage?	14
1.1.2	The evolutionary relationships of epithelial appendages	14
1.1.3	The development of epithelial appendages	21
1.1.4	Conclusion	27
1.2	Thesis rationale	27
1.3	Research summary	29
1.3.1	Chapter 2 summary	29
1.3.2	Chapter 3 summary	29
1.3.3	Chapter 4 summary	30
1.3.4	Chapter 5 summary	31
2.0	Chapter 2: Developing an ancient epithelial appendage: FGF signalling regulates early tail denticle formation in sharks	33
2.1	Abstract	34
2.2	Introduction	36
2.3	Results	42
2.3.1	Caudal denticle placode development reveals conserved morphogenetic mechanisms for integumentary organ formation	42
2.3.2	Gene expression from integumentary appendage development is conserved in sharks	45
2.3.3	Small molecule inhibition reveals dependency of caudal denticle development on FGF signalling	54

2.4	Discussion	59
2.4.1	An FGF-dependent GRN constructs the placodes of epithelial appendages throughout jawed vertebrates	59
2.5	Conclusion	62
2.6	Methods	62
2.6.1	Shark husbandry and fixation	63
2.6.2	Alizarin red clear and staining	63
2.6.3	Haematoxylin and eosin (H&E) staining	63
2.6.4	Micro-computed tomography (MicroCT) and light sheet fluorescence microscope (LSFM)	64
2.6.5	Small molecule gene perturbation experiments	64
2.6.6	Whole mount in situ hybridization (WMISH)	65
2.6.7	Section in situ hybridization (SISH)	66
2.6.8	Immunofluorescence	67
2.7	Acknowledgements	67
2.8	Additional materials	67
2.8.1	Additional file 1: additional figure	67
3.0	Chapter 3: An ancient Turing-like patterning mechanism regulates skin denticle development in sharks	70
3.1	Abstract	71
3.2	Introduction	72
3.3	Results	75
3.3.1	RD simulation and gene expression analyses suggest that a Turing-like system underlies shark body denticle patterning	75

3.3.2	RD-related genes are functionally conserved during patterning of shark body denticles	81
3.3.3	Retuning the RD model can explain the diversity of denticle patterning	84
3.4	Discussion	86
3.5	Methods	88
3.5.1	Shark and chick husbandry	88
3.5.2	Micro-CT and SEM	89
3.5.3	Alizarin red clear and staining	89
3.5.4	RD modelling	89
3.5.5	In situ hybridization	91
3.5.6	Bead implantation experiments	92
3.6	Acknowledgements	93
3.7	Supplementary materials	94
3.7.1	Supplementary file 1: Supplementary figures	94
3.7.2	Supplementary file 2: Python script for RD simulations	103
4.0	Chapter 4: Conserved gene signalling and a derived patterning mechanism underlie the development of avian footpad scales	108
4.1	Abstract	109
4.2	Introduction	110
4.3	Results	112
4.3.1	Avian and squamate scales exhibit morphological diversity	112
4.3.2	Conserved gene signalling is observed throughout the development of reticulate scales and other avian appendages	115

4.3.3	A derived patterning mechanism underlies chicken reticulate scale development	119
4.4	Discussion	123
4.5	Conclusion	126
4.6	Methods	126
4.6.1	Animal husbandry	126
4.6.2	Scanning electron microscopy (SEM)	126
4.6.3	Haematoxylin and eosin (H&E) staining	127
4.6.4	In situ hybridization	127
4.6.5	Immunofluorescence	127
4.6.6	Reaction-diffusion (RD) modelling	128
4.7	Acknowledgements	128
4.8	Additional materials	129
4.8.1	Additional file 1: additional figures	130
4.8.2	Additional file 2: Python script for reaction diffusion simulations	133
5.0	Chapter 5: Exogenous sonic hedgehog can trigger mineralised tissue deposition in the developing shark embryo	138
5.1	Abstract	139
5.2	Introduction	140
5.3	Results	142
5.3.1	Shark odontodes exhibit vast morphological diversity	142
5.3.2	Conserved markers of paired appendage outgrowth are expressed during denticle morphogenesis	144
5.3.3	Exogenous shh treatment results in the growth of ectopic, mineralised tissue	147

5.4	Discussion	150
5.5	Conclusion	153
5.6	Methods	153
5.6.1	Shark and chick husbandry	153
5.6.2	Scanning electron microscopy (SEM)	154
5.6.3	Alizarin red clear and staining	154
5.6.4	In situ hybridization	154
5.6.5	Whole mount immunofluorescence	154
5.6.6	Bead implantation experiments	155
5.6.7	Statistical analysis of mineralised tissue lengths	155
5.7	Acknowledgements	156
5.8	Supplementary materials	156
5.8.1	Supplementary file 1: Supplementary figures	156
5.8.2	Supplementary file 2: R code for statistical analysis	165
6.0	General Discussion	168
6.1	Discussion	168
6.2	Future directions	171
6.3	Limitations of using <i>Scyliorhinus canicula</i> as a model system	173
6.4	Limitations of reaction diffusion modelling	175
6.5	Conclusions	176
7.0	Appendix	178
7.1	Abbreviations	178
7.2	Solutions	180
8.0	References	183

1.0 Chapter 1:

General introduction

1.1 Introduction

1.1.1 What is an epithelial appendage?

Epithelial appendages are an incredibly diverse group of highly specialised organs located both upon and within an animal's body. Those found externally adorning the skin are collectively known as integumentary epithelial appendages. These structures include hair, feathers, scales and spines. Examples of internally located epithelial appendages include exocrine glands (Biggs and Mikkola, 2014; Pispa and Thesleff, 2003). It is the externally located integumentary epithelial appendages that will be the focus of this thesis. Despite their diversity in form, these units all arise from interactions between two adjacent tissue layers – the epithelium (derived from the ectoderm) and the mesenchyme (derived from the mesoderm or neural crest) (Pispa and Thesleff, 2003).

Epithelial appendages facilitate a huge range of functions that have enabled vertebrates to adapt to diverse modes of life. For example, mammalian hair plays an important role in thermoregulation (Ruxton and Wilkinson, 2011), feathers have enabled avian flight, camouflage and sexual selection (Dunn et al., 2015), and teleost fish scales provide a thin, flexible, defensive armour (Vernerey and Barthelat, 2014). The presence of clade-specific epithelial appendages has even aided the taxonomic descriptions of individual vertebrate classes (for example avian feathers and mammalian hair). Despite the importance of these structures in enabling the radiation of diverse vertebrate species, our understanding of both their evolution and development remains limited. Addressing this knowledge gap will be the broad focus of this thesis.

1.1.2 The evolutionary relationships of epithelial appendages

There is uncertainty regarding the evolutionary relationships of epithelial appendages, both within and between different taxonomic groups. This thesis will mostly focus upon the epithelial appendages of elasmobranchs (sharks, skates and rays) and birds.

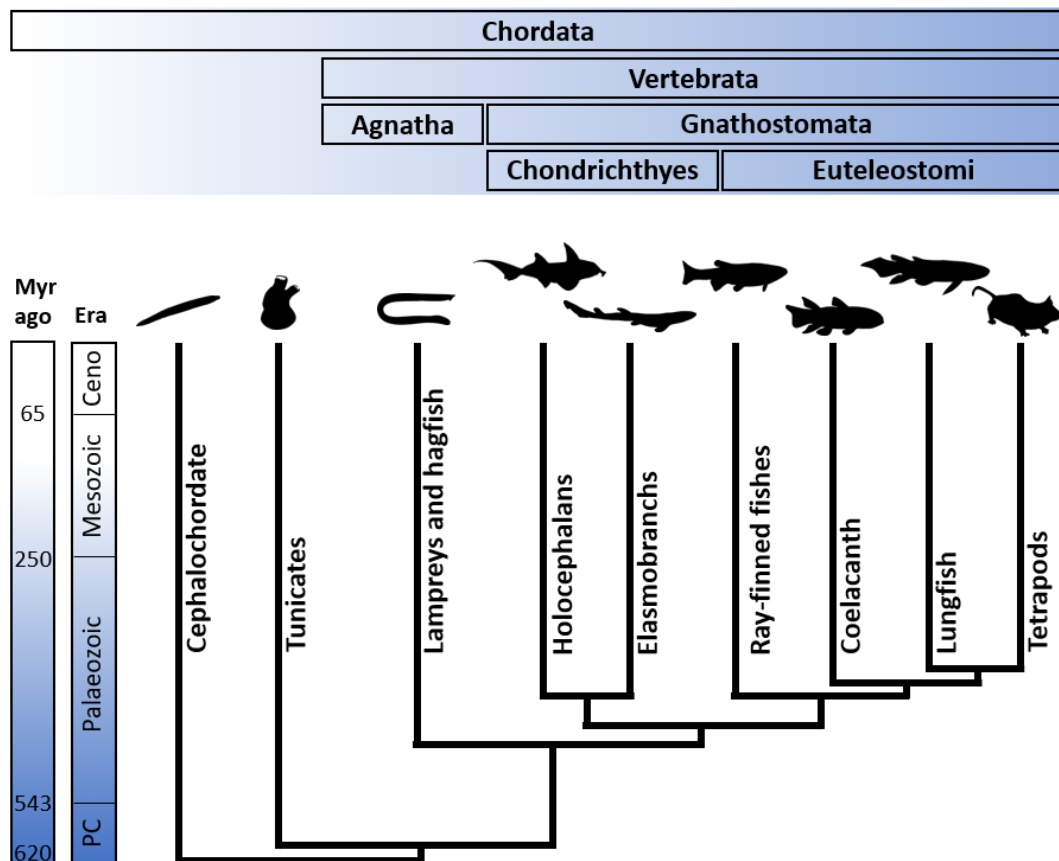


Figure 1: The phylogeny of chordates. Elasmobranchs are found within Chondrichthyes (cartilaginous fishes) and tetrapods are found within Euteleostomi (bony vertebrates). These two groups constitute the main focus of this thesis. Ceno - Cenozoic era, PC - Precambrian era. This phylogeny is based upon published work (Venkatesh et al., 2014). Silhouettes are from www.phylopic.org.

Elasmobranchs belong to a subclass of the cartilaginous fishes (Chondrichthyes), the sister lineage to bony vertebrates (Euteleostomi) (Fig. 1). They possess epithelial appendages collectively known as odontodes, which includes both teeth and dermal denticles (scales)

(Fig. 2). Odontodes have been observed in the fossil record in early thelodonts and shark-like fishes that lived as long as 450 million years ago (Karatajute-Talimaa, 1973; Sansom et al., 1996). They are one of the earliest known integumentary epithelial appendages to have arisen in gnathostomes (jawed vertebrates). Odontodes are structurally homologous to vertebrate teeth, consisting of a pulp cavity surrounded by a dentine layer encased within an enameloid (enamel-like) covering (Motta et al., 2012; Ørving, 1977). The morphological diversity and patterning of these structures has evolved to facilitate a plethora of different functions (Fig. 2), including drag reduction (Dean and Bhushan, 2010), defensive armour (Crooks et al., 2013), communication (Reif, 1985a), prevention of biofouling (Park et al., 2019; Sullivan and Regan, 2011) and feeding (Southall and Sims, 2003). Their role in facilitating drag reduction has even inspired the production of biomimetic shark skin, capable of improving hydrodynamic efficiency during locomotion (Domel et al., 2018; Oeffner and Lauder, 2012; Wen et al., 2015, 2014). In extant species, denticles are mostly restricted to elasmobranchs, although they are also found in some catfish species of the family *Loricariidae* (Rivera-Rivera and Montoya-Burgos, 2017), in which they provide similar defensive and drag reductive functions (Haspel et al., 2012; Schaefer, 1990). Despite our knowledge regarding the diverse functions of odontodes, our understanding of the evolutionary relationships between these structures remains contentious (Donoghue and Rücklin, 2016; Fraser et al., 2010).

There are contrasting theories for the evolutionary origins of odontodes (Donoghue and Rücklin, 2016). One such theory is that external dermal odontodes arose first, before odontode-competent ectoderm subsequently migrated inside the oral cavity to form teeth (the ‘outside-in’ hypothesis). In contrast, it has been suggested that odontodes first arose inside the pharyngeal cavity, before migrating outwards to form dermal denticles (the

‘inside-out’ hypothesis) (Donoghue and Rücklin, 2016; Fraser et al., 2010). This uncertainty has arisen due to contrasting fossil evidence from early jawless vertebrates,

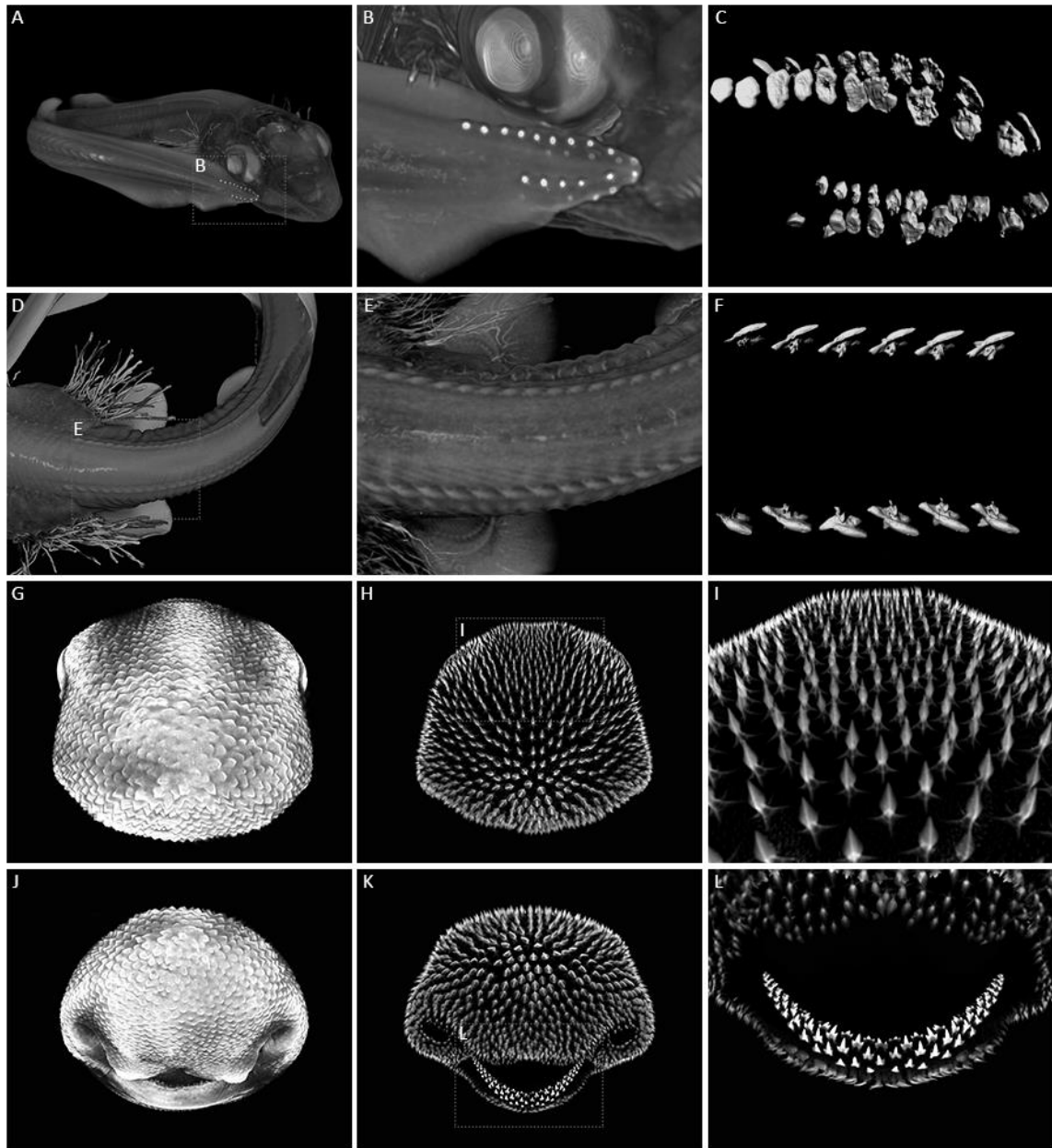


Figure 2: Dermal denticle diversity of the small spotted catshark (*Scyliorhinus canicula*). Caudal denticles (A-C) emerge at approximately stage 28 of development (A-B). They grow in four rows, ventrally and dorsally, on either side of the caudal most tip of the tail, from posterior to anterior. They show vast diversity in form, but generally have a petaliform shape with cusps pointing towards the posterior (C). Dorsal rows (D-F) emerge at approximately stage 30 of development in two distinct rows along the trunk. They are large and distinctly polarised when fully mineralised (F). General body denticles (G-I)

emerge close to the time of hatching and cover the animal's body. Primordia (G) morphogenesis is variable, giving rise to vast variations in morphology within the same individual (H-I). Teeth (J-L) are closely related to denticles (Donoghue and Rücklin, 2016; Fraser et al., 2010), however unlike denticles they regenerate continuously throughout an animal's life. All images are from MicroCT scan data and were rendered using Drishti, except for C and F which are from Light Sheet Fluorescence Microscopy (LSFM), rendered using Imaris.

including conodonts with oro-pharyngeal teeth and without external odontodes (Donoghue et al., 2006; Donoghue and Sansom, 2002; Purnell, 1995), ostracoderms with external dermal odontodes and without oro-pharyngeal denticles (Donoghue and Sansom, 2002; Reif, 1982; Sire et al., 2009), and thelodonts with both oro-pharyngeal teeth and external dermal odontodes (Smith and Coates, 1998). The current consensus is that odontodes arose as external dermal units, before co-option of the underlying gene regulatory network (GRN) gave rise to teeth (Donoghue and Rücklin, 2016; Fraser et al., 2010). Importantly, studies examining the development of these units at the molecular and cellular levels have helped to resolve questions regarding the evolutionary origins of these epithelial appendages (Fraser et al., 2010; Martin et al., 2016; Rasch et al., 2016).

Our understanding of the evolutionary relationships of comparatively derived epithelial appendages is also limited. The transition of tetrapods from water to land was facilitated by a range of fundamental anatomical changes, enabling animals to survive in a terrestrial environment. One such change was the radiation of keratinous integumentary epithelial appendages (Vandebergh and Bossuyt, 2012), including scales, spines, feathers and hair. The domestic chicken (*Gallus gallus domesticus*) has been an important avian model species for studying both the evolution and development of tetrapod epithelial appendages (Chuong et al., 2000a; Musser et al., 2015; Pispa and Thesleff, 2003). Chickens possess

Reticulate scale  Scutate scale  Feather 

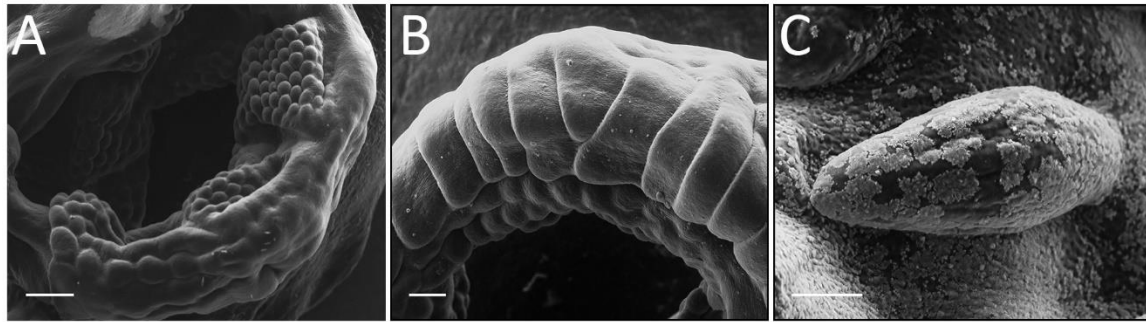


Figure 3: Avian epithelial appendage diversity. The chicken (*Gallus gallus domesticus*) possesses radially symmetrical reticulate scales on the ventral footpad surface, which are associated with grip and cushioning during locomotion (A). They also possess large, overlapping, rectangular shaped scutate scales on the dorsal foot surface and metatarsal shank, which provide a protective function (B). Additionally, they possess feathers, which develop from buds and cover the rest of the body (C). Scale bar lengths are A=250, B=125 μ m & C=50 μ m.

several types of feathers, which facilitate various functions including flight, communication (including sexual selection) and insulation (Chuong et al., 2000a; Dunn et al., 2015). Additionally, they possess large, overlapping, rectangular scutate scales on the anterior meta-tarsal shank and the dorsal surface of the foot (pes), and smaller, circular, radially symmetrical reticulate scales on the ventral surface of the foot and digits (Fig. 3). Scutate scales provide protection and prevent water loss, and reticulate scales are thought to provide grip and cushioning (Chuong et al., 2000a). These diverse functions demonstrate the importance of epithelial appendages for facilitating the evolution and diversification of vertebrate clades.

The evolutionary relationships of feathers, scutate scales and reticulate scales remain unclear. Although there have been multiple reports of feathered theropod dinosaurs (Chen et al., 1998; Foth et al., 2014; Fucheng et al., 2006), it is uncertain how widespread feathers

were amongst other dinosaur clades. It has been suggested that rare occurrences of ornithischian filamentous integumentary structures are likely independent acquisitions of novel feather-like structures (Barrett et al., 2015). Furthermore, it is unknown whether reticulate scales were present in the ancestral archosaur (Musser et al., 2018, 2015), or whether they are a comparatively more derived appendage type (Di-Poï and Milinkovitch, 2016). A recent molecular study revealed that scutate scales are secondarily derived from feathers, suggesting they are more evolutionarily distant from squamate scales than previously thought (Wu et al., 2018). Although limitations of the fossil record make it difficult to determine when particular structures arose, comparative developmental studies within and between extant species can help to elucidate their evolutionary relationships (Di-Poï and Milinkovitch, 2016; Musser et al., 2015).

One broad question that remains when assessing the evolutionary relationships of developmental structures, is whether we are observing deep or continuous (historical) homology (Scotland, 2010; Shubin et al., 2009; Wagner, 2007, 1989). The idea that evolutionary novelty can arise through the co-option of genetic regulatory circuits underpinning pre-existing structures, known as deep homology, is integral to evolutionary developmental biology (Shubin et al., 2009). Conversely to deep homology, continuous homology is considered to be the continual, historical persistence of a character (Wagner, 2007). It has been proposed that the continuity of genetic regulatory circuits, rather than individual genes, defines this continuous homology (Wagner, 2007, 1989). Regarding epithelial appendages, it is currently unclear whether they constitute continuously homologous structures across taxa, or deeply homology structures which have arisen independently through the repeated co-option of shared GRNs (Dhouailly, 2009; Sharpe, 2001). To unravel such questions of homology, it is essential to study the development of these structures in phylogenetically diverse species.

Research attempting to unravel the evolutionary relationships between odontodes and avian epithelial appendages shares a common theme. In both cases, examining the molecular and cellular basis of their development can complement palaeontological data and shed light upon the true evolutionary relationships of these structures. Morphological and structural analysis can produce contentious results when inferring evolutionary relationships of biological characters. The use of molecular developmental studies and GRN analysis will enable us to comprehensively address questions of homology throughout the gnathostomes (Wagner, 2007, 1989).

1.1.3 The development of epithelial appendages

Evolutionary novelty tends to emerge from the modification of pre-existing structures into new forms, rather than arising *de novo* (Shubin et al., 2009). Therefore, we expect a degree of homology to link the development of related structures, such as epithelial appendages (Biggs and Mikkola, 2014). Despite disparity in their adult forms, epithelial appendage development is a conserved process throughout phylogenetically diverse vertebrate groups (Biggs and Mikkola, 2014; Di-Poï and Milinkovitch, 2016; Pispá and Thesleff, 2003). A developmental unit known as an anatomical placode widely constitutes the common foundation of these organs (Fig. 4C-D) (Di-Poï and Milinkovitch, 2016). Variations in placode morphogenesis contributes to differences in their shapes, and variations in placode spatial distribution gives rise to differences in their patterning.

The anatomical placode is localised thickening of the epithelium, accompanied by a dermal condensation, characterised by signalling of conserved developmental genes in both the epithelium and underlying mesenchyme, and columnar epithelial cells with a reduced proliferation rate (Fig. 4C-D). Beta-catenin (β -cat) is one of the earliest expressed placode-specific regulators of development characterised from avian studies (Noramly et al., 1999),

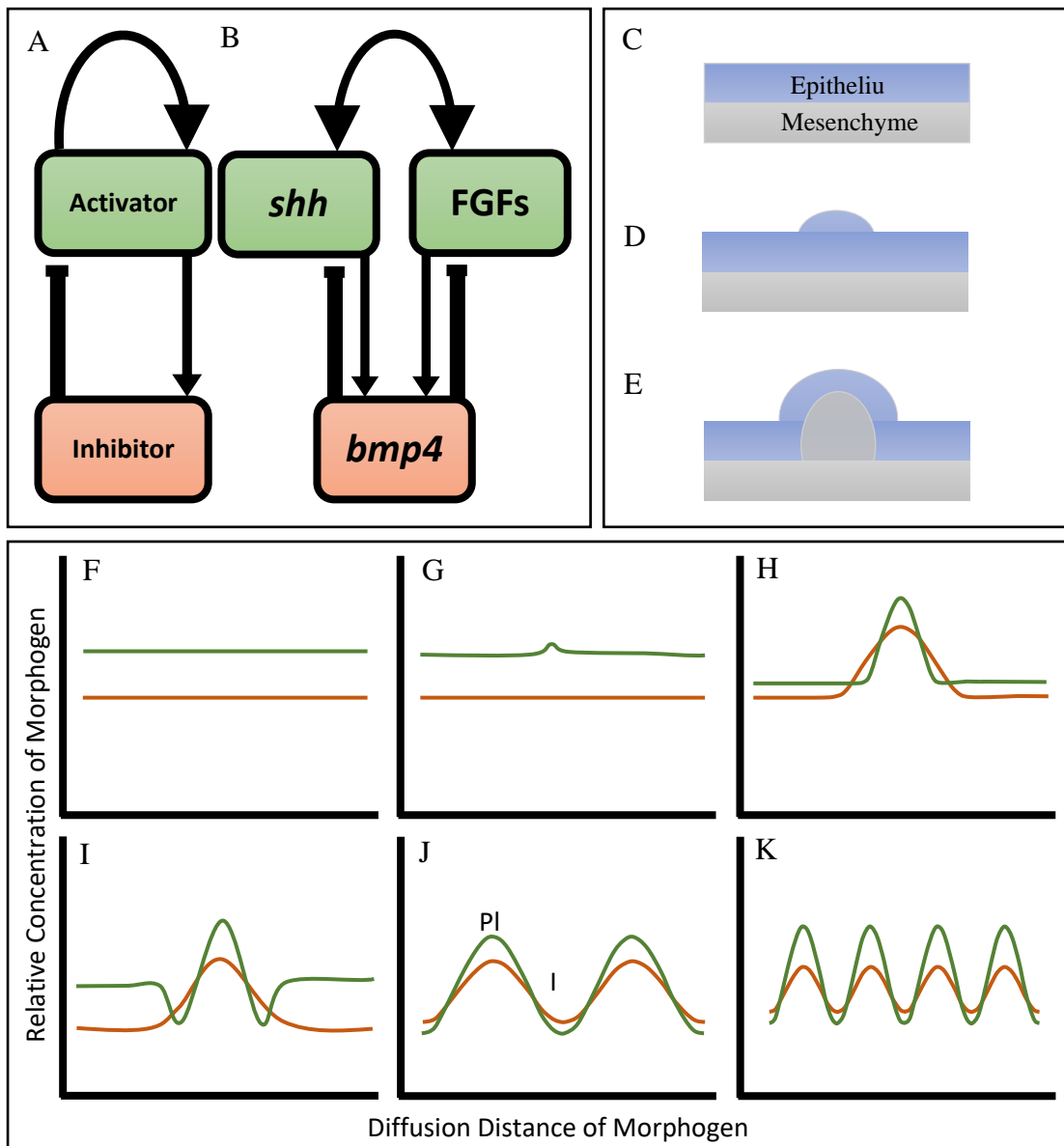


Figure 4: Patterning of Epithelial Appendages via Turing reaction-diffusion (RD).

Initiatory signals trigger the release of activators and inhibitors. Activators are autocatalytic, promoting their own expression and expression of the inhibitor, which then suppresses signalling of the activator (A). Examples of activators include *shh* and FGFs, and *bmp4* is an example of an inhibitor (B). Placodes form from a thickening of the epithelium (blue) which lies adjacent to the mesenchyme (grey) (C-D). They are characterised by conserved signalling in the epithelium and mesenchyme. A mesenchymal condensate forms underneath this thickening, forming a bud (E) that will later undergo morphogenesis, giving rise to the final adult form. Activator (green) signals diffuse over a shorter range compared to the inhibitor (red) (F). The autocatalytic activator promotes itself

(G), but also promotes the inhibitor (H), which then limits activator signalling (I). Turing demonstrated that this system can produce stable oscillations when concentrations are precisely tuned (J-K), defining placodal (Pl) and inter-placodal (I) regions, thereby dictating the patterning of epithelial appendages. F-K are adapted from (Kondo, 2002).

and observed throughout the initial growth of elasmobranch (Rasch et al., 2016), teleost (Aman et al., 2018), avian (Noramly et al., 1999) and mammalian (Chen et al., 2012) epithelial appendages. It is an important transcriptional regulator of target genes associated with cell proliferation and differentiation. Sonic hedgehog (*shh*), a ligand of the hedgehog (Hh) signalling pathway, is another conserved marker of placode growth, which influences both cellular proliferation and migration (Chuong et al., 2000b), along with bone morphogenetic proteins (BMPs) (Åberg et al., 1997) and fibroblast growth factors (FGFs) (Ornitz and Itoh, 2015). These signalling pathways interact throughout complex developmental feedback systems and GRNs, together dictating both the cellular migration and proliferation that controls appendage morphogenesis (although the relative contributions of these two processes in different systems remains poorly understood (Gritli-Linde, 2002; Magerl et al., 2001; Wessells, 1965)), as well as other diverse and essential aspects of development. As these important developmental pathways have been comprehensively characterised during avian and murine epithelial appendage development, it is possible for interesting comparisons to be drawn with other, comparatively less derived species, such as the shark. Although the evolution and radiation of new proteins such as the keratins is an incredibly important factor in contributing to epithelial appendage diversity (Vandebergh and Bossuyt, 2012), much of their diversity results from differential expression of conserved, re-deployed development genes (Pispa and Thesleff, 2003). This includes *β-cat*, *shh*, FGFs and BMPs (Pispa and Thesleff, 2003). In this sense, throughout their evolution vertebrates have employed a shared genetic toolkit to construct a remarkably

diverse array of epithelial structures. However, the specific mechanisms underpinning such diversity remain understudied, particularly in phylogenetically disparate taxa.

The spatial distribution of placodes defines the patterning of epithelial appendages. This patterning is major contributor to their diversity, and facilitates a plethora of functions ranging from thermoregulation to the provision of defensive armour (Maisey and Denton, 2016; Ruxton and Wilkinson, 2011). Alan Turing's reaction-diffusion (RD) system is considered a leading hypothesis to explain the autonomous formation of biological patterns (Kondo, 2002; Kondo and Miura, 2010; Torii, 2012; Turing, 1952). This mathematical model describes how morphogens diffusing differentially through a tissue can interact to produce patterns (Fig. 4A-B). These morphogens include a short-range autocatalytic activator that promotes its own expression, as well as the expression of a long-range inhibitor, which represses the activator. When parameters dictating the production, degradation and diffusion of either morphogen are appropriately tuned, stable oscillations of the activatory and inhibitory signals can arise (Fig. 4F-K) (Kondo, 2002; Kondo and Miura, 2010). Essentially, this dictates where placodes can and cannot form (Fig. 4F-K, P = placode, I = interplacode region), thereby controlling the spatial distribution, or patterning, of epithelial appendages.

Turing's patterning system has been widely used to explain pattern formation throughout diverse vertebrate groups. Such studies have used Turing's RD equations to produce patterns comparable to those observed in nature, for example the pigmentation of angelfish and leopards. These models can even predict changes in patterning throughout an animal's ontogeny (Kondo and Asai, 1995; Liu et al., 2006). However, experimental evidence supporting RD is relatively limited. Research involving the laser ablation of zebrafish pigmentation revealed stripe regeneration is consistent with RD simulation (Yamaguchi et al., 2007). Furthermore, researchers examining mouse epithelial appendage development

identified and experimentally tested activatory and inhibitory morphogens controlling RD patterning of hair (Sick et al., 2006), providing evidence for RD patterning of epithelial appendages in tetrapods.

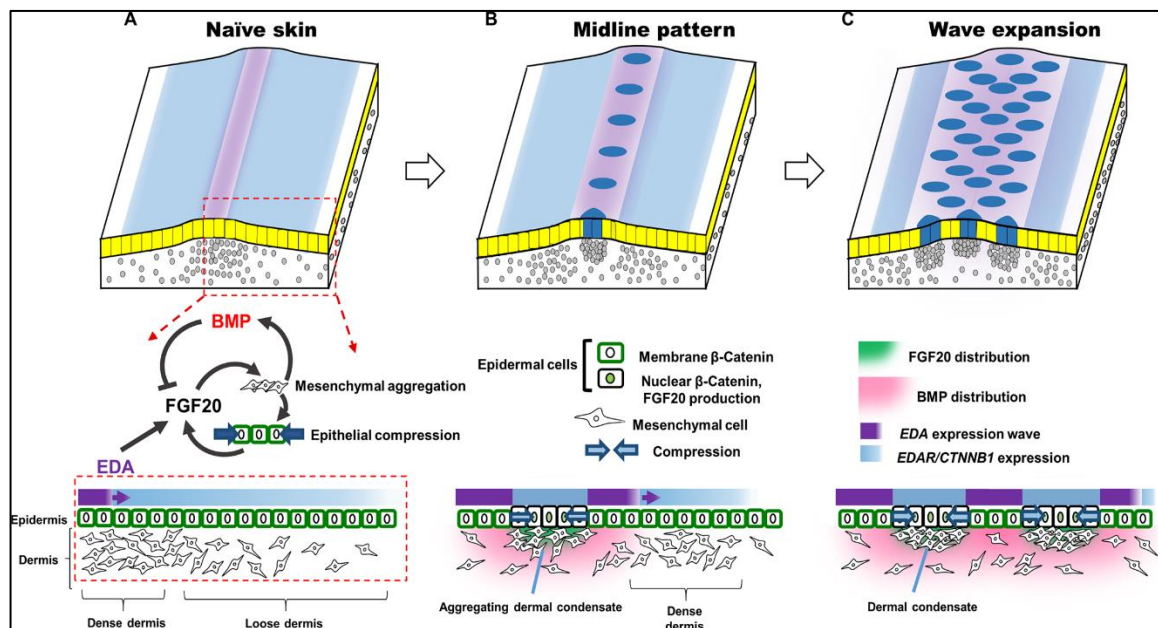


Figure 5: Schematic highlighting the role of tissue tension in feather patterning. A travelling wave of epithelial EDA triggers the release of FGF20, causing local aggregation of mesenchymal cells beneath the epithelium, subsequently compressing the epithelium, resulting in strengthened FGF20 expression and triggering patterning. Such patterning involves the release of other signalling molecules such as BMPs and β -cat, local to the mesenchyme and epithelium of developing placodes, respectively. Integration of molecular and mechanical aspects of patterning is termed reaction-diffusion-taxis. Schematic taken from (Ho et al., 2019).

More recently, researchers have proposed that mechanosensation also plays an important role in initiating pattern formation (Fig. 5) (Ho et al., 2019; Shyer et al., 2017). For example, tension of the avian dermis generated by the aggregation of mesenchymal cells is essential for breaking symmetry and activating β -cat production, thereby initiating feather placode

development (Fig. 5A-C) (Ho et al., 2019; Noramly et al., 1999; Shyer et al., 2017). A travelling wave of epithelial EDA can trigger the release of FGF20, resulting in local mesenchymal cellular aggregation, capable of compressing the adjacent epithelium (Ho et al., 2019). This process strengthens FGF20 expression, whilst triggering the release of other signal molecules localised to developing placodes, including epithelial β -cat and mesenchyme BMPs (Fig.5) (Ho et al., 2019). As the travelling wave expands, this combination of mechanical and molecular signalling produces a periodic pattern of feather primordia. Subtle alterations to mesenchymal tissue tension may even provide a mechanistic explanation for avian epithelial appendage pattern diversity. The integration of mechanical processes can complement morphogen-based RD systems, resulting in more comprehensive explanations of epithelial appendage patterning. Such integration has been termed a ‘reaction-diffusion-taxis system’ (Ho et al., 2019; Shyer et al., 2017).

Although there are many examples of biological patterns that conform to RD modelling, experimental evidence to support this system remains relatively limited, particularly outside of the tetrapods (Fig. 1) (Kondo, 2002; Kondo and Miura, 2010). Combining RD simulation with *in vivo* experimental manipulation of pattern formation will provide more robust support. By focusing such research efforts upon phylogenetically distinct taxa, we will begin to understand the relative importance and prevalence of this system throughout the epithelial appendage patterning of diverse gnathostomes.

Despite the wide-ranging explanatory potential of Turing’s patterning system, it is not ubiquitous. Previous research has demonstrated that the head scales of crocodiles (*Crocodylus niloticus*) emerge from the physical cracking of a highly keratinized skin domain (Milinkovitch et al., 2013). Rapid growth of the facial and jaw skeleton contributes to the mechanical stress that underpins this cracking, dividing the skin of the head into random polygonal units that do not arise from anatomical placodes, unlike other reptilian

scales and vertebrate epithelial appendages (Di-Poï and Milinkovitch, 2016; Milinkovitch et al., 2013). Additionally, mechanical stress can cause the hyper-keratinized skin of elephants (*Loxodonta africana*) to form an intricate network of crevices, which are essential for thermoregulation through the retention of water and mud (Lillywhite and Stein, 1987; Martins et al., 2018). Furthermore, development of the frilled dragon's (*Chlamydosaurus kingii*) erectile ruff is dependent upon elastic instability generated by homogenous growth of the frill skin, which is frustrated by attachment to surrounding tissue, resulting in the formation of characteristic folds (Montandon et al., 2019). These studies provide examples of how distinct physical and stochastic patterning systems can contribute to the diversity of integumentary structures adorning the skin of certain animals (Martins et al., 2018; Milinkovitch et al., 2013; Montandon et al., 2019). Furthermore, they highlight the need to study phylogenetically and ecologically diverse vertebrate species to gain a comprehensive understanding of the remarkable forms and morphologies displayed by different skin appendages.

1.1.4 Conclusion

As classic model organisms, chicken and mouse embryos have provided a wealth of information regarding epithelial appendage development (Chuong et al., 2000a; Hardy, 1992; St-Jacques et al., 1998; Stuart and Moscona, 1967). Such research has shed light upon the components of a shared genetic toolkit used to construct the foundations of epithelial appendages – the anatomical placode (Biggs and Mikkola, 2014; Di-Poï and Milinkovitch, 2016; Noramly et al., 1999; Pispa and Thesleff, 2003). Furthermore, these model species have provided us with experimental evidence describing how the spatial distribution of epithelial appendages is controlled, widely through Turing RD patterning (Jung et al., 1998; Sick et al., 2006). However, studies addressing more phylogenetically diverse study species are required for us to obtain a comprehensive understanding of how

epithelial appendages have arisen and diversified throughout gnathostomes. This will enable us to understand how developmental changes can produce such a remarkable variety of epithelial structures, and shed light upon how these structures are related across hundreds of millions of years of evolutionary time, throughout the gnathostomes.

1.2 Thesis rationale

Previous research examining epithelial appendages in classic model organisms has yielded a wealth of information regarding their evolution and development (Biggs and Mikkola, 2014; Chuong et al., 2000a; Pispá and Thesleff, 2003). However, to understand the remarkable diversity of these units that we observe in the natural world, it is essential to study diverse taxonomic groups which exhibit remarkable phenotypes. Such groups should be strategically selected to comprehensively cover the vertebrate phylogeny, allowing us to draw far reaching and widely applicable conclusions.

Studying sharks presents a unique opportunity to investigate epithelial appendage development in an ancient gnathostome lineage. As the cartilaginous fishes diverged from other bony vertebrates approximately 450 million years ago, comparing epithelial appendage development between either lineage allows us to draw broad inferences regarding these structures throughout the gnathostomes. Such research will complement data from classic model species, providing us with a more comprehensive understanding of how diverse epithelial appendages have arisen.

Using both elasmobranch (*S. canicula*) and avian (*G. domesticus*) models, this thesis aims to investigate three key questions regarding the evolution and development of gnathostome epithelial appendages.

- i) Chapter 2: Do anatomical placodes underpin epithelial appendage initiation throughout gnathostomes?

- ii) Chapters 3 & 4: How is the patterning of gnathostome epithelial appendages controlled?
- iii) Chapter 5: How is the morphogenesis of epithelial appendages regulated in gnathostomes?

1.3 Research summary

1.3.1 Chapter 2 summary

Epithelial placodes are thought to constitute the foundations upon which diverse epithelial appendages develop (Pispa and Thesleff, 2003). Recent research has shown these placodes underpin the development of epithelial appendages throughout the amniotes (Di-Poï and Milinkovitch, 2016; Musser et al., 2015). They are characterised by conserved signalling in the epithelial and mesenchyme, as well as columnar basal epithelial cells with a reduced proliferation rate (Di-Poï and Milinkovitch, 2016). I ask whether these placodes also provide the foundation of epithelial appendage development outside of the amniotes, by examining development in the shark. I demonstrate that placodes underpin the development of shark caudal denticles. These denticles contain an ancient dentine type associated with the oldest known sharks from the Silurian and Ordovician periods (Johanson et al., 2008). Therefore, it is likely that epithelial placodes provide the shared foundations upon which diverse epithelial appendages have arisen, throughout the gnathostomes.

1.3.2 Chapter 3 summary

RD patterning is important throughout diverse aspects of gnathostome development (Kondo and Miura, 2010; Turing, 1952). Despite a wealth of theoretical research examining the role of this system in controlling epithelial appendage patterning, experimental work is comparatively limited (Kondo, 2002; Kondo and Miura, 2010). Whilst previous studies

have found support for RD patterning of murine hair and avian feathers, there is limited experimental evidence outside of these tetrapod models (Jung et al., 1998; Sick et al., 2006). I provide evidence for RD patterning of shark denticles, using a combination of gene expression assays, RD modelling and experimental manipulations of normal development. I also show that alterations to RD parameters may explain variations in denticle patterns throughout elasmobranchs, demonstrating that this system is likely important in the evolution of the diverse functional traits facilitated by denticle patterning (Crooks et al., 2013; Dean and Bhushan, 2010; Oeffner and Lauder, 2012). As RD patterning is important in denticle development, it is likely that this system controls the patterning of diverse epithelial appendages, from sharks through to birds and mammals (Jung et al., 1998; Sick et al., 2006).

1.3.3 Chapter 4 summary

Reticulate scales are an avian epithelial appendage found on the ventral footpad surface, thought to aid grip and cushioning during locomotion (Chuong et al., 2000a). Previous research has suggested that these appendages do not develop from epithelial placodes, but instead arise as symmetrical elevations of the skin (Musser et al., 2015; Sawyer and Craig, 1977). However, research addressing the development of reticulate scales at the cellular and molecular levels is limited. Therefore, I examined gene expression and cellular proliferation during normal development of reticulate scales, and observed conserved markers of epithelial appendage development underpinning their formation. Additionally, I demonstrate that their patterning conforms to RD simulation, in which a primary circular domain subdivides into secondary units. This primary domain is likely either an enlarged placode or an initiatory field comparable to the feather tract. Comparisons with squamate footpad scale patterning suggests that this patterning system is unique to aves. Therefore, it likely arose after the divergence of squamates and aves from

a common diapsid ancestor, roughly 255 million years ago (Brusatte et al., 2015). This further demonstrates how alterations to widespread RD patterning systems can explain the development of diverse gnathostome epithelial appendages.

1.3.4 Chapter 5 summary

Shark denticles exhibit dramatic morphological variations, both within and between different elasmobranch species. These differences have arisen to facilitate a huge range of different functional traits, ranging from hydrodynamic drag reduction to the provision of defensive armour (Crooks et al., 2013; Dean and Bhushan, 2010). This chapter aims to uncover the molecular basis of this morphological diversity. I undertake gene expression assays of signalling pathways known to control paired appendage outgrowth, including sonic hedgehog (*shh*) and fibroblast growth factors (FGFs). Additionally, I attempt to experimentally manipulate normal denticle morphogenesis through treatment with ectopic SHH protein. These results show that gene signalled associated with the outgrowth of paired appendages underpins both denticle and avian feather morphogenesis. Furthermore, exogenous SHH treatment is sufficient to trigger the deposition of subepithelial ectopic mineralised tissue. Overall, this demonstrates that conserved genetic circuitry underpins shark denticle morphogenesis. Natural variations to this circuitry may underly the morphological diversity of denticles, providing a potential mechanism to explain how their diverse functional traits have arisen.

2.0 Chapter 2:

Developing an ancient epithelial appendage: FGF signalling regulates early tail denticle formation in sharks

Rory L. Cooper, Kyle J. Martin, Liam J. Rasch, Gareth J. Fraser*

*Correspondence: g.fraser@sheffield.ac.uk

Department of Animal and Plant Sciences, and the Bateson Centre, University of Sheffield, Sheffield, S10 2TN, UK

Citation: Cooper, R. L., Martin, K. J., Rasch, L. J., and Fraser, G. J. 2017, Developing an ancient epithelial appendage: FGF signalling regulates early tail denticle formation in sharks, *EvoDevo*, 8, 8, 1-19

2.1 Abstract

Introduction: Vertebrate epithelial appendages constitute a diverse group of organs that includes integumentary structures such as reptilian scales, avian feathers and mammalian hair. Recent studies have provided new evidence for the homology of integumentary organ development throughout amniotes, despite their disparate final morphologies. These structures develop from conserved molecular signalling centres, known as epithelial placodes. It is not yet certain whether this homology extends beyond the integumentary organs of amniotes, as there is a lack of knowledge regarding their development in basal vertebrates. As the ancient sister lineage of bony vertebrates, extant chondrichthyans are well suited to testing the phylogenetic depth of this homology. Elasmobranchs (sharks, skates and rays) possess hard, mineralised epithelial appendages called odontodes, which include teeth and dermal denticles (placoid scales). Odontodes constitute some of the oldest known vertebrate integumentary appendages, predating the origin of gnathostomes. Here, we used an emerging model shark (*Scyliorhinus canicula*) to test the hypothesis that denticles are homologous to other placode-derived amniote integumentary organs. To examine the conservation of putative gene regulatory network (GRN) member function, we undertook small molecule inhibition of fibroblast growth factor (FGF) signalling during caudal denticle formation.

Results: We show that during early caudal denticle morphogenesis, the shark expresses homologues of conserved developmental gene families, known to comprise a core GRN for early placode morphogenesis in amniotes. This includes conserved expression of FGFs, sonic hedgehog (*shh*) and bone morphogenetic protein 4 (*bmp4*). Additionally, we reveal that denticle placodes possess columnar epithelial cells with a reduced rate of proliferation, a conserved characteristic of amniote skin appendage development. Small molecule inhibition of FGF signalling revealed placode development is FGF dependent, and

inhibiting FGF activity resulted in downregulation of *shh* and *bmp4* expression, consistent with the expectation from comparison to the amniote integumentary appendage GRN.

Conclusion: Overall, these findings suggest the core GRN for building vertebrate integumentary epithelial appendages has been highly conserved over 450 million years. This provides evidence for the continuous, historical homology of epithelial appendage placodes throughout jawed vertebrates, from sharks to mammals. Epithelial placodes constitute the shared foundation upon which diverse vertebrate integumentary organs have evolved.

Keywords: Homology, Shark, Epithelial appendage, Anatomical placode, Dermal denticle

2.2 Introduction

The diversity of phenotypes among vertebrate epithelial appendages is vast and includes disparate structures of the integument such as feathers, hair, scales and teeth (Biggs and Mikkola, 2014; Pispa and Thesleff, 2003). These organs have evolved to facilitate wide-ranging aspects of survival and reproduction. Despite such diversity, these structures generally develop from patterns of reciprocal interactions between two adjacent tissue layers: the epithelium and underlying mesenchyme (Pispa and Thesleff, 2003). Where scale-like structures also arise from more derived mechanisms, for example the physical cracking of highly keratinised crocodile skin to form randomly spaced, polygonal head scales, placode-derived scales are also present on the body (Milinkovitch et al., 2013). Recent research has revealed shared ancestry among amniote epithelial appendages, based on the observation that reptilian scales, avian feathers and mammalian hair share a common foundation during early development (Di-Poï and Milinkovitch, 2016): the anatomical placode. This structure is characterised by conserved molecular markers and columnar epithelial cells with a reduced rate of proliferation. Placodes constitute a localised thickening of the epithelium together with an underlying dermal condensate (mesenchyme) (Sengel, 1990; Thesleff et al., 1995). Morphogenesis of the placode results in the adult form (Hardy, 1992) and is controlled by molecular signals that participate in a complex gene regulatory network (GRN). This placode GRN is thought to be largely conserved throughout amniotes (Di-Poï and Milinkovitch, 2016; Musser et al., 2015). However, there is a gap in our knowledge regarding the developmental processes guiding placode morphogenesis in non-amniote vertebrates. It is not known whether this GRN is conserved across all jawed vertebrates (Donoghue, 2002).

Chondrichthyans (sharks, rays and chimaeras) are the sister lineage of osteichthyans and occupy a basal position in jawed vertebrate phylogeny. They possess hard, mineralised epithelial appendages known as odontodes. Odontodes include both teeth and dermal denticles and have been observed in early vertebrates that lived as long as 450 million years ago (Karatajute-Talimaa, 1973; Sansom et al., 1996). Odontodes consist of a central pulp cavity surrounded by a dentine layer, encased within an enameloid (enamel-like) covering (Motta et al., 2012; Ørvig, 1977). Recent work has provided new genetic evidence for the old hypothesis that teeth and denticles share deep homology and that their development is controlled by a common odontode GRN (Martin et al., 2016). Since their likely origin as a form of body armour (Fraser et al., 2010), denticles have evolved to fulfil a plethora of functions: they reduce abrasive damage (Raschi and Tabit, 1992), aid feeding (Southall and Sims, 2003), deter parasites (Sullivan and Regan, 2011), enable communication (Reif, 1985a) and improve hydrodynamic efficiency (Dean and Bhushan, 2010; Oeffner and Lauder, 2012; Reif, 1985b). Chondrichthyan denticles exhibit broad morphological variation to facilitate these roles (Motta et al., 2012).

In the *Scyliorhinus canicula* embryo, this variation can broadly be categorised into 3 classes: (1) the precocious embryonic denticles of the caudal tail, (2) the dorsal trunk and (3) adult type general body denticles (Fig. 1) (Martin et al., 2016). Dorsal denticles (Fig. 1d, e) appear in two polarised rows at approximately 60–80 days post-fertilisation (dpf; Stage 31) and may trigger the subsequent emergence of general body denticles (Ballard et al., 1993), as observed during feather tract patterning (Oster et al., 1983). They are subsumed into general scalation soon after hatching (Martin et al., 2016). General body denticles (Fig. 1f, g) are the most prevalent denticle type, appearing just before hatching at 145–175 dpf (Stage 34) (Ballard et al., 1993), covering the skin in an intricate pattern when space is available and not in discrete rows (Fraser and Smith, 2011; Reif, 1982). Before

dorsal and body denticles appear, four rows of caudal denticles emerge at 52–60 dpf (Stage 30) (Ballard et al., 1993); two rows are present (dorsal and ventral) laterally on either side of the tail fin tip (Fig. 1b, c, j–m) (Johanson et al., 2008). Caudal denticle number can vary between 9 and 13 units which form on either dorsal row, and between 5 and 10 units which form on either ventral row (Ballard et al., 1993). The placodes of these denticles consist of a squamous epithelium overlying a basal epithelial layer of columnar cells, with condensing underlying mesenchyme (Fig. 3). They develop sequentially from posterior to anterior, approximately equidistant from one another (Ballard et al., 1993; Eames et al., 2007; Johanson et al., 2008, 2007). During morphogenesis, these denticles also mineralise in a posterior to anterior progression (Ballard et al., 1993). Despite being patterned in rows similarly to dorsal denticles, they display an irregular petaliform shape with variation in cusp number and have a less restricted polarity than other denticle types (Fig. 1l, m). These units have a dentine collar fusing the main cusp to the simple base (Johanson et al., 2008), anchored within the mesenchymal dermis via connective tissues. Caudal denticles are transient epithelial structures that are lost before or during the hatching phase when general body denticles develop to take over their positions. This morphological disparity between caudal denticles and other denticle types from the dorsal trunk and general body extends beyond their macrostructure.

Caudal denticles contain a dentine type that shares histological similarity to dentine from odontodes of the Ordovician and Silurian Periods (Johanson et al., 2008; Karatajute-Talimaa, 1973; Sansom et al., 1996). Unlike the orthodentine observed in the general body denticles of *S. canicula*, the tubules of this dentine exhibit a branching pattern (Johanson et al., 2008; W. E. Reif, 1980). The combination of this primitive-type dentine composition and the regulated, iterative patterning mechanism of these denticles, which are found in sharks at least across families Scyliorhinae and Heterodontidae, indicates that caudal

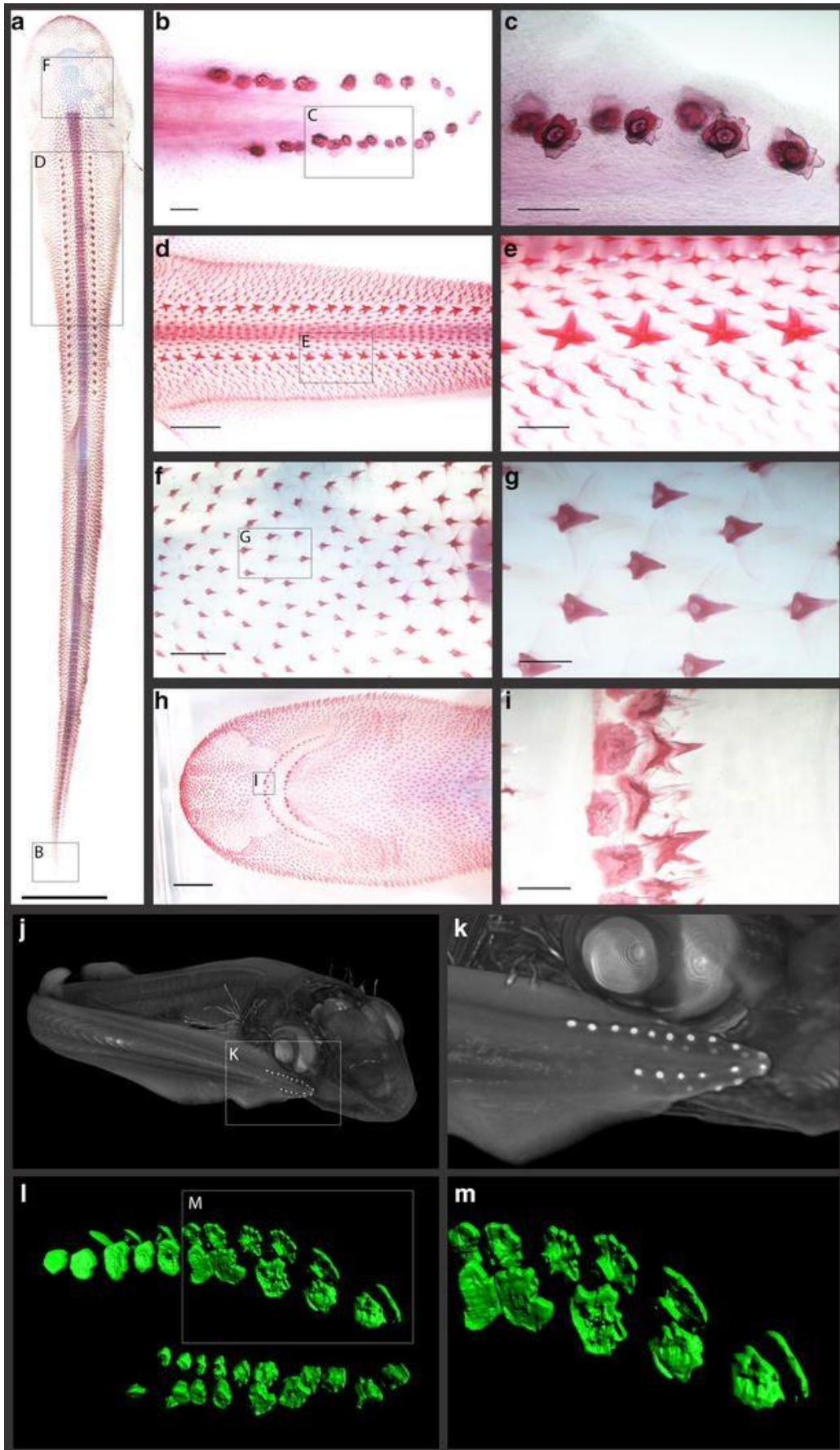


Figure 1: Odontode diversity of the pre-hatchling Catshark (*S. canicula*). Samples a–i are cleared and stained for calcium-rich tissue using alizarin red dye. Samples j–k are computerised tomography (CT) scans of a Stage 32 whole embryo, and samples l–m are light sheet fluorescence microscopy (LSFM) images of caudal denticles of a Stage 31 embryo, stained with alizarin red. The pre-hatchling (a) possesses three major external denticle types. The caudal denticles are the first to emerge, appearing on either side of the tip of the tail in dorsal and ventral rows (b, c, j–m) (Ballard et al., 1993). These denticles are not strongly polarised, although cusps generally point towards the posterior (Johanson et al., 2008). Next, the dorsal denticles emerge along the trunk of the embryo in two polarised rows (d, e). Finally, general body denticles emerge just before hatching, covering the whole body (f, g). These denticles are also highly polarised. Teeth emerge in the jaws at a similar stage to general body denticles (h, i). The scale bar for a = 1000 μm , b, c, g and i = 200 μm , d and h = 2500 μm , e and f = 500 μm

denticles may have a deep phylogenetic history and have been retained in extant sharks over 450 million years of evolution (Johanson et al., 2008, 2007). However, little is known about the developmental processes or GRN underlying the formation of caudal denticles or indeed other denticle types in chondrichthyans.

Fibroblast growth factor (FGF) signalling is essential for various aspects of both embryogenesis and adult homeostasis, such as tissue repair and regeneration (Ornitz and Itoh, 2015). FGFs have essential roles throughout vertebrate organogenesis, for example in limb, lung and brain development (Min et al., 1998a; Ohuchi et al., 2000; Trokovic et al., 2005). They mediate their responses by activating cell surface tyrosine kinase FGF receptors (FGFRs) (Ornitz and Itoh, 2015). FGF signalling is also widely involved in the development of taxonomically diverse epithelial appendages of the integumentary system, such as hair, feathers, scutes, scales and teeth (Jackman et al., 2004; Jung et al., 1998; Li et al., 2014; Moustakas-Verho et al., 2014; Rosenquist and Martin, 1996). Relative to the epithelial appendages of amniotes, little is known about the GRN controlling shark denticle

placode formation, although some recent work has documented signalling during shark tooth development (Rasch et al., 2016) and compared it to development of other odontode types (Debiais-Thibaud et al., 2015, 2011; Martin et al., 2016).

During feather placode development, ligands of the FGF signalling family (such as *Fgf4*) work together with sonic hedgehog (*Shh*) in a positive feedback loop, that promotes expression of both *Fgf4* and *Shh* whilst also inducing expression of bone morphogenetic protein 4 (*Bmp4*) (Jung et al., 1998; Widelitz et al., 1996). *Bmp4* then has an inhibitory effect upon both *Shh* and *Fgf4*, downregulating their expression to control patterning by limiting placode formation exclusively to the site of future organs (Ashique et al., 2002; Jung et al., 1998; Noramly and Morgan, 1998). This inhibitory action of mesenchymal *Bmp4* has also been observed during mouse hair development (Botchkarev et al., 1999). The mesenchymal expression of *Bmp4* is conserved during morphogenesis throughout amniote epithelial appendage development (Di-Poï and Milinkovitch, 2016). It is unknown whether this FGF, *Shh* and *Bmp4* signalling feedback system is conserved throughout all vertebrate epithelial appendage placode GRNs, although conservation of these markers is widely observed during amniote placode formation (Di-Poï and Milinkovitch, 2016).

This study examines whether the molecular signalling observed during early morphogenesis of amniote integumentary organs is conserved within the development of caudal denticles of the shark (*S. canicula*). By comparing gene expression to the development of other epithelial appendages and using functional experiments to examine gene interactions, it is possible to infer putative GRN relationships (Martin et al., 2016). A combination of anatomical, histological and molecular techniques including whole mount in situ hybridisation and immunohistochemistry was used to examine the development of shark caudal denticles, focusing on the role of the FGF signalling pathway and associated members of the putative core conserved placode GRN, inferred from studies in amniotes.

To study the conservation of placode GRN members between different odontode types, gene expression was also examined during development of general body denticles. The fibroblast growth factor receptor (FGFR) inhibitor SU5402 was used to examine the effect of suppressing signalling of this major developmental pathway. By examining the role of FGF signalling during epithelial appendage development in a chondrichthyan model and its effects upon the expression of other putative GRN members, it will be possible to elucidate the degree to which epithelial integumentary organ GRNs are conserved across jawed vertebrates, and evaluate their potential homology.

2.3 Results

2.3.1 Caudal denticle placode development reveals conserved morphogenetic mechanisms for integumentary organ formation

To determine the earliest time of caudal denticle morphogenesis in the shark (*S. canicula*), we charted the sequential development of these units. It has been documented that caudal denticles in *S. canicula* develop from a posterior to anterior direction in dorsal and ventral rows, on both sides of the caudal-most tip of the tail (Fig. 2) (Ballard et al., 1993; Johanson et al., 2008). Previous reports suggest their emergence occurs at 52–60 dpf (Stage 30) (Ballard et al., 1993) (Fig. 2f, g). However, our observations suggest placode development begins earlier, between 42 and 46 dpf (Stage 27) (Ballard et al., 1993) (Fig. 2b, c), although some variation in timing of denticle initiation was noted. One explanation for such variation in development is temperature of the surrounding environment (Ballard et al., 1993). Caudal denticles arise from distinct placodes (Figs. 2c4, 3a), which form from a thickened condensation of epithelial cells with an underlying mesenchymal condensate (Fig. 3). The first denticle placodes to form (most posterior) are also the first in the sequence to mineralise. This progresses in a posterior–anterior fashion (Fig. 2d4) and can be visualised using alizarin red staining (Fig. 2e4–i5).

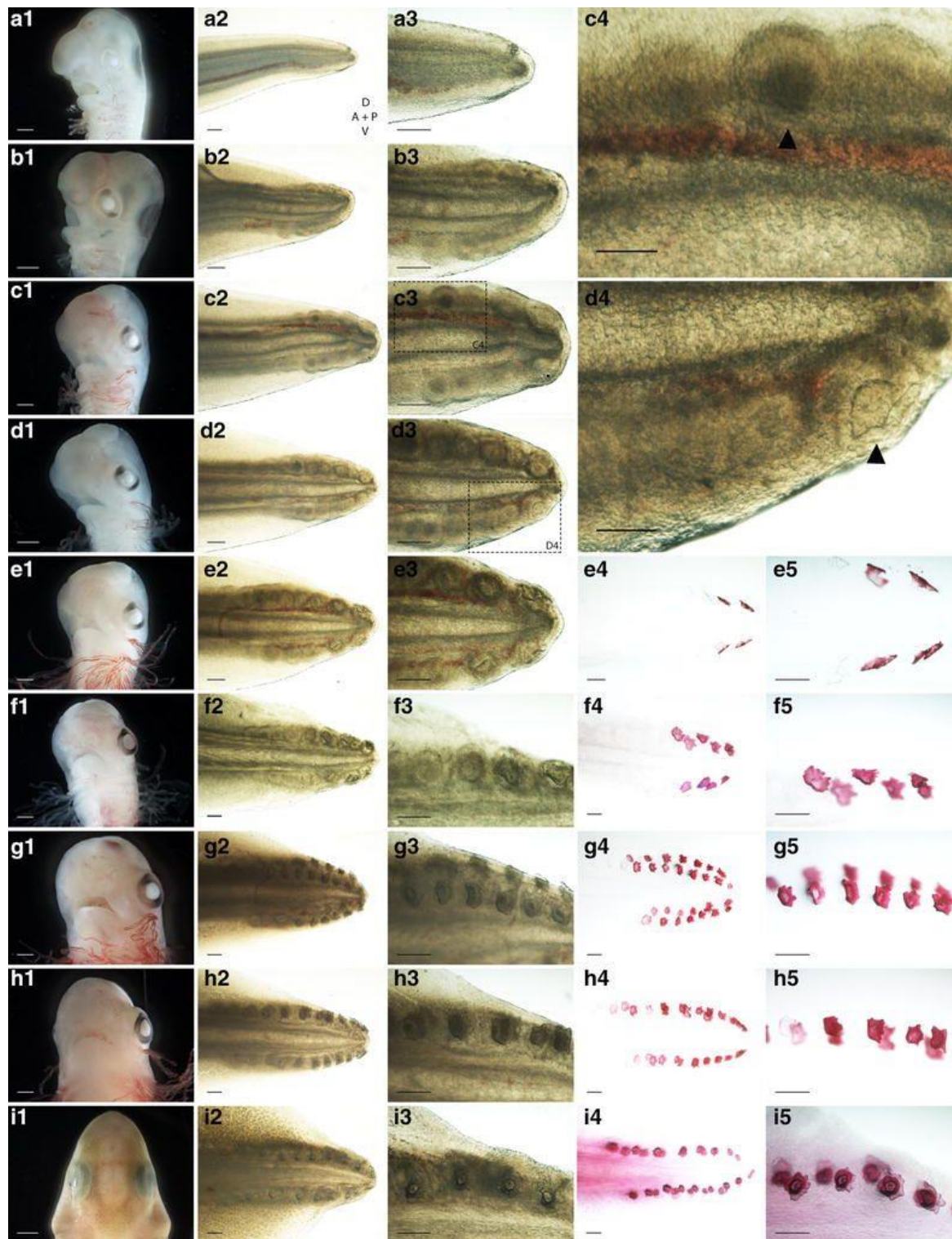


Figure 2: Sequential development of caudal denticles in the catshark. As the embryo develops from Stage 27 (a) to Stage 33 (i), the gills proliferate, the eyes are encircled with pigment of increasing darkness and the rostrum protrudes anterior to the mouth (Ballard et al., 1993). During this period, caudal denticles develop from posterior to anterior in dorsal

and ventral rows, on either side of the tail tip. At early Stage 27, no placodes can be detected (a2–a2). Epithelial thickenings then form from posterior to anterior (b2–b3, c2–c4). c4 shows a magnified view of c3, highlighting an individual placode (marked with an arrowhead). These placodes then accumulate their first layers of mineralised tissue during morphogenesis (d2–d4). d4 shows a magnified view of d3, highlighting a mineralising placode (marked with an arrowhead). Mineralisation of denticles also occurs sequentially from posterior to anterior (e2–e3, f2–f3, g2–g3, h2–h3 and i2–i3) and can be highlighted with alizarin red staining for calcium-rich tissue (e4–e5, f4–f5, g4–g5, h4–h5 and i4–i5). For the axis, D dorsal, V ventral, P posterior and A anterior. Scale bars are 1000 μm for a1, b1, c1, d1, e1, f1, g1, h1 and i1 and 200 μm for all other images

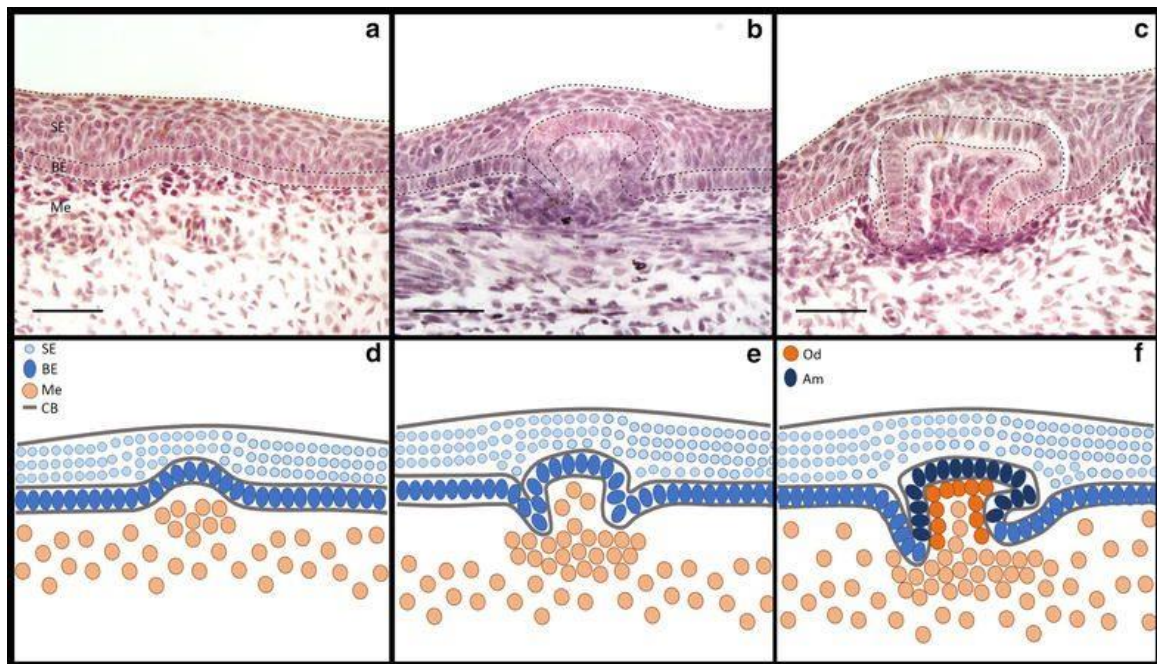


Figure 3: Morphogenesis of a caudal denticle. Caudal denticle placodes consist of a squamous epithelium (SE) overlying columnar cells of the basal epithelium (BE), which overlies the mesenchyme (Me) (a, d). During placode morphogenesis, condensing mesenchymal cells aggregate below columnar cells of the basal epithelium epithelial. The basal epithelium undergoes growth and folding (b, e) to form the posterior facing cusp (c, f). CB is cell layer boundary. Ameloblasts (Am) in the basal epithelial cusp (c, f) and odontodes (Od) in the papilla underlying the basal epithelium produce enameloid and dentine, respectively, to mineralise the unit (Rasch et al., 2016). Scale bars are 50 μm

The sequential development of this morphogenetic placode unit bears remarkable similarity to feather bud development in chicks (Di-Poï and Milinkovitch, 2016; Hogan, 1999; Jung et al., 1998; Stuart and Moscona, 1967) (Fig. 2). We wished to test whether members of the amniote epithelial appendage placode GRN are conserved in chondrichthyans (Di-Poï and Milinkovitch, 2016; Musser et al., 2015). Therefore, a selection of well-known GRN components assembled from the literature regarding feather, hair and tooth development were chosen (Fraser et al., 2004; Harris et al., 2008; Jung et al., 1998), and their expression during early placode morphogenesis of caudal denticles in *S. canicula* was examined.

2.3.2 Gene expression from integumentary appendage development is conserved in sharks

Recent research has revealed ectodysplasin signalling is conserved throughout development of amniote epithelial appendages (Di-Poï and Milinkovitch, 2016). Ectodysplasin-A (*Eda*) and its receptor (*Edar*) comprise some of the earliest markers of placode morphogenesis in vertebrates (including zebrafish, chick and mouse) (Drew et al., 2007; Fessing et al., 2006; Harris et al., 2008; Houghton et al., 2005; Mustonen et al., 2004). During early morphogenesis of shark caudal denticles, *eda* and *edar* expression is detected in the localised epithelial thickening (Fig. 4a–f). *eda* is also expressed during later denticle morphogenesis in epithelial cells in the signalling centre of the putative enameloid knot (EK) (Fig. 4b, bi). This shares similarity to mammalian tooth development, during which interactions between Eda/Edar and other signalling molecules (e.g. Shh, Fgf4 and Bmp4) regulate morphogenesis of the enamel knot (Tucker et al., 2000). During hair morphogenesis in mammals, Eda and Edar signalling induces expression of other signalling molecules, such as Shh (Pummila et al., 2007; Schmidt-Ullrich et al., 2006).

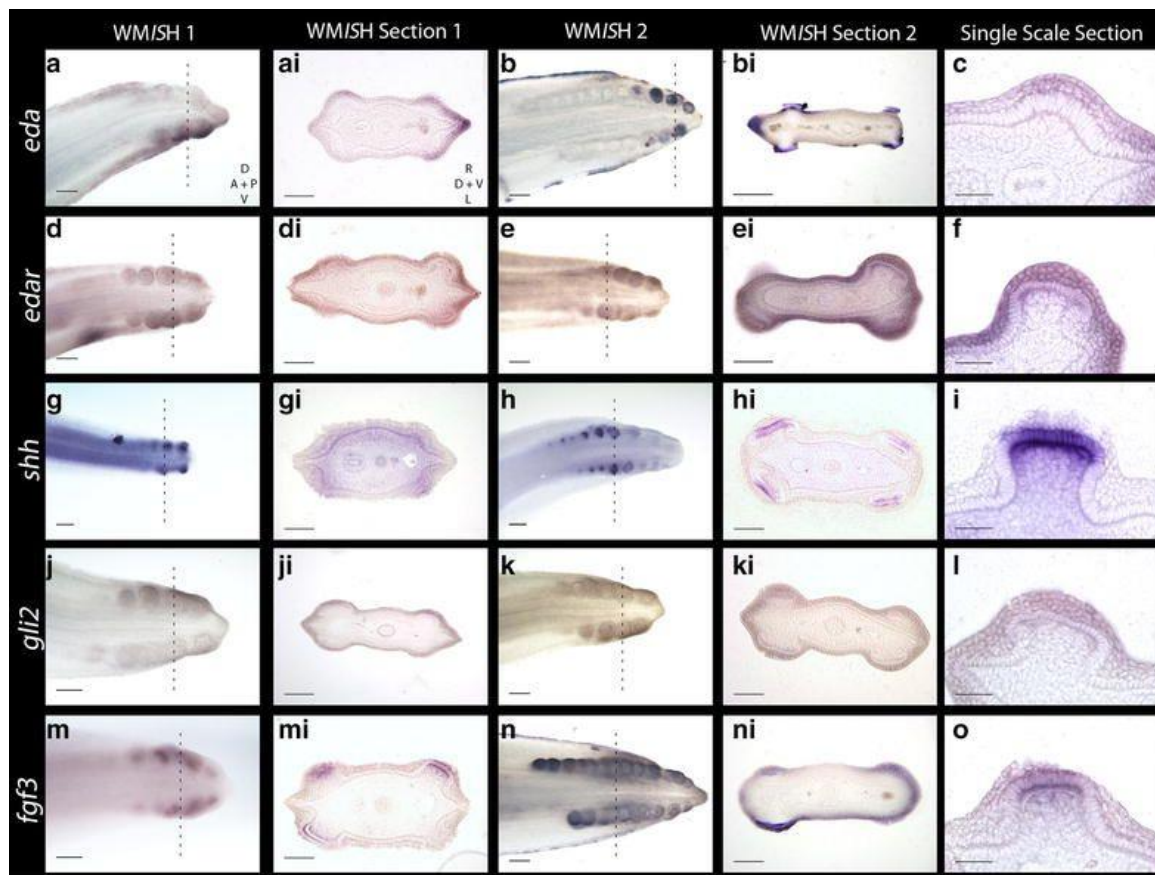


Figure 4: Gene expression analyses of early morphogenesis of caudal denticles. Expression of *eda* and its receptor *edar* are observed in the epithelium during early placode morphogenesis (a–f). *eda* can also be seen in tissue undergoing mineralisation later in morphogenesis (b–bi). *shh* is first observed in the epithelium during early morphogenesis, before becoming restricted to the basal epithelium later in morphogenesis (g–i). *gli2* is also seen in the epithelium early during placode formation (j–l). Expression of *fgf3* is first seen in the epithelium, before moving to both the epithelium and mesenchyme later in placode morphogenesis (m–o). The dashed lines show where in the WMISH the section was taken. WMISH Section 1 represents a younger stage specimen than WMISH Section 2. For the WMISH, D dorsal, V ventral, A anterior and P posterior. For WMISH sections, R right, L left, D dorsal and V ventral. For scale bars, a, b, d, e, g, h, j, k, m, n = 200 μ m, ai, bi, di, ei, gi, hi, ji, ki, mi, ni = 100 μ m, and c, f, i, l, o = 50 μ m

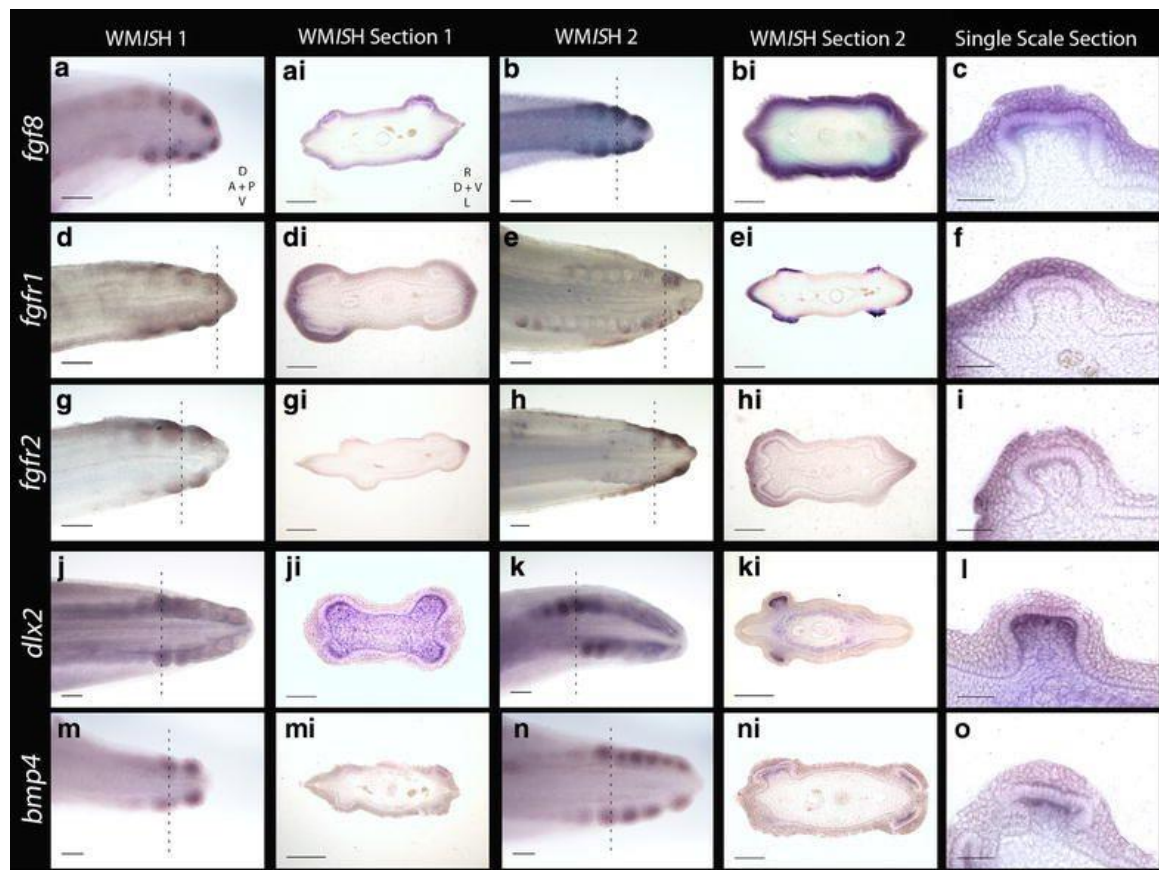


Figure 5: Gene expression analyses of early morphogenesis of caudal denticles (continued). *fgf8* signalling is largely retained in the epithelium throughout (a–c). *fgfr1* and *fgfr2* are both seen in the epithelium during early denticle morphogenesis (d–i). Expression of *dlx2* is restricted to the mesenchyme throughout early placode morphogenesis (j–l). Similarly, *bmp4* is observed in the mesenchyme during early placode morphogenesis (m–o). The dashed lines show where in the WMISH the section was taken. WMISH Section 1 represents a younger stage specimen than WMISH Section 2. For the WMISH, D dorsal, V ventral, A anterior and P posterior. For WMISH sections, R right, L left, D dorsal and V ventral. For scale bars, a, b, d, e, g, h, j, k, m, n = 200 μ m, ai, bi, di, ei, gi, hi, ji, ki, mi, ni = 100 μ m, and c, f, i, l and o = 50 μ m

Shh is a ligand of the Hedgehog (Hh) signalling pathway that marks early stages of epithelial morphogenesis in a diverse range of integumentary organs (Buchtová et al., 2008; Fraser et al., 2004; Smith et al., 2009), including shark teeth and chick feathers (Martin et al., 2016; Rasch et al., 2016; Smith et al., 2009; Ting-berreth and Chuong, 1996). *shh* is expressed throughout morphogenesis of shark caudal denticles (Fig. 4g–i). During early morphogenesis, *shh* is first expressed in the superficial squamous epithelium (Fig. 6m), before subsequently becoming restricted to the basal epithelium (Figs. 6n, o, 7). Previous research has shown that *Gli2* is expressed both downstream and upstream of Shh signalling (Ding et al., 1998; Pan et al., 2006; Sasaki et al., 1999) and is essential in hair follicle development as a promoter of cell proliferation (Mill et al., 2003). Here, we found that *gli2* is also expressed in the epithelial cells of developing placodes (Fig. 4j–l).

In various aspects of vertebrate appendage development, Shh and FGFs (*Fgf4*, *Fgf8*) exhibit interdependent positive feedback loops that promote the expression of either molecule (Gillis et al., 2009; Laufer et al., 1994). *Fgf3* expression is mesenchymal during early morphogenesis of both feathers (Mandler and Neubüser, 2004) and teeth, although in later tooth morphogenesis it is present in the epithelium of the primary enamel knot (Kettunen et al., 2000). In shark caudal denticles, *fgf3* expression is initially epithelial, although it is later seen in both the epithelium and mesenchyme, in a pattern similar to shark tooth and body denticle development (Martin et al., 2016; Rasch et al., 2016) (Figs. 4m–o, 6g–i, 7). *Fgf8* is an epithelial initiatory signal of mammalian tooth morphogenesis (Kettunen and Thesleff, 1998). In the shark, *fgf8* expression is observed in the epithelium during early caudal denticle morphogenesis, at a similar stage to *shh* (Figs. 5a–c, 6j–l, 7), and remains in the epithelium during later morphogenesis of the denticle cusps (Fig. 5l).

Studies from teleosts (medaka) and mammals (mouse) have indicated that *Fgf8* is a ligand of *Fgfr1* (Deng et al., 1994; Sun et al., 1999; Yokoi et al., 2007) that regulates enamel

formation during mammalian tooth morphogenesis (Takamori et al., 2008). During early caudal denticle morphogenesis, we observed expression of *fgfr1* in the squamous epithelium of placodes (Fig. 5d–f). *fgfr1* is also expressed throughout the epithelium later in morphogenesis during caudal denticle mineralisation (Fig. 5e–ei), which may be indicative of a conserved role regulating enameloid formation. Fgfr2 can transduce Fgf3 during mammalian development (Ornitz et al., 1996; Zhang et al., 2006). During early morphogenesis of caudal denticles, *fgfr2* is expressed in the squamous epithelium of the early developing placodes in *S. canicula* (Fig. 5g–i). This pattern is similar to epithelial expression of *fgf3*, suggesting the role of *fgfr2* as a *fgf3* signal transducer could be conserved.

Dlx2 is a member of the Dlx homeodomain transcription factor family, which is widely important throughout various aspects of vertebrate development, including epithelial appendage formation (Panganiban and Rubenstein, 2002; Rouzankina et al., 2004). Fgf8 regulates *Dlx2* expression in the underlying mesenchyme during both mouse tooth and branchial arch development (Bei and Maas, 1998; Thomas et al., 2000). Previously, *dlx* gene expression has been documented during caudal denticle morphogenesis in *S. canicula* (Debiais-Thibaud et al., 2011). Our results confirm *dlx2* is expressed in caudal denticles, and additionally we show that expression is restricted to the mesenchyme throughout early morphogenesis (Figs. 5j–l, 6d–f, 7), as observed during mouse tooth development (Bei and Maas, 1998).

Mesenchymal Bmp4 has an inhibitory role during amniote epithelial appendage development (Botchkarev et al., 1999; Jung et al., 1998; Pispá and Thesleff, 2003). Consistent with expression observed during feather, shark tooth and body denticle development (Botchkarev et al., 1999; Jung et al., 1998; Martin et al., 2016), *bmp4* is expressed in the mesenchyme during early morphogenesis of caudal denticle placodes

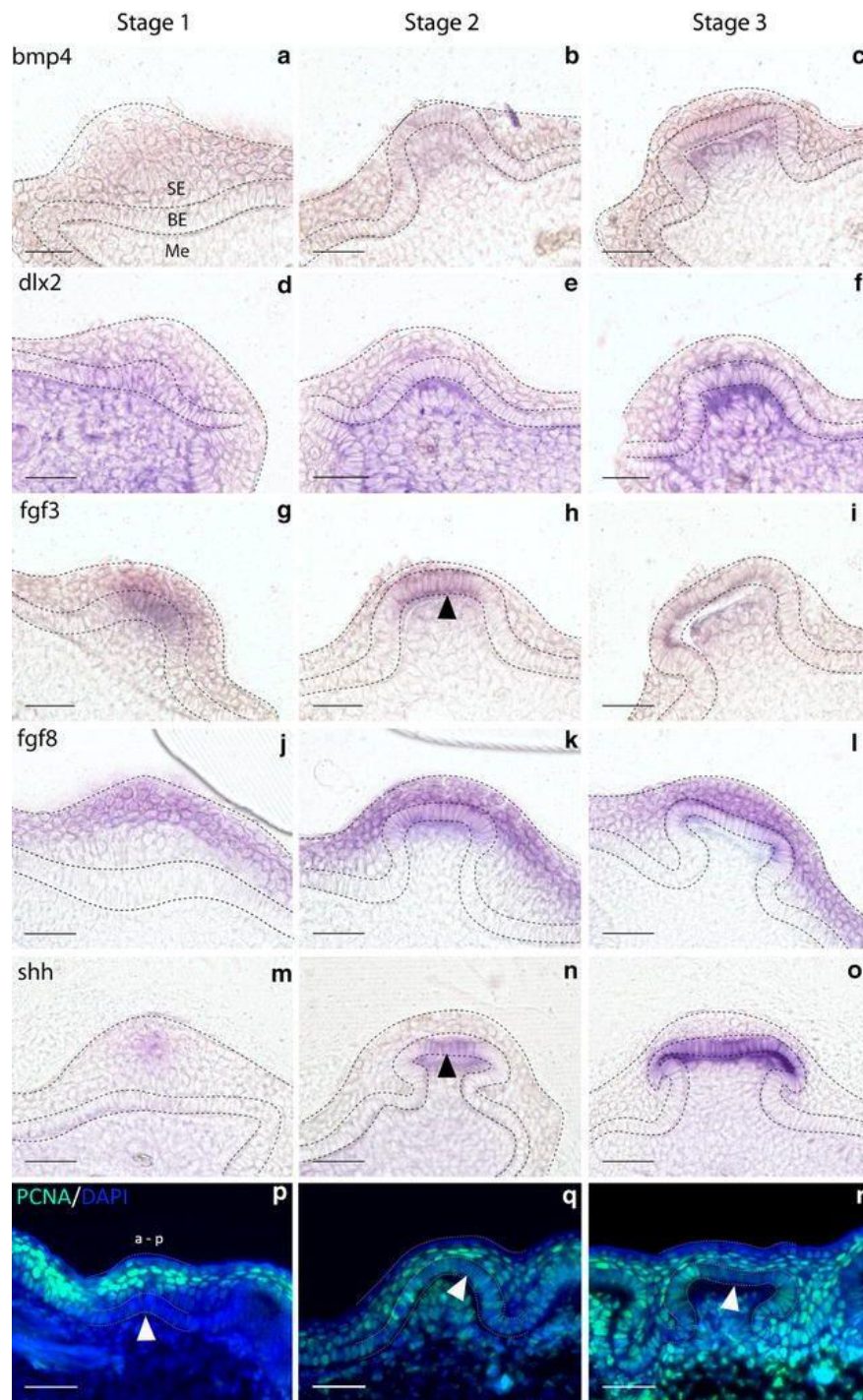


Figure 6: Gene expression/PCNA analysis of early caudal denticle morphogenesis. Gene expression is shown in 30- μ m transverse sections of wild-type *S. canicula* embryo tails post-WMISH, to highlight progressive stages of caudal denticle morphogenesis from the initial epithelial thickening. *bmp4* and *dlx2* expression is restricted to the mesenchyme throughout morphogenesis (Me) (a–f). *shh* and *fgf8* are first observed in the squamous epithelium (SE) before becoming restricted to the basal epithelium (BE) (m–o, j–l).

Expression of *fgf3* begins in the squamous and basal epithelium and is subsequently observed throughout the epithelium and mesenchyme (g–i). PCNA immunofluorescence is observed in the epithelium and mesenchyme throughout morphogenesis (p–r). Reduced activity (marked with an arrowhead) was noted in columnar cells of the epithelium during early morphogenesis (p) and in a central region of columnar cells of the basal epithelium during later morphogenesis (q–r). This region (q) overlaps with *fgf3* and *shh* expression in the basal epithelium (k, n) (marked with an arrowhead) and may be indicative of a basic primary enameloid knot. a is anterior, and p is posterior. Dashed lines separate the squamous epithelium (SE), basal epithelium (BE) and mesenchyme (Me). All scale bars are 50 μm in length

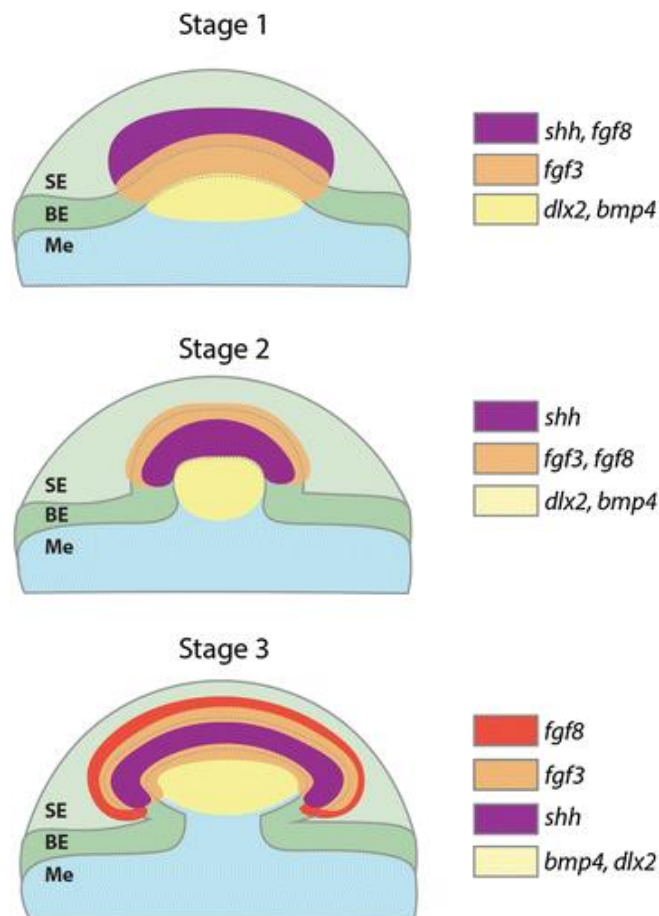


Figure 7: Schematic diagram of gene expression during early morphogenesis of caudal denticles. This diagram summarises the results from Figs. 4 and 5, representing expression of *fgf3*, *fgf8*, *shh*, *bmp4* and *dlx2* throughout progressive stages of early morphogenesis. SE is the squamous epithelium; BE is the basal epithelium and Me is the mesenchyme.

(Figs. 5m–o, 6a–c, 7). *bmp4* may also be acting as an internal inhibitor here (Jung et al., 1998; Pispas and Thesleff, 2003), helping to define the size of the placode and therefore the adult caudal denticle.

In addition to examining caudal denticle development, gene expression of these putative core GRN members was also examined in general body denticles to compare signalling between different odontode types (Figs. 1, 8). Expression of *shh* is restricted to the epithelium throughout early morphogenesis of general body denticles (Fig. 8a–c), whereas *fgf3* is first observed most strongly in the epithelium (Fig. 8d) before being expressed in both the epithelium and underlying mesenchyme (Fig. 8e, f). Epithelial *fgf3* overlaps with *shh* expression in the putative enameloid knot, whereas *bmp4* is restricted to the mesenchyme throughout morphogenesis (Fig. 8g–i). These results show conservation of gene expression patterns between caudal and general body denticles.

Proliferating cell nuclear antigen (PCNA) immunoreactivity marks several phases of cell division from late G1 to mitosis (Kurki et al., 1986). Developing body denticles are highly proliferative units similar to teeth and dental lamina (Debiais-Thibaud et al., 2015; Rasch et al., 2016) (Fig. 8j–l). During early morphogenesis, the columnar cells of these placodes are characterised by reduced proliferation (Fig. 8j), as also observed throughout amniote skin appendage development (Di-Poï and Milinkovitch, 2016). Interestingly, a region of the apical denticle cusp also shows marked reduction in PCNA immunoreactivity (Fig. 8k, l) that corresponds to a putative signalling centre comparable to the enameloid knot in shark teeth (Rasch et al., 2016). This set of cells appears to overlap with the region of *shh* and *fgf3* expression in the polarised cells that will become the apical cusp (Fig. 8a–f). Caudal denticles display comparable PCNA immunoreactivity during morphogenesis (Fig. 6p–r), including reduced proliferation of columnar cells during early morphogenesis compared to younger anterior epithelial tissue in which placode formation has not begun (Fig. 6p).

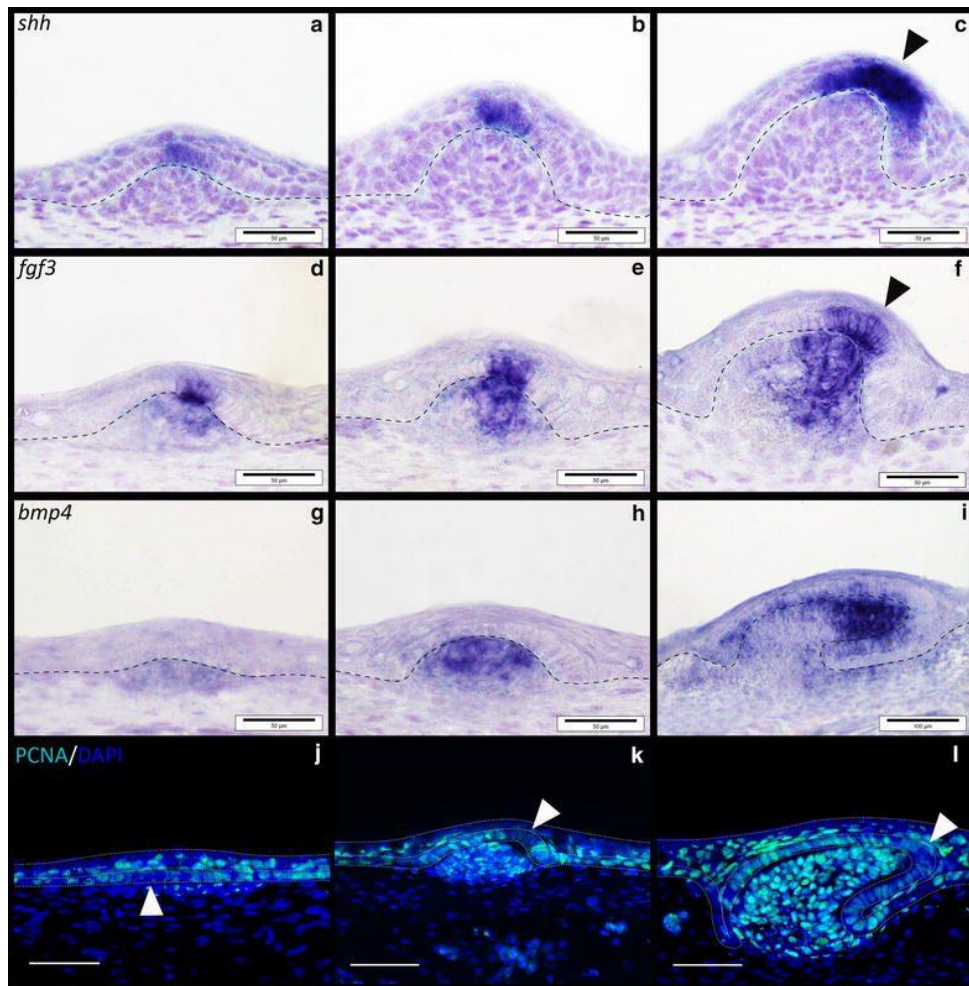


Figure 8: Gene expression analysis of putative placode GRN members, during general body denticle development. Section in situ hybridisation (SISH) was undertaken during early development of body denticles. Expression of *shh* was epithelial throughout development (a–c), whereas *fgf3* was observed in both the epithelium and mesenchyme (d–f). *bmp4* was mesenchymal throughout early morphogenesis (g–i). PCNA immunoreactivity was observed in the epithelial cells and condensing mesenchyme of emerging denticles (j–l). Reduced immunoreactivity was noted in columnar cells of the basal epithelium during placode formation (j) (white arrowed). *fgf3* and *shh* expression marks enameloid knot-like cells of the epithelium associated with denticle morphogenesis (c, f), which also show reduced PCNA immunoreactivity (l), characteristic of this signalling centre (black arrowheads). The dashed line separates the epithelium from the underlying mesenchyme (a–i), as well as the basal epithelium and squamous epithelium (j–l). All scale bars are 50 µm in length except for image i for which the scale bar is 100 µm

However, the region of reduced proliferation that occurs in columnar epithelial cells later during morphogenesis appears to be positioned more centrally than observed in body denticles, which have a distinct polarity (Fig. 6q, r). This region overlaps with expression of *fgf3* and *shh* (Fig. 6k–n), and could also be indicative of a putative primary enameloid knot, as observed in general body denticles (Fig. 8) (Rasch et al., 2016). The positional variation of this enameloid knot could reflect a shift in the morphology of these units, as caudal denticles display a less definitively polarised cusp than general body denticles (Fig. 1).

In the absence of functional data, it is not possible to test for the conserved action of GRN members, which could yield important clues regarding the putative homology of denticles and amniote epithelial appendages. We have therefore initiated a small-molecule-based targeted signalling pathway-knockdown screening assay in *S. canicula* to test the function of putative epithelial appendage GRN members, based on published results from other vertebrates.

2.3.3 Small molecule inhibition reveals dependency of caudal denticle development on FGF signalling

To elucidate the specific roles of FGF signalling during early caudal denticle placode morphogenesis, in vivo pathway perturbation assays were undertaken using SU5402. This chemical inhibits FGF signalling by blocking FGFR activity (Mohammadi et al., 1997; Paterson et al., 2004; Poss et al., 2000). Stage 28 *S. canicula* embryos were treated in their sealed egg cases by injection with SU5402 to a final concentration of ~10 μ M for 25 days and then allowed to develop for a further 35 days following the opening of their egg cases and washing with fresh artificial seawater. Treatment with SU5402 resulted in a single denticle knockout in 40% of the treated samples ($n = 5$) and none of the DMSO-treated

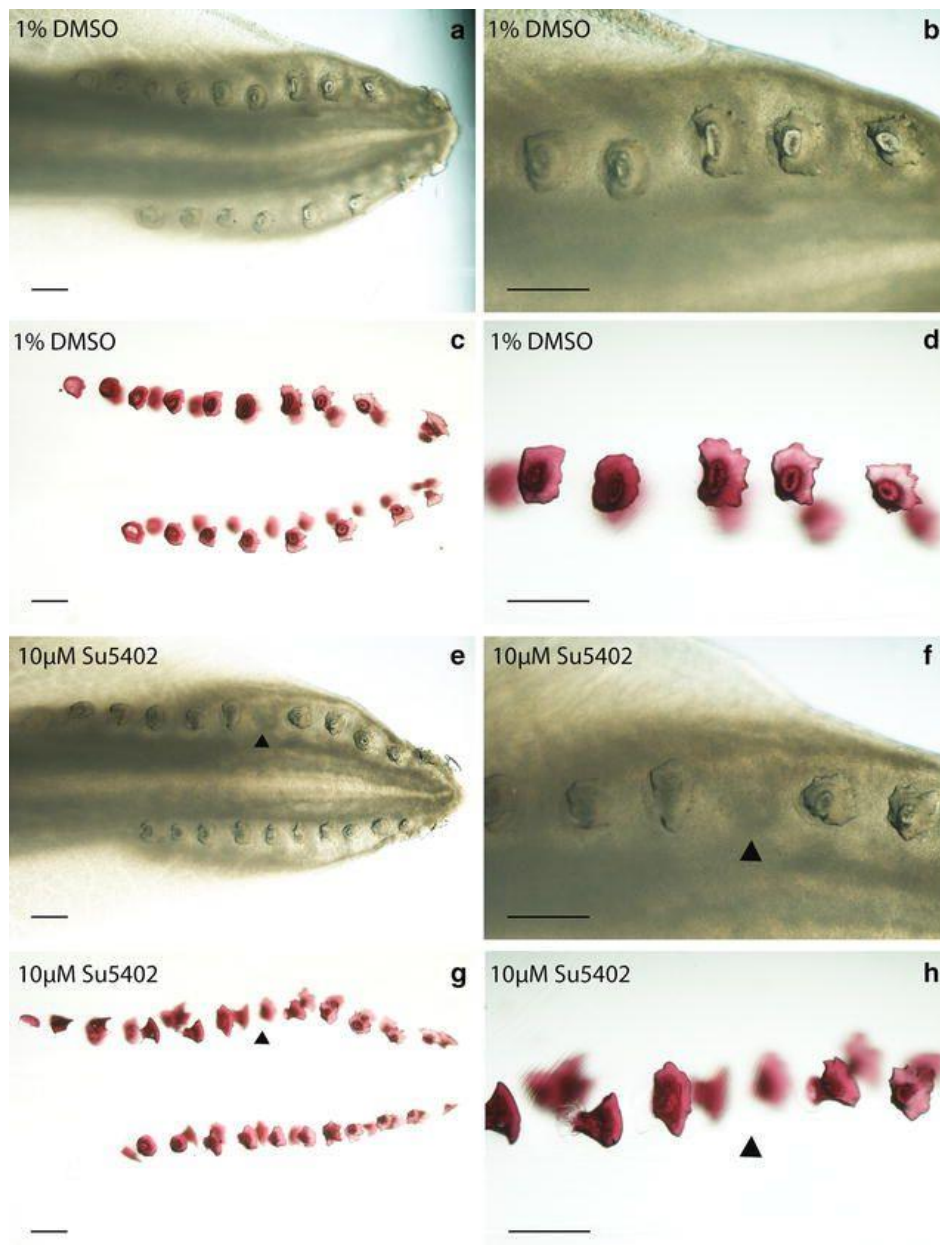


Figure 9: Phenotypic effect of FGF inhibition via SU5402 treatment (10 μ M) on caudal denticle development. The DMSO control specimen shown after fixation (a, b) and cleared and stained for calcium-rich tissue using alizarin red (c, d) possesses a full sequence of caudal denticles. However, the specimen treated with the FGF antagonist SU5402 has the 6th denticle missing from the sequence, shown after fixation (e, f) and cleared and stained (g, h). This is marked with a black arrowhead. This denticle knockout corresponds to the stage at which treatment occurred, and was observed in 40% of SU5402 treated specimens (n = 5). Scale bars are 200 μ m in length

control samples ($n = 5$) (Fig. 9). These units normally form equidistant from each other (Ballard et al., 1993; Eames et al., 2007; Johanson et al., 2007); however, in the drug treated specimen shown (Fig. 9e–h) the 6th denticle was missing in the left-side dorsal row. This corresponds to the time at which treatment took place, when approximately 5 caudal denticle placodes had developed in sequence on each row (Fig. 2c). Therefore, $\sim 10 \mu\text{M}$ SU5402 appears to prevent placode formation and subsequent morphogenesis, indicating this process is dependent upon FGF signalling. As only a single denticle was lost from the sequence, it is likely the chemical either diffused out of the egg case or decomposed within it after its initial inhibitory action. We observed a similar result in our preliminary SU5402 treatment trial (see Additional file 1), which revealed a vestige when stained with alcian blue, indicative of denticle abortion. The relatively short window of sensitivity to FGF inhibition by SU5402 treatment coupled with the offset in developmental timing of individual caudal denticle rows is likely to provide an explanation for the unilaterality of this denticle knockout. As subsequent placodes developed, the field of initiatory competence is likely to have already been in place, enabling the sequential, iterative patterning to proceed beyond the disturbance once the effect of SU5402 had subsided.

We sought to confirm a specific effect of SU5402 upon the FGF signalling pathway and the placode forming GRN by examining expression of participating network members. The prior assay required longer-term development of embryos to observe morphological effects (60 days) and subsequently used a lower drug concentration to avoid mortality, as this was an issue in preliminary trials. Experimental perturbation of FGF signalling was therefore repeated using a higher concentration of SU5402 ($1 \times 50 \mu\text{M}$ injection every 24 h, over a 96 hour period), in line with previously published assays (Fraser et al., 2013; Jackman et al., 2004; O’Shaughnessy et al., 2015), and embryos were fixed immediately after the 96-h period. Specimens were then processed for in situ hybridisation for a selection of the

same putative GRN members examined previously in wild-type embryos (Figs. 4, 5, 6). This allowed us to test whether perturbation of FGF signalling in shark denticles disrupted other members of the placode GRN in a manner consistent with a conserved relationship between network members.

FGF ligands exhibit positive feedback loops with Shh during many aspects of vertebrate embryogenesis, including epithelial appendage, limb bud and gill arch development (Gillis et al., 2009; Jung et al., 1998; Laufer et al., 1994; Lewandoski et al., 2000; Riddle et al., 1993). We observed a dramatic downregulation of *fgf3*, *fgf8*, *shh* and *dlx2* expression in the SU5402-treated individuals compared the DMSO-treated controls, in all but the youngest (most anterior) denticles (Fig. 10c–ji). Expression intensity of *bmp4* was also notably reduced compared to the control (Fig. 10a–bi). Two SU5402-treated specimens were used for WMISH for each marker, along with one DMSO control specimen. These results suggest that SU5402 blocked FGF/FGFR signalling (Mohammadi et al., 1997; Paterson et al., 2004; Poss et al., 2000), thereby reducing expression of *fgf3* and *fgf8* (Fig. 10e–hi). This is likely due to SU5402 blocking earlier FGF signalling required for expression of these ligands (Jackman et al., 2004), and interrupting the FGF–Shh positive feedback loop, which consequently limited expression of *shh*, *bmp4* and *dlx2* (Fig. 10a–di, i–ji) (Bei and Maas, 1998; Gillis et al., 2009; Jung et al., 1998; O’Shaughnessy et al., 2015). Dlx family members have a role downstream of FGFs during feather bud development (Rouzankina et al., 2004), indicating that this downregulation of *dlx2* is likely a result of FGF inhibition. These results suggest that during caudal denticle formation, the function of FGF signalling in the GRN which guides epithelial appendage morphogenesis is conserved between sharks and other vertebrates.

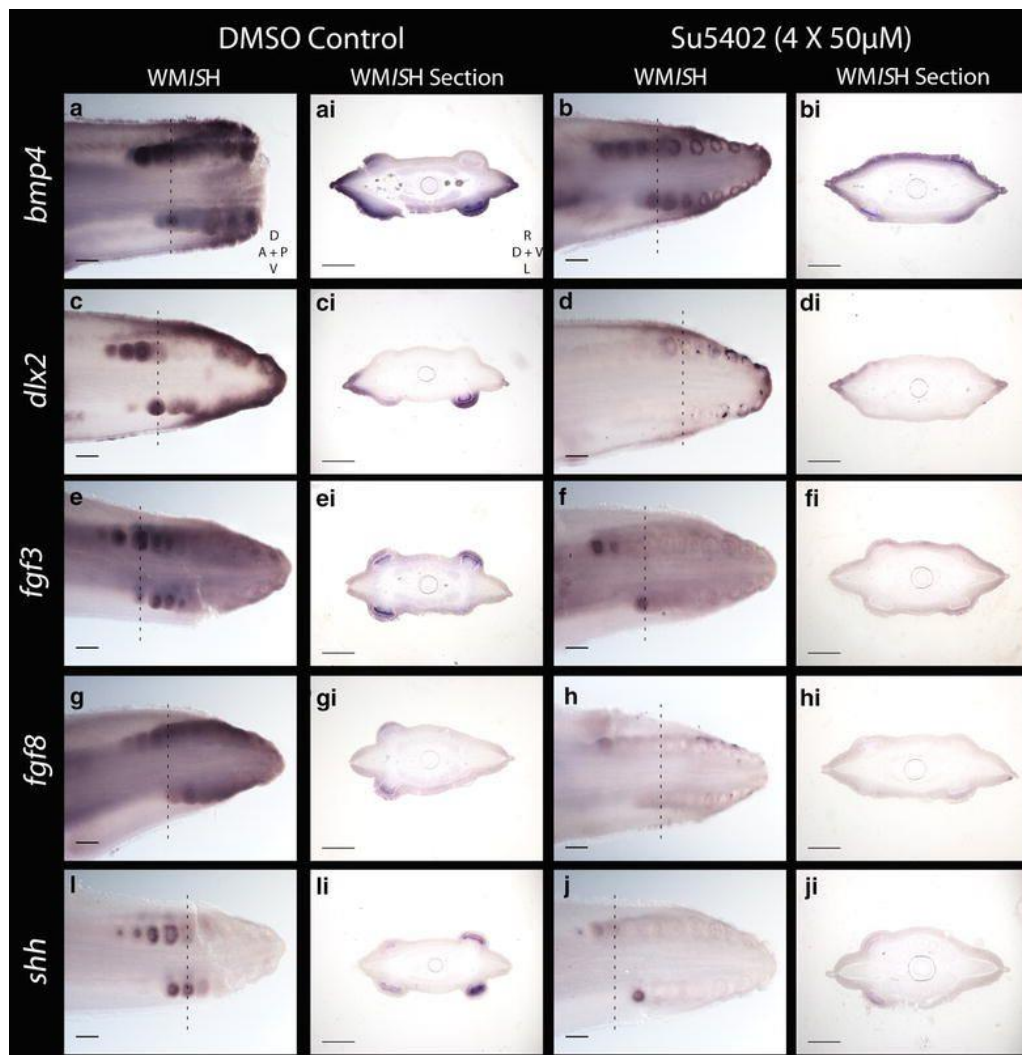


Figure 10: Genetic effect of FGF inhibition via SU5402 treatment (4 × 50 μ M) on caudal denticle development. There was a reduction in staining intensity of *bmp4* (a–bi), *dlx2* (c–di), *fgf3* (e–fi), *fgf8* (g–hi) and *shh* (i–ji) in SU5402-treated specimens compared to DMSO-treated controls. We propose this resulted from the interruptions to the following GRN interactions. SU5402 inhibits FGF activity by blocking FGFR activity, thereby reducing expression of *fgf3* and *fgf8* (e–hi). This reduced *shh* and *dlx2* expression as an FGF—*shh* positive feedback loops that would normally promote *shh* and *dlx2* expression (as observed during feather development) were interrupted (i–ji, c–di). The *fgf4*—*shh* positive feedback loop that promotes *bmp4* was also interrupted by the SU5402 treatment, reducing *shh* and *bmp4* expression (i–ji, a–bi). SU5402-treated and DMSO control specimens both underwent the colour reaction of the WMISH protocol for the same length of time. The dashed lines show where the section was taken from. Scale bars for WMISH are 200 μ m in length, and for the WMISH sections they are 100 μ m in length

2.4 Discussion

2.4.1 An FGF-dependent GRN constructs the placodes of epithelial appendages throughout jawed vertebrates

Our results suggest that a conserved core GRN, which includes *eda/edar*, *shh*, *gli2*, *fgf3*, *fgf8*, *bmp4* and *dlx2*, underlies the development of epithelial integumentary appendage placodes across jawed vertebrates (Figs. 4, 5, 6). These placodes possess columnar epithelial cells with a reduced rate of proliferation (Fig. 6p), which is considered a structural characteristic of amniote skin appendage development (Di-Poï and Milinkovitch, 2016). Functional experiments revealed that expression of these GRN members is influenced by the FGF signalling pathway and that normal denticle development is perturbed upon inhibition with SU5402 (Figs. 9, 10). Caudal denticles are considered an ancient epithelial appendage that may have originated in early vertebrates over 450 million years ago and have been retained in some extant chondrichthyans (Johanson et al., 2008; Karatajute-Talimaa, 1973; Sansom et al., 1996). The historical continuity of the anatomical placode and underlying GRN in both amniotes (Di-Poï and Milinkovitch, 2016) and chondrichthyans provides evidence for the historical homology of all vertebrate epithelial appendages (Wagner, 2007).

Previously, researchers have speculated that epithelial appendages have evolved independently in mammals, reptiles and birds and that therefore molecular similarity of GRNs could be a result of independent genetic co-option or deep homology (Dhouailly, 2009; Donoghue, 2002; Maderson, 2003, 1972; Shubin et al., 2009). However, recent evidence has suggested that integumentary epithelial appendages are historically homologous, at least throughout all amniotes on the basis of the anatomical placode with conserved expression and function of GRN members (Di-Poï and Milinkovitch, 2016). Our

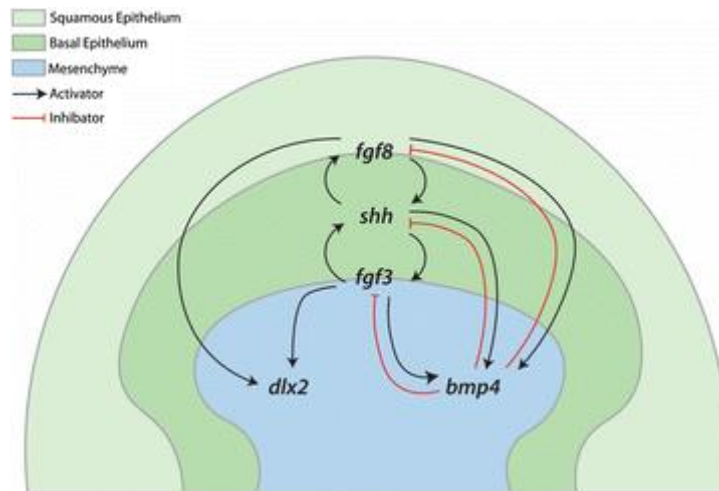


Figure 11: Putative relationship between FGF and associated GRN components during caudal denticle morphogenesis. As observed widely throughout epithelial appendage development, for example during feather placode development, FGF—*shh* positive feedback loops which promote mesenchymal *bmp4* are likely to promote early caudal denticle placode morphogenesis. *bmp4* may then act as an internal inhibitor, limiting the size of the final unit. FGF signalling can also promote mesenchymal expression of *dlx2*. This is a hypothetical GRN based on findings from previous research, gene expression data (Figs. 4, 5, 6, 8) and small molecule inhibition of FGF signalling during early caudal denticle morphogenesis, using SU5402 (Figs. 9, 10)

results suggest this historical homology extends even further into vertebrate phylogeny and may encompass the integumentary epithelial appendages of all extant jawed vertebrates.

During both mouse and zebrafish tooth morphogenesis, *Fgf8* signalling can promote *Dlx2* expression (Bei and Maas, 1998; Jackman et al., 2004; Thomas et al., 2000). Inactivation of *Fgf8* can result in both misregulation of *Fgf4* and *Shh* (Lewandoski et al., 2000), which are also known to work together in autocatalytic positive feedback loops during vertebrate development, for example in limb and feather patterning (Jung et al., 1998; Laufer et al., 1994). During early feather placode morphogenesis, this *Shh*–*Fgf4* feedback loop promotes *Bmp4* expression, which subsequently acts as an inhibitor to limit their expression in a

negative feedback loop (Jung et al., 1998). Our results regarding gene expression of FGF-perturbed shark embryos reveal this functional conservation likely extends to the denticles of sharks (Figs. 10, 11).

Despite the broad conservation of this GRN, our observations of gene expression patterns did highlight some taxonomic disparity. We showed that *fgf3* is expressed in both the epithelium and later the mesenchyme of denticle placodes, as observed during mouse and shark tooth development (Kettunen et al., 2000; Rasch et al., 2016). This contrasts with known expression patterns observed during zebrafish pharyngeal tooth and chick feather development (Jackman et al., 2004; Mandler and Neubüser, 2004). Similarly, *Fgf8* is an important inductive signal during mammalian tooth development (Kettunen and Thesleff, 1998) and is present during caudal denticle development, but is absent from feather or zebrafish tooth morphogenesis (Jackman et al., 2004; Ohuchi et al., 2000). There is potential for evolutionary alterations to gene expression and functionality throughout the FGF signalling family, and paralogs may perform the same developmental role in different taxa in a process known as function shuffling (McClintock et al., 2001), for example mammalian *Fgf8* may have a zebrafish specific paralog (Jackman et al., 2004).

Recent research has revealed chondrichthyan general body denticles and teeth are deeply homologous developmental units, despite differences in their regenerative capacities (Martin et al., 2016; Rasch et al., 2016). Our findings suggest this odontode GRN additionally encompasses caudal denticles, as conserved expression patterns were observed throughout early placode morphogenesis between caudal denticles and general body denticles. Caudal denticles are morphologically disparate from general body denticles, dorsal denticles and teeth (Fig. 1), and positional alterations to the putative enameloid knot may contribute to this variation (Figs. 6, 8). As predicted by an hourglass model of development (Kalinka et al., 2010), divergence in the GRN later in morphogenesis is also

likely to result in alterations to the adult form, constructing different structures upon a homologous foundation: the anatomical placode. Such divergence of networks is known to relate to variation in the adult structure of feathers and teeth (Chen et al., 2015; Jernvall and Thesleff, 2012).

2.5 Conclusion

The early morphogenesis of vertebrate epithelial appendages is likely to be a universal and highly conserved process retained over evolutionary time and modified to form the plethora of diverse skin appendages observed throughout all vertebrates, from sharks to mammals. The placodes of vertebrate epithelial appendages constitute the conserved foundations upon which integumentary structures have evolved, via alterations to an otherwise conserved GRN that take effect during later morphogenesis. The shark caudal denticle system provides an ideal set of sequentially developing integumentary epithelial appendages that can be studied further to decipher both complex functional GRNs and patterning mechanisms.

Combining techniques such as small molecule signalling pathway perturbation with gene expression analyses can help us begin to interpret the roles of putative GRN members. The set of genes investigated here were chosen due to their importance in the development of other epithelial appendages; however, there are many important molecules and interactions to further investigate, for example those associated with the Wnt/ β -catenin and Notch pathways (Felszeghy et al., 2010; Järvinen et al., 2006). A focus on investigating downstream GRN components responsible for later morphogenesis will enable us to elucidate how historically homologous placodes develop into the diverse range of epithelial appendages observed throughout vertebrates.

2.6 Methods

2.6.1 Shark husbandry and fixation

The University of Sheffield is a licensed establishment under the Animals (Scientific Procedures) Act 1986. All animals were culled by approved methods cited under Schedule 1 to the Act. Embryos were imported from ‘Station Biologique’ in Roscoff, France, and housed in tanks at The University of Sheffield, Animal and Plant Sciences, at 16 °C. Salinity was adjusted to replicate sea water using ‘Instant Ocean’ salt dissolved in dechlorinated water. Water was oxygenated with a submerged airflow. 50% water changes were undertaken on a weekly basis. Embryos were removed from their egg cases, anaesthetised using MS-222 (Tricaine) and fixed overnight at 4 °C in 4% paraformaldehyde (PFA). Samples were dehydrated through a graded series of PBS and MeOH and stored at –20 °C in MeOH.

2.6.2 Alizarin red clear and staining

Fixed specimens were rehydrated through a graded series of MeOH and PBS. Staining took place in darkness overnight in 0.01% alizarin red dissolved in 0.5% KOH. Specimens were treated with trypsin in saturated sodium borate and distilled water. For Additional file 1, the sample was stained with 0.1% alcian blue in EtOH and acetic acid before the alizarin red stain was applied. Samples were then run through a graded series of KOH and glycerol solutions, before imaging took place in glycerol, using a Nikon SMZ1500 stereomicroscope.

2.6.3 Haematoxylin and eosin (H&E) staining

Paraffin-embedded sections were deparaffinised in xylene and rehydrated through a graded series of MeOH and PBS, before staining with haematoxylin. Sections were then rinsed in ddH₂O, washed with HCl in EtOH and washed with 0.001 M Tris–HCL. Finally, sections were stained with eosin, dehydrated to MeOH and mounted used DePeX mounting

medium (VWR). Samples were imaged using an Olympus BX51 microscope and Olympus DP71 Universal digital camera attachment.

2.6.4 Micro-computed tomography (MicroCT) and light sheet fluorescence microscopy (LSFM)

High-resolution MicroCT scanning was carried out upon a Stage 32 embryo stained with 0.1% PTA (phosphotungstic acid) in 70% EtOH for 3 days, using an Xradia MicroXCT scanner at the Imaging and Analysis Centre of the Natural History Museum (London). Scans were rendered using the 3D volume exploration tool Drishti (www.github.com/nci/drishti) (Fig. 1j, k). LSFM was carried out upon alizarin-stained samples. A Zeiss Z1 light sheet microscope with two sCMOS cameras and an acquisition PC running Zen Black 2014 software was used to scan the tail of a Stage 31 embryo. Rendering was undertaken using the image analysis software Imaris (www.bitplane.com/imaris/imaris) by creating a signal intensity-based isosurface (Fig. 1l, m).

2.6.5 Small molecule gene perturbation experiments

For the first SU5402 treatment trial, Stage 28 *S. canicula* embryos (Ballard et al., 1993) were treated with the FGF-receptor inhibitor SU5402 (Sigma). At this stage, the egg case is sealed from the external environment, allowing administration of drugs via injection into the vitelline fluid. The egg case acts as a natural treatment chamber. 100 μ l of a 500 μ M stock solution of SU5402 in 1% DMSO in PBS was injected into 5 egg cases, to achieve a \sim 10 μ M concentration of SU5402 assuming an approximate egg case size of 5 ml. 5 control samples were treated with 100 μ l of 1% DMSO in PBS. At Stage 31 of development, the corners of the egg cases naturally open, allowing water to enter the case and replace the vitelline fluid and the chemical gene inhibitor. Once the first egg case had

opened, others were artificially opened to ensure that the treatment period remained constant between replicates. Egg cases remained sealed for 25 days before opening and were then allowed to develop for a further 35 days before fixation and morphological examination. After observing inhibition of denticle development (Fig. 9), a second round of drug treatments was conducted to examine the genetic effect of FGF inhibition via SU5402 treatment. WMISH was undertaken to examine caudal denticle morphogenesis for SU5402-treated samples and compared to control samples (treated with DMSO). The concentration of SU5402 was increased, with 10 specimens receiving a 50- μ l injection of a 5 mM stock solution of SU5402 in 1% DMSO in PBS, once every 24 h for 96 h, with each individual injection resulting in a \sim 50 μ M concentration. 5 control samples were treated with one 50 μ l injection of 1% DMSO in PBS, every 24 h for 96 h. Embryos were immediately fixed after the treatment period, before dissection and WMISH took place. Two SU5402-treated tails and one DMSO control tail were used to investigate expression of each gene. The concentrations used for chemical treatments were gleaned from studies undertaking similar gene perturbation experiments in teleosts and chondrichthyans, and honed using preliminary drug treatment trials in *S. canicula* (Fraser et al., 2013; Jackman et al., 2004; O'Shaughnessy et al., 2015) (see Additional file 1).

2.6.6 Whole mount in situ hybridization (WMISH)

Digoxigenin-labelled (DIG) antisense riboprobes were designed using partial skate (*Leucoraja erinacea*) and catshark (*S. canicula*) EST assemblies (Wyffels et al., 2014) (SkateBase; skatebase.org) and the Vertebrate TimeCapsule (VTcap; transcriptome.cdb.riken.go.jp/vtcap). Riboprobes were cloned from *S. canicula* cDNA, and DIG-labelled antisense riboprobes were generated using the Riboprobe System Sp6/T7 kit (Promega). WMISH was carried out as previously described (Fraser et al., 2013). Samples were rehydrated through a graded series of MeOH and PBS, and treated with proteinase K

(1 μ l/mg ProK for 60 min), to facilitate probe penetration. Next, samples were refixed in 4% PFA in PBS and incubated in pre-hybridisation buffer for 1 h at 61 °C. For the hybridisation stage, samples were placed in a shaker incubator overnight at 61 °C in 2 ml tubes (Eppendorf) containing 1 ml aliquots of hybridisation buffer and DIG-labelled antisense RNA probe. Samples were then washed in saline sodium citrate with 0.1% Tween-20 (SSCT), before incubation in blocking reagent (Roche). Antibody labelling occurred overnight at 4 °C in Maleic Acid Buffer with Tween-20 (MABT), using anti-DIG-ALP (0.2 μ l/ml) (Roche). This was followed by a series of washes and 48-h incubation in MABT at 4 °C. For the colour reaction, BM purple (Roche) was applied at room temperature, until the staining was sufficiently strong to represent gene expression. For WMISH undertaken upon SU5402 treated specimens, the colour reaction was run for the same length of time for SU5402 treated animals and DMSO controls. Samples were stored and imaged in 10% EtOH in PBS using Nikon SMZ1500 stereomicroscope. After WMISH and imaging, embryos were post-fixed with 4% PFA and embedded in chick albumin cross-fixed with 2.5% glutaraldehyde. A Leica Microsystems VT1000 vibratome was used to cut sections at 30 μ m. Vibratome sections were then mounted with Fluoromount (Sigma-Aldrich) and imaged using a BX51 Olympus Microscope.

2.6.7 Section in situ hybridization (SISH)

Fixed, dehydrated specimens were processed through a graded series of MeOH, chloroform and hot wax before being embedded in paraffin, and sectioned at 14 μ m with a microtome (Leica RM2145). Sections were rehydrated from MeOH, and SISH was carried out with solutions as described for WMISH. Sections were incubated in pre-hybridisation buffer, before overnight incubation with a DIG-labelled antisense RNA probe. Sections were then run through post-hybridisation washes. Antibody labelling occurred overnight incubation with anti-DIG-AP (Roche). After post-antibody washes, BM purple (Roche)

was used for the colour reaction. Sections were counterstained with haematoxylin and imaged using an Olympus BX51 Microscope and Olympus DP71 Universal digital camera attachment.

2.6.8 Immunofluorescence

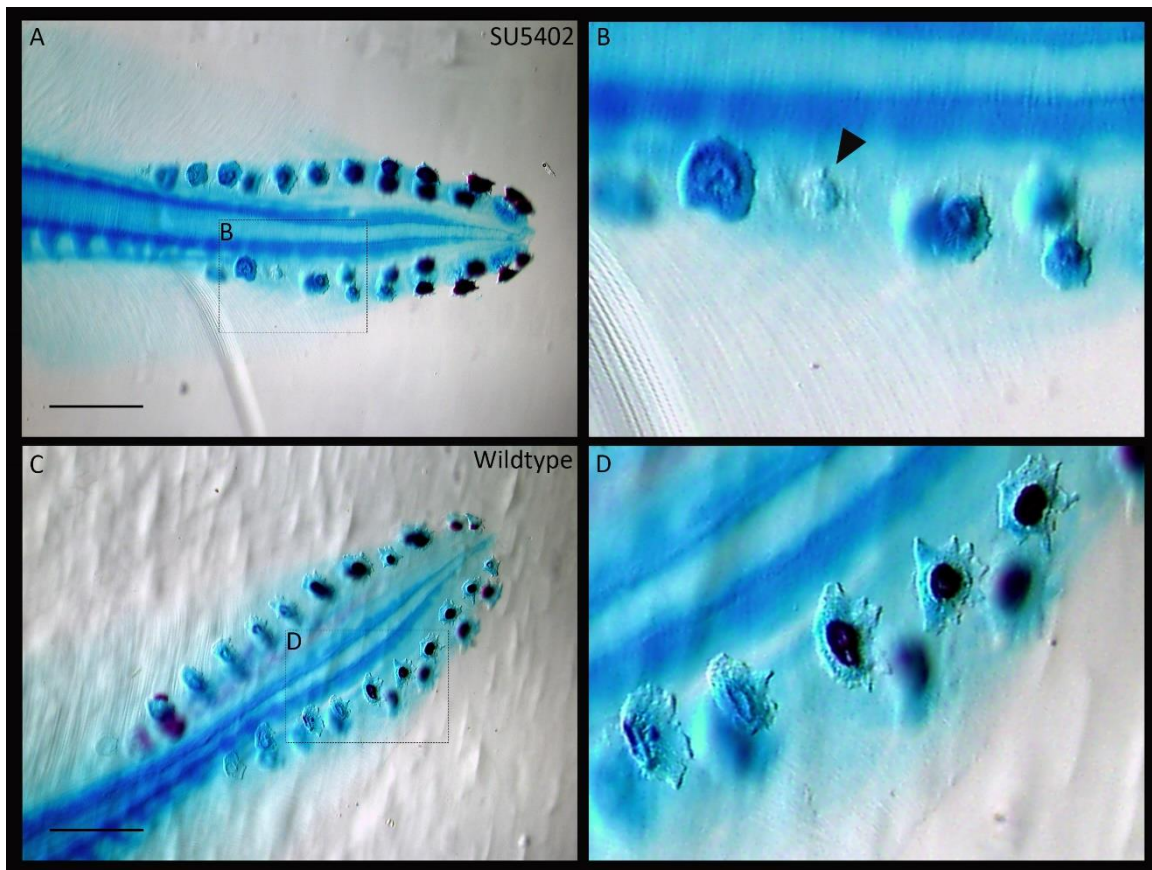
Sections were rehydrated from MeOH or EtOH as previously described for SISH. Antigen retrieval occurred in hot 0.01 M sodium citrate (pH 6.0) for 10 min, before blocking and antibody labelling. Primary antibody labelling was undertaken using mouse anti-PCNA antibody (ab29; Abcam), overnight at 4 °C. Secondary antibody incubation was undertaken with goat anti-mouse AlexaFluor-488 (Thermo Fisher), before counterstaining with DAPI (Sigma-Aldrich). Slides were mounted with Fluoromount (Sigma-Aldrich). Imaging was undertaken with an Olympus BX61 upright epifluorescent Microscope and Olympus DP71 Universal digital camera attachment, and visualised with the software Volocity 6.3.

2.7 Acknowledgements

We would like to thank Dr. Takanori Shono and Alex Thiery for providing laboratory assistance and expertise throughout the course of this project, and Phil Young for animal husbandry. We are grateful to Xavier Bailey and members of Station Biologique de Roscoff for the supply of shark embryos. MicroCT imaging was carried out with assistance from Dr. Zerina Johanson (Department of Earth Sciences), Dr. Farah Ahmed and Dr. Amin Garbout of the Imaging and Analysis Centre (Natural History Museum, London). Other imaging techniques were carried out with assistance from of Dr. Darren Robinson and Dr. Nick van Hateren of the Wolfson Light Microscopy Facility (The University of Sheffield).

2.8 Additional materials

2.8.1 Additional file 1: additional figure



Additional File 1: Caudal denticle abortion from preliminary SU5402 treatment trial.

A preliminary drug trial involved treating *S. canicula* embryos with a single injection resulting in a 50 μ M concentration of SU5402 in the egg case, which then remained sealed for 30 days. The egg case then opened, and the embryo was allowed an additional 30-day recovery period before fixation. The sample was then stained with alcian blue and alizarin red. There is a clear vestige (B, black arrowhead), indicating a single denticle from the sequence was aborted, as a result of this SU5402 treatment.

3.0 Chapter 3:

An ancient Turing-like patterning mechanism regulates skin denticle development in sharks

Rory L. Cooper¹, Alexandre P. Thiery¹, Alexander G. Fletcher², Daniel J. Delbarre³, Liam J. Rasch^{1,4}, Gareth J. Fraser^{1, 5, *}

*Correspondence: g.fraser@sheffield.ac.uk

¹Department of Animal and Plant Sciences, and the Bateson Centre, University of Sheffield, Sheffield, S10 2TN, UK

²School of Mathematics and Statistics, University of Sheffield, Sheffield, UK

³Department of Earth Sciences, University of Oxford, Oxford, UK

⁴Human Developmental Biology resource, Institute of Child Health, University College, London, UK

⁵Department of Biology, University of Florida, Gainesville, FL, USA

Citation: Cooper, R. L., Thiery, A. P., Fletcher, A. G., Delbarre, D. J., Rasch, L. J., and Fraser, G. J. 2018, An ancient Turing-like patterning mechanism regulates skin denticle development in sharks, *Science Advances*, 4, 11, eaau5484

3.1 Abstract

Vertebrates have a vast array of epithelial appendages, including scales, feathers, and hair. The developmental patterning of these diverse structures can be theoretically explained by Alan Turing's reaction-diffusion system. However, the role of this system in epithelial appendage patterning of early diverging lineages (compared to tetrapods), such as the cartilaginous fishes, is poorly understood. We investigate patterning of the unique tooth-like skin denticles of sharks, which closely relates to their hydrodynamic and protective functions. We demonstrate through simulation models that a Turing-like mechanism can explain shark denticle patterning and verify this system using gene expression analysis and gene pathway inhibition experiments. This mechanism bears remarkable similarity to avian feather patterning, suggesting deep homology of the system. We propose that a diverse range of vertebrate appendages, from shark denticles to avian feathers and mammalian hair, use this ancient and conserved system, with slight genetic modulation accounting for broad variations in patterning.

3.2 Introduction

Vertebrates have a plethora of diverse epithelial appendages, including hair, feathers, scales, spines, and teeth (Pispa and Thesleff, 2003). Recent research has revealed that these structures share extensive developmental homology, as they grow from a common foundation: the epithelial placode (Cooper et al., 2017; Di-Poï and Milinkovitch, 2016; Musser et al., 2015). Despite this shared ancestry, there are broad variations in both the final morphology and the spatial arrangement of these organs (Pispa and Thesleff, 2003). Such variation in patterning has evolved to facilitate diverse functions, for example, drag reduction, thermoregulation, and communication (Dean and Bhushan, 2010; Reif, 1985a; Ruxton and Wilkinson, 2011).

Alan Turing's reaction-diffusion (RD) model provides an explanation for the diversity of patterning observed in nature (Economou et al., 2012; Green and Sharpe, 2015; Kondo and Miura, 2010; Onimaru et al., 2016; Turing, 1952). This model describes how interactions between morphogens diffusing differentially through a tissue can give rise to autonomous patterning of epithelial appendages (Koch and Meinhardt, 1994; Turing, 1952). These morphogens typically constitute two interactive molecular signals that occupy the role of a short-range activator and long-range inhibitor (Gierer and Meinhardt, 1972). The autocatalytic activator promotes its own expression and expression of the inhibitor, which, in turn, represses the activator. Turing demonstrated that when tuned appropriately, the nonlinear reaction kinetics and difference in diffusion coefficients can result in the formation of a stable periodic pattern in a field of initially homogenous signal, in which peaks of activator alternate with the inhibitor (Kondo, 2002). This self-organizing system defines the spatial distribution of placodes and therefore the patterning of epithelial appendages. It is worth noting that in addition to RD, other factors such as mechanosensation of the tissue may be important for controlling skin appendage patterning

(Shyer et al., 2017). In this case, the patterning may still be via Turing instability, but using mechanical in addition to molecular RD interactions (Hiscock and Megason, 2015). We refer to this as a Turing-like system.

There is a growing body of experimental research supporting RD modelling throughout epithelial appendage development. This includes the role of RD in both patterning and morphogenesis of feathers and hair (Harris et al., 2005; Jiang et al., 1999; Jung et al., 1998; Sick et al., 2006). These studies have revealed that molecular signals such as fibroblast growth factors (FGFs) and sonic hedgehog (*Shh*) can play autocatalytic activatory roles, whereas bone morphogenetic proteins (BMPs) can act as inhibitors (Harris et al., 2002; Jung et al., 1998). Despite evidence for RD patterning in classic tetrapod model organisms (i.e., mouse and chick), our understanding of this system in earlier diverging lineages is limited.

Chondrichthyans (cartilaginous fishes) occupy the sister lineage to osteichthyans (bony vertebrates) and constitute an earlier diverging lineage with respect to tetrapods. The elasmobranchs (sharks, skates, and rays) are a subclass of Chondrichthyes, which have hard, mineralized epithelial appendages known as odontodes. Odontodes include teeth and dermal denticles, which consist of a pulp cavity encased within layers of dentine and enameloid (Ørvig, 1977). It is thought that odontogenic competence originated in the dermal skeleton, giving rise to denticles as a precursor to the oral dentition of vertebrates (Donoghue and Rücklin, 2016; Fraser et al., 2010; Martin et al., 2016). These structures have been observed in early vertebrates that lived as long as 450 million years ago (Karatajute-Talimaa, 1973; Sansom et al., 1996). Denticles have evolved to fulfil a variety of functions, including provision of drag reduction and protective armour (Dean and Bhushan, 2010; Raschi and Tabit, 1992). It has previously been suggested that shark denticles do not follow a strict spatial pattern (Fraser and Smith, 2011; Johanson et al.,

2007), although they do exhibit both intraspecific and interspecific variation in morphology and patterning, which closely relates to their function (Ferrón and Botella, 2017; Reif, 1985c). Recent research has suggested that a RD mechanism may underlie the arrangement of denticles in a fossil adult Cretaceous shark (*Tribodus limae*) (Maisey and Denton, 2016). However, experimental evidence addressing the initiation of patterning, and its genetic basis, is required to ascertain the role of this system in elasmobranchs.

Reif's inhibitory field concept is considered the leading hypothesis for explaining odontode patterning (W.-E. Reif, 1980). This theory describes how diffusion from existing odontodes can dictate the proximity of contemporaneous units, preventing placode formation within the perimeter of inhibition zones surrounding existing teeth or denticles (Reif, 1982; W.-E. Reif, 1980). However, no underlying molecular basis has been identified to support this idea. In fact, it has been described as a verbal description of a restricted parameterization of a RD system (Maisey and Denton, 2016).

There is thought to be early morphogenetic similarity between shark denticle and chick feather patterning, the latter of which is controlled by RD (Donoghue, 2002; Jung et al., 1998). Chick feathers initially develop sequentially in a dorsal longitudinal row along the embryo's midline. This initiator row triggers subsequent placode formation in adjacent parallel rows until the integument is covered (Hogan, 1999; Oster et al., 1983; Stuart and Moscona, 1967). This is consistent with a RD system (Jung et al., 1998; Turing, 1952). Embryonic sharks develop two dorsolateral rows of enlarged denticles that emerge before the subsequent eruption of intricately patterned body denticles (Fig. 1) (Ballard et al., 1993; Grover, 1974; Reif, 1982). Soon after hatching, these rows are subsumed into general scalation (Martin et al., 2016). As observed during feather patterning (Jung et al., 1998; Oster et al., 1983), shark dorsal denticles may act as initiator rows that trigger the emergence of surrounding body denticles, following a conserved Turing-like system.

This study investigates epithelial appendage patterning in an early diverging lineage, with respect to tetrapods, using the small-spotted catshark (*Scyliorhinus canicula*). Using a combination of RD modelling and gene expression analysis, we investigate the mechanism and underlying molecular basis of shark denticle patterning. We then use small-molecule gene pathway inhibition experiments to reveal functional conservation of these genes. Last, we use RD modelling to demonstrate that our experimental results conform to a conserved Turing-like patterning system. Rather than following a random distribution (Fraser and Smith, 2011), we find that shark denticle development is underpinned by a precise patterning mechanism that begins early in development. This conserved system may underlie the development of a broad range of epithelial appendages, thereby facilitating the evolution of diverse functional traits observed throughout vertebrates.

3.3 Results

3.3.1 RD simulation and gene expression analyses suggest that a Turing-like system underlies shark body denticle patterning

We first investigated the morphogenetic patterning of shark denticles. Two rows of dorsal denticle placodes are visible at stage 32 of development [~80 days postfertilization (dpf)] (Fig. 1A) (Ballard et al., 1993), preceding the emergence of body denticles (Fig. 1, C, D, and F). Compared to body denticles, dorsal denticles are larger and broader and do not have distinct ridges associated with hydrodynamic drag reduction (Fig. 1, D to F) (Dean and Bhushan, 2010). Simulation of a RD model was used to determine whether dorsal denticle rows can act as “initiator” rows, triggering the patterning of surrounding body denticles. Patterns were generated from a row of initiator spots representing dorsal denticles (Fig. 1K), from which waves of activatory and inhibitory morphogens radiated according to predefined values (Fig. 1L and table S1; see Materials and Methods for further details). Spots formed in rows adjacent and parallel to the initiator row. Upon reaching a steady

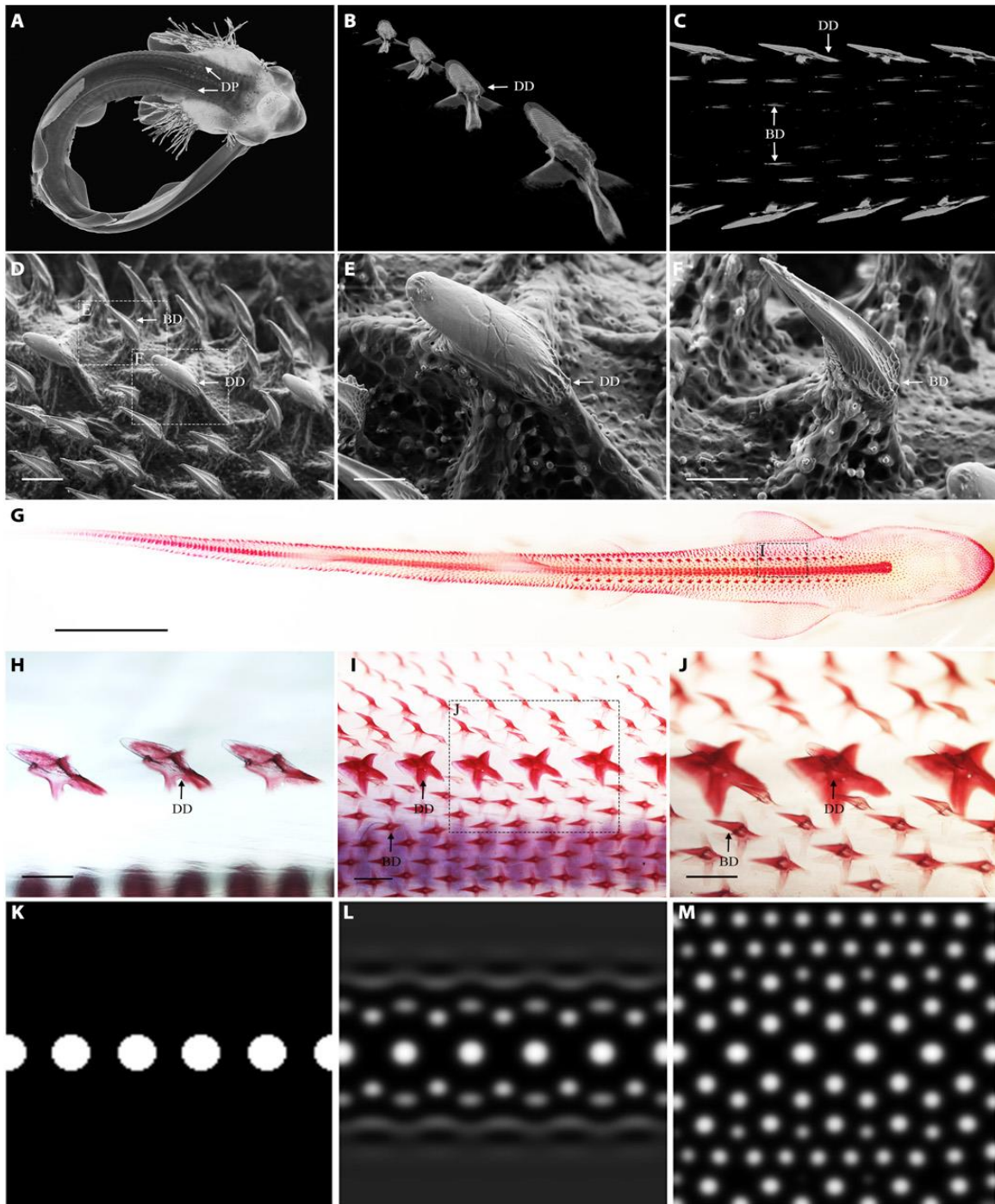


Figure 1: RD modelling can explain catshark denticle patterning. (A) Catsharks display two rows of dorsal denticle placodes (DP) at developmental stage 32 (~80 dpf). (B to E and G to J) These placodes undergo morphogenesis and mineralize to become dorsal denticles (DD). (C, D, F, and G to J) Their emergence precedes subsequent eruption of parallel, adjacent rows of body denticles (BD). Dorsal denticles also begin to mineralize (H) before body denticle development (I). Dorsal denticles are longer and broader than body denticles

(E, F, and J). RD modelling suggests that diffusion and interaction of an activator and inhibitor from an initiator row representing dorsal denticles (K) can explain the patterning of surrounding body denticles (L and M). (A) to (C) are computed tomography (CT) scans, (D) to (F) are scanning electron microscopy (SEM) images, and (G) to (J) show alizarin red-stained samples. See Materials and Methods for details of RD modelling. Scale bars, 250 μm (D), 200 μm (E), 100 μm (F), 10 mm (G), and 400 μm (H to J).

state, initiator spots remained larger than newly formed spots (Fig. 1M), reflecting squamation of the shark (Fig. 1, D to J). This model provides theoretical support for a Turing-like system controlling denticle patterning in sharks.

To compare the patterning of shark denticles and chick feathers, we examined the expression of β -catenin (*β -cat*), an early regulator of chick epithelial placode signalling (Fig. 2 and fig. S1) (Noramly et al., 1999). The chicken embryo expresses a dorsolateral stripe of *β -cat* at embryonic day 6 (E6) (Fig. 2, C and D). This stripe becomes compartmentalized into individual feather placodes at E7 (Fig. 2, G and H), which trigger the emergence of adjacent, parallel placode rows (Fig. 2, K and L) (Jung et al., 1998). The shark lateral line expresses *β -cat* at stage 31 (~70 dpf), shortly before denticle patterning begins (Fig. 2, A and B). A continuous stripe of expression was not observed in the shark; however, two dorsolateral rows of denticle placodes appeared simultaneously at stage 32 (~80 dpf), expressing *β -cat* (Fig. 2, E and F). These rows emerged parallel to either lateral line (Fig. 2, A to F). The smaller body denticle placodes subsequently emerged in rows adjacent to dorsal denticles later in stage 32 (~100 dpf) (Fig. 2, I and J). Shark dorsal denticles may be acting as initiator rows, triggering the emergence of surrounding units in a Turing-like mechanism comparable to feather patterning. Having noted this similarity between shark and chick epithelial appendage patterning, we next examined the expression of genes underlying a putative Turing-like patterning system in the shark.

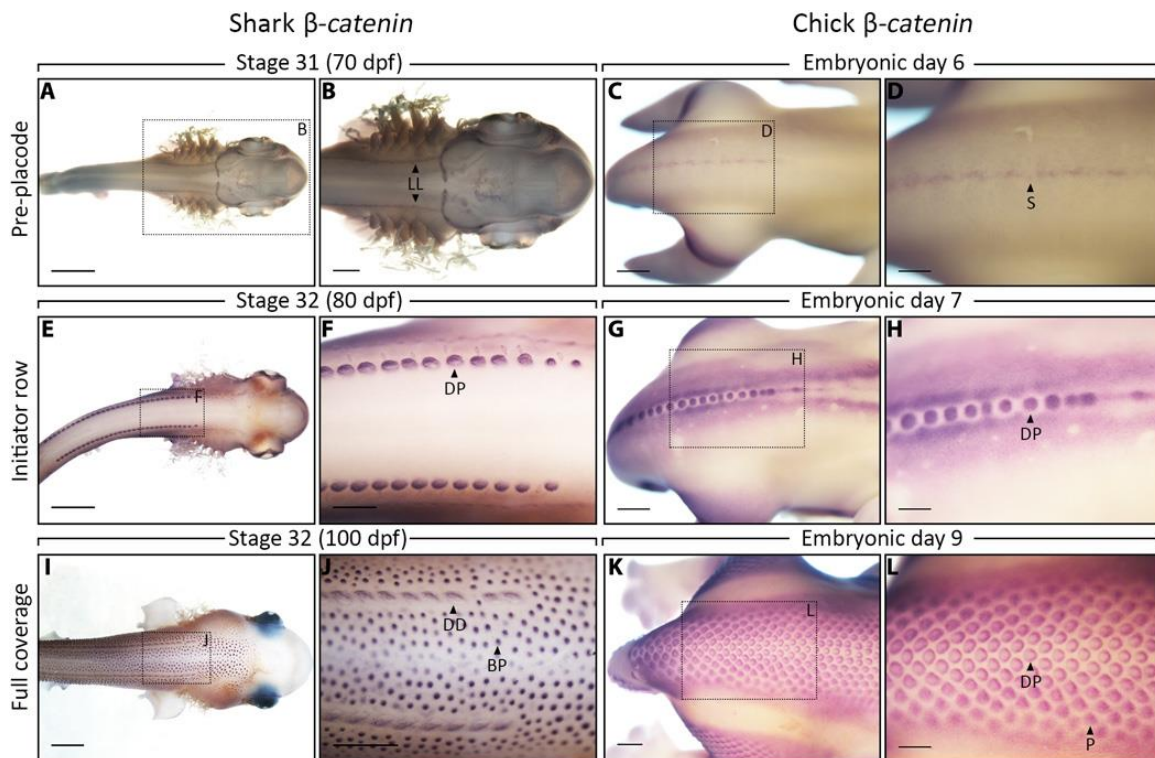


Figure 2: Conserved initiator rows may trigger surrounding epithelial placodes in the shark and chick. Whole-mount ISH for β -cat was undertaken throughout epithelial appendage patterning of shark denticles (A, B, E, F, I, and J) and chick feathers (C, D, G, H, K, and L). At E6, the chick displays a continuous stripe of β -cat expression (C and D), which then becomes compartmentalized into feather placodes (G and H). This initiator row triggers the emergence of surrounding feather placodes, following an RD system (Jung et al., 1998). (A and B) At stage 31 (~70 dpf), shark denticle placodes are not visible, although patterning of the lateral line sensory system is demarked by β -cat. (E and F) By stage 32 (~80 dpf), two dorsolateral rows of denticle placodes are visible. (I and J) Later in stage 32 (~100 dpf), surrounding rows of body denticle placodes also express β -cat. The shark dorsal denticle rows may be triggering body denticle emergence following a Turing-like system comparable to feather patterning. LL, lateral line; BP, body placode; P, placode. Scale bars, 2000 μ m (A, E, and I), 1000 μ m (B, C, G, J, and K), 500 μ m (D, F, and H), and 750 μ m (L).

Using in situ hybridization (ISH), we sought to identify the potential activators and inhibitors comprising this Turing-like patterning system. A suite of genes were selected on the basis of their importance during feather patterning (Jung et al., 1998), and their expression was analysed throughout squamation of the shark (Fig. 3 and fig. S1). At stage 31 (~70 dpf), dorsal denticle placodes were not detected (fig. S2), although β -cat expression labelled development of the lateral line sensory system (Fig. 2, A and B). By early stage 32 (~80 dpf), two dorsolateral rows of denticle placodes were visible, expressing the known activators of feather patterning, *fgf4* and *shh*, as well as the inhibitor *bmp4* (Fig. 3, A to C) (Ballard et al., 1993; Jung et al., 1998). Similar to feather patterning, *bmp4* was expressed within placodes rather than the interplacode regions, suggesting that its inhibitory action is indirect (Jung et al., 1998). The mesenchymal marker of feather bud development, *fgf3*, was also expressed in dorsal denticle rows (Fig. 3D) (Mandler and Neubüser, 2004), along with the runt domain transcription factor *runx2* (Fig. 3E), which is associated with FGF signalling throughout mammalian tooth morphogenesis and mineralization of other vertebrate skeletal elements (Åberg et al., 2004; D'Souza et al., 1999; Marcellini et al., 2010). An anterior to posterior gradient of dorsal denticle development was noted.

Later in developmental stage 32 (~100 dpf), body denticle placodes become visible in rows adjacent and parallel to dorsal denticle rows. Body denticles extend throughout the ventral trunk and eventually propagate to the entire flank and ventral surface. We understand that there are multiple initiation sites (Miyake et al., 1999), which are important for the extension of denticle patterning to the extremities, such as the paired pectoral fins. Redeployment of the same suite of genes expressed throughout dorsal denticle development was observed during patterning of these smaller body denticles (Fig. 3, F to O). Section ISH revealed that *shh* was expressed in the body denticle epithelium, whereas *fgf4*, *bmp4*, and *runx2* were expressed in the underlying mesenchyme (Fig. 3, P to R and T). The

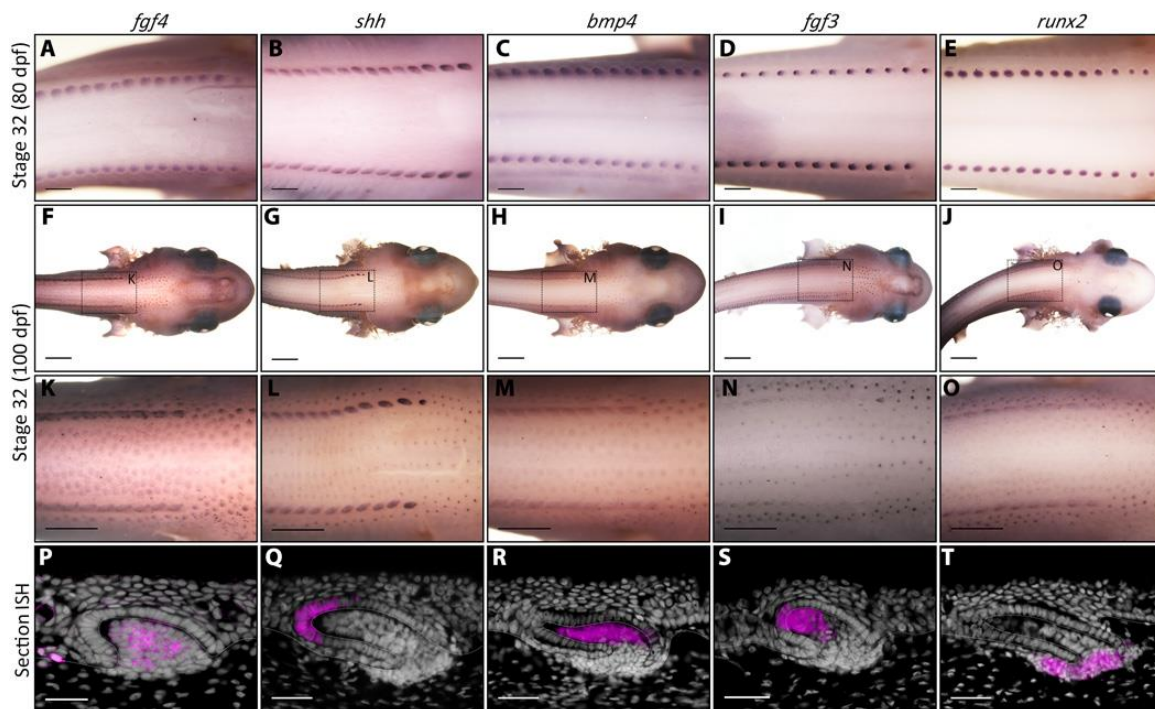


Figure 3: Conserved markers of RD are expressed during shark denticle patterning.

The expression of genes thought to control RD patterning of chick feathers was charted during shark denticle patterning (Hiscock and Megason, 2015). (A to C) At stage 32 (~80 dpf), shark dorsal denticle placodes express *fgf4* and *shh*, which are considered activators of feather patterning, and *bmp4*, which is considered an inhibitor (Hiscock and Megason, 2015). (D and E) Dorsal rows also express *fgf3*, a dermal marker of feather bud development, and *runx2*, which is associated with FGF signalling during mammalian tooth development (D'Souza et al., 1999; Mandler and Neubüser, 2004). (F to O) Later in stage 32 (~100 dpf), these genes are expressed during patterning of adjacent, parallel rows of body denticle placodes. (P to R and T) Section ISH of body denticles revealed epithelial expression of *shh* and mesenchymal expression of *fgf4*, *bmp4*, and *runx2*. (S) Expression of *fgf3* was observed in the epithelium and mesenchyme. White dashed lines separate columnar cells of the basal epithelium and the underlying mesenchyme. Scale bars, 500 μm (A to E), 2000 μm (F to J), 1000 μm (K to O), and 50 μm (P to T).

expression of *fgf3* was noted in both the epithelium and mesenchyme (Fig. 3S). Overall, these results revealed extensive conservation of RD-related gene expression between denticle and feather patterning (Jung et al., 1998; Noramly et al., 1999; Widelitz et al., 1996).

3.3.2 RD-related genes are functionally conserved during patterning of shark body denticles

To verify the functional conservation of genes expressed during denticle patterning, we undertook small-molecule gene pathway inhibition experiments. Embryos were treated with beads loaded with either the FGF receptor inhibitor SU5402 (Mohammadi et al., 1997) or dimethyl sulfoxide (DMSO) as a control. Beads were implanted beneath the epithelium in stage 31 embryos (~75 dpf), adjacent to rows of emerging dorsal denticle primordia (Fig. 4A). Development then continued before the genetic and phenotypic effects of treatment were examined at various time points.

First, ISH for RD-related genes was undertaken 5 days posttreatment (dpt). Localized inhibition of *shh* and *bmp4* expression was observed in dorsal denticle placodes treated with SU5402 beads, whereas the expression was unaltered in rows treated with DMSO beads (Fig. 4, C to J, and figs. S3 and S4, A to D). We propose that inhibition of FGF signalling disrupted a conserved activator-inhibitor feedback system between *fgf4*, *shh*, and *bmp4*, which similarly mediates feather patterning (Fig. 4B) (Jung et al., 1998). Furthermore, we observed down-regulation of sprouty 2 (*spry2*) expression (Fig. 4, K to N). As *spry2* is a downstream transcriptional readout of FGF signalling (Thisse and Thisse, 2005), this supports the idea that SU5402 treatment led to FGF inhibition in this system. Sections of whole-mount ISH samples revealed stunted development of denticle primordia (Fig. 4, C to N, and fig. S4), suggesting that inhibition of FGF signalling during early

morphogenesis is sufficient to restrict dorsal denticle growth. As dorsal denticles develop in an anterior to posterior gradient, the treatment effect was strongest in the units undergoing early morphogenesis at the time of beading, rather than simply the units closest to the bead (Fig. 4, C to N). For example, in Fig. 4K, the bead is positioned anterior to units with reduced gene expression, as the units closest to the bead are more advanced in their development. Posterior units undergoing early morphogenesis (demarcated with a black arrowhead) were affected by the treatment. Growth of the embryo may also affect proximity of the bead to the area of inhibition. These results suggest that there is functional conservation of a core gene regulatory network controlling shark denticle patterning, with FGF signalling playing an important activatory role.

Next, we examined the effect of the bead implants at 25 dpt, the stage at which smaller body denticles initiate (~100 dpf). Using ISH, we visualized *fgf4* expression to examine how the disruption of dorsal denticle development altered subsequent patterning (Fig. 4, O and P, and fig. S4, E and F). Dorsal denticle primordia failed to undergo morphogenesis following FGF inhibition, resulting in a gap in the row. This gap became infilled by smaller body denticle placodes (Fig. 4O), potentially as an inhibitory field surrounding dorsal denticles did not extend to this area. In contrast, control samples displayed a complete row of dorsal denticles (Fig. 4P). Alizarin red staining of SU5402 beaded samples fixed at 50 and 75 dpt revealed that this pattern was maintained throughout development, with smaller, mineralized body denticles occupying the gaps in the dorsal denticle rows (Fig. 4, Q and R, and figs. S5 and S6). Next, we examined whether this patterning response was consistent with a RD system. Therefore, we simulated the RD model (Fig. 1, K to M) with a unit missing from the initiator row (Fig. 4S) to mimic the functional experiment. The model output bore notable similarity to the pattern following bead implantation, with smaller units occupying the gap resulting from the missing initiator spot (Fig. 4, T and U). These results

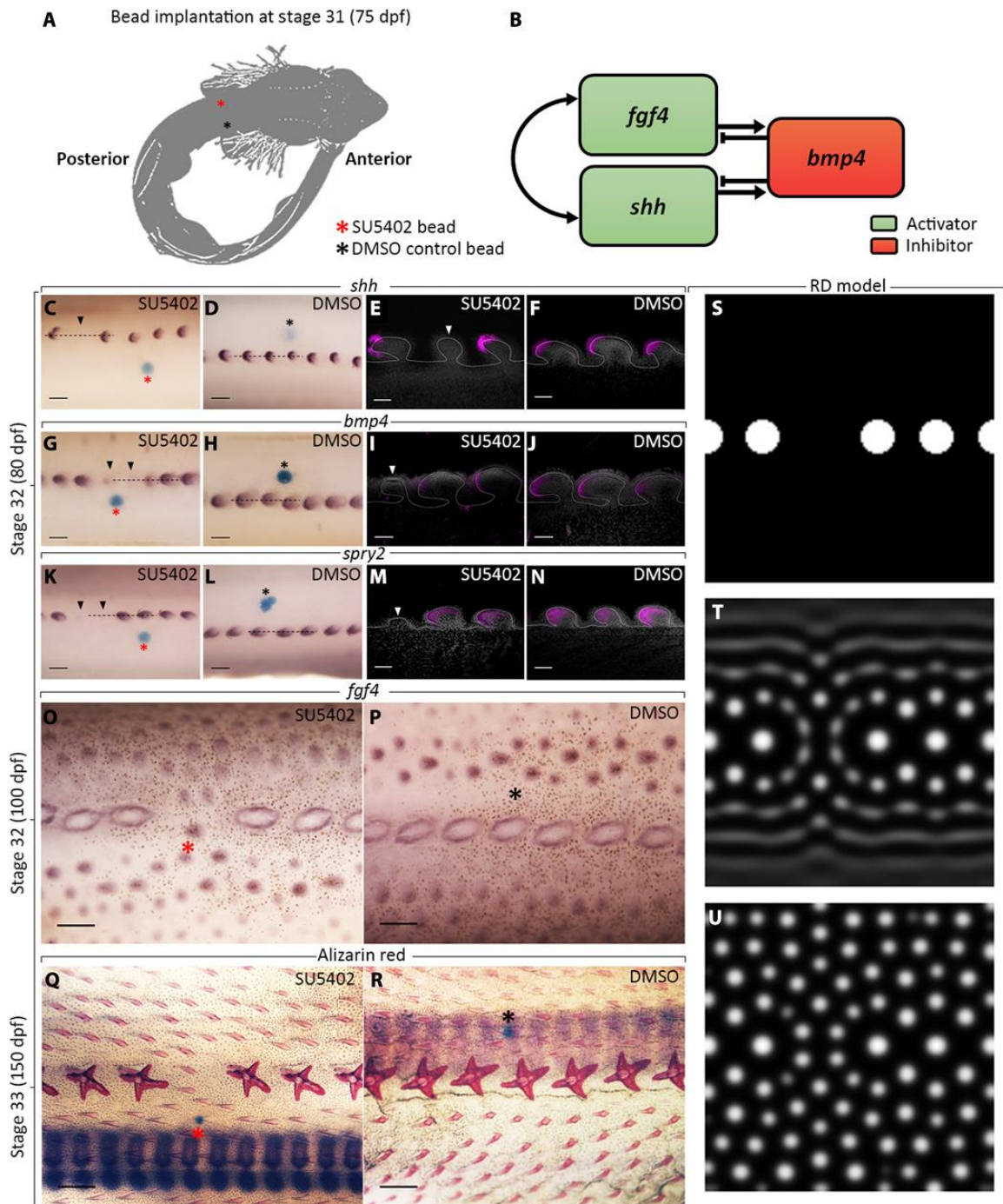


Figure 4: Bead inhibition experiments reveal functional conservation of RD-associated genes. (A) Beads loaded with the FGFR inhibitor SU5402 were implanted beneath the epithelium of shark embryos at 75 dpf. (C to N) First, we analysed gene expression at 5 dpt. We propose that breaking a conserved activator-inhibitor feedback system between *fgf4*, *shh*, and *bmp4* (B) led to localized down-regulation of both *shh* and *bmp4*, resulting in stunted growth of dorsal denticle primordia, highlighted by black and white arrowheads (C to J). (K to N) Expression of *spry2*, a transcriptional readout of FGF

signalling, was also reduced. We observed localized inhibition of gene expression at 5 dpt in all SU5402 beaded samples ($n = 5/5$) and no DMSO control samples ($n = 5/5$). (O) Expression of *fgf4* at 25 dpt showed that this inhibition resulted in a gap in the dorsal denticle row, which became occupied by smaller body denticles ($n = 2/2$). (P) No gap was observed in DMSO control samples ($n = 2/2$). Alizarin red staining revealed that this gap was maintained in 75% of SU5402-treated dorsal rows at 50 dpt ($n = 6/8$), whereas no gap was observed in rows treated with DMSO control bead ($n = 7/7$) (fig. S5). (Q) This pattern was maintained in SU5402 beaded dorsal rows at 75 dpt, once body denticles had begun to mineralize ($n = 7/8$). (R) DMSO control samples did not show a gap ($n = 9/9$). The output of RD simulation including a gap in the initiator row (S) was consistent with the experimental patterning observed; smaller units occupied the gap in the row (T and U). Dashed black lines show the location of vibratome sections from whole-mount ISH (E, F, I, J, M, and N). Scale bars, 200 μm (C, D, G, H, K, and L), 50 μm (E, F, I, J, M, and N), 300 μm (O and P), and 400 μm (Q and R).

provide further evidence that a Turing-like system controls shark denticle patterning, as the model response remains robust following experimental manipulation.

3.3.3 Retuning the RD model can explain the diversity of denticle patterning

Having found evidence for Turing-like denticle patterning in the catshark, we sought to examine the role of this system in other elasmobranch species. Among elasmobranchs, denticle density is diverse, with most sharks having a relatively dense coverage. Comparatively, denticle coverage of the thornback skate (*Raja clavata*) and the little skate (*Leucoraja erinacea*) is increasingly sparse (Fig. 5, A to F). We retuned parameters of activatory and inhibitory morphogens in the RD model to predict this diversity in elasmobranch denticle density.

Model parameters were initially set to result in a catshark-like denticle pattern (Figs. 1, K to M, and 5, D and G). The inhibitor's constitutive degradation rate (d_v) and maximum net

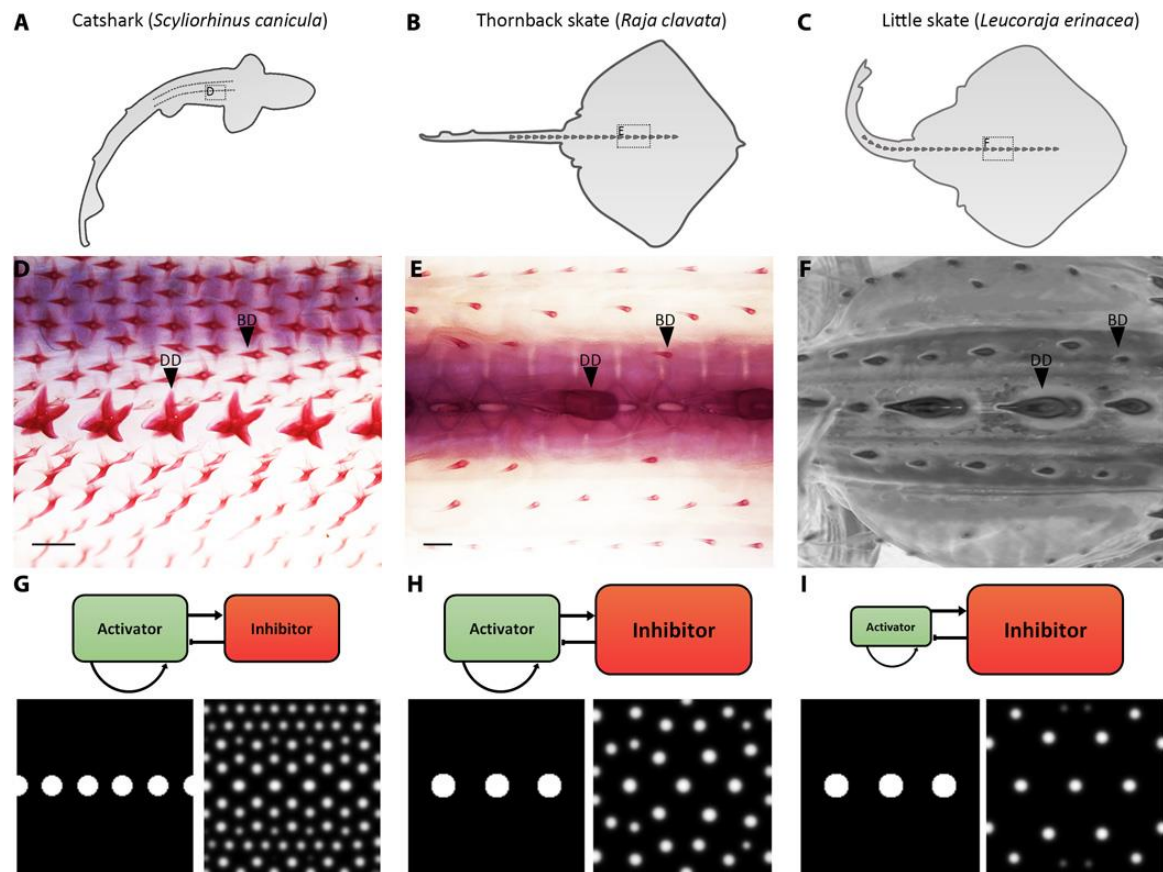


Fig. 5 Alterations to RD parameter values can explain denticle patterning diversity.

(A to F) Denticle diversity varies between elasmobranchs, with patterning becoming decreasingly dense from the catshark (*S. canicula*) to the thornback skate (*R. clavata*) and the little skate (*L. erinacea*). (G) Parameters of the RD model were initially set to result in catshark-like patterning. (H) Decreasing the inhibitor's constitutive degradation rate (d_v) and maximum net production rate (G_{max}) while increasing its diffusion coefficient (D_v) resulted in a less dense thornback skate-like pattern. (E) Initiator spots were made larger and placed further apart to reflect the skate's dorsal row. (I) Decreasing the activator's constitutive production rate (c_u) further reduced coverage density, resulting in a little skate-like pattern. See Materials and Methods for details of RD modelling and table S1 for specific parameter values. Scale bars, 400 μm (D) and 1000 μm (E).

production rate (G_{\max}) were then decreased, while its diffusion coefficient (D_v) was increased (table S1). Initiator spots were enlarged and spaced further apart to reflect the dorsal row of the skate (Fig. 5E). This led to decreased density of coverage, giving rise to patterning comparable to the thornback skate (Fig. 5, E and H). Next, the activator's constitutive production rate (c_u) was decreased (table S1). This further reduced the density of coverage, giving rise to patterning comparable to the little skate (Fig. 5, F to I). It is worth noting that numerous alternative combinations of parameter values could result in similar outputs to those shown here (Fig. 5, G to I), as well as outputs vastly more diverse (Kondo and Miura, 2010). Overall, these results demonstrate that simple alterations to parameters of the RD model can give rise to a wide diversity of patterning outcomes comparable to those seen in extant elasmobranch species. The plasticity of this system may underlie broad variations covering the vast spectrum of vertebrate epithelial appendage patterns.

3.4 Discussion

Our results provide both theoretical and experimental evidence to suggest that shark denticle patterning is controlled by a conserved Turing-like system also known to mediate the feather patterning of chicks (Jung et al., 1998). This mechanism has likely controlled epithelial appendage development for at least 450 million years, spanning the evolution of vertebrates, from sharks to mammals (Kondo and Miura, 2010; Sansom et al., 1996; Sick et al., 2006). This system includes a dorsolateral initiator row that triggers the emergence of surrounding appendages, controlled by functionally conserved activators and inhibitors, including *fgf4*, *shh*, and *bmp4* (Jung et al., 1998). In addition, we show that altering the parameters of this system can explain denticle pattern diversity observed between different elasmobranch species.

Previous experimental work investigating RD patterning has broadly focused on its role throughout amniotes, specifically mice and chicks (Jung et al., 1998; Sick et al., 2006). In addition, the rearrangement of zebrafish pigmentation following partial stripe ablation is concurrent with a RD system (Yamaguchi et al., 2007). Denticle patterning following bead implantation bore notable similarity to this experiment (Fig. 4); in both systems, the gap in the original row was occupied by infilling from adjacent rows. We provide evidence for Turing-like patterning in chondrichthyans. This supports both experimental and theoretical work, suggesting that Turing patterning is of widespread importance throughout vertebrate evolutionary history and is common to taxonomically diverse vertebrate groups (Kondo and Miura, 2010).

Furthermore, we demonstrate that alterations to the parameters of this system can explain the diversity of epithelial appendage patterns between different species (Fig. 5). Within elasmobranchs, this may have facilitated the evolution of various species-specific denticle functions, including protective armour, hydrodynamic drag reduction, feeding, and communication (Dean and Bhushan, 2010; Ferrón and Botella, 2017; Raschi and Tabit, 1992; Reif, 1985a; Southall and Sims, 2003). More broadly, this system may underlie epithelial appendage patterns throughout other vertebrates. For example, RD may control mammalian hair density, which is closely linked to thermoregulation (Ruxton and Wilkinson, 2011). Small changes to this conserved system may underpin pattern diversity throughout vertebrates.

Future research should address the formation of the initiator rows that trigger subsequent Turing patterning (Fig. 2). In the chick, this row originates as a continuous stripe, which then bifurcates into two rows, before the expression becomes localized to individual feather placodes (Chen et al., 2015). The shark has two initiator rows of denticle placodes (Jung et al., 1998; Oster et al., 1983), suggesting the single bifurcating initiator row of the chick

may be a derived feature. Transcriptome sequencing has shown that genes associated with neural development are significantly upregulated in the skin during patterning of the chick initiator row. This is indicative of developmental synchronicity between the nervous system and feather patterning (Gong et al., 2018). The shark lateral line is a system of innervated sensory organs that appear parallel to subsequent dorsal row placodes (Fig. 2, A and B, and fig. S2D). It is possible that these systems are synchronous in the shark, with the lateral line mediating the patterning of the shark denticle initiator row. Furthermore, the lateral line extends the entire length of the body and may mediate Turing-like patterning posterior to the dorsal rows, which extend approximately halfway along the dorsal trunk. In addition, there are multiple sites of pattern initiation, including those located on the wings and pectoral fins of the chick and elasmobranchs, respectively (Mayerson and Fallon, 1985; Miyake et al., 1999). Whether these sites have individual initiator rows is unknown, presenting a gap in our understanding of pattern initiation.

The importance of RD-controlled patterning has long been debated (Kondo and Miura, 2010). However, there is a growing body of both theoretical and experimental work supporting the relevance of this model (Economou et al., 2012; Harris et al., 2005; Jiang et al., 1999; Jung et al., 1998; Onimaru et al., 2016; Sick et al., 2006). Our findings provide support for this research, demonstrating that an ancient Turing-like system controls epithelial appendage patterning in chondrichthyans, which belong to an early diverging lineage, with respect to tetrapods. We suggest that diverse vertebrate groups share this common, conserved patterning mechanism, before deviation in later morphogenesis gives rise to clade-specific integumentary appendages, such as denticles, feathers, and hair.

3.5 Methods

3.5.1 Shark and chick husbandry

The University of Sheffield is a licensed establishment under the Animals (Scientific Procedures) Act 1986. All animals were culled by approved methods cited under Schedule 1 to the Act. Fertilized Bovan brown chicken eggs (Henry Stewart & Co., Norfolk, UK) were incubated at 37.5°C before overnight fixation in Carnoy's solution between E6 and E9. *S. canicula* embryos (North Wales Biologicals, Bangor, UK) were raised in oxygenated artificial saltwater (Instant Ocean) at 16°C. Shark embryos were culled with MS-222 (tricaine) at 300 mg/litre and fixed overnight in 4% paraformaldehyde in phosphate-buffered saline (PBS). After fixation, chicken and shark embryos were dehydrated through a graded series of PBS to ethanol (EtOH) and stored at -20°C.

3.5.2 Micro-CT and SEM

High-resolution micro-CT scanning was conducted using an Xradia Micro-XCT scanner at the Imaging and Analysis Centre, Natural History Museum, London. *S. canicula* embryos were stained with 0.1% phosphotungstic acid in 70% EtOH for 3 days to enhance contrast. Scans were rendered using the three-dimensional volume exploration tool Drishti (<https://github.com/nci/drishti>). SEM was undertaken using a Hitachi TM3030Plus Benchtop SEM scanner at 15,000 V.

3.5.3 Alizarin red clear and staining

Embryos were rehydrated from EtOH to PBS and stained overnight with alizarin red in potassium hydroxide (KOH), as previously described (Cooper et al., 2017). Samples were imaged in glycerol using a Nikon SMZ15000 stereomicroscope. Scale bars were created in Fiji (Schindelin et al., 2012).

3.5.4 RD modelling

RD modelling of shark body denticle patterning was undertaken using an activator-inhibitor model proposed by Kondo & Miura (Kondo and Miura, 2010), based on the equations

$$\frac{\partial u}{\partial t} = F(u, v) - d_u u + D_u \Delta u, \quad (1)$$

$$\frac{\partial v}{\partial t} = G(u, v) - d_v v + D_v \Delta v, \quad (2)$$

where $u(t, x, y)$ and $v(t, x, y)$ denote the concentrations of an activator and inhibitor, respectively, at time t and location (x, y) . Equations (1) and (2) describe the rate of change of these concentrations in time and space due to diffusion and regulated production and degradation of the molecular species. The nonlinear functions $F(u, v)$ and $G(u, v)$ are defined by

$$F(u, v) = \begin{cases} 0 & \text{if } a_u u + b_u v + c_u < 0, \\ F_{max} & \text{if } a_u u + b_u v + c_u > F_{max}, \\ a_u u + b_u v + c_u & \text{otherwise,} \end{cases} \quad (3)$$

$$G(u, v) = \begin{cases} 0 & \text{if } a_v u + b_v v + c_v < 0, \\ G_{max} & \text{if } a_v u + b_v v + c_v > G_{max}, \\ a_v u + b_v v + c_v & \text{otherwise.} \end{cases} \quad (4)$$

Equations (1) and (2) were solved in the two-dimensional square domain $0 < x < L, 0 < y < L$ for times $0 < t < T$ subject to no-flux boundary conditions and prescribed initial conditions that varied across simulations. For the simulations shown in Fig. 1K-M and Fig. 5G-I, the initial condition was given by

$$\begin{aligned} &u(0, x, y) \\ &= \begin{cases} u_0 & \text{if } (x - x_i)^2 + (y - y_i)^2 < (R_{spot})^2 \text{ for } i \in \{0, \dots, n_{spot} - 1\}, \\ 0 & \text{otherwise,} \end{cases} \end{aligned} \quad (5)$$

$$\begin{aligned} &v(0, x, y) \\ &= 0. \end{aligned} \quad (6)$$

where each (x_i, y_i) defines the centre of a spot in an ‘initiator’ row representing dorsal denticles of a given number (n_{spot}) and radius (R_{spot}). Fig. 1K-M and Fig. 5G were generated using $R_{spot} = 4.5$, $n_{spot} = 6$, and $(x_i, y_i) = (iL/5, L/2)$. Fig. 4S-U were generated using the same initial condition but with the spot centred at (x_2, y_2) removed. Fig. 5H was generated using $R_{spot} = 5.25$, $n_{spot} = 3$, and $(x_i, y_i) = ((3i + 2)L/10, L/2)$, reflecting fewer, larger, more widely spaced initiator spots.

The RD model was solved numerically using an explicit finite difference method, choosing a spatial discretization Δx and sufficiently small time step Δt to ensure numerical stability. Python code to generate Fig. 1K-M, Fig. 4S-U and Fig. 5G-I is provided in the Supplementary Material. The parameter values used to generate Fig. 1K-M and Fig. 4S-U were given by $d_u = 0.03$, $D_u = 0.02$, $a_u = 0.08$, $b_u = -0.08$, $c_u = 0.04$, $F_{max} = 0.2$, $d_v = 0.08$, $D_v = 0.6$, $a_v = 0.16$, $b_v = 0$, $c_v = -0.05$, $G_{max} = 0.5$, with a domain of size $L = 75$, end time $T = 1500$, spot radius $R = 4.5$, initial concentration $u_0 = 5$, and discretization $\Delta x = L/128 \approx 0.58$, $\Delta t = (\Delta x)^2/8D_v \approx 0.07$. These values were chosen based on an ad hoc exploration of parameter space around parameter values previously identified by Kondo and Miura as leading to patterning (Kondo and Miura, 2010). Parameter values for Figure 5 are given in Supplementary Table 1. For Fig. 5H-I, since the value of D_v was reduced, we updated the value of $\Delta t = (\Delta x)^2/8D_v \approx 0.04$ to maintain numerical stability.

3.5.5 In situ hybridization

Digoxigenin-labeled antisense riboprobes were designed using partial skate (*L. erinacea*) and catshark (*S. canicula*) EST (expressed sequence tag) assemblies (SkateBase; skatebase.org) (Wyffels et al., 2014), the Vertebrate TimeCapsule (VtCap; transcriptome.cdb.riken.go.jp/vtcap), and transcriptome data from RNA sequencing

(unpublished). Sequences of forward and reverse primers (Sigma) are as follows: chick *β-cat*, TCTCACATCACCGTGAAGGC (forward) and CCTGATGTCTGCTGGTGAGG (reverse); shark *β-cat*, GGTGAAAATGCTTGGGTCT (forward) and GGACAAGGGTTCCTAGAAGA (reverse); shark *fgf4*, ATGTTGATCAGGAAGCTGCG (forward) and GTATGCGTTGGATTCGTAGGC (reverse); shark *shh*, TGACTCCCAATTACAACCCGG (forward) and TCAGGTCCTTCACTGACTTGC (reverse); shark *bmp4*, GATCTCTACAGGCTGCAGTCC (forward) and GATCTCTACAGGCTGCAGTCC (reverse); shark *fgf3*, CTTGCTCAACAGTCTTAAGTTATGG (forward) and CGGAGGAGGCTCTACTGTG (reverse); shark *runx2*, ATCTCTCAATCCTGCACCAGC (forward) and CCAGACAGACTCATCAATCCTCC (reverse); and shark *spry2*, AACTAGCACTGTGAGTAGCGG (forward) and GTTCCGAGGAGGTAACTGGG (reverse). Riboprobes were synthesized using the Riboprobe System SP6/T7 Kit (Promega) and DIG RNA Labelling Mix (Roche). Whole-mount and section ISH was performed as previously described (Cooper et al., 2017; Rasch et al., 2016). To compare sequences between the chick and shark, phylogenetic gene trees were reconstructed from protein coding sequences extracted from www.ensembl.org, aligned to *S. canicula* sequences obtained during probe synthesis (see fig. S1 for details) (Edgar, 2004; Guindon et al., 2005). Whole-mount ISH samples were imaged using a Nikon SMZ15000 stereomicroscope, and sections were imaged using an Olympus BX51 microscope and Olympus DP71 Universal digital camera attachment. Vibratome sections shown in Fig. 4 were cut at a thickness of 30 μm. Adjustments to image contrast and brightness were made to improve clarity. Scale bars were added using Fiji (Schindelin et al., 2012).

3.5.6 Bead implantation experiments

Embryos were treated with Affi-Gel Blue beads (Bio-Rad) loaded with SU5402 (2 mg/ml; Sigma) in DMSO. Control beads were loaded with DMSO. Stage 31 (~75 dpf) embryos were removed from their egg cases and anaesthetized before beads were surgically implanted using sharpened tungsten wire. Embryos were then cultured in six-well plates with artificial saltwater and 1% penicillin-streptomycin (Thermo Fisher Scientific). At stage 32 (~100 dpf), embryos were transferred to 70-ml plastic containers (Sarstedt) floating in a 200-liter tank. The number of replicates and observed effects for different analyses are shown in Table 1 (below).

Table 1: Summary of the number of replicates for bead inhibition experiments (shown in Fig. 4 and figs. S4 and S5).

Stage fixed (dpf)	Analysis type	SU5402 bead (number of dorsal rows affected/total)	DMSO control bead (number of dorsal rows unaffected/total)
80	ISH	5/5	5/5
100	ISH	2/2	2/2
125	Alizarin red	6/8	7/7
150	Alizarin red	7/8	9/9
	Total	20/23 = 87%	23/23 = 100%

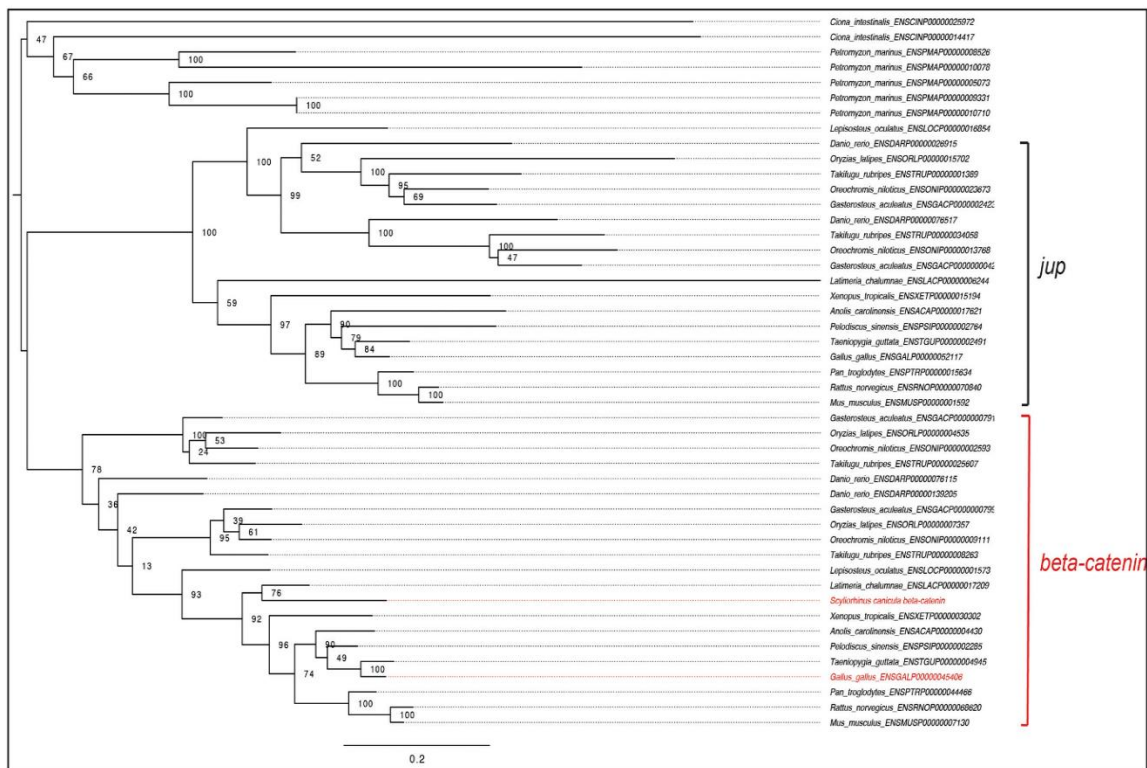
3.6 Acknowledgements

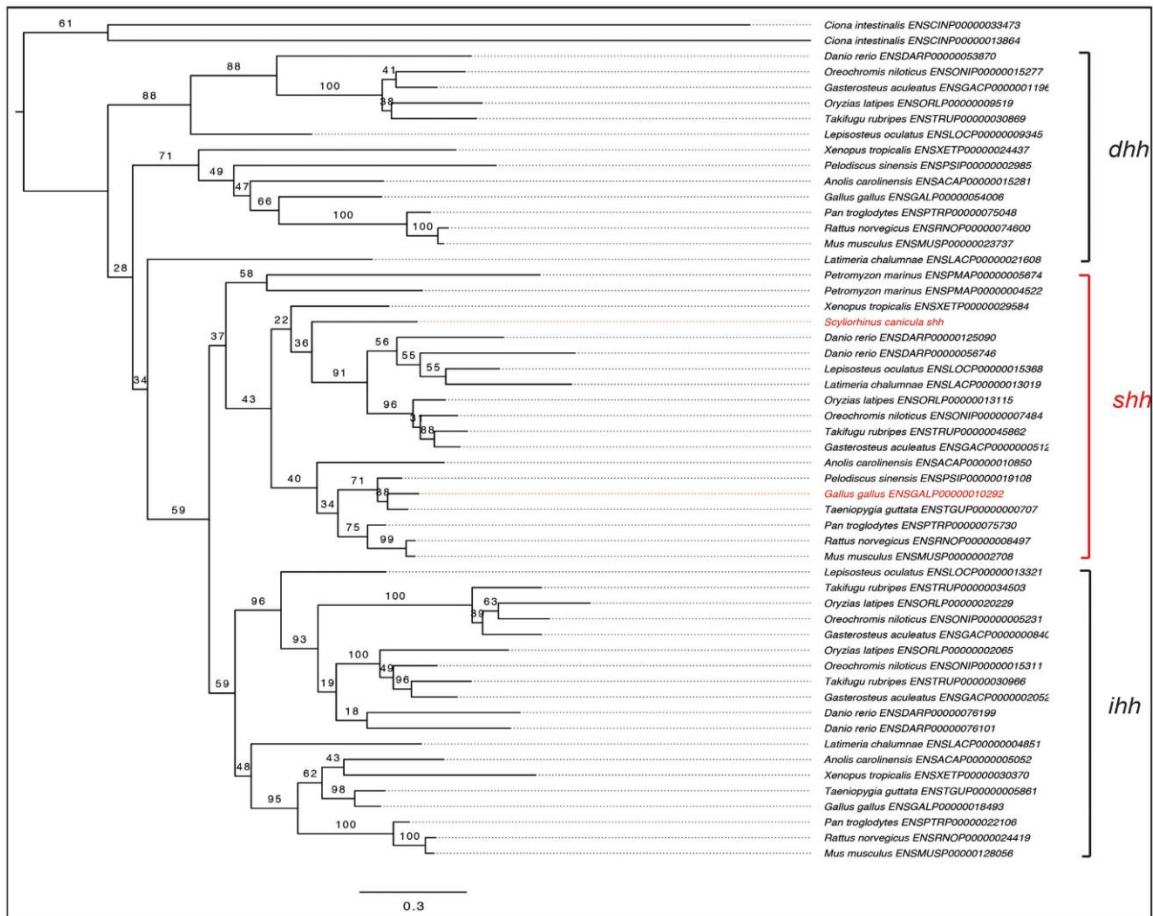
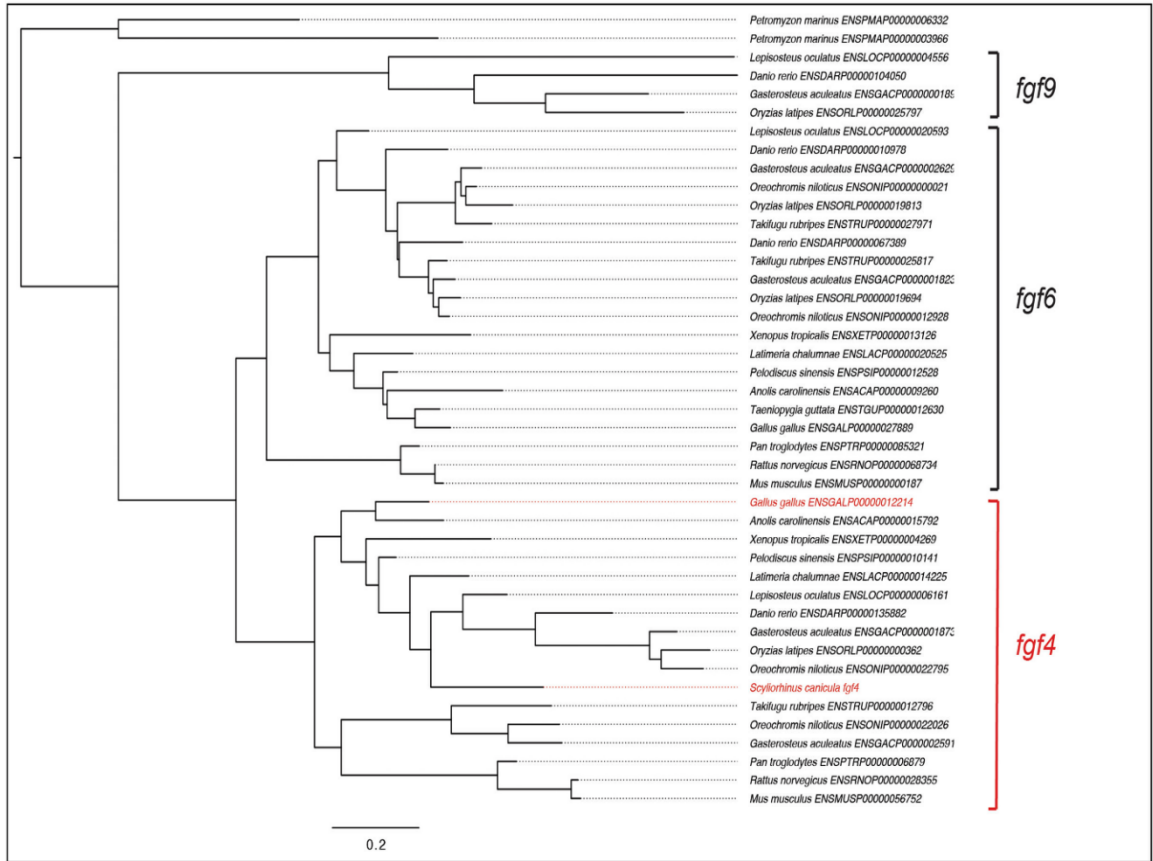
We would like to thank N. Monk (School of Mathematics and Statistics, University of Sheffield) for initial discussions regarding RD modelling. We also extend our gratitude to K. Martin, Z. Johanson (Department of Earth Sciences, Natural History Museum, London), F. Ahmed, and A. Garbout (Imaging and Analysis Centre, Natural History

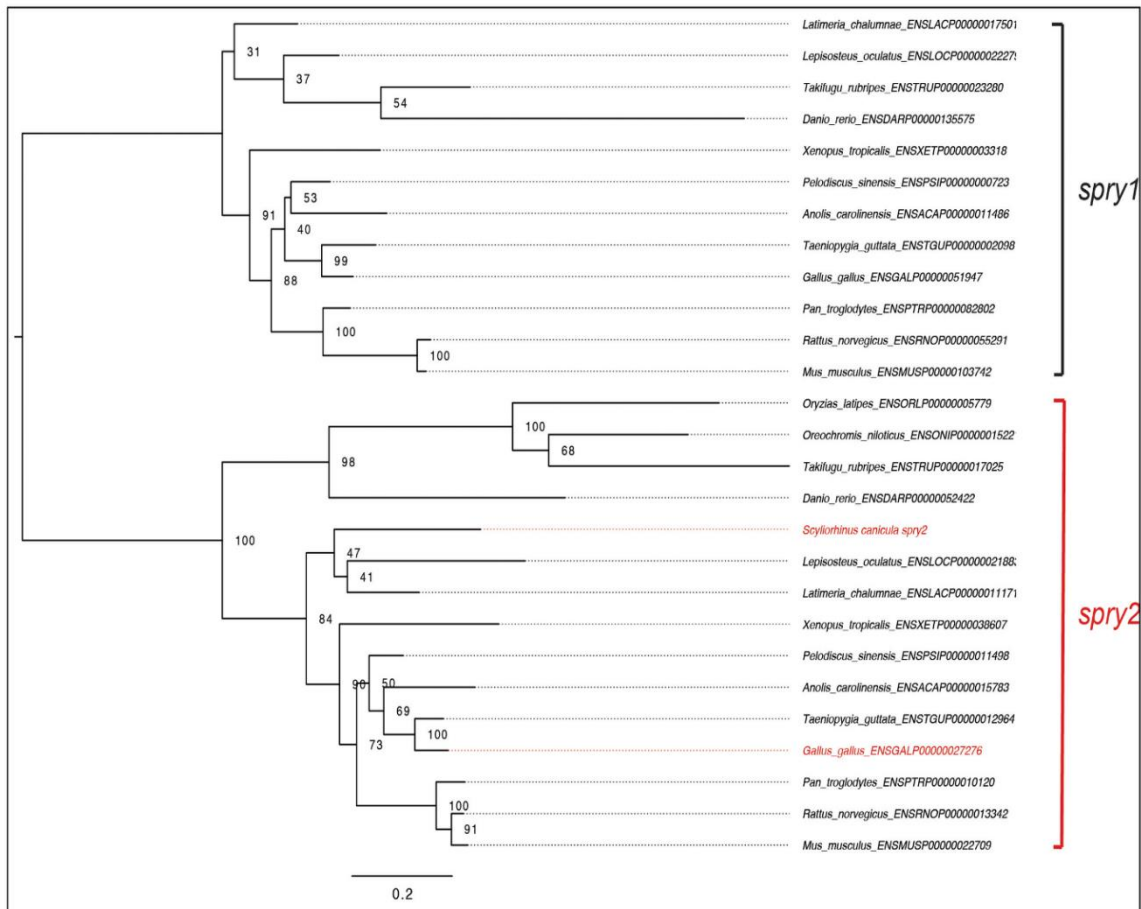
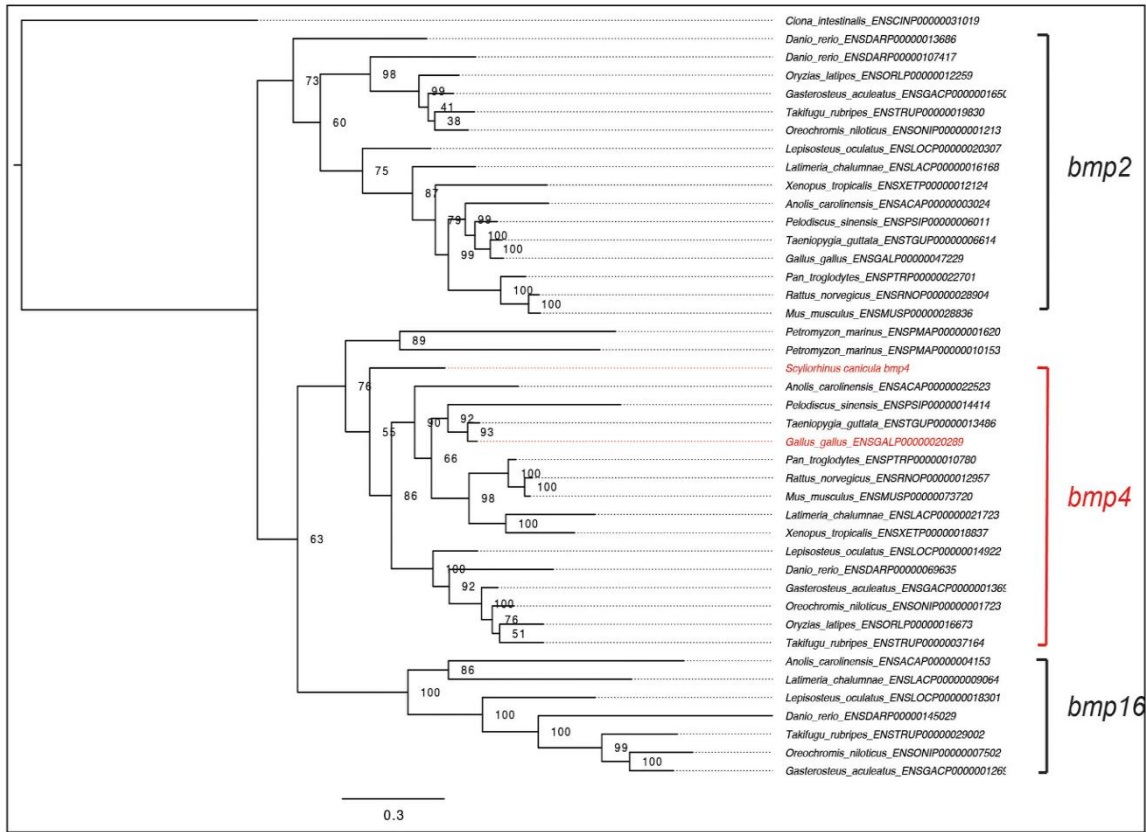
Museum, London) for assistance with micro-CT imaging. Thornback ray (*R. clavata*) embryos were donated by the Native Marine Centre, Weymouth, UK, and little skate (*L. erinacea*) embryos were sourced from the Marine Biological Laboratories (MBL), Woods Hole, MA, USA. Last, we thank M. Placzek for the gift of Affi-Gel Blue beads (Bio-Rad) and K. Onimaru for advice on experimental methods.

3.7 Supplementary materials

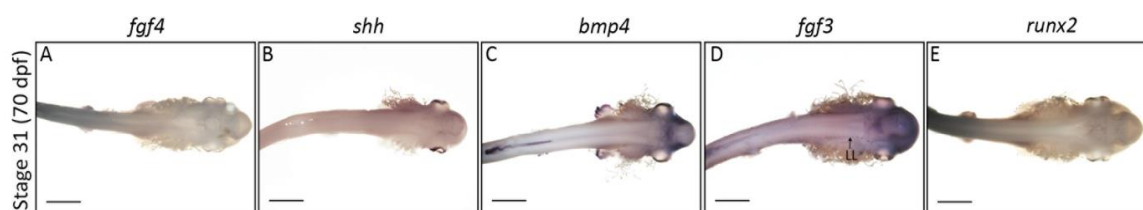
3.7.1 Supplementary file 1: supplementary figures



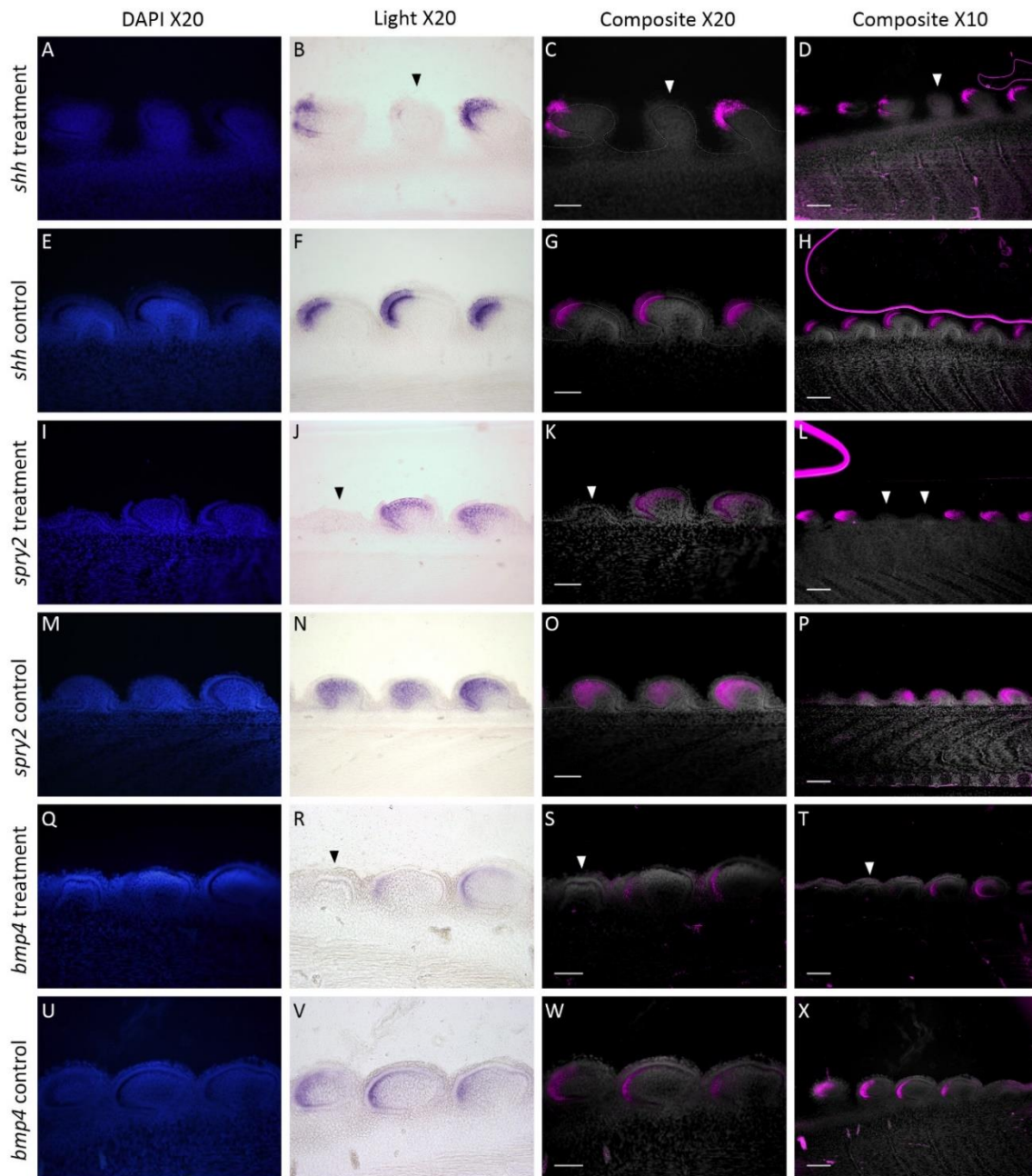




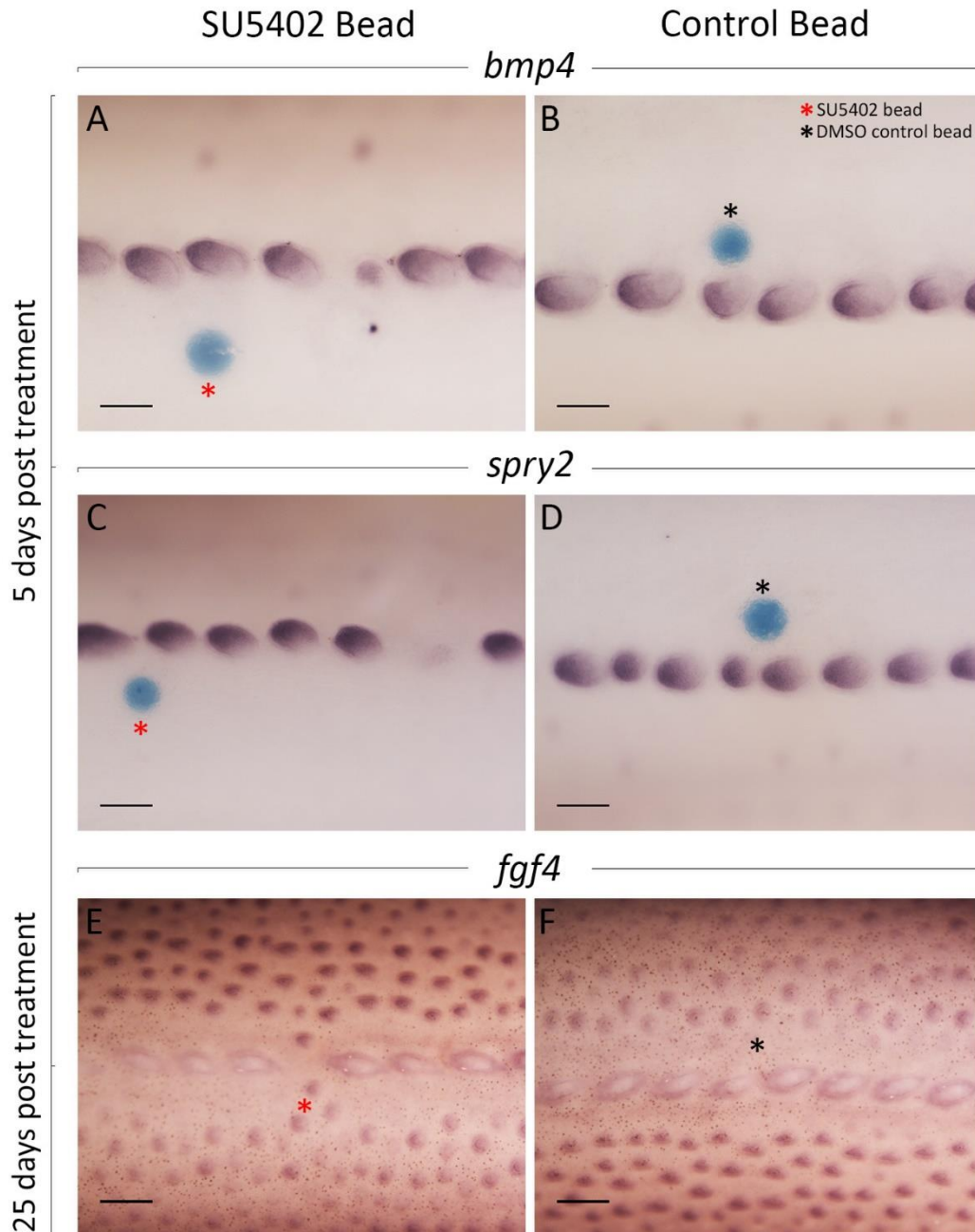
Supplementary Figure 1: Phylogenetic gene trees reconstructed from protein coding sequences (CDS) extracted from www.ensembl.org. Species included in the analysis were selected based on their phylogenetic position. Ensembl sequences were aligned to *S. canicula* sequences obtained during probe synthesis steps (see methods). Sequences were aligned using MUSCLE (Edgar, 2004). A maximum likelihood tree was generated from 100 bootstrap replications using PHYML with a GTR substitution model (Guindon et al., 2005). Trees were edited in FigTree v1.4.3



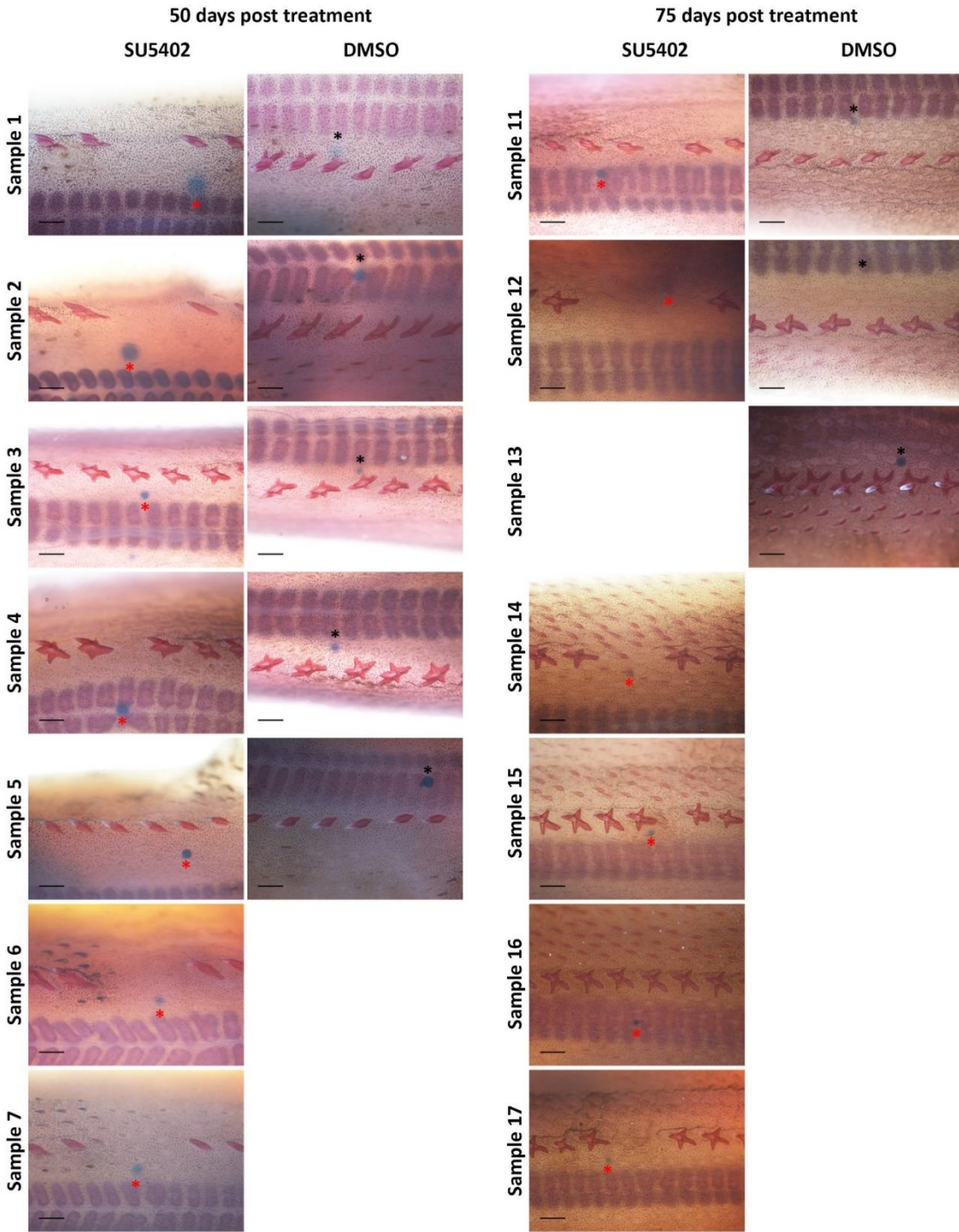
Supplementary Figure 2: Dorsal denticle placodes are not visible at Stage 31 (~70 dpf). Wholemount ISH for *fgf4*, *shh*, *bmp4*, *fgf3* and *runx2* revealed that dorsal denticle placodes were not present at developmental Stage 31 (~70 dpf). Patterning of the lateral line sensory system (LL) is visible, expressing *fgf3*. Scale bars are 2000 μ m.

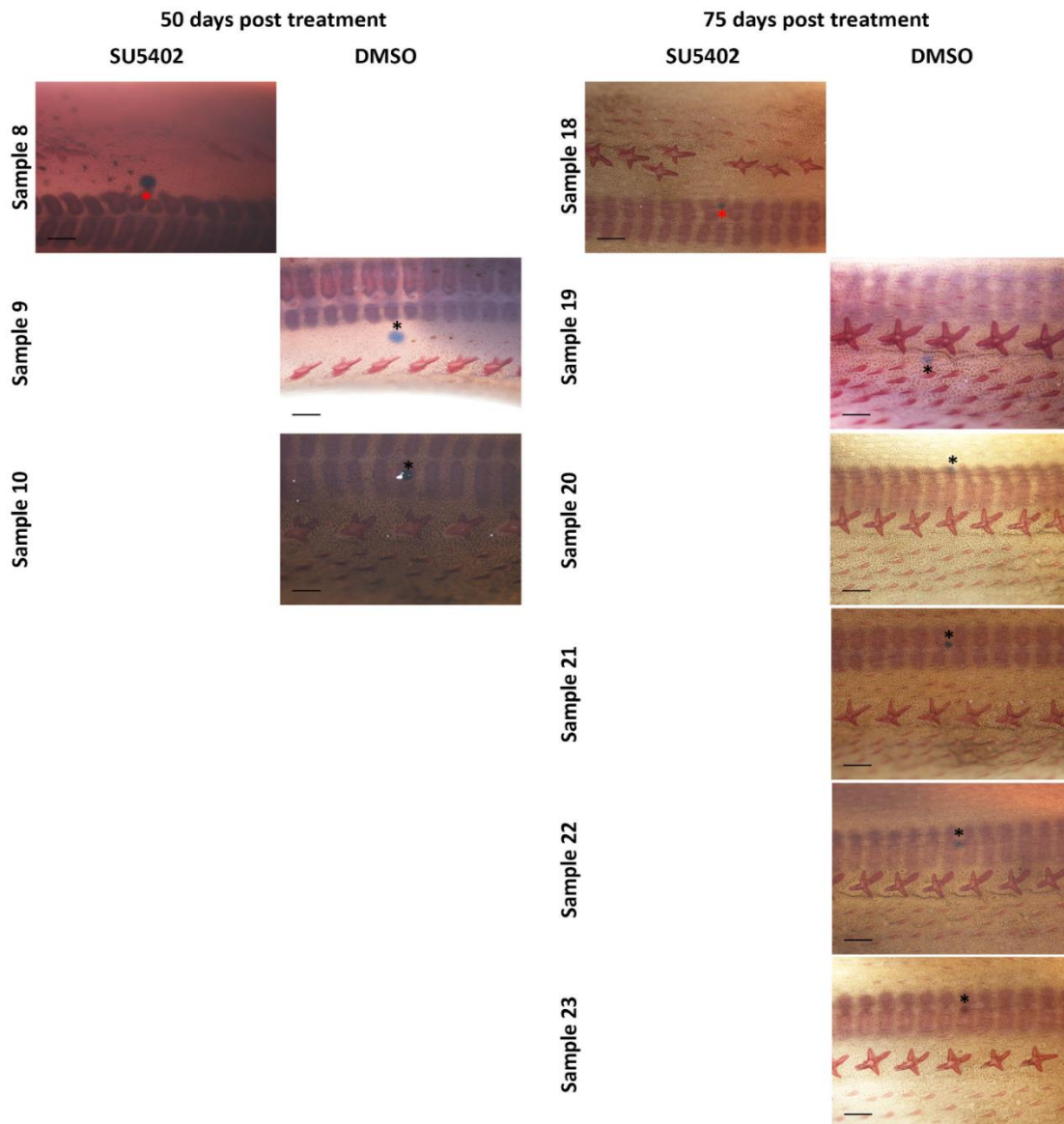


Supplementary Figure 3: Individual vibratome section images comprising false coloured *in situ* hybridization composite images. Vibratome sections of whole mount *ISH* are shown, for both SU5402 (treatment) and DMSO (control) beaded samples. Images are shown for both DAPI (blue) and light channels. The composite images are shown at both X10 and X20 magnification. Scale bars lengths are D, H, L, P, T and X = 100 μ m, and C, G, K, O, S and W = 50 μ m.

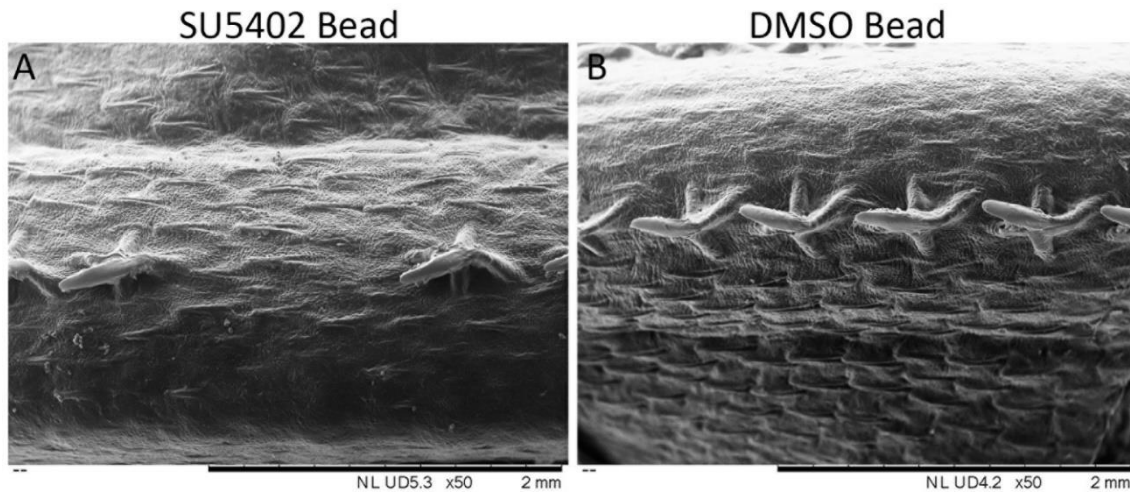


Supplementary Figure 4: Replicates of beaded shark embryos after whole mount *in situ* hybridization. Whole mount *ISH* show additional shark embryo replicates after beading with SU5402 and DMSO as a control. Scale bar lengths are A-D = 200 μ m, and E, F = 300 μ m.





Supplementary Figure 5: Replicates of clear and stained shark embryos showing RD response to SU5402 beading. Replicates of alizarin red stained embryos treated with either SU5402 or DMSO loaded beads are shown at 50 dpt and 75 dpt. Embryos were treated with either one SU5402 bead and one DMSO bead adjacent to each dorsal row (Samples 1-5, Samples 11-12), or only one bead type per embryo (Samples 6-10, Samples 13-23). The SU5402 bead did not have an effect upon Samples 3, 5 and 16. Red asterisks mark SU5402 beads and black asterisks mark DMSO control beads. Scale bar lengths are 400µm.



Supplementary Figure 6: Scanning electron microscope images of shark embryo 75 days post beading. These scanning electron microscope images show sample 14 (A) and sample 19 (B) from Supplementary Figure 5. They are 75 dpt, at developmental Stage 33 (150 dpf), and infilling of body denticles is visible in the SU5402 beaded individual (A). Tissue had to be dry when scanned, consequently resulting in distortion of the sample. Scale bar lengths are 2mm.

<i>Species</i>	<i>Activator values (u)</i>						<i>Inhibitor values (v)</i>					
	d_u	D_u	a_u	b_u	c_u	F_{max}	d_v	D_v	a_v	b_v	c_v	G_{max}
Catshark	0.03	0.02	0.08	-0.08	0.04	0.2	0.08	0.6	0.16	0.0	-0.05	0.5
Thornback ray	0.03	0.02	0.08	-0.08	0.04	0.2	<u>0.035</u>	<u>0.895</u>	0.16	0.0	-0.05	<u>0.3</u>
Little skate	0.03	0.02	0.08	-0.08	<u>0.01</u>	0.2	0.035	0.895	0.16	0.0	-0.05	0.3

Supplementary Table 1: Activator and inhibitor values for RD model. These are the RD model parameter values specified for patterning resembling squamation of the catshark, thornback ray and little skate (see Figure 5). Parameter values shown in red and underlined have been altered from the previous row. See ‘Methods’ for more information on RD modelling.

3.7.2 Supplementary file 2: Python script for RD simulations

```
# -*- coding: utf-8 -*-  
"""
```

Created on Tue May 29 12:14:28 2018

Python code for the numerical solution of a 2D reaction-diffusion system. Using an explicit finite difference method, with a timestep chosen sufficiently small to ensure numerical stability, we solve the coupled PDEs

$$u_t = D_u(u_{xx} + u_{yy}) + F(u,v) - d_u u,$$
$$v_t = D_v(v_{xx} + v_{yy}) + G(u,v) - d_v v$$

on the square domain $0 < x, y < L$, for $0 < t < T$. We impose no-flux boundary conditions, and initial conditions corresponding to a row of 'initiator' spots as defined in the main text. The nonlinear functions F and G are defined by

$$F(u,v) = \min(\max(a_u u + b_u v + c_u, 0), F_{\max}),$$
$$G(u,v) = \min(\max(a_v v + b_v u + c_v, 0), G_{\max}).$$

The precise initial conditions and parameter values are varied in each simulation, generating Figs 1K-M, 4S-U and 5G-I.

```
@author: Alexander Fletcher  
"""
```

```
import numpy as np  
from numpy.linalg import norm  
import matplotlib.pyplot as plt
```

```
def solve_RD_model(spot_centres, plot_times, plot_names, *params):  
    """Function to solve the reaction-diffusion system and output to file"""  
    # Specify grid size and time step to ensure numerical stability  
    M = 128  
    dx2 = (L/M)**2  
    dt = 0.5 * dx2 / (4 * max(D_u, D_v))  
    N = int(T / dt)  
  
    # Specify initial conditions  
    U, V, U_pen, V_pen = [np.zeros((M, M)) for _ in range(4)]  
    c_y = int(M/2)  
    centres = [int(x*M/L) for x in spot_centres]  
    for c_x in centres:  
        for i in range(M):  
            for j in range(M):  
                if (i - c_x)**2 + (j - c_y)**2 < int(R_spot**2/dx2):  
                    U[i,j] = u_0  
  
    # Set up plotting
```

```

plot_timesteps = [round(i/ dt) for i in plot_times]

# Solve the PDE system numerically
for n in range(N+2):

    # Store penultimate state of system to assess convergence to steady state
    if n == N+1:
        U_pen[:] = U
        V_pen[:] = V

    # Plot state of system if at plotting times
    if n in plot_timesteps:
        idx = plot_timesteps.index(n)
        plt.figure()
        fig =
plt.imshow(np.transpose(U),interpolation='bilinear',cmap='binary_r',extent=[0,L,0,L],orig
in='lower')
        plt.axis('off')
        fig.axes.get_xaxis().set_visible(False)
        fig.axes.get_yaxis().set_visible(False)
        plt.savefig(plot_names[idx]+' .png',bbox_inches='tight',pad_inches=0)

    d2U = (U[1:-1,0:-2]+U[1:-1,2:]+U[2:,1:-1]+U[0:-2,1:-1]-4*U[1:-1,1:-1])/dx2
    d2V = (V[1:-1,0:-2]+V[1:-1,2:]+V[2:,1:-1]+V[0:-2,1:-1]-4*V[1:-1,1:-1])/dx2

    Uc = U[1:-1, 1:-1]
    Vc = V[1:-1, 1:-1]
    F = np.minimum(np.maximum(a_u*Uc + b_u*Vc + c_u,0), F_max)
    G = np.minimum(np.maximum(a_v*Uc + b_v*Vc + c_v,0), G_max)

    # Update u and v
    U[1:-1, 1:-1] = Uc + dt*(D_u*d2U + F - d_u*Uc)
    V[1:-1, 1:-1] = Vc + dt*(D_v*d2V + G - d_v*Vc)

    # Impose no-flux boundary conditions
    for Z in (U, V):
        Z[0,:] = Z[1,:]
        Z[-1,:] = Z[-2,:]
        Z[:,0] = Z[:,1]
        Z[:, -1] = Z[:, -2]

    # Check for convergence to steady state
    tol = 1e-2
    if norm(U - U_pen) < tol and norm(V - V_pen) < tol:
        print('System has reached steady state')
    else:
        print('System has not yet reached steady state')

if __name__ == '__main__':

```

```

##### Fig. 1K-M #####

# Specify parameters for Fig. 1K-M
D_u, a_u, b_u, c_u, d_u, F_max = 0.02, 0.08, -0.08, 0.04, 0.03, 0.2
D_v, a_v, b_v, c_v, d_v, G_max = 0.6, 0.16, 0.0, -0.05, 0.08, 0.5
u_0 = 5
L, T = 75, 1500
R_spot = 0.06*L

p_dict = {'D_u':D_u,'a_u':a_u,'b_u':b_u,'c_u':c_u,'d_u':d_u,'F_max':F_max,
          'D_v':D_v,'a_v':a_v,'b_v':b_v,'c_v':c_v,'d_v':d_v,'G_max':G_max,
          'u_0':u_0,'R_spot':R_spot,'L':L,'T':T}

# Specify spot locations and plotting times for Fig. 1K-M
spot_centres = [0, L/5, 2*L/5, 3*L/5, 4*L/5, L]

# Specify spot locations and plotting times for Fig. 1K-M
plot_times = [0, 0.25*T, T]
plot_names = ['Figure1K', 'Figure1L', 'Figure1M']

# Save images for Fig. 1K-M
solve_RD_model(spot_centres, plot_times, plot_names, p_dict)

##### Fig. 4S-U #####

# Re-specify spot locations and plotting times for Fig. 4S-U
spot_centres = [0, L/5, 3*L/5, 4*L/5, L]
plot_times = [0, 0.4*T, T]
plot_names = ['Figure4S', 'Figure4T', 'Figure4U']

# Save images for Fig. 4S-U
solve_RD_model(spot_centres, plot_times, plot_names, p_dict)

##### Fig. 5G-I #####

# NB Fig. 5G is the same as Figs 1K,M

# Re-specify parameters, spot locations and plotting times for Fig. 5H
R_spot = 0.07*L
T = 3000
d_v = 0.035
D_v = 0.895
G_max = 0.3
spot_centres = [L/5, L/2, 4*L/5]
plot_times = [0, T]
plot_names = ['Figure5H_start', 'Figure5H_end']

# Save images for Fig. 5H
solve_RD_model(spot_centres, plot_times, plot_names, p_dict)

```

```
# Re-specify parameters, spot locations and plotting times for Fig. 5I
R_spot = 0.07*L
c_u = 0.01
spot_centres = [L/5, L/2, 4*L/5]
plot_times = [0, T]
plot_names = ['Figure5I_start', 'Figure5I_end']

# Save images for Fig. 5I
solve_RD_model(spot_centres, plot_times, plot_names, p_dict)
```


4.0 Chapter 4:

Conserved gene signalling and a derived patterning mechanism underlie the development of avian footpad scales

Rory L. Cooper^{1^}, Victoria J. Lloyd^{1^}, Nicolas Di-Poi², Alexander G. Fletcher³, Paul M. Barrett⁴ & Gareth J. Fraser^{5, *}

*Correspondence: g.fraser@sheffield.ac.uk

[^]These authors contributed equally to this work

¹Department of Animal and Plant Sciences, University of Sheffield, Sheffield, UK

²Program in Developmental Biology, Institute of Biotechnology, University of Helsinki, Helsinki, Finland

³School of Mathematics and Statistics, University of Sheffield, Sheffield, UK

⁴Department of Earth Sciences, Natural History Museum, London, UK

⁵Department of Biology, University of Florida, Gainesville, USA

Citation: Cooper, R. L., Lloyd, V. J., Di-Poi, N., Fletcher, A. G., Barrett, P. M., and Fraser, G. J. 2019, Conserved gene signalling and a derived patterning mechanism underlie the development of avian footpad scales, *EvoDevo*, 10, 19, 1-11

4.1 Abstract

Introduction: Vertebrates possess a diverse range of integumentary epithelial appendages, including scales, feathers and hair. These structures share extensive early developmental homology, as they mostly originate from a conserved anatomical placode. In the context of avian epithelial appendages, feathers and scutate scales are known to develop from an anatomical placode. However, our understanding of avian reticulate (footpad) scale development remains unclear.

Results: Here, we demonstrate that reticulate scales develop from restricted circular domains of thickened epithelium, with localised conserved gene expression in both the epithelium and underlying mesenchyme. These domains constitute either anatomical placodes, or circular initiatory fields (comparable to the avian feather tract). Subsequent patterning of reticulate scales is consistent with reaction–diffusion (RD) simulation, whereby this primary domain subdivides into smaller secondary units, which produce individual scales. In contrast, the footpad scales of a squamate model (the bearded dragon, *Pogona vitticeps*) develop synchronously across the ventral footpad surface.

Conclusions: Widely conserved gene signalling underlies the initial development of avian reticulate scales. However, their subsequent patterning is distinct from the footpad scale patterning of a squamate model, and the feather and scutate scale patterning of birds. Therefore, we suggest reticulate scales are a comparatively derived epithelial appendage, patterned through a modified RD system.

4.2 Introduction

Integumentary epithelial appendages are a diverse group of organs that includes scales, feathers, teeth and hair (Pispa and Thesleff, 2003). These structures facilitate a broad range of functions, such as communication, protection, thermoregulation and locomotion (Dean and Bhushan, 2010; Reif, 1985a; Ruxton and Wilkinson, 2011). Recent research has revealed they share developmental homology, as they mostly originate from a conserved epithelial placode, which develops within an initiatory field such as a feather tract (Cooper et al., 2017; Di-Poï and Milinkovitch, 2016; Jung et al., 1998; Musser et al., 2015). This placode is characterised by conserved patterns of gene expression in the epithelium and underlying mesenchyme, as well as columnar basal epithelial cells which exhibit a reduced rate of proliferation (Ahtiainen et al., 2014; Di-Poï and Milinkovitch, 2016; Tanaka and Kato, 1983). The spatial distribution of these conserved placodes during development, and therefore the ultimate pattern of adult epithelial appendages, is important for facilitating their diverse functions.

Epithelial appendage patterning is thought to be controlled by a reaction–diffusion (RD) system, whereby interactions between differentially diffusing activatory and inhibitory morphogens give rise to autonomous pattern formation (Kondo and Miura, 2010; Turing, 1952). Previous research has indicated that RD is of widespread importance during epithelial appendage patterning of species from a diverse range of taxonomic groups, from sharks to mammals (Cooper et al., 2018; Jung et al., 1998; Sick et al., 2006). RD mediates the spatial distribution of individual epithelial placodes, which subsequently undergo morphogenesis and differentiate into their final adult form.

However, further research has demonstrated that there are exceptions to this patterning mechanism. The head scales of crocodiles are not individual developmental units. Instead,

they arise from the physical cracking of highly keratinised skin, presenting a stochastic patterning system distinct from RD (Milinkovitch et al., 2013). Additionally, mechanosensory forces in the tissue are considered to be important for the initiation of follicle patterning in avian skin (Ho et al., 2019; Shyer et al., 2017). This demonstrates that alternative processes contribute to the diversity of vertebrate epithelial appendage patterning.

The chicken embryo is an important model for studying epithelial appendage development and associated RD patterning (Jung et al., 1998). Chickens possess a range of epithelial appendages, including feathers (of which there are several types, from filoplume to flight feathers (Prum, 1999)) and various scale types (Stettenheim, 2000) (Fig. 1A–C). Overlapping scutate scales are found on the anterior metatarsal shank and the dorsal surface of the foot, whereas radially symmetrical reticulate scales are typically found on the ventral surface of the foot and digits (Fig. 1B–C) (Chuong et al., 2000a), presumably to provide cushioning and grip during locomotion.

There is uncertainty regarding the evolutionary relationships between different squamate and avian scale types (Dhouailly, 2009; Di-Poï and Milinkovitch, 2016). It has been hypothesised that squamate reptilian scales share more similarity with avian reticulate scales than avian scutate scales (Sawyer et al., 1986). However, the identification of an anatomical placode in squamate scale development indicates that reticulate scales might be derived structures (Brush and Wyld, 1980; Di-Poï and Milinkovitch, 2016; Musser et al., 2015). Reticulate scales may be distinct from other amniote epithelial appendages due to the apparent lack of individual epithelial placodes (Musser et al., 2015; Sawyer and Craig, 1977). A recent transcriptome sequencing (RNA-seq) analysis showed that gene expression during feather development is more similar to that of scutate scale development than expression during reticulate scale development (Musser et al., 2018). One conclusion from

this study suggested that reticulate scales are comparatively less derived than feathers and scutate scales, potentially representing a more primitive state. Separate research compared avian epithelial appendage development and proposed that scutate scales are secondarily derived from feathers (Wu et al., 2018); however, this study did not examine reticulate scales.

Although feathers have provided a widely used model system for studying avian epithelial appendage development (Harris et al., 2005; Jung et al., 1998), the development of reticulate scales has been largely unexplored at both cellular and molecular levels. Developmental studies exploring reticulate scales are absolutely necessary to improve our understanding of both the evolutionary relationships between different avian and squamate epithelial appendage types, and the evolution of avian-specific epithelial appendages.

Here, we examine the development of epithelial appendages in the chicken (*Gallus gallus*), focusing upon the patterning of reticulate scales. Using scanning electron microscopy (SEM), in situ hybridisation (ISH) and immunofluorescence, we ask whether the development of reticulate scales is underpinned by conserved gene signalling, known to be important throughout the development of other avian and squamate epithelial appendage types. Additionally, we investigate whether reticulate scale development follows a patterning mechanism consistent with RD simulation during their propagation throughout the footpad.

4.3 Results

4.3.1 Avian and squamate scales exhibit morphological diversity

First, we aimed to investigate the diversity of both avian and squamate epithelial appendages. To do this, we used scanning electron microscopy (SEM) to examine morphological variations in the epithelial appendages of these evolutionarily distinct

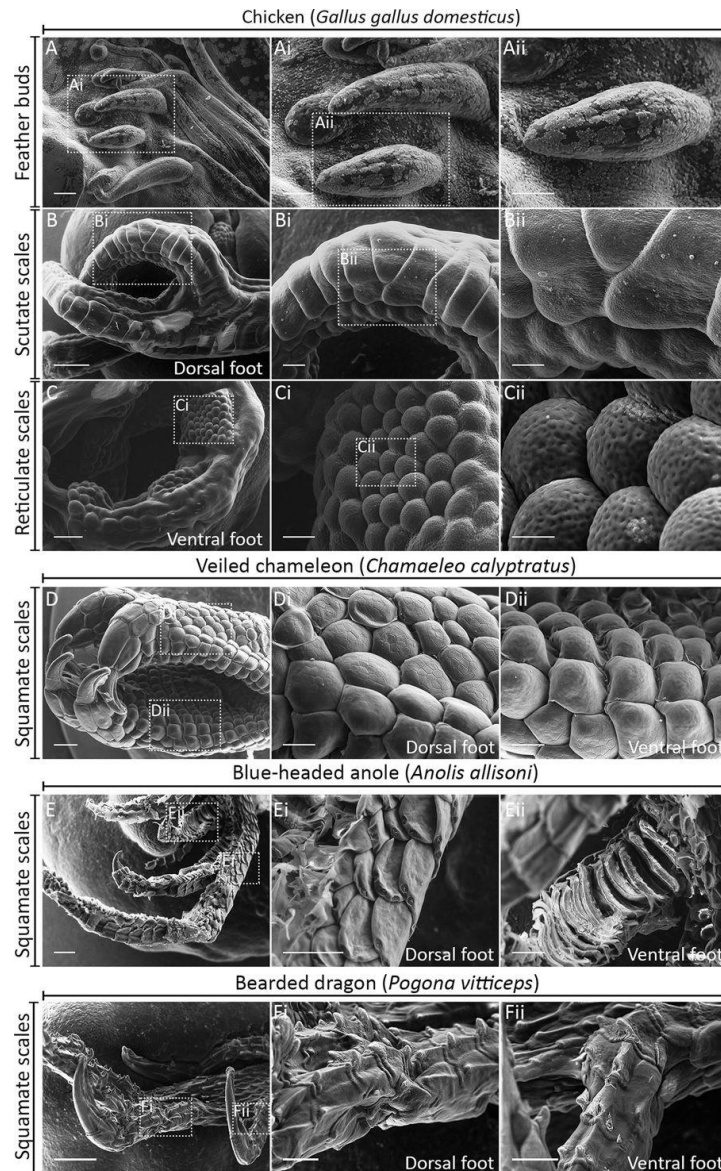


Figure 1: Morphological diversity of avian and reptilian integumentary appendages.

Scanning electron microscopy (SEM) was used to examine the morphological characteristics of avian and reptilian appendage types. The E14 chicken embryo (*Gallus gallus*) possesses feathers (A), scutate scales on the metatarsal shank and dorsal foot surface (B), and reticulate scales on ventral foot surface (C). The hatchling veiled chameleon (*C. calytratus*) possesses bilateral scales on the dorsal and ventral foot surface, which bare morphological similarity to reticulate scales (D). The hatchling blue-headed anole (*A. allisoni*) (E) and the E46 bearded dragon (*Pogona vitticeps*) (F) possess large overlapping scales, more similar to avian scutate scales. Scale bar lengths are: A, Bi, Di, Dii, Ei, Eii, Fi, Fii = 125 μm , Ai, Aii = 50 μm , B, D, F = 500 μm , Bii, Ci = 75 μm , C, E = 250 μm , Cii = 25 μm

groups. Birds and squamates share a common ancestry within Diapsida, but their respective lineages diverged from each other approximately 255 million years ago (Brusatte et al., 2015). Diverse feather types develop in tracts from the proximal–distal elongation of feather buds, covering most of the chicken embryo’s body (Fig. 1A). Scutate scales are large, overlapping, approximately rectangular structures found on the metatarsal shank and dorsal surface of the foot (Chuong et al., 2000a; Sawyer, 1972). Both feathers and scutate scales display anterior–posterior asymmetry (Fig. 1A, B) after developing from a radially symmetrical placode (Fig. 2A–P, Fig. 3A–H) (Chuong et al., 2000a). Reticulate scales form on the ventral surface of the footpad and digits (Fig. 1C). Unlike feathers and scutate scales, they maintain radial symmetry in their adult form.

We next examined the morphology of squamate scales belonging to three lizard species, to discern the diversity of these structures. This included the veiled chameleon (*Chamaeleo calytratus*) and the bearded dragon (*Pogona vitticeps*) which are members of Acrodonta, and the blue-headed anole (*Anolis allisoni*), which belongs to Pleurodonta (Wiens et al., 2012). Hatchling *C. calytratus* possess bilateral overlapping scales on the dorsal surface of the feet (Fig. 1D). Scales on the ventral foot surface retain a similar shape to the dorsal scales, but do not overlap and appear thicker than those on the dorsal surface (Fig. 1D). These ventral foot scales are morphologically similar to chicken reticulate scales (Fig. 1C). Scales of hatchling *A. allisoni* are large, overlapping and approximately rectangular, with those on the ventral foot surface appearing comparable to chicken scutate scales, in terms of their general morphology (Fig. 1E). The scales of pre-hatchling (E46) *P. vitticeps* are similar to those of *A. allisoni*, as they are large, overlapping structures on both the dorsal and ventral foot surfaces (Fig. 1F).

Overall, there appears to be less morphological diversity between the scales present on ventral and dorsal foot surfaces of the lizard species examined here than observed in the

chicken. Furthermore, we observed no clear boundary separating dorsal and ventral squamate scale types. Therefore, the scales on lizard dorsal and ventral foot surfaces may be modifications of a similar squamate scale morphology, whereas the chicken possesses morphologically distinct scale types: the scutate and reticulate scales (Chuong et al., 2000a).

4.3.2 Conserved gene signalling is observed throughout the development of reticulate scales and other avian appendages

Next, we aimed to compare and understand the developmental pathways and mechanisms underlying the early formation of different avian epithelial appendages, including reticulate scales. Most epithelial appendages have been shown to develop from the initial formation of an anatomical placode, which arises within an initiatory field such as a feather tract (Di-Poï and Milinkovitch, 2016; Jung et al., 1998; Pispá and Thesleff, 2003). The anatomical placode is defined by an epithelial thickening with columnar cells exhibiting a reduced rate of proliferation, along with conserved molecular signalling in both the epithelium and underlying mesenchyme (Di-Poï and Milinkovitch, 2016). First, to investigate cellular proliferation rate, we examined immunoreactivity of proliferating cell nuclear antigen (PCNA) during early development of avian epithelial appendages (Fig. 2).

As shown previously, avian feathers and scutate scales both develop from anatomical placodes which first arise within initiatory fields at embryonic day 7 (E7) and E10, respectively (Harris et al., 2002; Jung et al., 1998; Musser et al., 2015). These placodes exhibit columnar cells of the basal epithelium with a characteristically reduced rate of proliferation compared to surrounding cells (Di-Poï and Milinkovitch, 2016) (Fig. 2A, I, white arrowheads). Notably, PCNA immunoreactivity indicated that reticulate scales first develop from comparatively larger epithelial thickenings that emerge along the ventral side

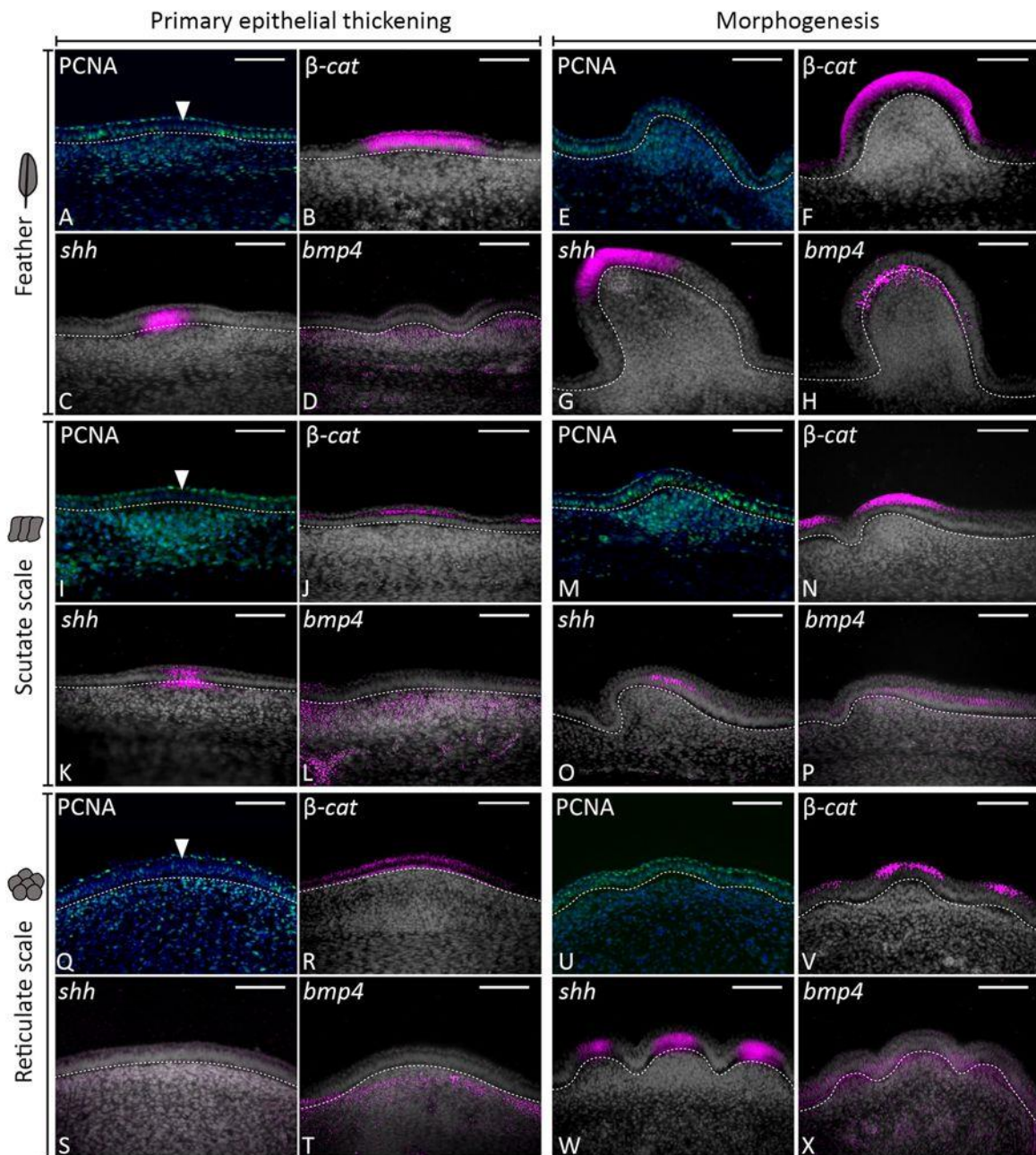


Figure 2: Conserved gene signalling underlies the development of feathers, scutate and reticulate scales. Vibratome sectioning of whole-mount ISH samples was done to examine tissue layer-specific expression of β -cat, *Shh* and *Bmp4* during development of avian epithelial appendages. Sections shown are false coloured, with DAPI in grey and gene expression in pink. Immunoreactivity of PCNA was also examined, with DAPI in blue and PCNA in green. PCNA immunoreactivity revealed columnar cells of the basal epithelium with reduced proliferation compared to surrounding cells during the primary epithelial thickening stage, for feathers, scutate and reticulate scales (A, I, Q) (white arrowheads). β -cat expression was localised to the epithelium during both the primary stage

and morphogenesis of chick feather, scutate and reticulate scale development (B, F, J, N, R, V). Similarly, *Shh* expression was localised to the epithelium, although at the reticulate scale primary epithelial thickening stage, localised expression was not observed (C, G, K, O, S, W). Expression of *Bmp4* was mesenchymal during the primary stage and observed in both the epithelium and mesenchyme during morphogenesis (D, H, L, P, T, X). Overall, these results suggest avian appendage development is underpinned by conserved gene signalling. White dashed lines separate the basal epithelium from the mesenchyme. Scale bars are 75 μm in length

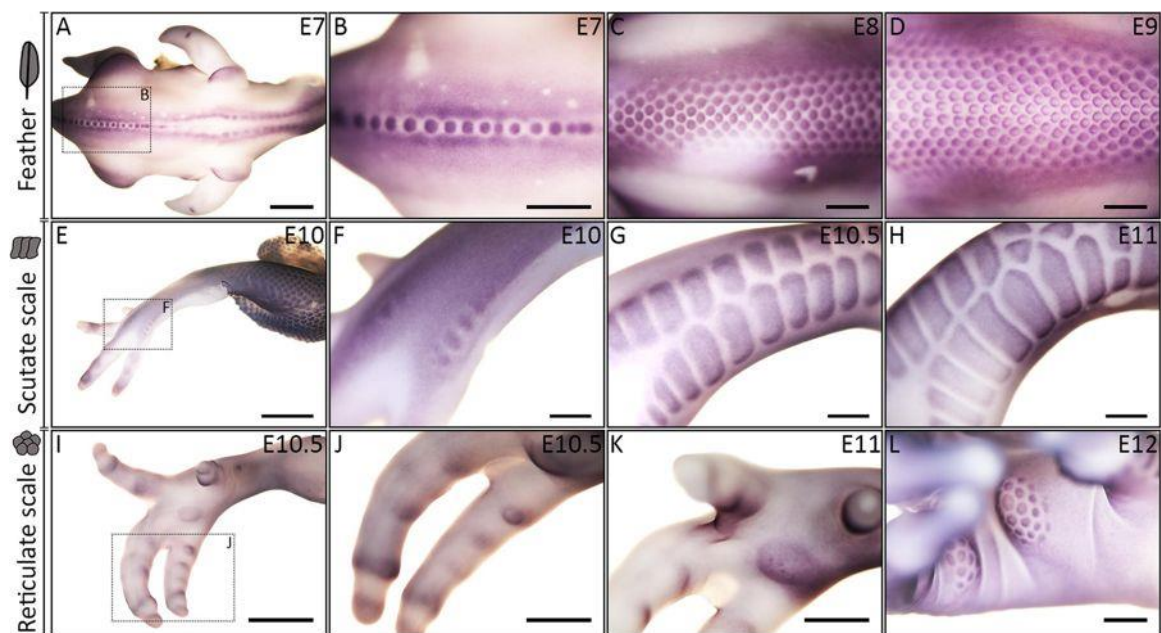


Figure 3: Localised β -catenin expression demarks feather, scutate and reticulate scale development. Whole-mount ISH for β -cat was performed to examine patterning of avian epithelial appendages. Feather patterning begins at E7, with a bifurcating dorsolateral row of feathers developing within an initiatory tract, triggering RD patterning of adjacent feathers (Jung et al., 1998) (A–D). Scutate scales form along the anterior metatarsal shank and dorsal foot surface, beginning at E10 (E–H). Restricted circular domains of β -cat preceding individual reticulate scales are visible at E10.5 along the ventral surface of the footpad and digits (I–K). These domains appear to subsequently subdivide into smaller units at E12 (L), which then form individual reticulate scales. Scale bar lengths are as follows: A, E = 2000 μm , B, C, D, I, = 1000 μm , J, K, L = 500 μm , F, G, H = 400 μm

of the footpad and digits at E10.5. These placodes also possess columnar basal epithelial cells with a slightly reduced proliferation compared to surrounding cells (Fig. 2Q, white arrowhead, Additional file 1: Figure S1).

We next aimed to investigate whether conserved molecular signalling in the epithelium and mesenchyme underlies the development of chicken epithelial appendages. First, we examined expression of the transcriptional cofactor β -catenin (*β -cat*), one of the earliest known epithelial regulators of primordium-specific gene expression (Noramly et al., 1999) (Figs. 2, 3). Whole-mount ISH revealed *β -cat* demarcates the development of feathers, scutate and reticulate scales, from initiation through to morphogenesis (Fig. 3) (Noramly et al., 1999; Widelitz et al., 2000). Whilst feather development involves anterior to posterior and lateral addition of primordia (Fig. 3A–D), similar to zebrafish scale patterning (Aman et al., 2018), scutate scale patterning occurs through the spread of placodes proximally along the metatarsal shank and distally along the digits (Fig. 3E–H). Some scutate scale placodes may fuse to produce enlarged scale buds (Wu et al., 2018). Notably, localised expression of *β -cat* marks restricted circular domains along the ventral footpad and digits (E10.5, Fig. 3I–K), which appear to subsequently subdivide into individual reticulate scales (E12, Fig. 3L).

Sectioning of whole-mount ISH samples revealed that expression of *β -cat* was specific to the epithelium of developing feathers, scutate and reticulate scales, during both the primary epithelial thickening and morphogenesis stages (Fig. 2B, F, J, N, R, V). Additionally, we examined expression of a conserved regulator of epithelial appendage development, sonic hedgehog (*Shh*) (Chiang et al., 1999; Jung et al., 1998; Morgan et al., 1998; Ting-berreth and Chuong, 1996). *Shh* expression was observed in the epithelium of developing appendages at both the placode and morphogenesis stages of development for feathers and scutate scales (Fig. 2C, G, K, O) (Jung et al., 1998). Expression of *Shh* was not localised to

the primary epithelial thickening stage of reticulate scales at E10.5, although we observed weak expression in the epithelium and underlying mesenchyme (Fig. 2S). During morphogenesis, expression of *Shh* was strong and specific to individual elevations of the epithelium (Fig. 2W). Finally, we charted the expression of bone morphogenetic protein 4 (*Bmp4*), a mesenchymal marker of placode development (Di-Poï and Milinkovitch, 2016; Jung et al., 1998). *Bmp4* expression was limited to the mesenchyme during the primary epithelial thickening stage of feathers, scutate and reticulate scales (Fig. 2D, L, T), before also shifting to the epithelium during morphogenesis (Fig. 2H, P, X). We also observed localised expression of additional conserved markers including bone morphogenetic protein 2 (*Bmp2*) and sprouty 2 (*Spry2*) during reticulate scale development (Additional file 1: Figure S2). Together, these results demonstrate that conserved molecular signalling in both the epithelium and underlying mesenchyme regulates the early development of chick epithelial appendages, including reticulate scales.

Overall, these results support previous research suggesting that feathers and scutate scales develop from an anatomical placode (Jung et al., 1998; Morgan et al., 1998; Ting-berreth and Chuong, 1996). This character is typified by columnar epithelial cells exhibiting a reduced rate of proliferation and conserved molecular signalling in both the epithelium and mesenchyme (Di-Poï and Milinkovitch, 2016; Musser et al., 2015; Noramly et al., 1999). Additionally, we provide new developmental evidence that reticulate scales may develop following a similar system, initiating at E10.5.

4.3.3 A derived patterning mechanism underlies chicken reticulate scale development

Previously, it has been suggested that reticulate scales do not develop from an anatomical placode but instead appear as symmetrical elevations at E12, although this event

may be preceded by a placode spanning the entire foot or toe pad (Musser et al., 2015). Here, we have provided evidence that circular domains of conserved localised gene expression arise upon the ventral surface of the footpad and digits before subsequent development of reticulate scales.

The epithelial thickenings that subsequently give rise to reticulate scales emerge along the digits at E10.5 (Figs. 2Q–T, 3I–L). These circular domains are larger than the initial placodes that give rise to feathers and scutate scales, and appear to subdivide into smaller, secondary units, which radiate outwards sequentially from a central unit (Fig. 4A–D). They subsequently undergo morphogenesis to become radially symmetrical reticulate scales (Fig. 1C). Such periodic patterning bears striking similarity to a RD system, similar to that which underlies avian feather patterning (Jung et al., 1998). Feather patterning involves a bifurcating dorsolateral initiator row of placodes triggering the emergence of parallel, adjacent rows (Jung et al., 1998). During reticulate scale patterning, we observed enlarged placode-shaped domains, which appear to subdivide into radially arranged smaller secondary units, as opposed to the emergence of placodes in parallel, adjacent rows in feather development (Jung et al., 1998) (Fig. 3I–L). Reticulate scale patterning may follow a derived RD mechanism, adapted from the system that underpins feather or scutate scale development.

Diverse vertebrate epithelial appendages are thought to be patterned through RD, in which interactions between diffusing activatory and inhibitory morphogens result in autonomous pattern formation (Cooper et al., 2018; Jung et al., 1998; Sick et al., 2006). Therefore, we examined whether RD simulation can explain the propagation of reticulate scales from a single, circular initiatory domain (Fig. 4E–H). We initialised a RD simulation with a central spot representing the primary epithelial thickening (Fig. 4E). Numerical exploration revealed a range of model parameter values for which waves of activatory and inhibitory

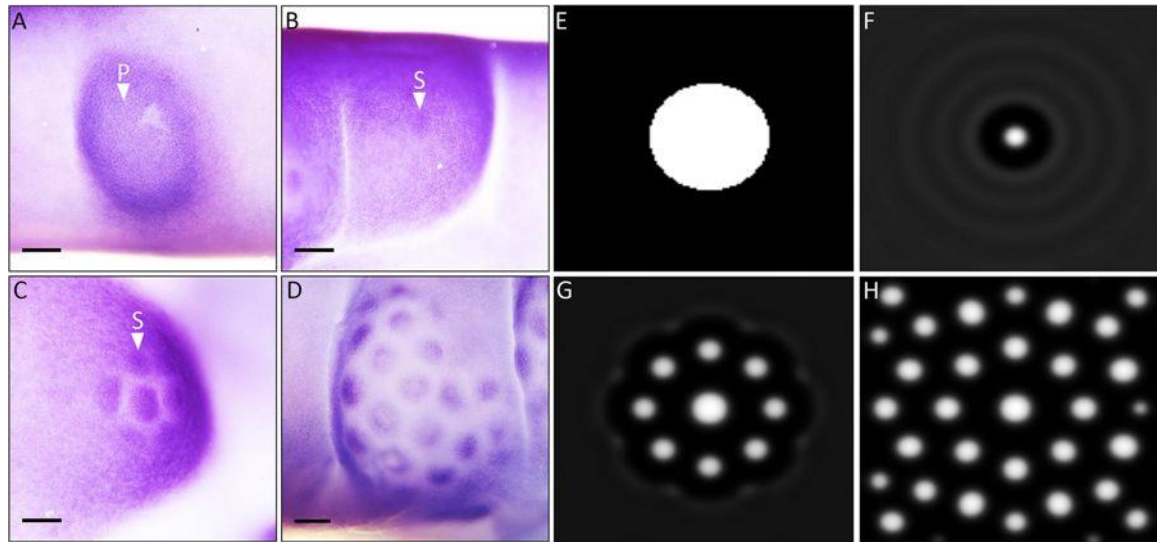


Figure 4: Reaction–diffusion simulation can explain the patterning of avian reticulate scales. Whole-mount ISH revealed that reticulate scale development begins with a circular domain (A, white arrowhead P), which subsequently subdivides into smaller secondary units, radiating outwards sequentially out from a central unit (B–D, white arrowhead S). RD simulation suggests that interactions between diffusing activatory and inhibitory morphogens can explain this patterning process (E–H). See “Methods” section for further details of RD modelling. Scale bars are 250 μm in length

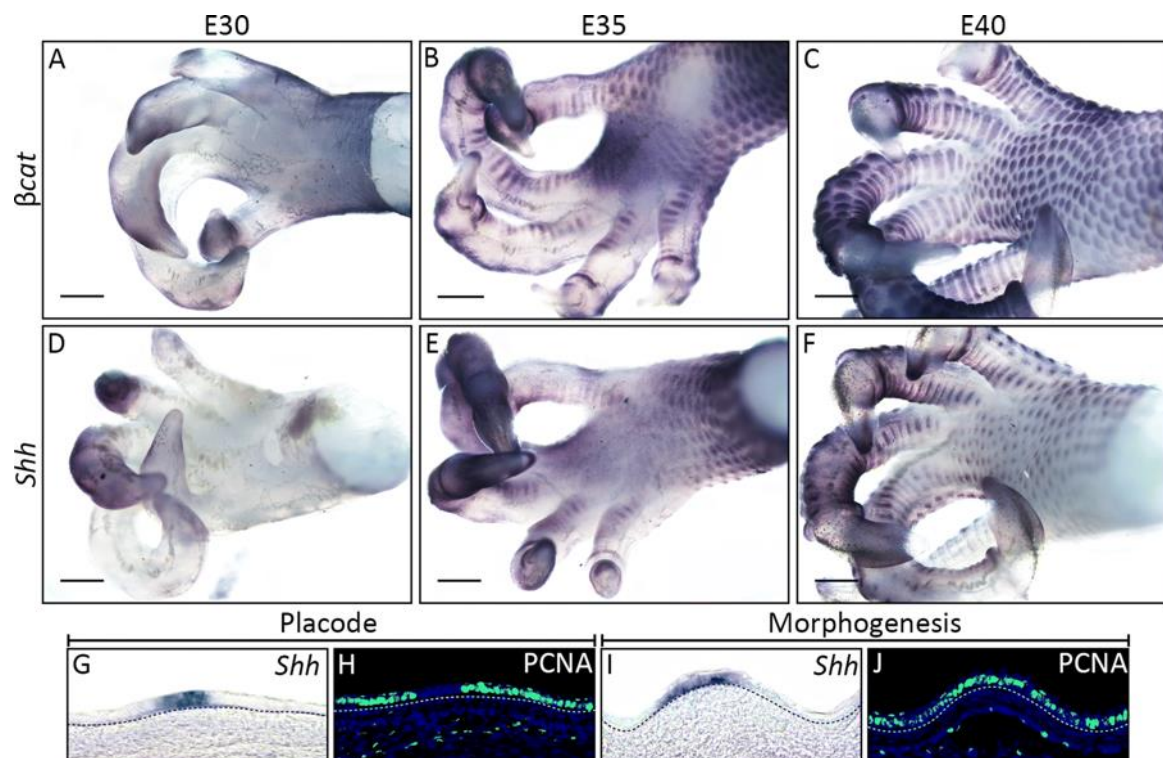


Figure 5: Scales of the bearded dragon ventral footpad arise synchronously from individual placodes. Whole-mount ISH was performed to investigate gene expression during scale development of the bearded dragon's (*P. vitticeps*) ventral foot surface. At E30, no placodes were visible (A, D). By E35, placodes were visible emerging synchronously over the footpad and digits, expressing both β -cat and *Shh* (B, E). By E40, these units had developed to cover the footpad and digits, still expressing β -cat and *Shh* (C, F). Section ISH of bearded dragon body scales revealed that *Shh* expression is epithelial during both placode stage and morphogenesis (G, I), as previously described (Di-Poï and Milinkovitch, 2016). PCNA immunoreactivity revealed that columnar cells of the basal epithelium exhibit a reduced rate of proliferation in the placode stage (H), compared to morphogenesis (J). Dashed lines separate the basal epithelium from the underlying mesenchyme. Scale bars are 500 μ m in length

signals radiated from the primary placode (Fig. 4E–H, see “Methods” for further details). From this simulation, we observed the enlarged primary domain subdividing into smaller secondary units, added sequentially from a central unit in a radial arrangement (Fig. 4E–H). This is comparable to expression patterns of β -cat observed from E10.5 to E12 (Fig. 4A–D). These results demonstrate that RD can theoretically explain the derived patterning mechanism underpinning the development of reticulate scales.

Squamates also possess distinct epithelial appendages on the ventral surfaces of their feet. This observation, in combination with the presence of reticulate scales in birds, led to the suggestion that the ancestral archosaur would have also possessed distinct reticulate scales (Musser et al., 2018). To test this hypothesis, we examined scale development on the ventral footpad of a reptilian squamate, the bearded dragon (*P. vitticeps*) (Fig. 5A–J). Reptilian body scales are known to develop from anatomical placodes (Di-Poï and Milinkovitch, 2016) (Fig. 5G–J). ISH of *P. vitticeps* samples revealed that scales of the ventral footpad and digits also develop from individual placodes that begin to emerge

synchronously at E35, and express both *Shh* and β -*cat* (Fig. 5A–F). Therefore, the footpad scales of *P. vitticeps* are developmentally distinct from avian reticulate scales in terms of their patterning, as reticulate scales arise from restricted, circular domains which subdivide into individual units (Figs. 2, 3, 4). This provides evidence that reticulate scales are derived epithelial appendages that are not present in squamates, at least in the bearded dragon, rendering the condition in the ancestral archosaur ambiguous.

4.4 Discussion

Overall, we provide evidence that conserved gene signalling underlies the development of avian reticulate scales. Restricted, circular domains of conserved localised gene expression appear along the ventral footpad surface at E10.5. These domains appear to subdivide into individual radially arranged reticulate scales by E12, following a pattern consistent with RD simulation.

One important question that remains is whether this primary initiatory domain constitutes an enlarged anatomical placode or an initiatory field, comparable to the avian feather tract. Anatomical placodes are characterised by conserved gene expression in the epithelium and underlying mesenchyme, and a local epithelial reduction in cell proliferation (Di-Poï and Milinkovitch, 2016). We show some evidence for this in avian reticulate scales (Figs. 2Q–X, 3I–J, Additional file 1: Figure S2), although we did not observe localised expression of *Shh*, a widely conserved marker of skin appendage development, in the primary circular domain (Chuong et al., 2000b). Therefore, it remains uncertain whether these circular domains are anatomical placodes, or a series of initiatory fields. Comparative transcriptome analysis of this primary circular domain with both feather tracts and placodes would help to resolve this question.

Our results demonstrate that the patterning of reticulate scales from an initial circular domain can be explained through RD simulation. RD controls the patterning of various vertebrate epithelial appendages (Jung et al., 1998; Sick et al., 2006), and alterations to this system can give rise to diverse patterns both within and between different species, facilitating important functional traits (Cooper et al., 2018). We propose that reticulate scale patterning may follow a modified RD system, derived from the patterning of feathers or scutate scales. Although the patterning of reticulate scales appears distinct from the patterning of other avian epithelial appendages, it is likely still underpinned by a RD system.

It has been suggested that squamate scales are more similar to avian reticulate scales than feathers or scutate scales (Sawyer et al., 1986). However, our developmental findings support the hypothesis that reticulate scales are derived structures (Di-Poï and Milinkovitch, 2016), thus suggesting a new evolutionary relationship between different squamate and avian scale types. Fossil evidence has revealed that structures comparable to feathers, scutate and reticulate scales were present in coelurosaurian theropods (Cuesta et al., 2015; Fucheng et al., 2006), although the prevalence of feathers in other dinosaur groups remains controversial (Barrett et al., 2015; Godefroit et al., 2014; Yang et al., 2019). Scale impressions are known for ornithischian and sauropodomorph dinosaurs, from both footprints and body fossils, but on the basis of the available morphological evidence it is currently ambiguous whether these were developmentally homologous with those of squamates or birds. However, one recent phylogenetic analysis of dinosaur evolution suggested that ornithischians and theropods share a sister group relationship, forming the clade Ornithoscelida (Baron et al., 2017). If correct, this hypothesis might increase the likelihood that ornithischian ‘feathers’ and scales, which have been suggested to include both scutate and reticulate scales (Godefroit et al., 2014), were homologous with those of

theropods as these could have been features present in the ornithoscelidan ancestor (Baron et al., 2017; Godefroit et al., 2014; Yang et al., 2019) (Additional file 1: Figure S3). Consequently, current evidence supports the appearance of reticulate scales early in theropod evolution (Cuesta et al., 2015), prior to the origin of birds, and it is plausible that they are an even more ancient dinosaurian feature.

Recent RNA-seq analysis of avian epithelial appendage types has indicated that feathers and scutate scales are more similar to each other, and to alligator scale types, than reticulate scales (Musser et al., 2018). Researchers proposed that reticulate scales may have therefore arisen relatively earlier in tetrapod evolution. However, our results demonstrate that reticulate scales develop from restricted circular domains at E10.5, which may constitute an anatomical placode. Prior research has suggested that reticulate scales emerge as symmetrical elevations at E12 (Musser et al., 2015). Therefore, this analysis may not have compared true placode stages between epithelial appendage types, providing an explanation for this dissimilarity. Additionally, this previous study showed that gene expression of scutate scales clustered with that of reticulate scales during morphogenesis (Musser et al., 2018), which is indicative of their developmental similarity in later development. Reticulate scales may be more developmentally similar to other avian appendage types than previously thought, as it is possible that they develop from an anatomical placode.

There is a degree of morphological similarity between squamate scales of the veiled chameleon (*C. calyptratus*) and avian reticulate scales (Fig. 1C, D). However, based on the development of these units we propose this similarity is a result of convergent evolution, with scales on the ventral foot surfaces of both groups having evolved to fulfil similar functions, such as grip and cushioning (Chang et al., 2009; Chuong et al., 2000a). Despite their similarity in appearance, reptilian ventral footpad scales are developmentally distinct

from reticulate scales, as their patterning follows the synchronous emergence of individual placodes at E35, rather than the subdivision of a circular domain (Figs. 4, 5).

4.5 Conclusion

Overall, we demonstrate that the development of avian epithelial appendages, including feathers, scutate and reticulate scales, is regulated by the signalling of conserved developmental genes. During reticulate scale development, circular domains of localised gene expression are observed along the ventral footpad at E10.5, constituting either anatomical placodes or circular initiatory fields. These domains subsequently subdivide into individual reticulate scales, following a patterning mechanism consistent with RD simulation. This is distinct from the patterning of squamate (*P. vitticeps*) ventral footpad scales. Therefore, we suggest that reticulate scales are derived epithelial appendages patterned through a modified RD system.

4.6 Methods

4.6.1 Animal husbandry

The University of Sheffield is a licensed establishment under the Animals (Scientific Procedures) Act 1986. All animals were culled by approved methods cited under Schedule 1 to the Act. Fertilised chicken eggs (Bovan Brown, Henry Stewart & Co., Norfolk, UK) were incubated at 37.5 °C and fixed overnight in Carnoy's solution. Embryos were dehydrated into ethanol (EtOH) and stored at –20 °C. *A. allisoni* and *C. calypttratus* specimens were a gift from Oldřich Zahradníček. *P. vitticeps* embryos were obtained from reptile breeding facility at the University of Helsinki (licence ESAVI/13139/04.10.05/2017).

4.6.2 Scanning electron microscopy (SEM)

SEM was performed using a Hitachi TM3030Plus Benchtop SEM scanning at 15,000 V. Samples were rehydrated to PBS, washed in ddH₂O and air-dried before scanning.

4.6.3 Haematoxylin and eosin (H&E) staining

H&E staining was performed as previously described (Cooper et al., 2017). Imaging was carried out using an Olympus BX51 microscope and Olympus DP71 Universal digital camera attachment.

4.6.4 In situ hybridization (ISH)

Whole-mount ISH was performed as previously described (Cooper et al., 2017), using riboprobes synthesised from the Riboprobe System Sp6/T7 kit (Promega) and DIG labelling mix (Roche). Primer sequences are as follows: Chick *β-cat* (forward: TCTCACATCACCGTGAAGGC, reverse: CCTGATGTCTGCTGGTGAGG). Data obtained from plasmids used to synthesise bearded dragon *β-cat* and *Shh*, and chick *Spry2*, *Shh*, *Bmp2* and *Bmp4*, have previously been published (Chambers and Mason, 2000; Di-Poï and Milinkovitch, 2016; Pickering et al., 2017; Riddle et al., 1993). A minimum of 6 samples were used for ISH for each gene at each stage of chicken development. As bearded dragon embryos were comparatively scarce, 3 samples were used per gene at each developmental stage. Samples were imaged using a Nikon SMZ15000 stereomicroscope. Vibratome sections were cut at a thickness of 30 μm and imaged using an Olympus BX51 microscope and Olympus DP71 universal digital camera attachment. Brightness and contrast were adjusted to improve clarity. Scale bars were added using Fiji (Schindelin et al., 2012). Cryosections after whole-mount ISH in bearded dragon were performed as previously described (Di-Poï and Milinkovitch, 2016).

4.6.5 Immunofluorescence

Immunofluorescence for PCNA was done as previously described (Cooper et al., 2017; Di-Poï and Milinkovitch, 2016). Imaging was carried out with an Olympus BX61 upright epifluorescent microscope and Olympus DP71 universal digital camera attachment, using the software Volocity 6.3.

4.6.6 Reaction-diffusion (RD) modelling

RD modelling of reticulate scale patterning was undertaken using an activator-inhibitor model proposed by Kondo & Miura (Kondo and Miura, 2010), as previously described (Cooper et al., 2018). Briefly, this model describes the diffusion of, and nonlinear reaction between, activator (u) and inhibitor (v) molecules in a two-dimensional domain. Parameter values were as follows: $d_u = 0.02$, $D_u = 0.02$, $a_u = 0.06$, $b_u = -0.07$, $c_u = 0.015$, $F_{max} = 0.19$, $d_v = 0.031$, $D_v = 0.4$, $a_v = 0.0608$, $b_v = 0.004$, $c_v = -0.025$, $G_{max} = 0.184$. For the simulations shown in Fig. 4E-H, we specified the initial condition

$$u(0, x, y) = \begin{cases} u_0 & \text{if } (x - L/2)^2 + (y - L/2)^2 < R^2, \\ 0 & \text{otherwise,} \end{cases} \quad (1)$$

$$\begin{aligned} v(0, x, y) \\ = 0, \end{aligned} \quad (2)$$

defined in a square spatial domain $0 < x, y < L$ with no-flux boundary conditions. Parameter values used were $L = 75$, $L = 1.5$. This central ‘spot’ represents a primary reticulate placode. These values were determined based on an ad hoc exploration around values previously shown to result in patterning (Kondo and Miura, 2010). See Cooper *et al.* 2018 for further details of reaction-diffusion modelling (Cooper et al., 2018).

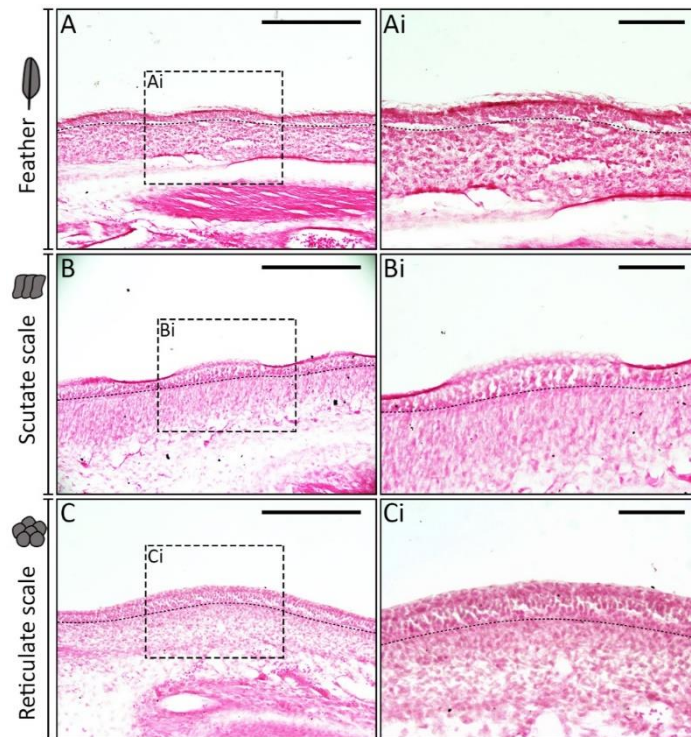
4.7 Acknowledgements

We would like to thank Oldřich Zahradníček (Charles University, Prague) for the gift of *A. allisoni* and *C. calyptratus* specimens. We also extend our gratitude to Anthony

Graham (MRC Centre, Developmental Neurobiology, Kings College London) and Matthew Towers (Department of Biomedical Science and The Bateson Centre, The University of Sheffield), for the gift of chicken plasmids.

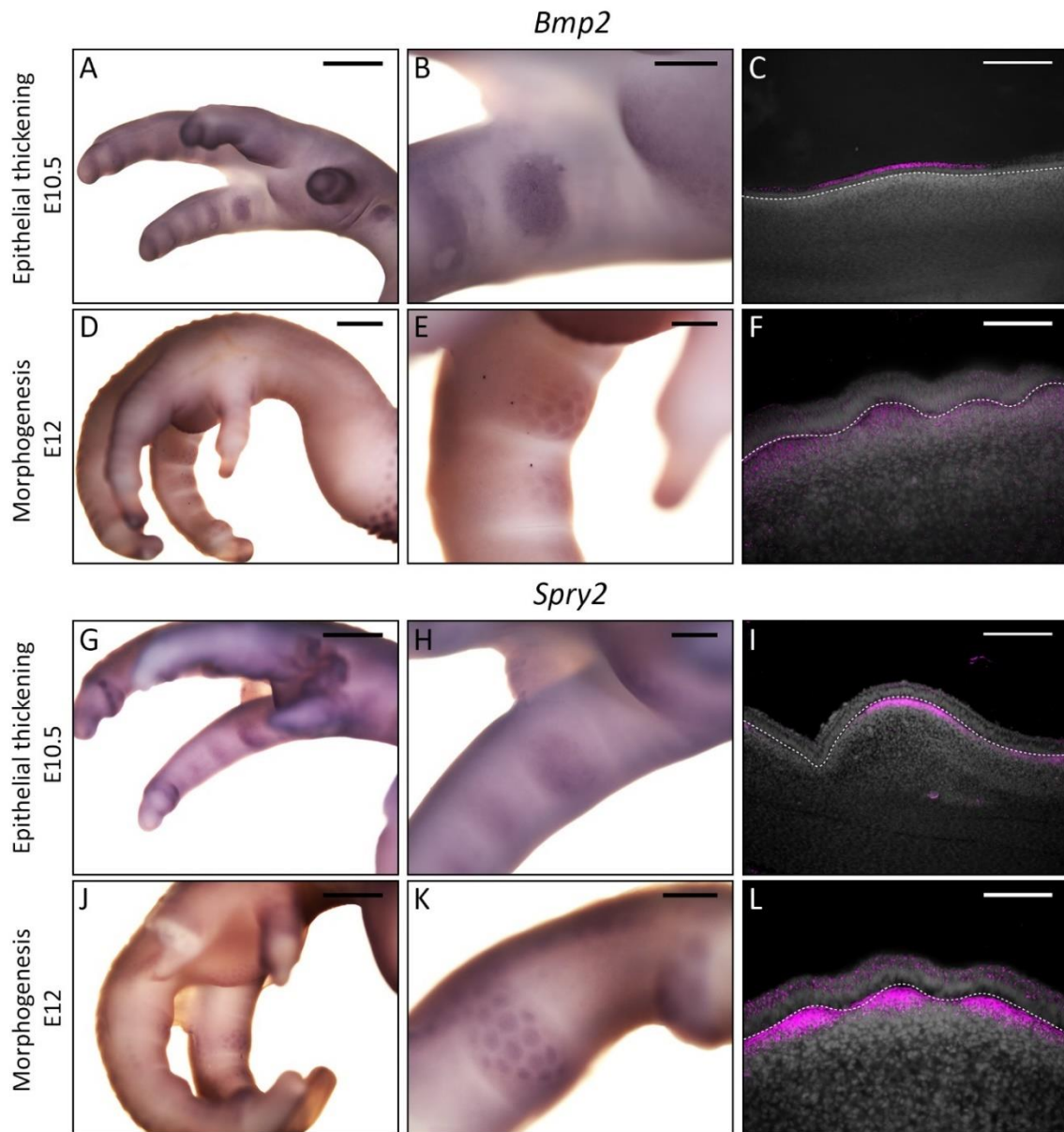
4.8 Additional materials

4.8.1 Additional file 1 – additional figures



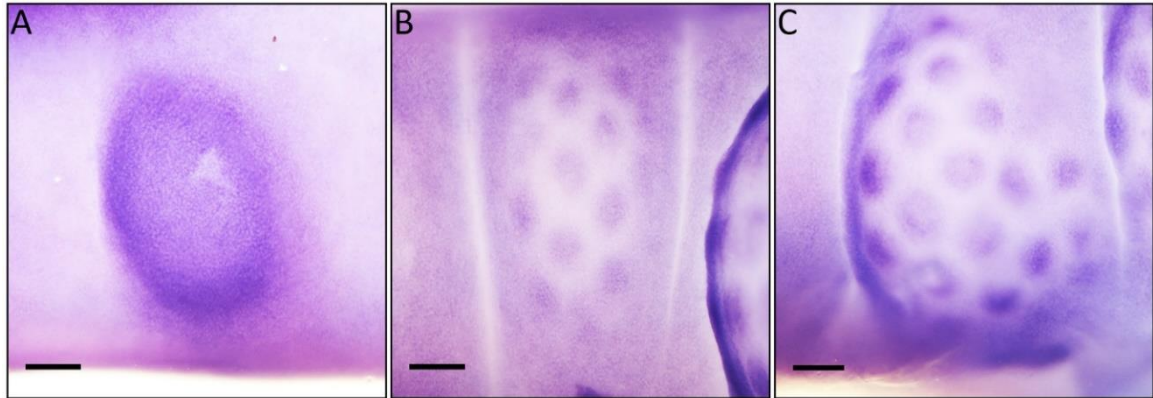
Additional Figure S1: Haematoxylin and eosin staining of chick appendage placodes.

Paraffin embedded E10.5 chicken embryos were microtome sectioned and stained with haematoxylin and eosin. As previously shown (Musser et al., 2015), feathers and scutate scales develop from a placode with localised columnar epithelial cells (A, B). Additionally, we observed localised thickening of columnar basal epithelial cells specific to early reticulate scale development (C). Black dashed lines separate the basal epithelium from the mesenchyme. Scale bar lengths are: A, B, C =150 μ m, and Ai, Bi, Ci = 75 μ m.

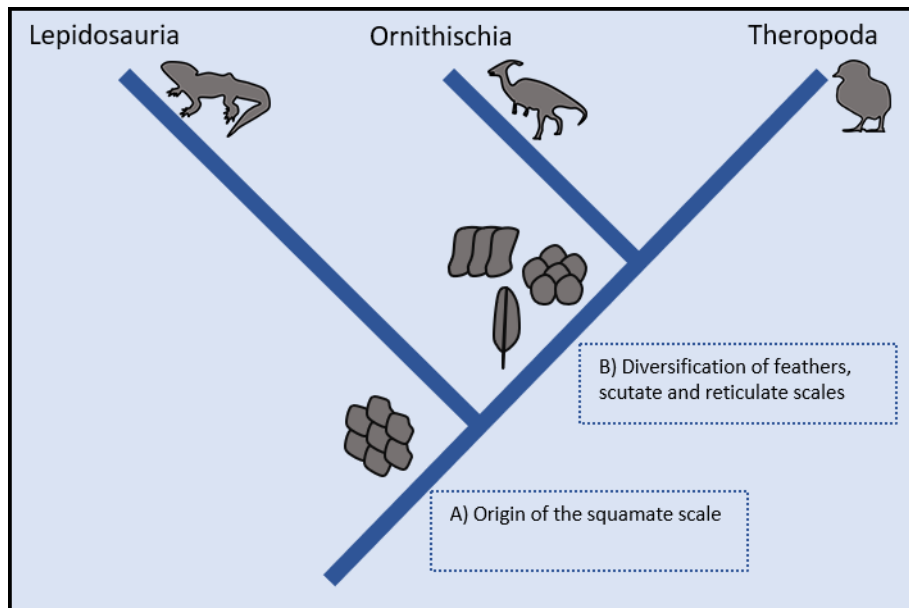


Additional Figure S2: Additional conserved gene expression during reticulate scale development. Similarly to feather development (Harris et al., 2002), we observed expression of *Bmp2* in the epithelial thickening during chick reticulate placode development (E10.5) (A-C), and the mesenchyme during morphogenesis (E12) (D-F). Furthermore, we observed mesenchymal expression of *Spry2*, a regulator of fibroblast growth factor signalling (Moura et al., 2011; Thisse and Thisse, 2005). In the epithelial thickening stage (E10.5) (G-I), *Spry2* expression was mesenchymal, and during morphogenesis weak expression was also observed in the epithelium (E12) (J-L). White dashed lines separate the basal epithelium from the underlying mesenchyme. Scale bar

lengths are as follows: A, D, G, J = 1000 μ m, B, E, H, K = 300 μ m, C, I = 150 μ m, F, L = 75 μ m.



Additional Figure S3: β -catenin staining during reticulate scale patterning (additional data). Reticulate scale patterning begins with the formation of a primary epithelial thickening at E10.5 (A). This thickening then appears to subdivide into individual units, which radiate sequentially from a central unit (B-C), in accordance with RD simulation (Fig. 4). The sequential addition of units in a radial pattern indicates that they initiate from a central point. Scale bars are 250 μ m in length.



Additional Figure S4: A hypothesis for the evolutionary relationships between squamate and avian appendage types. We propose that feathers, scutate scales and reticulate scales diversified after the divergence of Lepidosauria (which includes squamates), and prior to the divergence of Ornithischia, as they have been observed in both ornithischian and theropod fossils (Cuesta et al., 2015; Godefroit et al., 2014). These structures are retained in extant avian species, which arose from theropod dinosaurs (Brusatte et al., 2015).

4.8.2 Additional file 2: Python script for reaction diffusion simulations

```
# -*- coding: utf-8 -*-
```

```
"""
```

```
Created on Tue May 29 12:14:28 2018 for Cooper et al. 2018 -
```

```
"An ancient Turing-like patterning mechanism regulates skin denticle development in sharks"
```

```
Edited by Rory Cooper on Tue October 30 09:58:00 2018 for Cooper et al. 2019 -
```

```
"Conserved gene signalling and a derived patterning mechanism underlie the development of avian footpad scales"
```

```
Python code for the numerical solution of a 2D reaction-diffusion system. Using an explicit finite difference method, with a timestep chosen sufficiently small to ensure numerical stability, we solve the coupled PDEs
```

$$u_t = D_u(u_{xx} + u_{yy}) + F(u,v) - d_u u,$$

$$v_t = D_v(v_{xx} + v_{yy}) + G(u,v) - d_v v$$

```
on the square domain  $0 < x,y < L$ , for  $0 < t < T$ . We impose no-flux boundary conditions, and initial conditions corresponding to an 'initiator' spot as defined in the main text. The nonlinear functions F and G are defined by
```

$$F(u,v) = \min(\max(a_u u + b_u v + c_u, 0), F_{\max}),$$

$$G(u,v) = \min(\max(a_v u + b_v v + c_v, 0), G_{\max}).$$

```
@author: Alexander Fletcher
```

```
"""
```

```
import numpy as np
```

```
from numpy.linalg import norm
```

```
import matplotlib.pyplot as plt
```

```

def solve_RD_model(spot_centres, plot_times, plot_names, *params):
    """Function to solve the reaction-diffusion system and output to file"""
    # Specify grid size and time step to ensure numerical stability
    M = 128
    dx2 = (L/M)**2
    dt = 0.5 * dx2 / (4 * max(D_u, D_v))
    N = int(T / dt)

    # Specify initial conditions
    U, V, U_pen, V_pen = [np.zeros((M, M)) for _ in range(4)]
    c_y = int(M/2)
    centres = [int(x*M/L) for x in spot_centres]
    for c_x in centres:
        for i in range(M):
            for j in range(M):
                if (i - c_x)**2 + (j - c_y)**2 < int(R_spot**2/dx2):
                    U[i,j] = u_0

    # Set up plotting
    plot_timesteps = [round(i/ dt) for i in plot_times]

    # Solve the PDE system numerically
    for n in range(N+2):

        # Store penultimate state of system to assess convergence to steady state
        if n == N+1:
            U_pen[:] = U
            V_pen[:] = V

        # Plot state of system if at plotting times
        if n in plot_timesteps:
            idx = plot_timesteps.index(n)

```

```

plt.figure()

fig
plt.imshow(np.transpose(U),interpolation='bilinear',cmap='binary_r',extent=[0,L,0,L],orig
in='lower')

plt.axis('off')

fig.axes.get_xaxis().set_visible(False)

fig.axes.get_yaxis().set_visible(False)

plt.savefig(plot_names[idx]+' .png',bbox_inches='tight',pad_inches=0)

d2U = (U[1:-1,0:-2]+U[1:-1,2:]+U[2:,1:-1]+U[0:-2,1:-1]-4*U[1:-1,1:-1])/dx2
d2V = (V[1:-1,0:-2]+V[1:-1,2:]+V[2:,1:-1]+V[0:-2,1:-1]-4*V[1:-1,1:-1])/dx2

Uc = U[1:-1, 1:-1]
Vc = V[1:-1, 1:-1]
F = np.minimum(np.maximum(a_u*Uc + b_u*Vc + c_u,0), F_max)
G = np.minimum(np.maximum(a_v*Uc + b_v*Vc + c_v,0), G_max)

# Update u and v
U[1:-1, 1:-1] = Uc + dt*(D_u*d2U + F - d_u*Uc)
V[1:-1, 1:-1] = Vc + dt*(D_v*d2V + G - d_v*Vc)

# Impose no-flux boundary conditions
for Z in (U, V):
    Z[0,:] = Z[1,:]
    Z[-1,:] = Z[-2,:]
    Z[:,0] = Z[:,1]
    Z[:, -1] = Z[:, -2]

# Check for convergence to steady state
tol = 1e-2
if norm(U - U_pen) < tol and norm(V - V_pen) < tol:
    print('System has reached steady state')
else:

```

```

print('System has not yet reached steady state')

if __name__ == '__main__':

##### Fig. 4C-F #####

# Specify parameters for Fig. 4C-F
D_u, a_u, b_u, c_u, d_u, F_max = 0.02, 0.06, -0.07, 0.015, 0.02, 0.190
D_v, a_v, b_v, c_v, d_v, G_max = 0.4, 0.0608, 0.004, -0.025, 0.031, 0.184
u_0 = 5
L, T = 75, 4500
R_spot = 0.2*L

p_dict = {'D_u':D_u,'a_u':a_u,'b_u':b_u,'c_u':c_u,'d_u':d_u,'F_max':F_max,
          'D_v':D_v,'a_v':a_v,'b_v':b_v,'c_v':c_v,'d_v':d_v,'G_max':G_max,
          'u_0':u_0,'R_spot':R_spot,'L':L,'T':T}

# Specify spot locations and plotting times for Fig. 4C-F
spot_centres = [3*L/5.75]
# Specify spot locations and plotting times for Fig. 4C-F
plot_times = [0, 0.2*T, 0.5*T, T]
plot_names = ['Figure4C', 'Figure4D', 'Figure4E', 'Figure4F']

# Save images for Fig. 4C-F
solve_RD_model(spot_centres, plot_times, plot_names, p_dict)

```


5.0 Chapter 5:

Exogenous sonic hedgehog protein can trigger mineralised tissue deposition in the developing shark embryo

Rory L. Cooper¹, Victoria J. Lloyd¹, Philip C. J. Donoghue² & Gareth J. Fraser^{3,*}

*Correspondence: g.fraser@sheffield.ac.uk

¹Department of Animal and Plant Sciences, University of Sheffield, Sheffield, UK

³Department of Earth Sciences, University of Bristol, Bristol, UK

²Department of Biology, University of Florida, Gainesville, USA

5.1 Abstract

Shark denticles are an ancient evolutionary innovation capable of facilitating diverse functional traits. This includes both hydrodynamic drag reduction and the provision of defensive armour. To facilitate these functions, dermal denticle morphology varies both within and between different elasmobranch species. However, the developmental basis of this morphological diversity is poorly understood. Here, we use a combination of in situ hybridization and immunofluorescence to investigate molecular signalling during denticle morphogenesis in the shark (*Scyliorhinus canicula*). We then use bead implantation treatments with exogenous sonic hedgehog (SHH) protein to manipulate normal development, at the time of first-generation denticle development. Rather than a divergence in denticle morphology, this treatment triggered the growth of subepithelial, ectopic mineralised tissue. Our results suggest that conserved genetic circuitry associated with paired appendage outgrowth also regulates denticle morphogenesis. Alterations to this genetic circuitry can result in the deposition of spheritic mineralised tissue. We suggest that such mineral deposition may have contributed to the morphological diversity of denticles throughout elasmobranchs. This provides a potential developmental explanation for the origin of their remarkable range of functions, including drag reduction and the provision of defensive armour.

5.2 Introduction

Vertebrates possess a remarkable array of epithelial appendages, including scales, spines, teeth, feathers and hair. Despite their vast morphological diversity, the development of these organs is often conserved, as they widely arise from a characteristic epithelial placode (Biggs and Mikkola, 2014; Cooper et al., 2017; Di-Poi and Milinkovitch, 2016; Pispá and Thesleff, 2003). Divergence in morphogenesis contributes to the development of distinct structures, built upon this common foundation. This divergence in form has facilitated the evolution of clade-specific functional traits, ranging from the drag reductive capacity of shark denticles, to the thermoregulative properties of mammalian hair (Dean and Bhushan, 2010; Ruxton and Wilkinson, 2011).

Morphogenesis is the process by which a conserved epithelial placode develops a specific shape (Biggs and Mikkola, 2014; Pispá and Thesleff, 2003). Sonic hedgehog (*Shh*) is a conserved ligand of the Hedgehog signalling pathway known to mediate diverse aspects of morphogenesis (Chuong et al., 2000b), including the outgrowth of paired appendages, such as limbs (Bénazet et al., 2009; Chuong et al., 2000b; Dahn et al., 2007; Gillis and Hall, 2016; Petit et al., 2017; Pickering et al., 2019; Tickle and Towers, 2017; Zuniga, 2015). During limb bud morphogenesis, *Shh* defines a mesenchymal signalling centre at the posterior margin, known as the zone of polarising activity (ZPA) (Hill, 2007; Riddle et al., 1993). The ZPA directs anterior-posterior patterning and mediates proximodistal limb bud outgrowth (Laufer et al., 1994; Niswander et al., 1994; Towers et al., 2008; Zhu et al., 2008), through various interactions including the upregulation of both gremlin 1 (*grem1*) in the posterior-distal mesenchyme and fibroblast growth factors (FGFs) in the apical ectodermal ridge (AER) (Bénazet et al., 2009; Zúñiga et al., 1999). Recent research has suggested that parallel activation of genetic circuitry controlling paired appendage development also underpins development of the cuttlefish limbs (Tarazona et al., 2019).

Therefore, this paired appendage outgrowth-associated genetic circuitry is appears widely conserved both throughout and beyond the gnathostomes.

These conserved signalling pathways are also essential for the patterning and morphogenesis of diverse vertebrate epithelial appendages (Biggs and Mikkola, 2014; Chuong et al., 2000b; Pispá and Thesleff, 2003), including both avian feathers and shark dermal denticles (Busby et al., 2019; Cooper et al., 2018; Jung et al., 1998; Lin et al., 2006; Ting-berreth and Chuong, 1996). *Shh* is likely involved with the both the determination of feather bud polarity (Ting-berreth and Chuong, 1996), and the induction of flight feathers buds (Busby et al., 2019; Kondo et al., 2018). Overall, *Shh* is important for mediating diverse morphogenetic processes, including the outgrowth of both paired and epithelial appendages.

Sharks possess a group of hard, mineralised epithelial appendages collectively known as odontodes, which includes both dermal denticles and teeth (Ørvig, 1977). These structures have been observed in the fossil record from as long as 450 million years ago (Karatajute-Talimaa, 1973; Sansom et al., 1996). They exhibit dramatic interspecific and intraspecific morphological variation (Motta et al., 2012), facilitating a range of functional traits, ranging from hydrodynamic drag reduction (Dean and Bhushan, 2010; Oeffner and Lauder, 2012), to sexually dimorphic protective armour (Crooks et al., 2013). Despite recent research highlighting the molecular basis of shark odontode development and regeneration (Cooper et al., 2018; Martin et al., 2016; Rasch et al., 2016), the mechanisms underlying their dramatic morphological diversity remain unclear.

Here, we ask whether conserved genetic circuitry associated with the regulation of paired appendage outgrowth also regulates the outgrowth of epithelial appendages in the shark. Using in situ hybridization and immunofluorescence, we examine the signalling of genes

associated with paired appendage outgrowth during shark denticle morphogenesis. We then use bead implantation experiments to functionally manipulate *shh* signalling during denticle morphogenesis, resulting in the deposition of subepithelial, ectopic mineralised tissue. Overall, our results suggest that conserved genetic circuitry associated with paired appendage outgrowth underlies the morphogenesis of denticles in the shark.

5.3 Results

5.3.1 Shark odontodes exhibit vast morphological diversity

The morphology of odontodes varies dramatically both within and between different elasmobranch species (Crooks et al., 2013; Motta et al., 2012). Using scanning electron microscopy (SEM), we investigate denticle diversity of the small-spotted catshark (*Scyliorhinus canicula*).

The catshark possesses three distinct types of denticles. Caudal denticles emerge first in the embryonic catshark, in regular dorsal and ventral rows either side of the caudal fin tip at ~60 days post fertilisation (dpf) (Ballard et al., 1993; Cooper et al., 2017; Johanson et al., 2008, 2007). They are irregular structures with highly variable posterior facing cusps (Fig. 1A). These units contain an ancient Palaeozoic dentine-type, making them distinct from other denticles of the catshark (Johanson et al., 2008). They are shed close to the time of hatching. Dorsal denticles are the next type to emerge at ~75 dpf (Ballard et al., 1993; Cooper et al., 2018). These large units form in two regularly spaced dorsolateral rows (Fig. 1B). They have a single posterior facing cusp. Dorsal denticles are subsumed into general scalation close to the time of hatching (Martin et al., 2016).

Dorsal denticle rows trigger the emergence of body denticles at ~100 dpf (Fig. 1C-E), which cover the shark following a Turing-like patterning system (Cooper et al., 2018). They exhibit morphological variation across the shark's body. In the hatchling catshark, those

located on the head between the gill arches have sharp posterior facing cusp, and ridges associated with hydrodynamic drag reduction (Fig. 1C). Body denticles on the rostrum are petal-shaped, with a single central ridge (Fig. 1D). Units from the lateral flank region are similar to those found between the gill arches, although they appear relatively smaller (Fig. 1E). Sharks also possess continuously regenerating multicuspoid teeth (Fig. 1F) (Martin et al., 2016; Rasch et al., 2016), which are structurally homologous to body denticles. Overall, there is vast morphological diversity within odontodes of the hatchling catshark. However, the molecular mechanisms underpinning this diversity remain poorly understood.

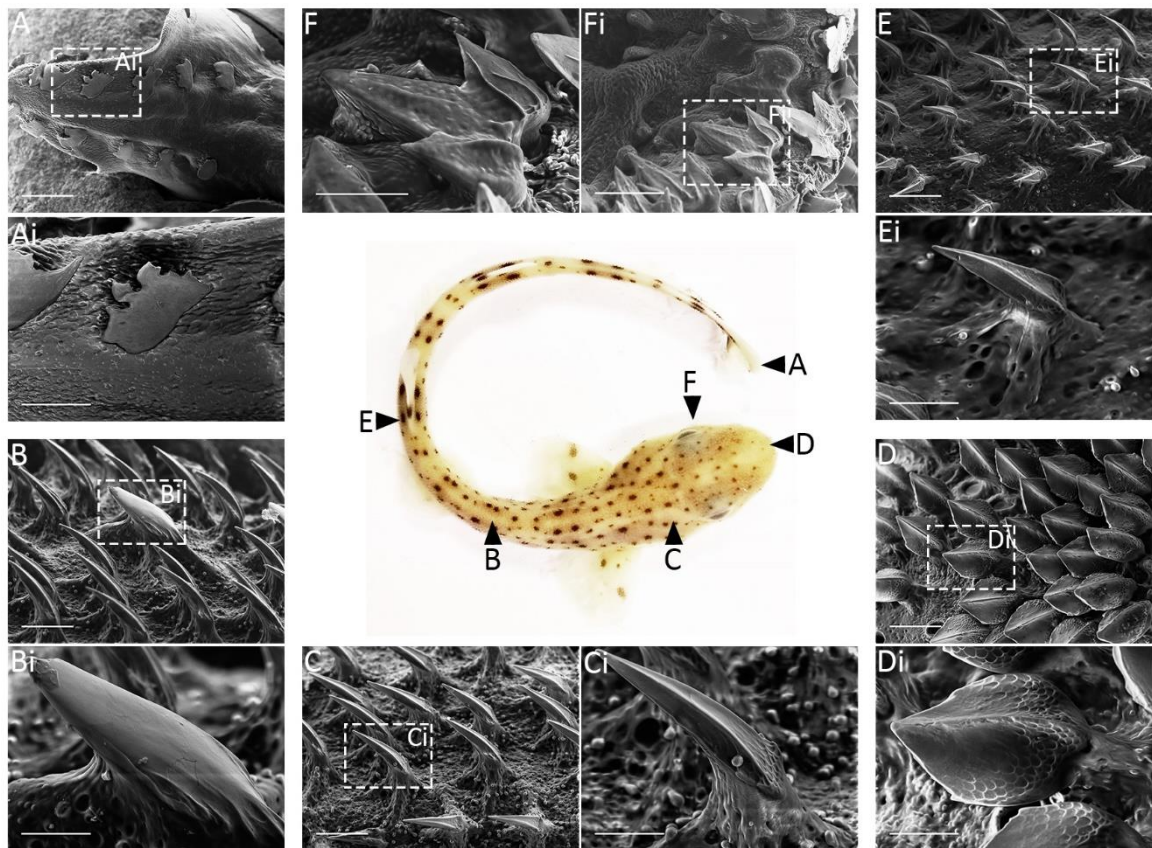


Figure 1: Scanning electron microscopy reveals intraspecific denticle diversity in the small-spotted catshark. Different areas of the catshark's (*S. canicula*) body were imaged using an SEM, to examine the diversity of denticle morphology. Regular dorsal and ventral rows of caudal denticles are the first to emerge at ~60 dpf. When mineralised, these denticles have highly variable, posterior facing cusps (A-Ai). Two dorsolateral rows of

regularly spaced dorsal denticles emerge at ~75 dpf. These units have a single large posterior facing cusp (B-Bi). Body denticles emerge at ~100 dpf, covering the body of the shark. Units located on the head between the gill arches have a single, sharp cusp, and ridges associated with drag reduction (C-Ci). Body denticles from the rostrum are petal-shaped and have a single, central ridge (D-Di). Those from the lateral flank have a sharp cusp and distinct ridges (E-Ei). Shark teeth are multicuspoid, regenerative structures (F-Fi). Scale bars for A-F are 250 μm in length, and scale bars for Ai-Fi are 100 μm in length.

5.3.2 Conserved markers of paired appendage outgrowth are expressed during denticle morphogenesis

Having observed this dramatic morphological variation in catshark odontodes, we next aimed to characterise its developmental basis. Using whole mount in situ hybridization (WMISH) and immunofluorescence, we examined signalling of developmental genes associated with vertebrate paired appendage outgrowth, during body denticle morphogenesis in the shark.

Distal outgrowth of the mouse limb bud is mediated by feedback between *Shh*, *Grem1*, and FGFs in the AER (Bénazet et al., 2009). We observed strong expression of *shh* concentrated at the posterior facing cusp of shark denticles throughout early morphogenesis (Fig. 2A-B). Furthermore, we noted expression of fibroblast growth factor 4 (*fgf4*) and bone morphogenetic protein 4 (*bmp4*) adjacent and anterior to this posterior *shh* signalling (Fig. 2C-D, G-H). Expression of fibroblast growth factor 8 (*fgf8*) was also observed, localised to individual denticle primordia (Fig. 2E-F). Immunofluorescence of SHH and proliferating cell nuclear antigen (PCNA) revealed local accumulation of SHH in the highly proliferative, early stage denticle primordia at 100 dpf (Fig. 2I-J). Interestingly, we observed spatially comparable expression patterns during feather development in the chicken embryo (Fig. 2K-T). Overall, this is indicative of conserved gene signalling associated with paired appendage outgrowth, during epithelial appendage morphogenesis.

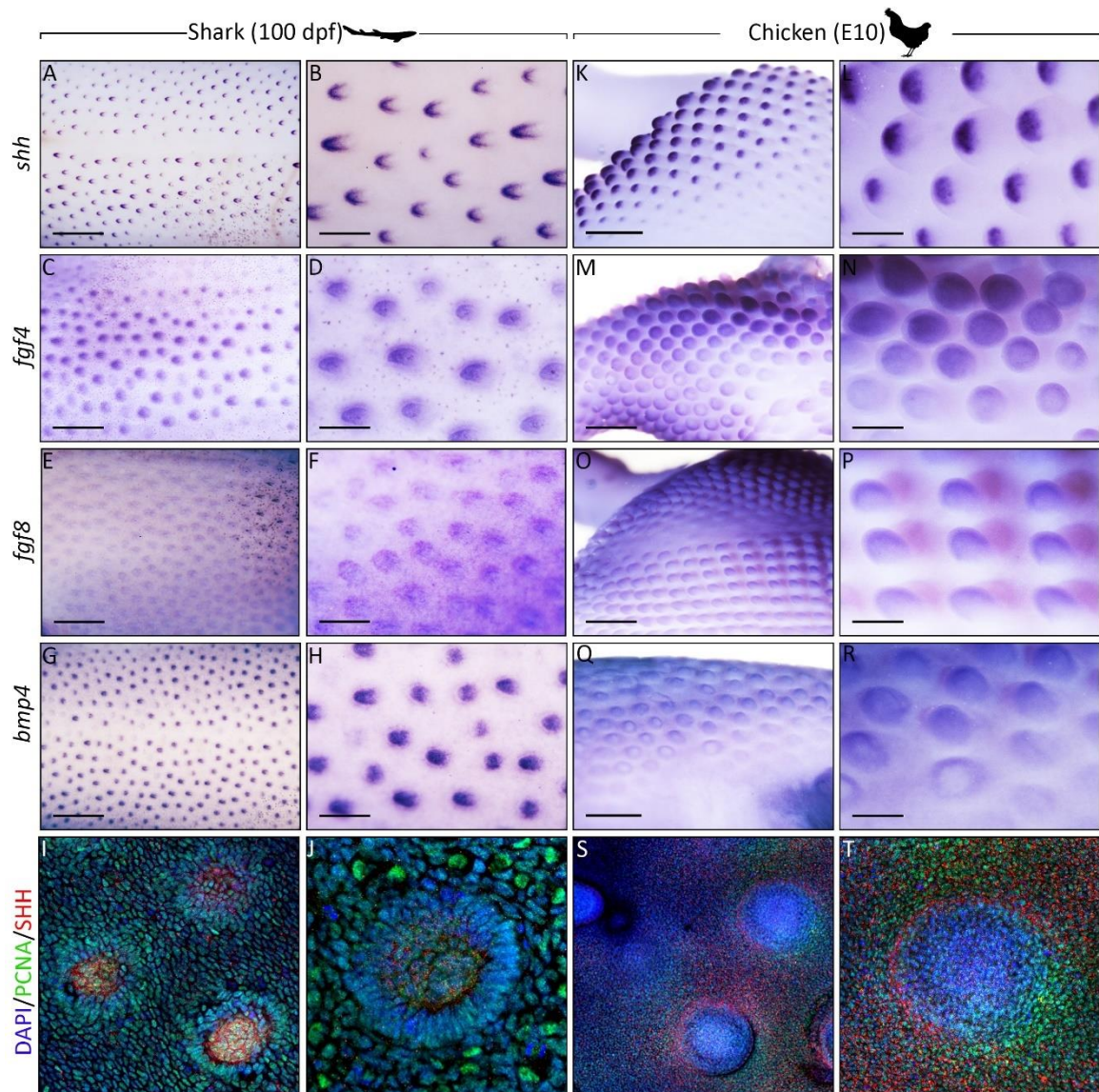


Figure 2: Expression patterns of conserved paired appendage-associated genes during shark denticle and chicken feather morphogenesis. In the shark (*S. canicula*) embryo at 100 dpf, WMISH revealed expression of *shh* restricted to the posterior facing tip of developing denticles (A-B). Furthermore, we observed expression of *fgf4* (C-D) and *bmp4* (G-H) anterior to this region of *shh* expression. Expression of *fgf8* was also noted, specific to denticle primordia (E-F). Immunofluorescence revealed SHH (red) localised to proliferative denticle primordia (PCNA shown in green, DAPI shown in blue) (I-J). Comparable expression patterns were noted during avian feather development at E10 (K-T). Scale bar lengths are: A, C, E, G, K, M, O & Q are 1000 μ m, B, D, F, H are 200 μ m, and L, N, P & R are 250 μ m in length. Silhouettes are from www.phylopic.org.

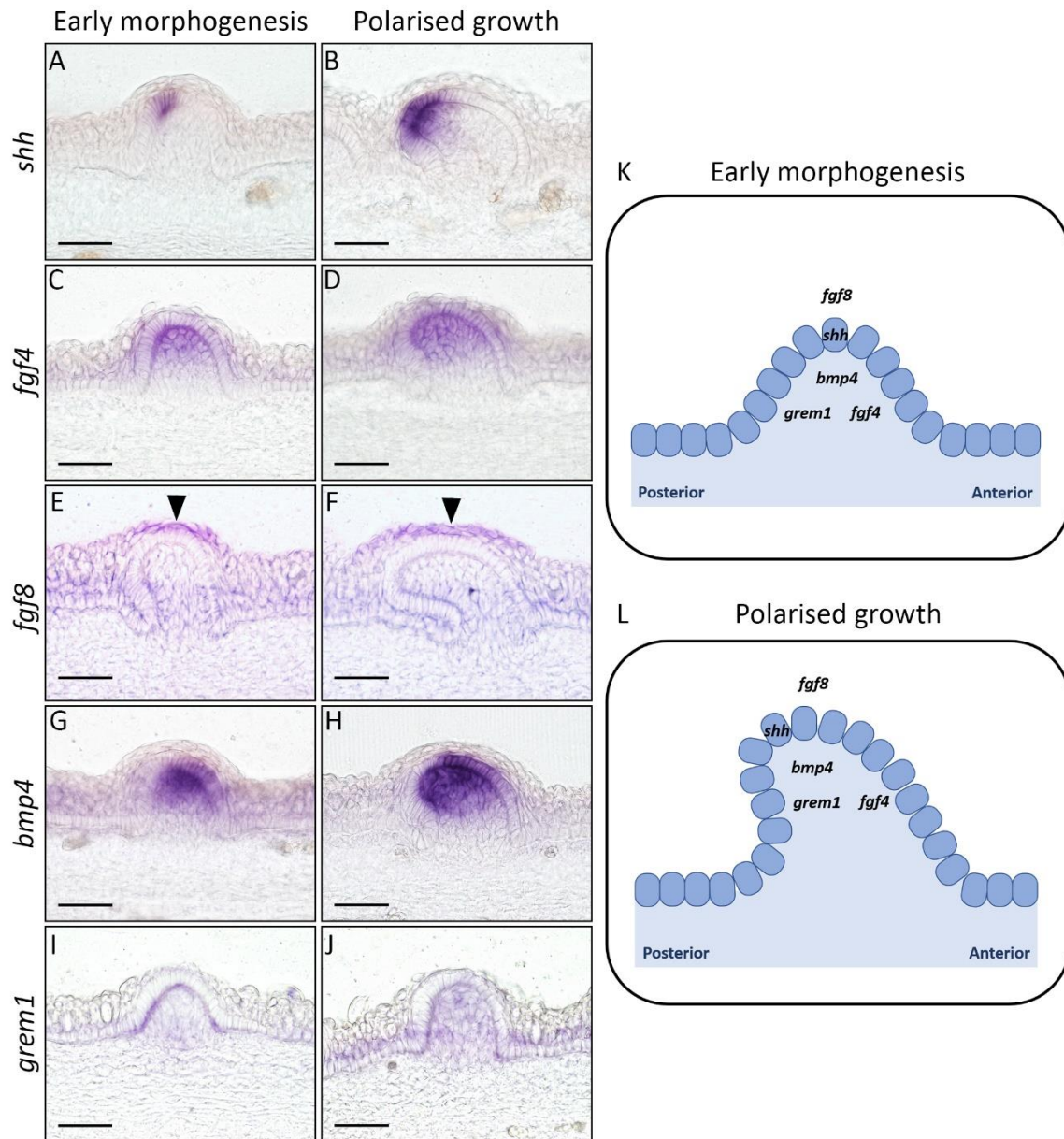


Figure 3: Sections of WMISH samples reveals tissue layer specific expression patterns of limb bud-associated genes. Vibratome sectioning of WMISH samples revealed epithelial expression of *shh* in the denticle tip during the early morphogenesis and polarised growth stages (A-B). Expression of *fgf4* (C-D), *bmp4* (G-H) and *grem1* (I-J) was mesenchymal. *fgf8* was observed in the squamous epithelial cells overlying developing denticles (E-F, black arrowheads). These gene expression patterns are summarised in the schematic diagrams (K-L) (dark blue represents columnar basal epithelial cells and light blue represents mesenchyme). Scale bars are 50 μ m in length.

In order to reveal tissue layer specific expression patterns of these genes, we next sectioned shark WMISH samples (Fig. 2). Expression of *shh* was localised to columnar basal epithelial cells of the posterior denticle tip, during both the early morphogenesis and polarised growth stages (Fig. 3A-B, K-L). Expression of *fgf8* was localised to the squamous epithelial cells overlying the columnar basal epithelial cells of the developing denticle cusp (Fig. 3E-F, black arrowheads, K-L). We also noted mesenchymal expression of *fgf4*, *bmp4* and *grem1* (Fig. 3C-D, G-L).

There are spatial differences in gene expression patterns between denticle morphogenesis and limb bud development (Bénazet et al., 2009; Zuniga, 2015). Although we observed comparable mesenchymal expression of *bmp4* and *grem1* development (Fig. 3G-J), *shh* was noted at the posterior epithelial denticle tip, rather than a mesenchymal signalling centre comparable to the ZPA (Fig. 3A-B), and *fgf4* expression was mesenchymal rather than epithelial (Fig. 3C-D). *fgf8* was expressed in the superficial epithelial cells associated with the denticle outgrowth (Fig. 3E-F), which could be considered comparable to expression in the AER during limb bud outgrowth (Bénazet et al., 2009; Zuniga, 2015). Overall, we observed conserved expression of genes known to regulate the distal outgrowth of paired appendages (Bénazet et al., 2009; Zuniga, 2015), during the morphogenesis of both shark denticles and chicken feathers (Fig. 2, Fig. 3), although we noted some shifts in tissue layer specific expression patterns.

5.3.3 Exogenous SHH treatment results in the growth of ectopic, mineralised tissue

We next aimed to establish whether these genes also exhibit functional conservation and whether variations to the gene signalling underpinning denticle morphogenesis can influence morphological diversity. Therefore, we treated embryos with recombinant SHH

protein at ~100 dpf, during the development of the first generation of body denticles, to assess the effect of upregulating the activity of this signalling pathway upon subsequent gene signalling and morphogenesis.

Beads loaded with recombinant SHH protein were implanted beneath the epithelium of the dorsal region of shark embryos at 100 dpf (Fig. 4A, supplementary figures 1-6). First, samples were fixed at 5 days post treatment (dpt, 105 dpf) and WMISH was undertaken to examine shifts in gene expression patterns (see supplementary table 1 for information regarding replicates). We noted a dramatic increase in epithelial expression of *fgf4* overlying SHH beads compared to PBS/BSA control beads (Fig. 4C-J, Supplementary figure 1, Supplementary figure 3). We did not observe shifts in expression patterns of *bmp4* as a result of SHH beading, or PBS/BSA control beading (Supplementary figure 2, Supplementary figure 4). This may indicate that the upregulation of *bmp4* in response to SHH is dose dependent. Overall, this demonstrates that SHH beading is sufficient to shift expression patterns of specific, associated genes.

Next, we fixed samples at 75 dpt (180 dpf) and undertook alizarin red staining to assess whether the treatment had produced shifts in denticle phenotypes after the first generation of body denticles were fully mineralised. Interestingly, rather than alterations to denticle morphologies, we observed the growth of ectopic, subepithelial mineralised tissue surrounding SHH loaded beads (Fig. 4 K-N, Supplementary figure 5, see supplementary table 1 for information regarding replicates). No growth of ectopic tissue was observed in PBS/BSA control beaded samples (Fig. 4O-R, Supplementary figure 6). These subepithelial ectopic tissues appeared to exhibit a specific orientation, with individual growths facing posteriorly in accordance with dermal denticles (Fig. 4K-L, supplementary figure 5). This may be indicative of an endogenous signal controlling epithelial appendage

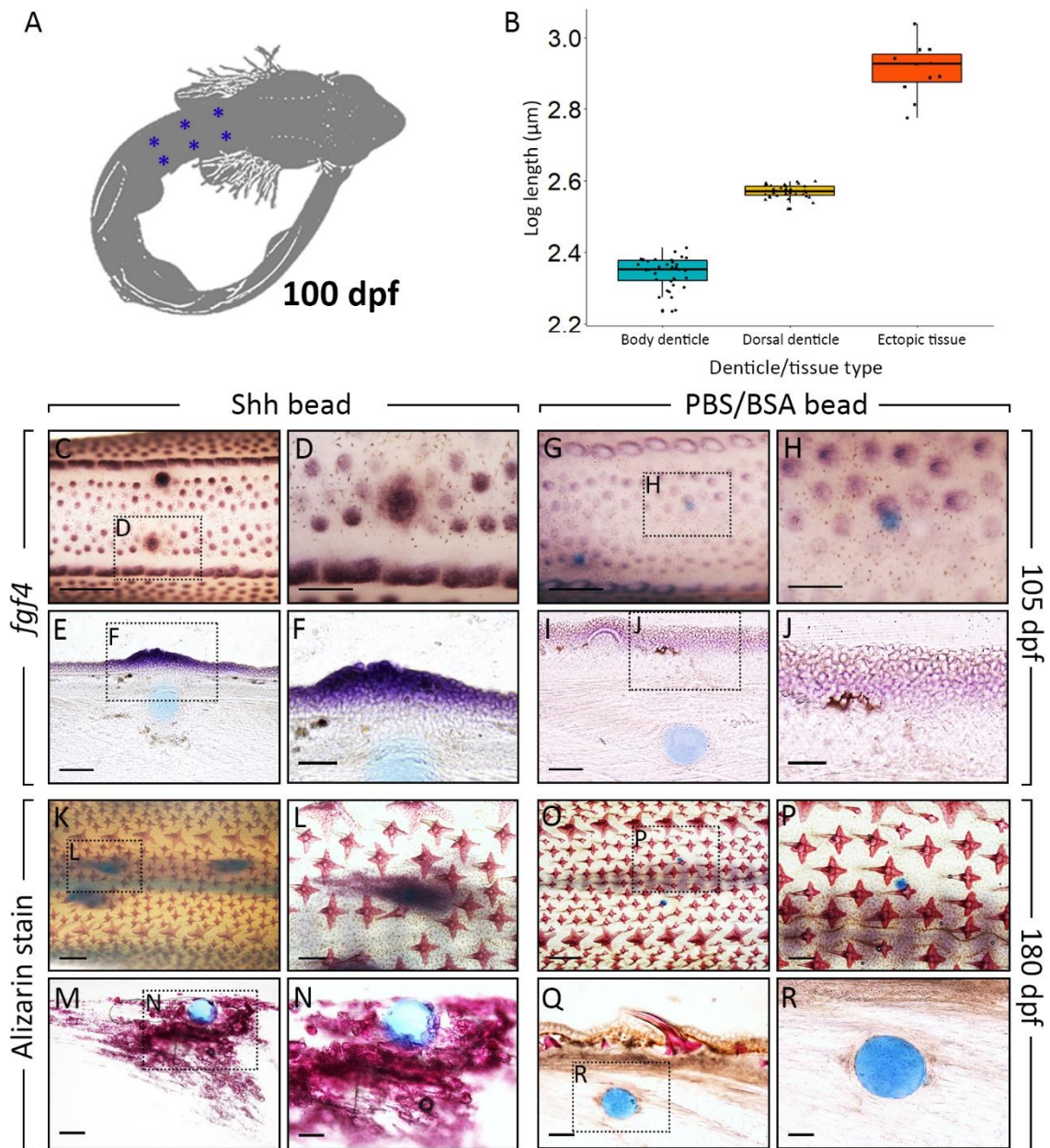


Figure 4: Exogenous SHH treatment triggers the growth of ectopic mineralised tissue.

Treatment beads loaded with SHH in PBS with 0.1% BSA, or control beads loaded with PBS with 0.1% BSA, were implanted beneath the dorsal epithelium of shark embryos at 100 dpf (A). Samples were fixed at 105 dpf to assess shifts in gene expression. A dramatic increase in local expression of epithelial *fgf4* was noted as a result of beading in SHH treated samples compared to controls (C-J, supplementary figure 1, supplementary figure 3, supplementary table 1). No alteration to expression patterns of *bmp4* were observed (supplementary figures 2, supplementary figure 4, supplementary table 1). Samples were

also fixed at 180 dpf, and stained with alizarin red to assess phenotypic alterations. Subepithelial ectopic masses of disorganised, granular mineralised tissue were observed surrounding SHH beads (K-N, supplementary figure 5, supplementary table 1). No ectopic mineralisation was observed in control samples (O-R, supplementary figure 6, supplementary table 1). These tissue masses were significantly longer than both normal body denticles (Tukey comparison, $P < 0.001$) and dorsal denticles (Tukey comparison, $P < 0.001$) (B) (supplementary table 2, supplementary file 2, see methods for details regarding statistical analysis). Scale bar lengths are: C & G are 1000 μm , D, H, K & O are 400 μm , E, I, M & Q are 100 μm , F, J, N & R are 50 μm , L & P are 200 μm .

orientation. The log length of ectopic tissue growths was significantly greater than both body denticles (Tukey comparison, $P < 0.001$) and dorsal denticles (Tukey comparison, $P < 0.001$) (Fig. 4B, supplementary table 2, supplementary file 2, see methods for details of statistical analysis). Sectioning of these samples revealed a disorganised mass of granular, mineralised tissue surrounding the SHH loaded bead (Fig. 4M-N). Overall, this demonstrates that subepithelial SHH beading during shark denticle development is sufficient to trigger the deposition of mineralised tissue.

5.4 Discussion

Our results demonstrate that conserved genes associated with the outgrowth of paired appendages are expressed during the early morphogenesis of shark denticles (Fig. 2, Fig. 3). Furthermore, we show that the local application of exogenous SHH can alter normal gene expression during denticle morphogenesis (Fig. 4C-J), and subsequently trigger the deposition of subepithelial, disorganised, granular, mineralised tissue (Fig. 4K-R). The morphology of denticles exhibits dramatic interspecific and intraspecific diversity (Fig. 1), associated with a plethora of different functions including hydrodynamic drag reduction and the provision of defensive armour (Crooks et al., 2013; Motta et al., 2012;

Oeffner and Lauder, 2012; Southall and Sims, 2003). We suggest that natural variations in the signalling of *shh* and associated pathways may influence the deposition of mineralised tissue during denticle development, thereby contributing to this morphological diversity. Overall, this provides a potential developmental explanation for how the remarkable range of functional traits facilitated by dermal denticles has arisen.

The disorganised mass of granular mineralised tissue we observed as a result of SHH beading is indicative of spheritic mineralisation (Fig. 4K-N), a type of rapid mineral growth lacking a coherent organic matrix (Ørvig, 1967). This contrasts to inotropic mineralisation, which is deposited upon an organic matrix, such as a collagen matrix. As it does not require the construction of a matrix, spheritic mineralisation is relatively fast and energy efficiency (Ørvig, 1968, 1951). It has been associated with cartilage, dermal bone, dentine and enameloid (Boyde and Sela, 1978; Downs and Donoghue, 2009; Keating and Donoghue, 2016). The spheritic-like mineralised tissue observed in this study bares notable similarity to dentine found in early shark-like fishes from the Ordovician period (Andreev et al., 2016, 2015). Identifying the specific cell and tissue type and underlying the ectopic mineralised tissue mass produced here (Fig. 4K-N) remains an important question regarding our study. This could be achieved through high resolution imaging, such as synchrotron or atomic force microscopy.

Interestingly, studies examining avian feather development have yielded similar results to those presented here (Jung et al., 1998; Morgan et al., 1998). The stage specific forced expression of SHH in the chicken embryo's skin can result in the formation of large, abnormal feather buds or the development of feathers in areas which are normally apteric (Morgan et al., 1998). Although the mineralised tissue observed in our study is subepithelial and lacks the structural characteristics of a denticle, manipulations to the *shh* pathway may contribute to the morphological diversity of epithelial appendages throughout

phylogenetically distinct taxa. Previous research has demonstrated that ectopic expression of *shh* via plasmid construct injection is sufficient to induce the deposition of bone material, resulting in the fusion of ray branches during zebrafish fin development (Avaron et al., 2006). This may be due to increased proliferation and/or differentiation of bone-secreting cells (Quint et al., 2002). Furthermore, *shh* and limb-associated signalling mediates both the anteroposterior patterning and proliferative expansion of gill arches in the little skate (*Leucoraja erinacea*) (Gillis and Hall, 2016). Additionally, SHH beading experiments have proven capable of inducing the growth of clasper-associated cartilage in the little skate (*Leucoraja erinacea*), through interactions with limb bud outgrowth circuitry (O'Shaughnessy et al., 2015). We suggest that alterations to this outgrowth genetic circuit and subsequent cellular proliferation and/or differentiation may be an important contributor to the diversity of vertebrate epithelial appendages, as well as paired appendages.

One notable difference between gene expression patterns of limb bud and epithelial appendage development is that in the latter, expression of *shh* is epithelial. It has previously been suggested that this shift is due to the relative proportion of epithelial/mesenchymal components of either structure, with limb buds having a relatively greater mesenchymal component (Ting-berreth and Chuong, 1996). These researchers suggested that if *Shh* is playing a major role in morphogenesis it should occupy the location of this major morphogenetic event. For epithelial appendages, this is the epithelium (Ting-berreth and Chuong, 1996). Furthermore, the site of initiation may be an important factor. The induction of limb bud development is mesodermal, whereas epithelial appendage development is initiated from the epithelium (Boulet et al., 2004; Min et al., 1998b; Nishimoto et al., 2015; Pispá and Thesleff, 2003; Xu et al., 1998). Although we see shifts in tissue layer specific expression patterns of genes when comparing limb bud to epithelial

appendage outgrowth, it is likely there is conservation of both gene functions and interactions underpinning their development.

Such shifts in tissue layer specific gene expression patterns may correspond to dramatic morphogenetic changes. For example, zebrafish scale formation involves the accumulation of mesenchymal cells below the epithelial placode (Harris et al., 2008), resulting in epithelial appendages that are distinct from the comparatively superficial shark denticles. Our subepithelial SHH beading experiment resulted in the formation of subepithelial mineralised tissue (Fig. 4K-N), demonstrating how shifting tissue layer specific signalling may result in dramatic phenotypic variation. The relative components of epithelial-mesenchymal interactions varies throughout vertebrate epithelial appendage development (Harris et al., 2008), and contributes to the remarkable morphological diversity of these structures.

5.5 Conclusion

Overall, we suggest that conserved, genetic circuitry associated with paired appendage outgrowth also underlies the morphogenesis of shark dermal denticles. Alterations to this conserved genetic circuitry can result in phenotypic shifts, including the deposition of ectopic mineralised tissue. This provides a potential developmental explanation for the evolution of the morphological diversity of shark denticles, which may explain how the diverse functional traits facilitated by these units have arisen.

5.6 Methods

5.6.1 Shark and chick husbandry

The University of Sheffield is a licensed establishment under the Animals (Scientific Procedures) Act 1986. All animals were culled by approved methods cited under Schedule 1 to the Act. *S. canicula* embryos were purchased from North Wales Biologicals,

UK, and raised in oxygenated artificial saltwater (Instant Ocean) at 16°C. Embryos were culled using MS-222 (Tricaine) at 300 mg/litre and fixed overnight in 4% paraformaldehyde in phosphate-buffered saline (PBS). Fertilized Bovan brown chicken eggs were purchased from Henry Stewart & Co., Norfolk, UK, incubated at 37.5°C, and fixed overnight in Carnoy's solution. Following fixation, shark and chicken embryos were dehydrated through a graded series of PBS to ethanol (EtOH) and stored at -20°C.

5.6.2 Scanning electron microscopy (SEM)

SEM was undertaken using a Hitachi TM3030Plus Benchtop SEM scanner at 15,000 V.

5.6.3 Alizarin red clear and staining

Fixed, dehydrated shark embryos were rehydrated into PBS and stained overnight in alizarin red in potassium hydroxide (KOH), as previously described (Cooper et al., 2017). Imaging was conducted using a Nikon SMZ15000 stereo-microscope, and scale bars were created using Fiji (Schindelin et al., 2012).

5.6.4 In situ hybridization

The design of digoxigenin-labelled antisense riboprobes and subsequent *in situ* hybridization was undertaken as previously described (Cooper et al., 2018, 2017). Whole mount samples were imaged using a Nikon SMZ15000 stereomicroscope and then embedded in gel albumin and sectioned with a vibratome (Leica VT1000S). Sections were imaged using an Olympus BX51 microscope and Olympus DP71 Universal digital camera attachment. Fiji was just to adjust brightness and contrast of whole images to improve clarity, and add scale bars (Schindelin et al., 2012).

5.6.5 Whole mount immunofluorescence

Samples were rehydrated from EtOH through a graded series of PBS with 0.5% Triton (PBS-T) and treated with 10µg/ml proteinase k for 20 minutes. Samples were then incubated in 5% goat serum with 1% bovine serum albumin in PBS for the blocking stage. Primary antibody staining took place for 2 days at 4°C, using both Anti-SHH (AV44235, Sigma-Aldrich) and Anti-PCNA (ab29, Abcam) at a concentration of 1:500. Incubation in the secondary antibody was performed under the same conditions, using goat anti-mouse Alexa Fluor 488 and goat anti-rabbit Alexa Fluor 647 (Thermo Fisher) respectively. Samples were counterstained with DAPI before imaging with a Zeiss LMS 880 with Airyscan. Images shown in Figure 2 were composed using the standard deviation projection of a Z-series in Fiji (Schindelin et al., 2012).

5.6.6 Bead implantation experiments

Shark embryos were treated with Affigel-blue beads (Bio-Rad) loaded with human recombinant SHH protein (1mg/ml; RayBiotech), diluted in PBS with 0.1% BSA. Control beads were soaked in PBS with 0.1% BSA. Shark embryos at ~100 dpf were removed from their egg cases and anaesthetised using MS-222 (Tricaine), before beads were surgically implanted using sharpened tungsten wire. Embryos were implanted with either 4 or 6 beads, depending on the time taken for implantation. See supplementary table 1 for replicates regarding bead implantation experiments. Embryos were then cultured in 70ml plastic containers (Sarstedt) floating in a 200-litre tank and fixed for analysis at either 5- or 80-days post-treatment. Clear and stained samples were first imaged using a Nikon SMZ15000 microscope, and then embedded in gel albumin and sectioned using a vibratome (Leica VT10000S). Sections were imaged using an Olympus BX51 microscope and Olympus DP71 Universal digital camera attachment.

5.6.7 Statistical analysis of mineralised tissue lengths

Using R, we assessed differences in log lengths of mineralised tissues (body denticles, dorsal denticles and ectopic mineralised tissue) between groups using a linear mixed effects model with the lmer function of the lme4 package (Bates et al., 2015). We included sample as an intercept only random effect and assessed statistical significance using a likelihood ratio test with a Chi-squared distribution. Finally, we assessed pairwise comparisons between groups, using Tukey multiple comparison test with the glht function from the multcomp package (Hothorn et al., 2008). The R code used to generate box plots from Figure 4 and undertake this statistical analysis are included as supplementary file 2.

5.7 Acknowledgements

We would like to thank Darren Robinson and Nick Van Hateren for assistance with confocal microscopy. We extend our gratitude to Moya Smith and Mason Dean for discussions regarding the interpretation of results from our functional experiments.

5.8 Supplementary materials

5.8.1 Supplementary file 1: Supplementary figures

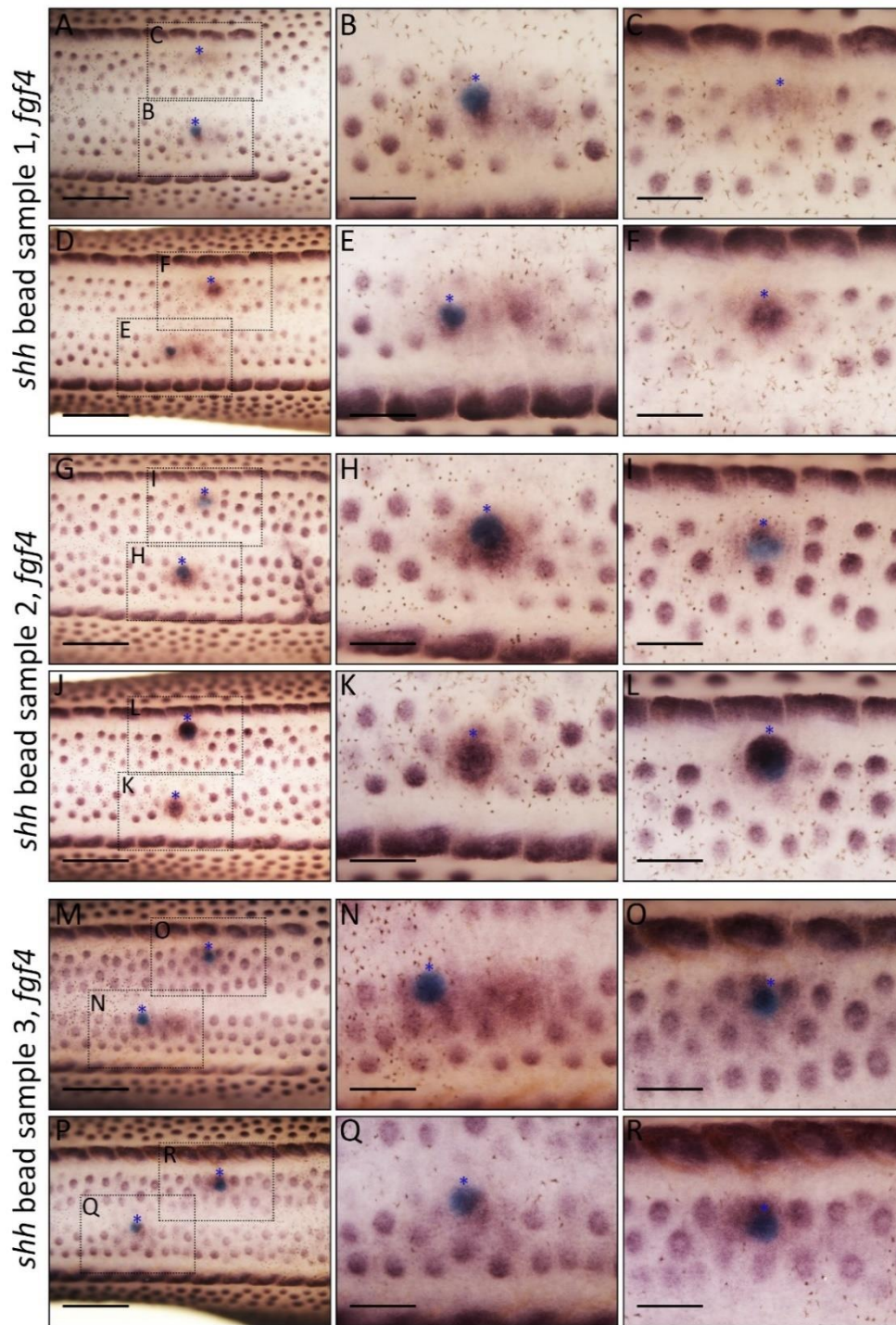
Supplementary table 1: Summary of the number of replicates for bead inhibition experiments (shown in Figure 3 and supplementary figures 1-6)

Stage fixed (dpf)	Analysis type	SHH bead (number affected/total)	PBS/BSA control bead (unaffected/total)
105	ISH – <i>fgf4</i>	12/12 (100%)	12/12 (100%)
105	ISH – <i>bmp4</i>	0/12 (0%)	12/12 (100%)
180	Alizarin red	11/32 (34.38%)	24/24 (100%)

Supplementary table 2: data used to generate box plots (Figure 4B). Lengths and log lengths of mineralised tissues – body denticles, dorsal denticles and SHH bead induced mineralised tissue. The script to generate R code is provided in Supplementary file

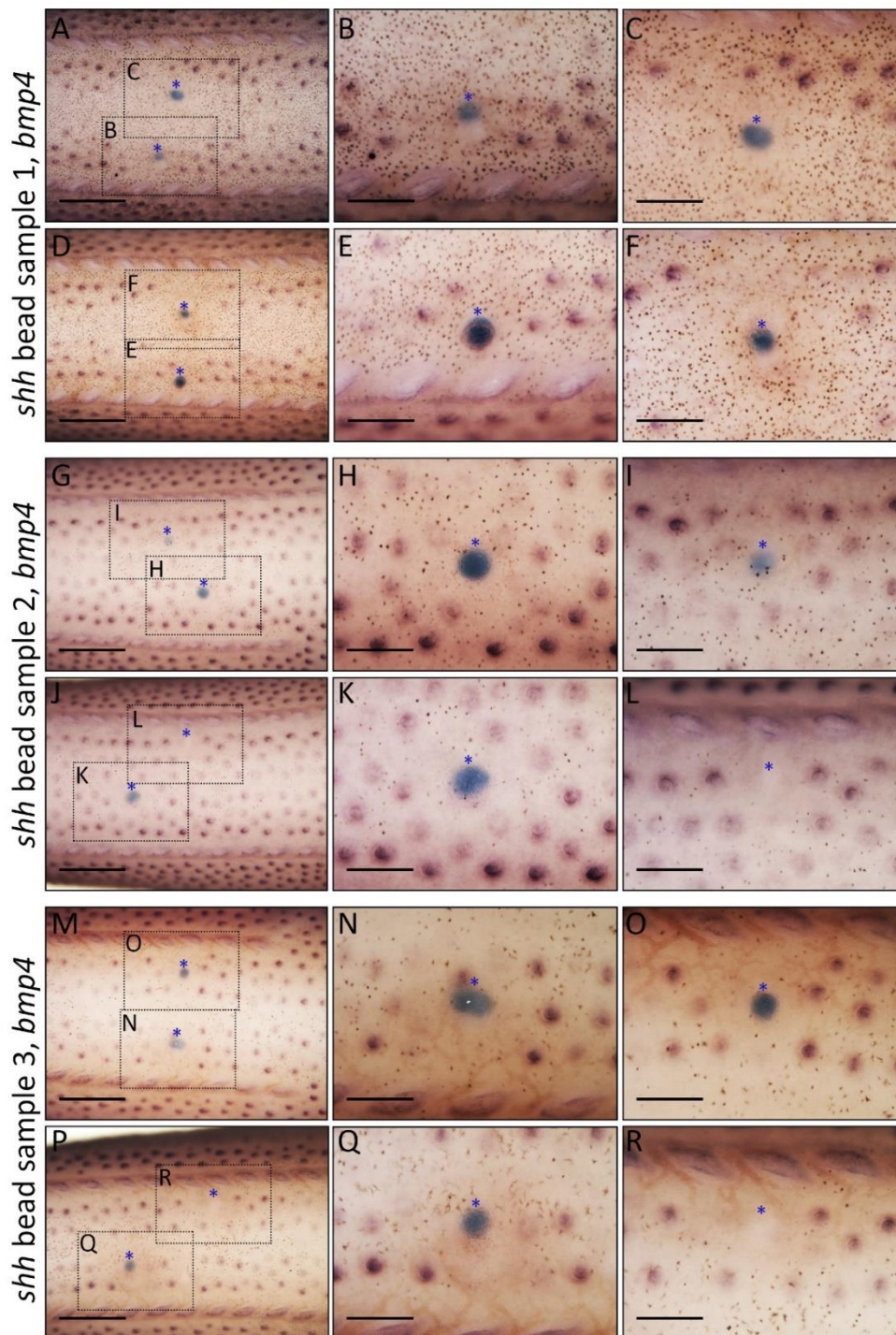
Sample	group	Denticle_number	Denticle_length_pixels	Denticle_length_μm	Log_denticle_length_μm
1	body_denticle	1	146	195	2.290034611
1	body_denticle	2	130	173	2.238046103
1	body_denticle	3	141	188	2.274157849
1	body_denticle	4	158	211	2.324282455
1	body_denticle	5	129	172	2.235528447
1	dorsal_denticle	1	270	360	2.556302501
1	dorsal_denticle	2	264	352	2.546542663
1	dorsal_denticle	3	275	367	2.564666064
1	dorsal_denticle	4	249	332	2.521138084
1	dorsal_denticle	5	258	344	2.536558443
1	shh_bead_denticle	1	633	844	2.926342447
1	shh_bead_denticle	2	693	924	2.965671971
1	shh_bead_denticle	3	579	772	2.8876173
1	shh_bead_denticle	4	583	777	2.890421019
1	shh_bead_denticle	5	693	924	2.965671971
2	body_denticle	1	177	236	2.372912003
2	body_denticle	2	182	243	2.385606274
2	body_denticle	3	169	225	2.352182518
2	body_denticle	4	171	228	2.357934847
2	body_denticle	5	174	232	2.365487985
2	dorsal_denticle	1	276	368	2.565847819
2	dorsal_denticle	2	288	384	2.584331224
2	dorsal_denticle	3	279	372	2.57054294
2	dorsal_denticle	4	273	364	2.561101384
2	dorsal_denticle	5	291	388	2.588831726
2	shh_bead_denticle	1	486	648	2.811575006
3	body_denticle	1	141	188	2.274157849
3	body_denticle	2	180	240	2.380211242
3	body_denticle	3	156	208	2.318063335
3	body_denticle	4	159	212	2.326335861
3	body_denticle	5	147	196	2.292256071
3	dorsal_denticle	1	285	380	2.579783597
3	dorsal_denticle	2	282	376	2.575187845
3	dorsal_denticle	3	273	364	2.561101384
3	dorsal_denticle	4	294	392	2.593286067
3	dorsal_denticle	5	279	372	2.57054294
3	shh_bead_denticle	1	633	844	2.926342447
3	shh_bead_denticle	2	819	1092	3.038222638
3	shh_bead_denticle	3	546	728	2.862131379
3	shh_bead_denticle	4	654	872	2.940516485
3	shh_bead_denticle	5	447	596	2.77524626
4	body_denticle	1	171	228	2.357934847

4	body_denticle	2	178	237	2.374748346
4	body_denticle	3	158	211	2.324282455
4	body_denticle	4	189	252	2.401400541
4	body_denticle	5	174	232	2.365487985
4	dorsal_denticle	1	268	357	2.552668216
4	dorsal_denticle	2	271	361	2.557507202
4	dorsal_denticle	3	280	373	2.571708832
4	dorsal_denticle	4	296	395	2.596597096
4	dorsal_denticle	5	278	371	2.56937391
5	body_denticle	1	174	232	2.365487985
5	body_denticle	2	180	240	2.380211242
5	body_denticle	3	152	203	2.307496038
5	body_denticle	4	168	224	2.350248018
5	body_denticle	5	179	239	2.378397901
5	dorsal_denticle	1	268	357	2.552668216
5	dorsal_denticle	2	281	375	2.574031268
5	dorsal_denticle	3	292	389	2.589949601
5	dorsal_denticle	4	283	377	2.57634135
5	dorsal_denticle	5	270	360	2.556302501
6	body_denticle	1	167	223	2.348304863
6	body_denticle	2	164	219	2.340444115
6	body_denticle	3	183	244	2.387389826
6	body_denticle	4	160	213	2.328379603
6	body_denticle	5	151	201	2.303196057
6	dorsal_denticle	1	291	388	2.588831726
6	dorsal_denticle	2	297	396	2.597695186
6	dorsal_denticle	3	276	368	2.565847819
6	dorsal_denticle	4	293	391	2.592176757
6	dorsal_denticle	5	289	385	2.58546073
7	body_denticle	1	194	259	2.413299764
7	body_denticle	2	169	225	2.352182518
7	body_denticle	3	181	241	2.382017043
7	body_denticle	4	179	239	2.378397901
7	body_denticle	5	172	229	2.359835482
7	dorsal_denticle	1	288	384	2.584331224
7	dorsal_denticle	2	273	364	2.561101384
7	dorsal_denticle	3	277	369	2.567026366
7	dorsal_denticle	4	282	376	2.575187845
7	dorsal_denticle	5	265	353	2.547774705

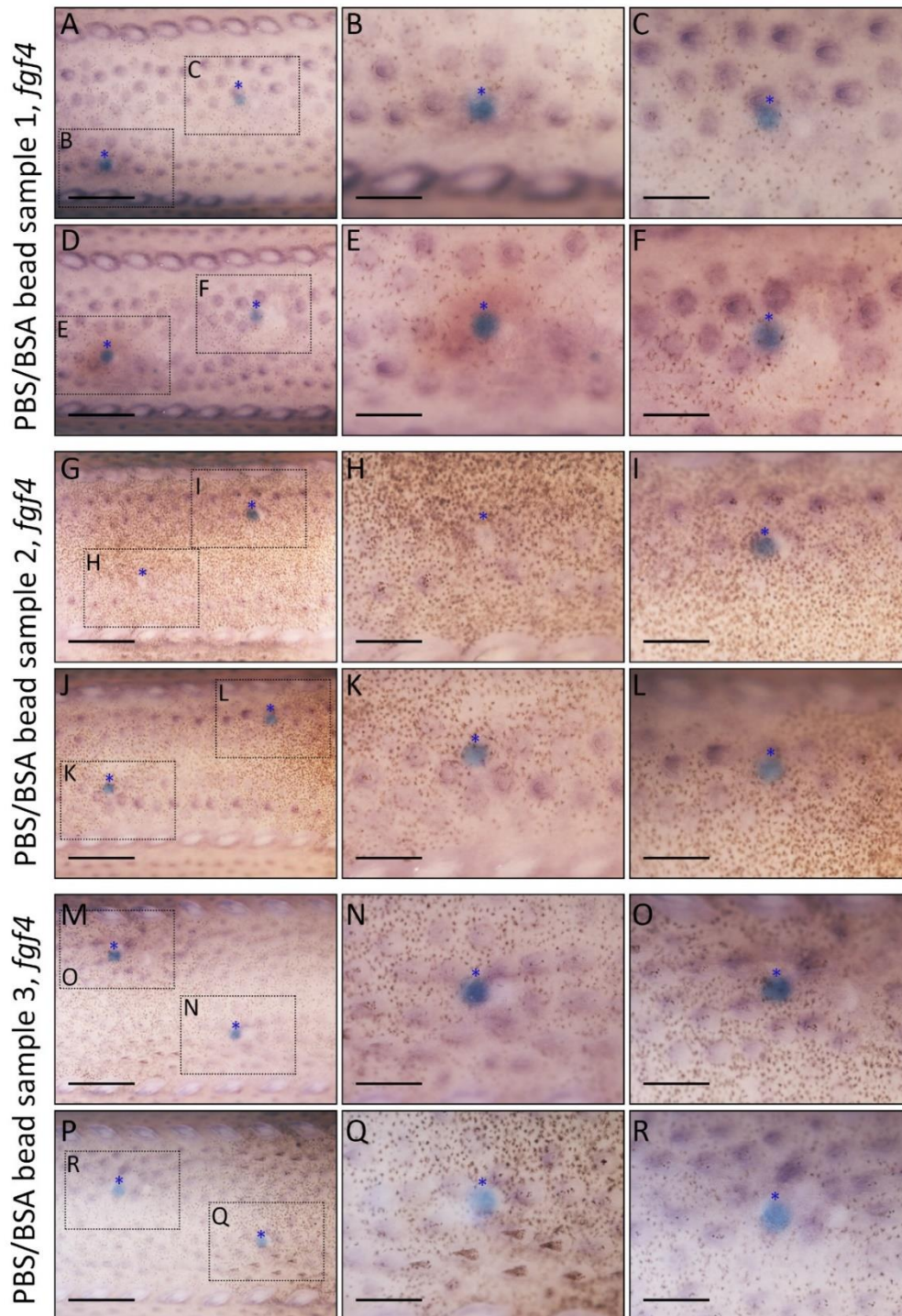


Supplementary figure 1: replicates of *fgf4* expression after SHH bead implantation.

These images show replicates of panels Fig. 4C-D, with samples beaded with SHH at 100 dpf and fixed at 105 dpf. SHH beading causes local upregulation of *fgf4* expression. The approximate site of beading is demarked with a blue asterisk. Some beads were dislodged during processing. Scale bars for A, D, G, J, M & P are 1000 μm , and B, C, E, F, H, I, K, L, N, O, Q, & R are 400 μm .



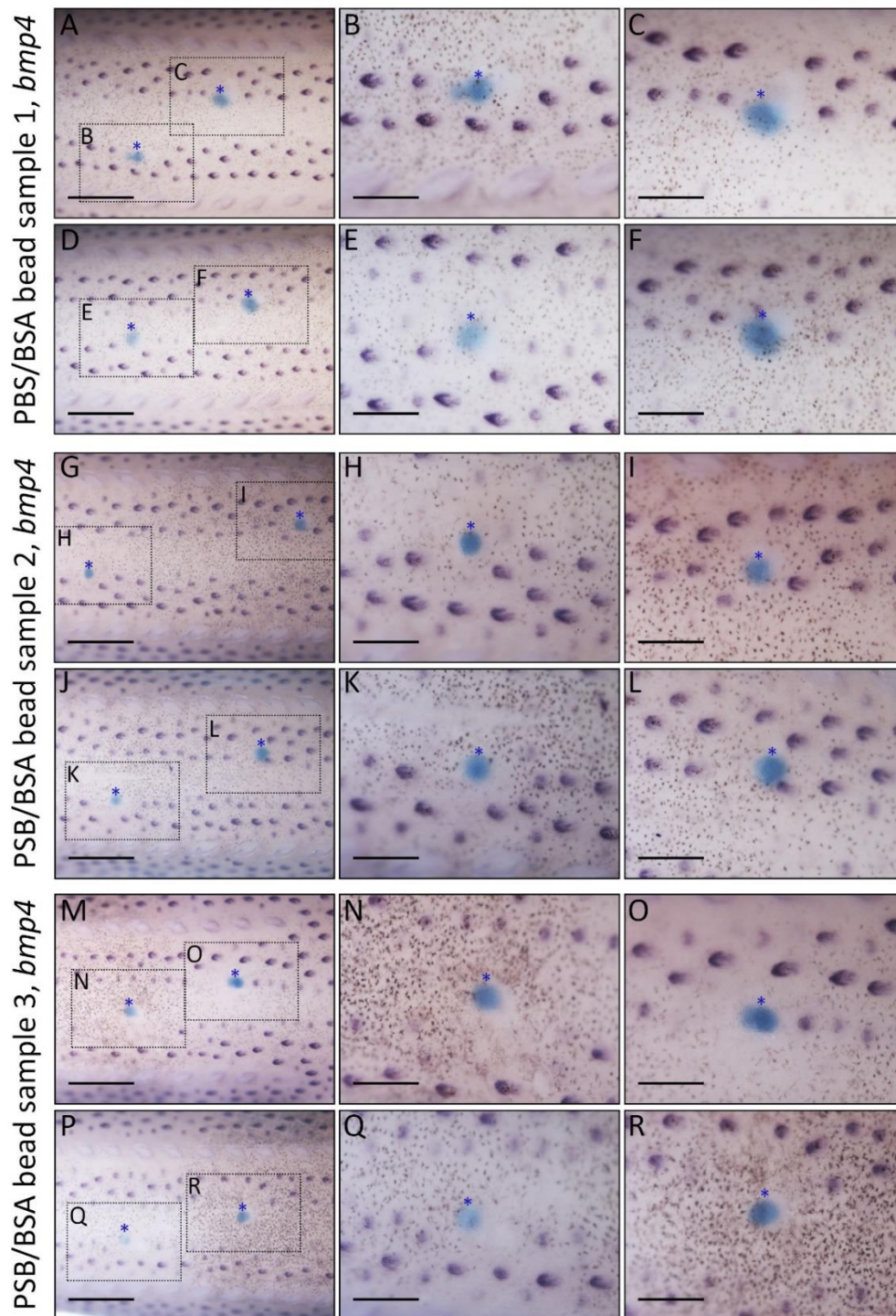
Supplementary figure 2: *bmp4* expression after SHH bead implantation. These images show *bmp4* expression in with samples beaded with SHH at 100 dpf and fixed at 105 dpf. SHH beading does not appear to disrupt local *bmp4* expression. The approximate site of beading is demarked with a blue asterisk. Some beads were dislodged during processing. Scale bars for A, D, G, J, M & P are 1000 μ m, and B, C, E, F, H, I, K, L, N, O, Q, & R are 400 μ m



Supplementary figure 3: *fgf4* expression after control PBS/BSA bead implantation.

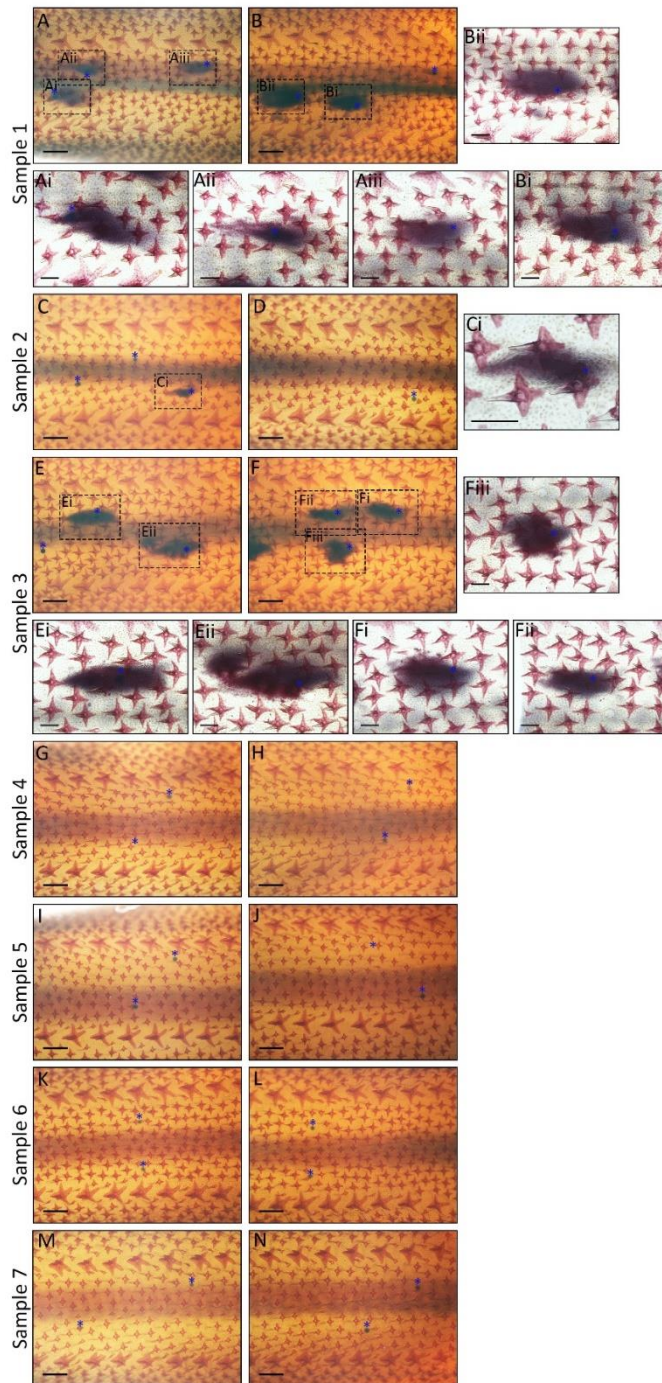
These images show *fgf4* expression in with samples beaded with control beads at 100 dpf and fixed at 105 dpf. Control beading does not appear to disrupt local *fgf4* expression.

The approximate site of beading is demarked with a blue asterisk. Some beads were dislodged during processing. Scale bars for A, D, G, J, M & P are 1000 μm , and B, C, E, F, H, I, K, L, N, O, Q, & R are 400 μm



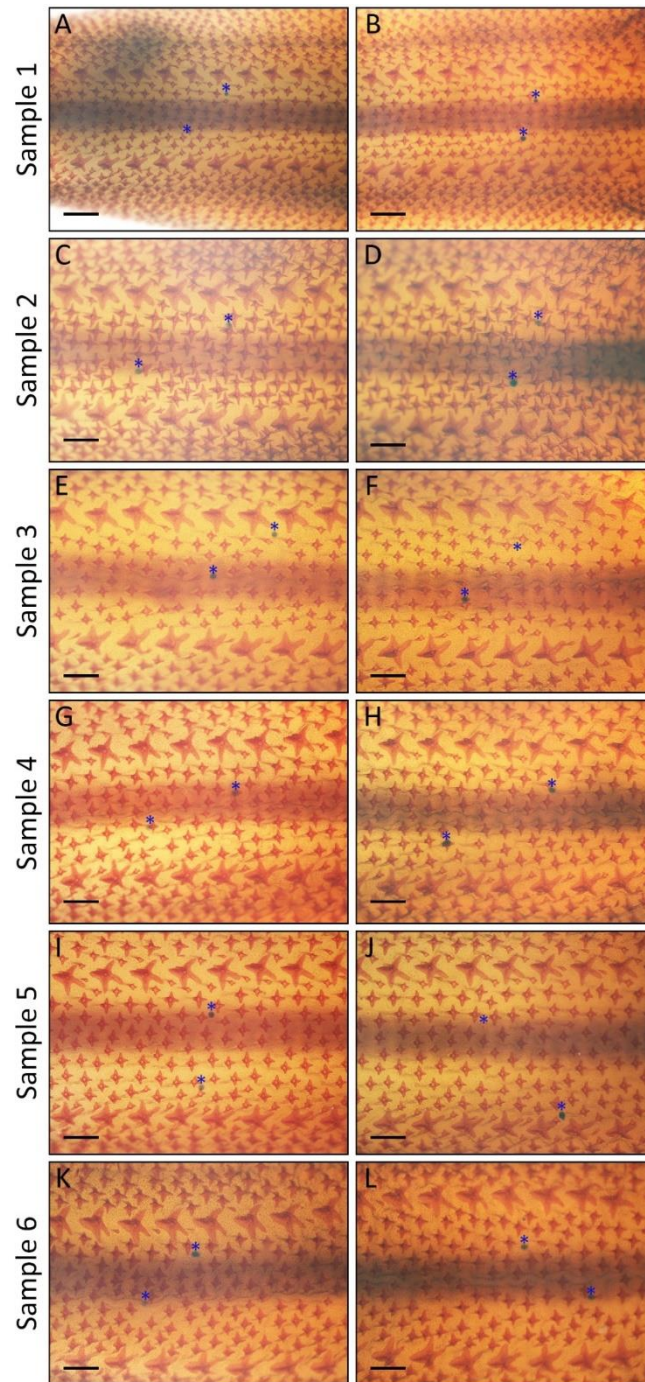
Supplementary figure 4: *bmp4* expression after control PBS/BSA bead implantation.

These images show *bmp4* expression in with samples beaded with control beads at 100 dpf and fixed at 105 dpf. Control beading does not appear to disrupt local *bmp4* expression. The approximate site of beading is demarked with a blue asterisk. Some beads were dislodged during processing. Scale bars for A, D, G, J, M & P are 1000 μm , and B, C, E, F, H, I, K, L, N, O, Q, & R are 400 μm



Supplementary figure 5: Clear and stained samples after SHH bead implantation.

These images show alizarin red staining of mineralised tissue after beading at 100 dpf with SHH loaded beads and fixation at 180 dpf. In samples 1-3, we saw growth of sub epithelial ectopic mineralised tissue at the point of beading. The approximate site of beading is demarked with a blue asterisk. Some beads were dislodged during processing. Scale bar lengths for A, B, C, D, E, F, G, H, I, J, K, L, M & N are 400 μ m, and Ai, Aii, Aiii, Bi, Bii, Ci, Ei, Eii, Fi, Fii, Fiii are 200 μ m



Supplementary figure 6: Clear and stained samples after control bead implantation.

These images show alizarin red staining of mineralised tissue after beading at 100 dpf with control beads (PBS/BSA) and fixation at 180 dpf. No growth of ectopic mineralised tissue was observed. The approximate site of beading is demarked with a blue asterisk. Some beads were dislodged during processing. Scale bar lengths are 400 μ m.

5.8.2 Supplementary file 2: R code for statistical analysis

```
# 30/09/19, R.L.C: Box plots and mixed model for mineralised tissue length analysis
```

```
# Set working directory and import data
```

```
setwd("D:/PhD Work/University Work/Fraser Lab Work/ZPA paper")
my_data <- read.csv("Denticle_lengths_data_grp.csv")
head(my_data)
levels(my_data$group)
```

```
# Box plot of log denticle lengths for different denticle types
```

```
library(ggplot2)
library(ggpubr)
ggboxplot(my_data, x="group", y="Log_denticle_length_um",
color = "black",
size = 0.8,
fill = "group", palette = c("#00AFBB", "#E7B800", "#FC4E07"),
add="jitter",
shape = "group") +
theme(axis.title.x = element_blank(),
axis.title.y = element_blank(),
axis.text.y = element_text(size=32),
axis.text.x = element_blank(),
legend.position = "none")
```

```
# ANOVA as a mixed model
```

```
library(lme4)
library(ggfortify)
modnull <- lmer((Log_denticle_length_um) ~ (1|Sample), data = my_data)
mod1 <- lmer((Log_denticle_length_um) ~ group + (1|Sample), data = my_data)
summary(mod1)
anova(modnull, mod1)
```

```
# Tukey's HSD post hoc test on mixed effect model
```

```
library(multcomp)
summary(glht(mod1, linfct = mcp (group="Tukey")))
```


6.0 Chapter 6:

General Discussion

6.1 Discussion

Overall, this thesis has provided new insights into the evolution and development of epithelial appendages throughout the gnathostomes. My results demonstrate that in many cases, small alterations to widely conserved genetic circuitry and developmental mechanisms can explain a wealth of diversity across phylogenetically disparate groups.

First, I provide evidence that epithelial placodes constitute the foundation of shark caudal denticles (Cooper et al., 2017). These placodes are thought to underpin epithelial appendage development across the amniotes (Di-Poï and Milinkovitch, 2016). They are characterised by conserved molecular signalling in the epithelium and underlying mesenchyme, and a reduced proliferation rate in columnar basal epithelial cells (Di-Poï and Milinkovitch, 2016; Musser et al., 2015). Caudal denticles are considered to be an ancient epithelial appendage found in ancestral sharks from the Silurian and Ordovician periods (Johanson et al., 2008). Therefore, my results indicate that these epithelial placodes have provided a conserved foundation for the development of diverse skin appendages throughout gnathostome evolution (Cooper et al., 2017). The evolution of different epithelial appendage types upon this common, recycled foundation has facilitated the radiation of diverse structures and their associated functional traits, ultimately enabling the adaptation of gnathostomes to wide-ranging ecological niches.

Second, I demonstrate that a Turing-like RD system is consistent with the spatial distribution of body denticles in the shark (Cooper et al., 2018). Experimental evidence for this RD patterning system during epithelial appendage development is lacking in comparison to theoretical research (Kondo and Miura, 2010). Previous work has provided

support for this system in avian feather and murine hair development (Jung et al., 1998; Sick et al., 2006), however our knowledge of its role outside of tetrapods has been limited (Kondo and Miura, 2010). I have provided experimental evidence that this system can control shark denticle patterning in the small-spotted catshark, and may even explain interspecific pattern variation between different elasmobranchs. This system is likely important in epithelial appendage patterning throughout the gnathostomes, all the way from sharks through to tetrapods (Cooper et al., 2018). The precise patterning of epithelial appendages is essential for facilitating their diverse functional traits (Crooks et al., 2013; Motta et al., 2012; Ruxton and Wilkinson, 2011).

Third, I show that retuning the parameters of a RD system can explain how avian reticulate scales form (Cooper et al., 2019). These units were previously thought to arise simultaneously as symmetrical elevations of the skin, rather than developing from epithelial placodes (Sawyer and Craig, 1977). However, my developmental study suggests that they actually arise within a primary domain on the ventral footpad, which may constitute either an enlarged epithelial placode or an initiatory field comparable to the feather tract (Cooper et al., 2019). Reticulate scale patterning is distinct from squamate footpad scale patterning, suggesting that as developmental units, reticulate scales arose after the divergence of squamates and aves from their common diapsid ancestor, approximately 255 million years ago (Brusatte et al., 2015). Again, this study highlights how small alterations to a conserved developmental patterning mechanism found throughout gnathostomes, can produce vast phenotypic diversity, which facilitates functional traits.

Finally, I demonstrate that conserved gene signalling associated with the outgrowth of paired appendages also mediates shark denticle morphogenesis. This includes gene signalling that typically defines the ZPA and AER during paired appendage outgrowth,

such as the Hh and FGF pathways. Interestingly, bead implantation experiments delivering recombinant SHH protein were sufficient to locally upregulate epithelial *fgf4* expression, and trigger the subepithelial deposition of disorganised, ectopic, mineralised tissue masses. These ectopic tissues bore characteristics of spheritic mineralisation, a type of rapid and efficient mineral growth lacking a coherent organic matrix (Ørvig, 1968, 1967, 1951). I propose that conserved morphogenetic circuitry underpins shark denticle development. Small alterations to this circuitry may contribute to the natural diversity of denticle morphology, in this case through the deposition of mineralised tissue. This provides a potential developmental explanation for the remarkable range of functional traits facilitated by diverse shark denticle morphologies, such as hydrodynamic drag reduction and the provision of defensive armour (Crooks et al., 2013; Motta et al., 2012; Oeffner and Lauder, 2012).

This thesis has demonstrated that different aspects of epithelial appendage initiation, patterning and morphogenesis are underpinned by conserved developmental systems, shared between taxonomically diverse gnathostomes (Cooper et al., 2019, 2018, 2017). This supports the concept of deep homology in development, and idea that new structures tend to arise through the modification of established genetic circuitry and developmental systems, rather than arising *de novo* (Shubin et al., 2009). Future studies conducted throughout a comprehensive spectrum of evolutionarily diverse gnathostomes will be required to determine whether continuous homology also underpins epithelial appendage development between related species (Wagner, 2007, 1989). Studying the epithelial appendages of evolutionarily diverse species will also uncover doubtlessly numerous cases that present exceptions to the developmental mechanisms presented in this thesis, which constitute the RD patterning of placode-derived appendages (Cooper et al., 2019, 2018, 2017).

6.2 Future directions

The head scales of alligators, skin crevices of elephants and elaborate neck ruff of the frilled dragon are examples of epithelial appendages which develop through the integration of physical processes (such as mechanical stress and elastic instability), and biological processes (such as molecular signalling) (Martins et al., 2018; Milinkovitch et al., 2013; Montandon et al., 2019). Such physical processes are comparatively understudied, although they are becoming considered increasingly significant in contributing to epithelial appendage diversity. Studying these phenotypes in diverse taxa, with an increased focus upon physical developmental processes, is essential for obtaining a comprehensive understanding of epithelial appendage evolution and development.

Physical processes at the cellular level have recently been proven an important aspect of feather patterning (Ho et al., 2019; Shyer et al., 2017). The aggregation of mesenchymal cells is sufficient to induce tension in adjacent epithelial cells, triggering the local release of β -cat, and activating RD patterning of feathers (Shyer et al., 2017). Experiments culturing tissue explants under different tensions have demonstrated such alterations can result in variations in feather primordia density (Shyer et al., 2017). It is thought that a wave of EDA induces this initial cellular aggregation, in what has been termed a reaction-diffusion-taxis system (Ho et al., 2019). Interestingly, this EDA wave is lost in flightless birds such as the emu and ostrich, which have developed alternative patterning systems (Ho et al., 2019). This demonstrates that different patterning systems can arise within a taxon, highlighting the importance of studying a wide range of species to broadly characterise such systems. Examining the role of mesenchymal cellular aggregation in triggering RD patterning of epithelial appendages in non-avian models is an important future direction, and will uncover whether this mechanical aspect of patterning is important throughout the gnathostomes. However, variations in such cellular aggregation may

provide an alternative mechanism for the evolution of pattern diversity, in addition to RD. This demonstrates that considering both mechanical and molecular systems is essential when attempting to understand how the diversity of epithelial appendages has arisen.

Comparative transcriptomics is becoming an increasingly popular tool for expanding our understanding of the development and regeneration of epithelial appendages and other aspects of the vertebrate body plan, both within and between different species (Johanson et al., 2019; Musser et al., 2018; Salomies et al., 2019). Through the use of transcriptomics, it is possible to identify new candidate genes that are important at specific time points of development. Candidate genes can then be functionally tested using various experimental approaches, such as small molecule gene inhibition, or CRISPR-cas9 genome editing (Cong et al., 2013; Mali et al., 2013). Furthermore, it is possible to quantify differences in the expression levels of conserved genes both throughout comparable developmental stages in different species, and at different developmental stages within a species (Musser et al., 2018). Such an approach will help to shed light upon how conserved genetic circuitry is modified between different species to produce diverse phenotypes. Additionally, comparative multi-omics approaches simultaneously investigating the genome, transcriptome and proteome are becoming increasingly important for resolving discrepancies between mRNA and protein level sequencing (Ghazalpour et al., 2011; Liu et al., 2019; Manzoni et al., 2018). As the cost of sequencing declines and its accuracy increases, transcriptomics will only become more powerful in advancing our understanding of the genetic origins of evolutionary diversity.

Additionally, research into epithelial appendage development should be expanded to encompass animals situated outside of the gnathostomes. A recent study examining limb development in the cuttlefish (*Sepia officinalis*), discovered that conserved genetic circuitry regulates development of both limbs and suckers in this highly derived

invertebrate (Tarazona et al., 2019). This study concluded that such circuitry was present in the bilaterian common ancestor. This demonstrates how far the conservation of gene regulatory networks and therefore homology can extend (Shubin et al., 2009; Wagner, 2007). To understand the evolutionary origins of epithelial appendages, it is becoming increasingly apparent that we must look back beyond the gnathostomes.

6.3 Limitations of using *Scyliorhinus canicula* as a model system

Most of the research presented in this thesis has been undertaken in the small-spotted catshark (*S. canicula*), an emerging model for studying evolutionary developmental biology (Dahn et al., 2007; Gillis et al., 2009; Rasch et al., 2016). As sharks belong to the ancient sister lineage to bony vertebrates, the cartilaginous fishes, studying them enables us to draw broad inferences regarding the evolutionary conservation of developmental processes throughout the gnathostomes. However, there are limitations regarding their use in research.

Using genome editing techniques such as CRISPR-cas9 is very difficult in the shark. To ensure that genome editing targets each individual cell, CRISPR constructs must be injected into embryos very early in development, at the first cell stage (Cong et al., 2013; Mali et al., 2013). The small-spotted catshark is an oviparous species. Accessing embryos inside the egg cases at such an early developmental stage is not only very difficult, but invariably results in embryonic death (Ballard et al., 1993). However, new advances in CRISPR-cas9 delivery methods may provide a solution to this problem. Researchers have recently undertaken CRISPR-cas9 genome editing through the microinjection of constructs into immature, unfertilised oocytes of the brown anole (*Anolis sagrei*), following a surgical procedure to expose the ovaries (Rasys et al., 2019). The success rate of this procedure was relatively low, with an overall mutation frequency of 6.2% of all injected eggs.

Furthermore, successful mutation only occurred within a specific size range of oocytes. However, even with a low success rate, this technique can be used to generate CRISPR mutants and subsequently mutant lines, without direct access to an early stage embryo. Additionally, this study demonstrates that it is possible to undertake genome modification in non-model, oviparous species (Rasys et al., 2019). Limitations regarding CRISPR-cas9 genome editing in the shark may be overcome in the future, as delivery methods continue to advance.

Another current limitation of research using *S. canicula* as a model, is the absence of a high-quality genome. Recent years have seen the publication of new genomes from different elasmobranch species, including the white shark, brown banded bamboo shark and cloudy catshark (Hara et al., 2018; Marra et al., 2019). Such work has the potential to greatly improve the alignment of transcriptome data to reference

genomes, as previously *de novo* assemblies based on more distantly related species such as the whale shark and elephant shark has been required (Read et al., 2017; Venkatesh et al., 2014). Furthermore, the publication of the *S. canicula* genome is imminent. This will help to propel the status of this species as a model for research in developmental biology.

In the absence of genome editing techniques, the research presented in this thesis has used small molecule gene inhibition and recombinant protein treatments to manipulate normal molecular signalling. In chapter 2, we present results regarding whole embryo immersion in an inhibitor of FGFR signalling (Cooper et al., 2017). One limitation of such a technique, is that it may have off-target effects upon the whole embryo, which can be difficult to measure and account for. Furthermore, the toxicity of small molecules can often result in premature embryonic death. To reduce such effects, I developed a bead implantation protocol in the shark, which was used to acquire results presented in chapters 3 and 5. This

technique allowed the highly localised and specific delivery of both small molecules and recombinant SHH protein (Cooper et al., 2018). Embryos treated with beads had a much lower mortality rate than those used for whole embryo immersion treatments, reducing the total quantity of embryos required for experimentation. The synthesis of new, highly specific small molecules will continue to facilitate similar functional experiments, helping us to unravel the roles and interactions of complex genetic circuitry.

Another limitation regarding the use of sharks as a model for studying epithelial appendage development, is that tissue culture protocols have not yet been developed. The experimental manipulation of live tissue explants has been integral for advancing our understanding of feather development (Ho et al., 2019; Jung et al., 1998; Shyer et al., 2017). The use of live imaging, small molecule treatments and recombinant protein treatments are comparatively easier to undertake in culture rather than in living embryos. Tissue culture has been employed to examine tooth regeneration in the corn snake (*Pantherophis guttatus*), demonstrating that its use is achievable in emerging model species (Gaete and Tucker, 2013). Developing such a technique in sharks would facilitate the employment of additional, targeted functional manipulations of appendage development, for example electroporation (Neumann et al., 1982).

6.4 Limitations of reaction-diffusion modelling

In chapters 3 and 4 of this thesis, we present simulations of pattern formation based on the Turing RD system (Kondo and Miura, 2010; Turing, 1952). As assumed with any modelling, these simulations present dramatic simplifications of a biological process. Our model simulates interactions between a single activatory signal and a single inhibitory morphogen (Cooper et al., 2019, 2018). In reality, complex, interactive signalling cascades are likely to control development, consisting of numerous activatory and inhibitory signals.

Furthermore, our model assumes a consistently sized, two-dimensional field in which patterns form. In reality, pattern forming domains are dynamic, and will grow throughout ontogeny (Maini et al., 2012). Furthermore, they have specific, three-dimensional geometries that are likely to impact pattern formation (Manukyan et al., 2017). Many assumptions regarding parameterisation have been made in the model presented in Chapters 3 and 4, due to a lack of data regarding real diffusion and degradation rates of different morphogens *in vivo*. Therefore, additional work is required to validate such parameters in specific developmental scenarios. Such research will provide a stronger foundation for parameterisation, thereby increasing our confidence in such modelling. Increasingly advanced RD models that account for multiple morphogens, three-dimensional growth, and diffusion across specific tissue layers are being developed, particularly in medical research fields (Bendahmane et al., 2019; De Oliveira Vilaca et al., 2019; Fried and Iber, 2014). Models are inherently a simplification of a process. Nonetheless, they are invaluable tools for understanding complex biological systems. The integration of computer science and mathematics with developmental biology will advance model development in this field, giving rise to increasingly comprehensive tools for addressing biological research questions, including those regarding pattern formation.

6.5 Conclusion

The ever-advancing availability of phylogenetically diverse model species with remarkable phenotypes is fuelling research into evolutionary developmental biology, and the field of epithelial appendage development is no exception. New studies addressing structures such as elaborate scales, spines and teeth are complimenting both classic and modern studies addressing feather and hair development (Cooper et al., 2019, 2018, 2017; Ho et al., 2019; Jung et al., 1998; Noramly et al., 1999; Rasch et al., 2016; Shono et al., 2019; Shyer et al., 2017; Sick et al., 2006). This is providing us with a more holistic view

of the molecular control underpinning the formation of these epithelial organs. Integrating our understanding of biological development, with comparatively understudied physical principles that also govern growth at multiple scales (Martins et al., 2018; Milinkovitch et al., 2013; Shyer et al., 2017), will further our understanding of this research field. Ultimately, this will help us to uncover both the evolutionary and developmental relationships of diverse of epithelial appendages and other biological structures.

7.0 Appendix

7.1 Abbreviations

<i>β-cat</i>	Gene, beta-catenin
<i>Bmp2</i>	Gene, bone morphogenetic protein 2
<i>Bmp4</i>	Gene, bone morphogenetic protein 4
CDS	Coding sequence
MicroCT	Micro computed tomography
DAPI	4',6-diamindino-2phenylindole
ddH ₂ O	Double distilled water
DEPC	Diethyl pyrocarbonate
DIG	Digoxigenin
<i>dlx2</i>	Gene, distal-less homeobox 2
DPF	Days post fertilisation
DPT	Days post treatment
DMSO	Dimethyl sulfoxide
<i>Eda</i>	Gene, ectodysplasin A
<i>Edar</i>	Gene, ectodysplasin A receptor
EK	Enamel/Enameloid Knot
EtOH	Ethanol
FGF	Fibroblast growth factor
<i>fgf3</i>	Gene, fibroblast growth factor 3
<i>fgf4</i>	Gene, fibroblast growth factor 4
<i>fgf8</i>	Gene, fibroblast growth factor 5
FGFR	Fibroblast growth factor receptor

<i>fgfr1</i>	Gene, fibroblast growth factor receptor 1
<i>fgfr2</i>	Gene, fibroblast growth factor receptor 2
<i>gli2</i>	Gene, gli family zinc finger 2
GRN	Gene regulatory network
ISH	In situ hybridization
KOH	Potassium hydroxide
LSFM	Light sheet fluorescence microscopy
MAB	Maleic acid buffer
MS-222	Tricaine mesylate
MUSCLE	Multiple sequence comparison by log-expectation
PBS	Phosphate buffered saline
PCNA	Proliferating cell nuclear antigen
PFA	Paraformaldehyde
PHYML	Phylogenetic inferences using maximum likelihood
RD	Reaction diffusion
<i>runx2</i>	Gene, runt-related transcription factor 2
SEM	Scanning electron microscopy
<i>Shh</i>	Gene, sonic hedgehog
SISH	Section in situ hybridization
<i>Spry2</i>	Gene, sprouty 2
SSC	Saline sodium citrate
SU5402	Small molecule FGFR inhibitor, C ₁₇ H ₁₆ N ₂ O ₃
WMISH	Whole mount in situ hybridization
ZPA	Zone of polarising activity

7.2 Solutions

DEPC ddH ₂ O	1L Double distilled water, 500μl DEPC, autoclave
10X PBS (1L)	80g NaCl, 2g KCL, 17.2g Na ₂ HPO ₄ ·2H ₂ O, 2.4g KH ₂ PO ₄ , ddH ₂ O to 1L, pH to 7.6, autoclave
DEPC PBS (1L)	100ml 10X PBS in 900ml DEPC ddH ₂ O
0.5M EDTA (1L)	186.1g C ₁₀ H ₁₈ N ₂ Na ₂ O ₁₀ , 20g NaOH, DEPC ddH ₂ O to 1L, autoclave
4% PFA (1L)	40g paraformaldehyde in PBS (total volume of 1L) (heated to 60°C). Add 2M NaOH until PFA dissolves, pH to 7.6 and store at -20°C
20X SSC (1L)	175.2g NaCl, 88.2g Na ₃ C ₆ H ₅ O ₇ ·2H ₂ O, ddH ₂ O to 1L, autoclave
2X SSC (1L)	100ml 20X SSC in 900ml ddH ₂ O
0.2X SSC (1L)	100ml 2X SSC in 900ml ddH ₂ O
Blocking reagent (100ml)	2g Roche blocking reagent in 100ml MAB, heat for 2 minutes until dissolved
10X MAB (1L)	116g Maleic Acid, 87.6g NaCl, 8g NaOH, ddH ₂ O to 1L, pH to 7.6, autoclave
MAB (1L)	100ml 10X MAB in 900ml ddH ₂ O
NTMT (500ml)	10ml 5M NaCl, 25ml 1M MgCl, 50ml 1M Tris pH 9.5, 500μl Tween20, ddH ₂ O to 500ml

Alizarin red solution	0.02g alizarin red in 100ml 0.1% KOH
Sodium citrate (1M)	29.4g $\text{Na}_3\text{C}_6\text{H}_5\text{O}_7$, DEPC-ddH ₂ O to 100ml, pH to 6.0
Prehybridization buffer (1L)	500ml deionised-formamide, 250ml 20X SSC, 10ml 1M sodium citrate, 500 μ l Tween 20, DEPC ddH ₂ O to 1L, pH to 6, store at -20°C
10X TBS	24g Tris base, 88g NaCl, ddH ₂ O to 1L, pH to 7.6, autoclave
TBS	100ml 10X TBC in 900ml ddH ₂ O

8.0 References

Åberg, T., Wang, X.P., Kim, J.H., Yamashiro, T., Bei, M., Rice, R., Ryoo, H.M.,

- Thesleff, I., 2004. Runx2 mediates FGF signaling from epithelium to mesenchyme during tooth morphogenesis. *Dev. Biol.* 270, 76–93.
- Åberg, T., Wozney, J., Thesleff, I., 1997. Expression patterns of bone morphogenetic proteins (Bmps) in the developing mouse tooth suggest roles in morphogenesis and cell differentiation. *Dev. Dyn.* 210, 383–396.
- Ahtiainen, L., Lefebvre, S., Lindfors, P.H., Renvoisé, E., Shirokova, V., Vartiainen, M.K., Thesleff, I., Mikkola, M.L., 2014. Directional Cell Migration, but Not Proliferation, Drives Hair Placode Morphogenesis. *Dev. Cell* 28, 588–602.
- Aman, A.J., Fulbright, A.N., Parichy, D.M., 2018. Wnt/ β -catenin regulates an ancient signaling network during zebrafish scale development. *Elife* 7, 1–22.
- Andreev, P., Coates, M.I., Karatajute-Talimaa, V., Shelton, R.M., Cooper, P.R., Wang, N.Z., Sansom, I.J., 2016. The systematics of the Mongolepidida (Chondrichthyes) and the Ordovician origins of the clade. *PeerJ* 2016, 1–38.
- Andreev, P.S., Coates, M.I., Shelton, R.M., Cooper, P.R., Smith, M.P., Sansom, I.J., 2015. Upper Ordovician chondrichthyan-like scales from North America. *Palaeontology* 58, 691–704.
- Ashique, A.M., Fu, K., Richman, J.M., 2002. Signalling via type IA and type IB bone morphogenetic protein receptors (BMPR) regulates intramembranous bone formation, chondrogenesis and feather formation in the chicken embryo. *Int. J. Dev. Biol.* 46, 243–253.
- Avaron, F., Smith, A., Akimenko, M., 2006. Sonic Hedgehog Signaling in the Developing and Regenerating Fins of Zebrafish. In: *Shh and Gli Signalling and Development*. Springer, New York, pp. 1549–1564.

- Ballard, W., Mellinger, J., Lechenault, H., 1993. A Series of Normal Stages for Development of *Scyliorhinus canicula*, the Lesser Spotted Dogfish (Chondrichthyes : Scyliorhinidae). *J. Exp. Zool.* 267, 318–336.
- Baron, M.G., Norman, D.B., Barrett, P.M., 2017. A new hypothesis of dinosaur relationships and early dinosaur evolution. *Nature* 543, 501–506.
- Barrett, P.M., Evans, D.C., Campione, N.E., 2015. Evolution of dinosaur epidermal structures. *Biol. Lett.* 11.
- Bates, D., Mächler, M., Bolker, B.M., Walker, S.C., 2015. Fitting linear mixed-effects models using lme4. *J. Stat. Softw.* 67.
- Bei, M., Maas, R., 1998. FGFs and BMP4 induce both *Msx1*-independent and *Msx1*-dependent signaling pathways in early tooth development. *Development* 125, 4325–33.
- Bénazet, J.-D., Bischofberger, M., Tiecke, E., Gonçalves, A., Martin, J.F., Zuniga, A., Naef, F., Zeller, R., 2009. A Self-Regulatory System of Interlinked Signaling Feedback Loops Controls Mouse Limb Patterning. *Science* 323, 1050–1053.
- Bendahmane, M., Erraji, E., Karami, F., 2019. A 3D reaction–diffusion system describing calcium dynamics in cardiac cell. *Math. Model. Nat. Phenom.* 14, 205.
- Biggs, L.C., Mikkola, M.L., 2014. Early inductive events in ectodermal appendage morphogenesis. *Semin. Cell Dev. Biol.* 25–26, 11–21.
- Botchkarev, V.A., Botchkareva, N. V, Roth, W., Nakamura, M., Chen, L.H., Herzog, W., Lindner, G., McMahon, J.A., Peters, C., Lauster, R., McMahon, A.P., Paus, R., 1999. Noggin is a mesenchymally derived stimulator of hair-follicle induction. *Nat. Cell Biol.* 1, 158–64.

- Boulet, A.M., Moon, A.M., Arenkiel, B.R., Capecchi, M.R., 2004. The roles of Fgf4 and Fgf8 in limb bud initiation and outgrowth. *Dev. Biol.* 273, 361–372.
- Brusatte, S.L., O'Connor, J.K., Jarvis, E.D., 2015. The origin and diversification of birds. *Curr. Biol.* 25, R888–R898.
- Brush, A.H., Wyld, J.A., 1980. Molecular correlates of morphological differentiation: Avian scutes and scales. *J. Exp. Zool.* 212, 153–157.
- Buchtová, M., Handrigan, G.R., Tucker, A.S., Lozanoff, S., Town, L., Fu, K., Diewert, V.M., Wicking, C., Richman, J.M., 2008. Initiation and patterning of the snake dentition are dependent on Sonic hedgehog signaling. *Dev. Biol.* 319, 132–45.
- Busby, L., Aceituno, C., McQueen, C., Rich, C.A., Ros, M.A., Towers, M., 2019. A positional information gradient of sonic hedgehog is required for flight feather formation in avian wings. *bioRxiv* 1–35.
- Chambers, D., Mason, I., 2000. Expression of sprouty2 during early development of the chick embryo is coincident with known sites of FGF signalling. *Mech. Dev.* 91, 361–364.
- Chang, C., Wu, P., Baker, R.E., Maini, P.K., Alibardi, L., Chuong, C.M., 2009. Reptile scale paradigm: Evo-Devo, pattern formation and regeneration. *Int. J. Dev. Biol.* 53, 813–826.
- Chen, C.-F., Foley, J., Tang, P.-C., Li, A., Jiang, T.X., Wu, P., Widelitz, R.B., Chuong, C.M., 2015. Development, regeneration, and evolution of feathers. *Annu. Rev. Anim. Biosci.* 3, 169–95.
- Chen, D., Jarrell, A., Guo, C., Lang, R., Atit, R., 2012. Dermal β -catenin activity in response to epidermal Wnt ligands is required for fibroblast proliferation and hair

- follicle initiation. *Development* 139, 1522–33.
- Chen, P., Dong, Z., Zhen, S., 1998. An exceptionally well-preserved theropod dinosaur from the Yixian Formation of China. *Nature* 391, 147–152.
- Chiang, C., Swan, R.Z., Grachtchouk, M., Bolinger, M., Litingtung, Y., Robertson, E.K., Cooper, M.K., Gaffield, W., Westphal, H., Beachy, P.A., Dlugosz, A.A., 1999. Essential Role for Sonic hedgehog during Hair Follicle Morphogenesis. *Dev. Biol.* 9, 1–9.
- Chuong, C., Chodankar, R., Widelitz, R.B., Ting-Xin, J., 2000a. Evo-Devo of feathers and scales: building complex epithelial appendages. *Curr. Opin. Genet. Dev.* 10, 449–456.
- Chuong, C., Patel, N., Lin, J., Jung, H.S., Widelitz, R.B., 2000b. Sonic hedgehog signaling pathway in vertebrate epithelial appendage morphogenesis: Perspectives in development and evolution. *Cell. Mol. Life Sci.* 57, 1672–1681.
- Cong, L., Ran, F.A., Cox, D., Lin, S., Barretto, R., Habib, N., Hsu, P.D., Wu, X., Jiang, W., Marraffini, L.A., Zhang, F., 2013. Multiplex Genome Engineering Using CRISPR/Cas Systems. *Science* 339, 819–823.
- Cooper, R.L., Lloyd, V.J., Di-Poi, N., Fletcher, A.G., Barrett, P.M., Fraser, G.J., 2019. Conserved gene signalling and a derived patterning mechanism underlie the development of avian footpad scales. *Evodevo* 10, 19.
- Cooper, R.L., Martin, K.J., Rasch, L.J., Fraser, G.J., 2017. Developing an ancient epithelial appendage: FGF signalling regulates early tail denticle formation in sharks. *Evodevo* 8, 1–19.
- Cooper, R.L., Thiery, A.P., Fletcher, A.G., Delbarre, D.J., Rasch, L.J., Fraser, G.J., 2018.

- An ancient Turing-like patterning mechanism regulates skin denticle development in sharks. *Sci. Adv.* 4, eaau5484.
- Crooks, N., Babey, L., Haddon, W.J., Love, A.C., Waring, C.P., 2013. Sexual Dimorphisms in the Dermal Denticles of the Lesser-Spotted Catshark, *Scyliorhinus canicula* (Linnaeus, 1758). *PLoS One* 8, e76887.
- Cuesta, E., Díaz-Martínez, I., Ortega, F., Sanz, J.L., 2015. Did all theropods have chicken-like feet? First evidence of a non-avian dinosaur podotheca. *Cretac. Res.* 56, 53–59.
- D'Souza, R.N., Aberg, T., Gaikwad, J., Cavender, a, Owen, M., Karsenty, G., Thesleff, I., 1999. *Cbfa1* is required for epithelial-mesenchymal interactions regulating tooth development in mice. *Development* 126, 2911–2920.
- Dahn, R.D., Davis, M.C., Pappano, W.N., Shubin, N.H., 2007. Sonic hedgehog function in chondrichthyan fins and the evolution of appendage patterning. *Nature* 445, 311–314.
- De Oliveira Vilaca, L.M., Milinkovitch, M.C., Ruiz-Baier, R., 2019. Numerical approximation of a 3D mechanochemical interface model for skin patterning. *J. Comput. Phys.*
- Dean, B., Bhushan, B., 2010. Shark-skin surfaces for fluid-drag reduction in turbulent flow: a review. *Philos. Trans. A. Math. Phys. Eng. Sci.* 368, 4775–806.
- Debiais-Thibaud, M., Chiori, R., Enault, S., Oulion, S., Germon, I., Martinand-Mari, C., Casane, D., Borday-Birraux, V., 2015. Tooth and scale morphogenesis in shark: an alternative process to the mammalian enamel knot system. *BMC Evol. Biol.* 15, 292.
- Debiais-Thibaud, M., Oulion, S., Bourrat, F., Laurenti, P., Casane, D., Borday-Birraux,

- V., 2011. The homology of odontodes in gnathostomes: insights from *Dlx* gene expression in the dogfish, *Scyliorhinus canicula*. *BMC Evol. Biol.* 11, 307.
- Deng, C.X., Wynshaw-Boris, A., Shen, M.M., Daugherty, C., Ornitz, D.M., Leder, P., 1994. Murine *FGFR-1* is required for early postimplantation growth and axial organization. *Genes Dev.* 8, 3045–3057.
- Dhouailly, D., 2009. A new scenario for the evolutionary origin of hair, feather, and avian scales. *J. Anat.* 214, 587–606.
- Di-Poi, N., Milinkovitch, M.C., 2016. The anatomical placode in reptile scale morphogenesis indicates shared ancestry among skin appendages in amniotes. *Sci. Adv.* 2, 1–8.
- Ding, Q., Motoyama, J., Gasca, S., Mo, R., Sasaki, H., Rossant, J., Hui, C.C., 1998. Diminished Sonic hedgehog signaling and lack of floor plate differentiation in *Gli2* mutant mice. *Development* 125, 2533–43.
- Domel, A.G., Saadat, M., Weaver, J.C., Haj-Hariri, H., Bertoldi, K., Lauder, G. V., 2018. Shark skin-inspired designs that improve aerodynamic performance. *J. R. Soc. Interface* 15.
- Donoghue, P.C.J., 2002. Evolution of Development of the Vertebrate Dermal and Oral Skeletons: Unraveling Concepts, Regulatory Theories and Homologies. *Palaeobiology* 28, 474–507.
- Donoghue, P.C.J., Rücklin, M., 2016. The ins and outs of the evolutionary origin of teeth. *Evol. Dev.* 18, 19–30.
- Donoghue, P.C.J., Sansom, I.J., 2002. Origin and early evolution of vertebrate skeletonization. *Microsc. Res. Tech.* 59, 352–372.

- Donoghue, P.C.J., Sansom, I.J., Downs, J.P., 2006. Early Evolution of Vertebrate Skeletal Tissues and Cellular Interactions, and the Canalization of Skeletal Development. *J. Exp. Zool. Part B Mol. Dev. Evol.* 306B, 122-278–294.
- Drew, C.F., Lin, C.M., Jiang, T.X., Blunt, G., Mou, C., Chuong, C.M., Headon, D.J., 2007. The Edar subfamily in feather placode formation. *Dev. Biol.* 305, 232–245.
- Dunn, P.O., Armenta, J.K., Whittingham, L.A., 2015. Natural and sexual selection act on different axes of variation in avian plumage color. *Sci. Adv.* 1, e1400155.
- Eames, B.F., Allen, N., Young, J., Kaplan, A., Helms, J.A., Schneider, R.A., 2007. Skeletogenesis in the swell shark *Cephaloscyllium ventriosum*. *J. Anat.* 210, 542–554.
- Economou, A.D., Ohazama, A., Porntaveetus, T., Sharpe, P.T., Kondo, S., Basson, M.A., Gritli-Linde, A., Cobourne, M.T., Green, J.B.A., 2012. Periodic stripe formation by a Turing mechanism operating at growth zones in the mammalian palate. *Nat. Genet.* 44, 348–351.
- Edgar, R.C., 2004. MUSCLE: Multiple sequence alignment with high accuracy and high throughput. *Nucleic Acids Res.* 32, 1792–1797.
- Felszeghy, S., Suomalainen, M., Thesleff, I., 2010. Notch signalling is required for the survival of epithelial stem cells in the continuously growing mouse incisor. *Differentiation* 80, 241–248.
- Ferrón, H.G., Botella, H., 2017. Squamation and ecology of thelodonts, *Plos One*.
- Fessing, M.Y., Sharova, T.Y., Sharov, A.A., Atoyán, R., Botchkarev, V.A., 2006. Involvement of the Edar signaling in the control of hair follicle involution (catagen). *Am. J. Pathol.* 169, 2075–84.

- Foth, C., Tischlinger, H., Rauhut, O.W.M., 2014. New specimen of Archaeopteryx provides insights into the evolution of pennaceous feathers. *Nature* 511, 79–82.
- Fraser, G.J., Bloomquist, R.F., Streelman, J.T., 2013. Common developmental pathways link tooth shape to regeneration. *Dev. Biol.* 377, 399–414.
- Fraser, G.J., Cerny, R., Soukup, V., Bronner-Fraser, M., Streelman, T., 2010. The Odontode Explosion: The origin of tooth-like structures in vertebrates. *Bioessays* 32, 808–817.
- Fraser, G.J., Graham, A., Smith, M.M., 2004. Conserved deployment of genes during odontogenesis across osteichthyans. *Proc. Biol. Sci.* 271, 2311–7.
- Fraser, G.J., Smith, M.M., 2011. Evolution of developmental pattern for vertebrate dentitions: An oro-pharyngeal specific mechanism. *J. Exp. Zool. Part B Mol. Dev. Evol.* 316 B, 99–112.
- Fried, P., Iber, D., 2014. Dynamic scaling of morphogen gradients on growing domains. *Nat. Commun.* 5, 1–12.
- Fucheng, Z., Zhonghe, Z., Dyke, G., 2006. Feathers and ‘feather-like’ integumentary structures in Liaoning birds and dinosaurs. *Geol. J.* 41, 395–404.
- Gaete, M., Tucker, A.S., 2013. Organized Emergence of Multiple-Generations of Teeth in Snakes Is Dysregulated by Activation of Wnt/Beta-Catenin Signalling. *PLoS One* 8, e74484.
- Ghazalpour, A., Bennett, B., Petyuk, V.A., Orozco, L., Hagopian, R., Mungrue, I.N., Farber, C.R., Sinsheimer, J., Kang, H.M., Furlotte, N., Park, C.C., Wen, P.Z., Brewer, H., Weitz, K., Camp, D.G., Pan, C., Yordanova, R., Neuhaus, I., Tilford, C., Siemers, N., Gargalovic, P., Eskin, E., Kirchgessner, T., Smith, D.J., Smith, R.D.,

- Lusis, A.J., 2011. Comparative analysis of proteome and transcriptome variation in mouse. *PLoS Genet.* 7.
- Gierer, A., Meinhardt, H., 1972. A theory of biological pattern formation. *Kybernetik* 12, 30–39.
- Gillis, J.A., Dahn, R.D., Shubin, N.H., 2009. Shared developmental mechanisms pattern the vertebrate gill arch and paired fin skeletons. *Proc. Natl. Acad. Sci. U. S. A.* 106, 5720–4.
- Gillis, J.A., Hall, B.K., 2016. A shared role for sonic hedgehog signalling in patterning chondrichthyan gill arch appendages and tetrapod limbs. *Development* 143, 1313–1317.
- Godefroit, P., Sinitsa, S.M., Dhouailly, D., Bolotsky, Y.L., Sizov, A. V., McNamara, M.E., Benton, M.J., Spagna, P., 2014. A Jurassic ornithischian dinosaur from Siberia with both feathers and scales. *Science* 345, 451–456.
- Gong, H., Wang, H., Wang, Y.X., Bai, X., Liu, B., He, J.F., Wu, J.H., Qi, W.M., Zhang, W.G., 2018. Skin transcriptome reveals the dynamic changes in the Wnt pathway during integument morphogenesis of chick embryos. *PLoS One* 13, 1–17.
- Green, J.B.A., Sharpe, J., 2015. Positional information and reaction-diffusion: two big ideas in developmental biology combine. *Development* 142, 1203–1211.
- Gritli-Linde, A., 2002. Shh signaling within the dental epithelium is necessary for cell proliferation, growth and polarization. *Development* 129, 5323–5337.
- Grover, A.C., 1974. Juvenile denticles of the swell shark *Cephaloscyllium ventriosum*: function in hatching. *Can. J. Zool.* 52, 359–363.
- Guindon, S., Lethiec, F., Duroux, P., Gascuel, O., 2005. PHYML Online - A web server

for fast maximum likelihood-based phylogenetic inference. *Nucleic Acids Res.* 33, 557–559.

Hara, Y., Yamaguchi, K., Onimaru, K., Kadota, M., Koyanagi, M., Keeley, S.D., Tatsumi, K., Tanaka, K., Motone, F., Kageyama, Y., Nozu, R., Adachi, N., Nishimura, O., Nakagawa, R., Tanegashima, C., Kiyatake, I., Matsumoto, R., Murakumo, K., Nishida, K., Terakita, A., Kuratani, S., Sato, K., Hyodo, S., Kuraku, S., 2018. Shark genomes provide insights into elasmobranch evolution and the origin of vertebrates. *Nat. Ecol. Evol.* 2, 1761–1771.

Hardy, M.H., 1992. The secret life of the hair follicle. *Trends Genet.* 8, 55–61.

Harris, M.P., Fallon, J.F., Prum, R.O., 2002. Shh-Bmp2 signaling module and the evolutionary origin and diversification of feathers. *J. Exp. Zool.* 294, 160–76.

Harris, M.P., Rohner, N., Schwarz, H., Perathoner, S., Konstantinidis, P., Nüsslein-Volhard, C., 2008. Zebrafish *eda* and *edar* mutants reveal conserved and ancestral roles of ectodysplasin signaling in vertebrates. *PLoS Genet.* 4.

Harris, M.P., Williamson, S., Fallon, J.F., Meinhardt, H., Prum, R.O., 2005. Molecular evidence for an activator-inhibitor mechanism in development of embryonic feather branching. *Proc. Natl. Acad. Sci.* 102, 11734–11739.

Haspel, G., Schwartz, A., Streets, A., Camacho, D.E., Soares, D., 2012. By the teeth of their skin, cavefish find their way. *Curr. Biol.* 22.

Hill, R.E., 2007. How to make a zone of polarizing activity: Insights into limb development via the abnormality preaxial polydactyly. *Dev. Growth Differ.* 49, 439–448.

Hiscock, T.W., Megason, S.G., 2015. Mathematically guided approaches to distinguish

- models of periodic patterning. *Development* 142, 409–419.
- Ho, W.K.W., Freem, L., Zhao, D., Painter, K.J., Woolley, T.E., Gaffney, E.A., McGrew, M.J., Tzika, A., Milinkovitch, M.C., Schneider, P., Drusko, A., Matthäus, F., Glover, J.D., Wells, K.L., Johansson, J.A., Davey, M.G., Sang, H.M., Clinton, M., Headon, D.J., 2019. Feather arrays are patterned by interacting signalling and cell density waves, *PLOS Biology*.
- Hogan, B.L.M., 1999. Morphogenesis. *Cell* 96, 225–233.
- Hothorn, T., Bretz, F., Westfall, P., 2008. Simultaneous inference in general parametric models. *Biometrical J.* 50, 346–363.
- Houghton, L., Lindon, C., Morgan, B.A., 2005. The ectodysplasin pathway in feather tract development. *Development* 132, 863–872.
- Jackman, W.R., Draper, B.W., Stock, D.W., 2004. Fgf signaling is required for zebrafish tooth development. *Dev. Biol.* 274, 139–57.
- Järvinen, E., Salazar-Ciudad, I., Birchmeier, W., Taketo, M.M., Jernvall, J., Thesleff, I., 2006. Continuous tooth generation in mouse is induced by activated epithelial Wnt/beta-catenin signaling. *PNAS* 103, 18627–18632.
- Jernvall, J., Thesleff, I., 2012. Tooth shape formation and tooth renewal: evolving with the same signals. *Development* 139, 3487–97.
- Jiang, T.X., Jung, H.S., Widelitz, R.B., Chuong, C.M., 1999. Self-organization of periodic patterns by dissociated feather mesenchymal cells and the regulation of size, number and spacing of primordia. *Development* 126, 4997–5009.
- Johanson, Z., Martin, K., Fraser, G., James, K., 2019. The Synarcual of the Little Skate, *Leucoraja erinacea*: Novel Development Among the Vertebrates. *Front. Ecol. Evol.*

7, 1–19.

Johanson, Z., Smith, M.M., Joss, J.M.P., 2007. Early scale development in *Heterodontus* (Heterodontiformes; Chondrichthyes): A novel chondrichthyan scale pattern. *Acta Zool.* 88, 249–256.

Johanson, Z., Tanaka, M., Chaplin, N., Smith, M., 2008. Early Palaeozoic dentine and patterned scales in the embryonic catshark tail. *Biol. Lett.* 4, 87–90.

Jung, H., Francis-West, P.H., Widelitz, R.B., Jiang, T.-X., Ting-Berreth, S., Tickle, C., Wolpert, L., Chuong, C.-M., 1998. Local Inhibitory Action of BMPs and Their Relationships with Activators in Feather Formation: Implications for Periodic Patterning. *Dev. Biol.* 196, 11–23.

Kalinka, A.T., Varga, K.M., Gerrard, D.T., Preibisch, S., Corcoran, D.L., Jarrells, J., Ohler, U., Bergman, C.M., Tomancak, P., 2010. Gene expression divergence recapitulates the developmental hourglass model. *Nature* 468, 811–814.

Karatajute-Talimaa, V., 1973. *Elegestolepis grossi* gen. et sp. nov., ein neuer Typ der Placoidschuppe aus dem oberen Silur der Tuwa. *Palaeontogr. A* 143, 35–50.

Kettunen, P., Laurikkala, J., Itäranta, P., Vainio, S., Itoh, N., Thesleff, I., 2000. Associations of FGF-3 and FGF-10 with signaling networks regulating tooth morphogenesis. *Dev. Dyn.* 219, 322–332.

Kettunen, P., Thesleff, I., 1998. Expression and function of FGFs-4, -8, and -9 suggest functional redundancy and repetitive use as epithelial signals during tooth morphogenesis. *Dev. Dyn.* 211, 256–268.

Koch, A., Meinhardt, H., 1994. Biological pattern formation: from basic mechanisms to complex structures. *Rev. Mod. Phys.* 66, 1481–1507.

- Kondo, M., Sekine, T., Miyakoshi, T., Kitajima, K., Egawa, S., Seki, R., Abe, G., Tamura, K., 2018. Flight feather development: Its early specialization during embryogenesis. *Zool. Lett.* 4, 1–11.
- Kondo, S., 2002. The reaction-diffusion system: A mechanism for autonomous pattern formation in the animal skin. *Genes to Cells* 7, 535–541.
- Kondo, S., Asai, R., 1995. A reaction-diffusion wave on the skin of the marine angelfish *Pomacanthus*. *Nature* 376, 765–768.
- Kondo, S., Miura, T., 2010. Reaction-Diffusion Model as a Framework of Understanding Biological Pattern Formation. *Science* 329, 1616–1620.
- Kurki, P., Vanderlaan, M., Dolbeare, F., Gray, J., Tan, E.M., 1986. Expression of proliferating cell nuclear antigen (PCNA)/cyclin during the cell cycle. *Exp. Cell Res.* 166, 209–219.
- Laufer, E., Nelson, C.E., Johnson, R.L., Morgan, B.A., Tabin, C., 1994. Sonic hedgehog and Fgf-4 act through a signaling cascade and feedback loop to integrate growth and patterning of the developing limb bud. *Cell* 79, 993–1003.
- Lewandoski, M., Sun, X., Martin, G.R., 2000. Fgf8 signalling from the AER is essential for normal limb development. *Nat. Genet.* 26, 460–463.
- Li, C.-Y., Prochazka, J., Goodwin, A.F., Klein, O.D., 2014. Fibroblast growth factor signaling in mammalian tooth development. *Odontology* 102, 1–13.
- Lillywhite, H.B., Stein, B.R., 1987. Surface sculpturing and water retention of elephant skin. *J. Zool.* 211, 727–734.
- Lin, C.M., Jiang, T.X., Widelitz, R.B., Chuong, C.M., 2006. Molecular signaling in feather morphogenesis. *Curr. Opin. Cell Biol.* 18, 730–741.

- Liu, R.T., Liaw, S.S., Maini, P.K., 2006. Two-stage Turing model for generating pigment patterns on the leopard and the jaguar. *Phys. Rev. E* 74, 011914–8.
- Liu, Y., Yang, M., Deng, Y., Su, G., Guo, C.C., Zhang, D., Kim, D., 2019. High-Spatial-Resolution Multi-Omics Atlas Sequencing of Mouse Embryos via Deterministic Barcoding in Tissue. *bioRxiv*.
- Maderson, P.F., 1972. When? Why? and How?: Some Speculations on the Evolution of the Vertebrate Integument. *Am. Zool.* 12, 159–171.
- Maderson, P.F., 2003. Mammalian skin evolution : a reevaluation. *Exp. Dermatol.* 12, 233–236.
- Magerl, M., Tobin, D.J., Mu, S., Hagen, E., Lindner, G., Mckay, I.A., Paus, R., 2001. Patterns of Proliferation and Apoptosis during Murine Hair Follicle Morphogenesis. *J. Invest. Dermatol.* 947–955.
- Maini, P.K., Woolley, T.E., Baker, R.E., Gaffney, E.A., Seirin Lee, S., 2012. Turing’s model for biological pattern formation and the robustness problem. *Interface Focus* 2, 487–496.
- Maisey, J.G., Denton, J.S.S., 2016. Dermal denticle patterning in the Cretaceous hybodont shark *Tribodus limae* (Euselachii, Hybodontiformes), and its implications for the evolution of patterning in the chondrichthyan dermal skeleton. *J. Vertebr. Paleontol.* 36, e1179200.
- Mali, P., Yang, L., Esvelt, K.M., Aach, J., Guell, M., DiCarlo, J.E., Norville, J.E., Church, G.M., 2013. RNA-guided human genome engineering via Cas9. *Science* 339, 823–826.
- Mandler, M., Neubüser, A., 2004. FGF signaling is required for initiation of feather

- placode development. *Development* 131, 3333–3343.
- Manukyan, L., Montandon, S.A., Fofonjka, A., Smirnov, S., Milinkovitch, M.C., 2017. A living mesoscopic cellular automaton made of skin scales. *Nature* 544, 173–179.
- Manzoni, C., Kia, D.A., Vandrovcova, J., Hardy, J., Wood, N.W., Lewis, P.A., Ferrari, R., 2018. Genome, transcriptome and proteome: The rise of omics data and their integration in biomedical sciences. *Brief. Bioinform.* 19, 286–302.
- Marcellini, S., Bruna, C., Henríquez, J.P., Albistur, M., Reyes, A.E., Barriga, E.H., Henríquez, B., Montecino, M., 2010. Evolution of the interaction between Runx2 and VDR, two transcription factors involved in osteoblastogenesis. *BMC Evol. Biol.* 10, 1–12.
- Marra, N.J., Stanhope, M.J., Jue, N.K., Wang, M., Sun, Q., Bitar, P.P., Richards, V.P., Komissarov, A., Rayko, M., Kliver, S., Stanhope, B.J., Winkler, C., O’Brien, S.J., Antunes, A., Jorgensen, S., Shivji, M.S., 2019. White shark genome reveals ancient elasmobranch adaptations associated with wound healing and the maintenance of genome stability. *Proc. Natl. Acad. Sci. U. S. A.* 116, 4446–4455.
- Martin, K.J., Rasch, L.J., Cooper, R.L., Metscher, B.D., Johanson, Z., Fraser, G.J., 2016. Sox2+ progenitors in sharks link taste development with the evolution of regenerative teeth from denticles. *PNAS* 113, 14769–14774.
- Martins, A.F., Bennett, N.C., Clavel, S., Groenewald, H., Hensman, S., Hoby, S., Joris, A., Manger, P.R., Milinkovitch, M.C., 2018. Locally-curved geometry generates bending cracks in the African elephant skin. *Nat. Commun.* 9, 1–8.
- Mayerson, P.L., Fallon, J.F., 1985. The spatial pattern and temporal sequence in which feather germs arise in the White Leghorn chick embryo. *Dev. Biol.* 109, 259–267.

- McClintock, J.M., Carlson, R., Mann, D.M., Prince, V.E., 2001. Consequences of Hox gene duplication in the vertebrates: an investigation of the zebrafish Hox paralogue group 1 genes. *Development* 128, 2471–84.
- Milinkovitch, M.C., Manukyan, L., Debry, A., Di-Poi, N., Martin, S., Singh, D., Lambert, D., Zwicker, M., 2013. Crocodile Head Scales Are Not Developmental Units But Emerge from Physical Cracking. *Science* 339, 78–81.
- Mill, P., Mo, R., Fu, H., Grachtchouk, M., Kim, P.C.W., Dlugosz, A.A., Hui, C., 2003. Sonic hedgehog-dependent activation of Gli2 is essential for embryonic hair follicle development. *Genes Dev.* 17, 282–94.
- Min, H., Danilenko, D.M., Scully, S.A., Bolon, B., Ring, B.D., Tarpley, J.E., DeRose, M., Simonet, W.S., 1998a. Fgf-10 is required for both limb and lung development and exhibits striking functional similarity to *Drosophila* branchless. *Genes Dev.* 12, 3156–3161.
- Min, H., Danilenko, D.M., Scully, S.A., Bolon, B., Ring, B.D., Tarpley, J.E., DeRose, M., Simonet, W.S., 1998b. Fgf-10 is required for both limb and lung development and exhibits striking functional similarity to *Drosophila* branchless. *Genes Dev.* 12, 3156–3161.
- Miyake, T., Vaglia, J.L., Taylor, L.H., Hall, B.K., 1999. Development of dermal denticles in skates (Chondrichthyes, Batoidea): Patterning and cellular differentiation. *J. Morphol.* 241, 61–81.
- Mohammadi, M., McMahon, G., Sun, L., Tang, C., Hirth, P., Yeh, B.K., Hubbard, S.R., Schlessinger, J., 1997. Structures of the tyrosine kinase domain of fibroblast growth factor receptor in complex with inhibitors. *Science* 276, 955–960.

- Montandon, S.A., Fofonjka, A., Milinkovitch, M.C., 2019. Elastic instability during branchial ectoderm development causes folding of the *Chlamydosaurus* erectile frill. *Elife* 8, 1–23.
- Morgan, B.A., Orkin, R.W., Noramly, S., Perez, A., 1998. Stage-Specific Effects of Sonic Hedgehog Expression in the Epidermis. *Dev. Biol.* 201, 1–12.
- Motta, P., Habegger, M.L., Lang, A., Hueter, R., Davis, J., 2012. Scale morphology and flexibility in the shortfin mako *Isurus oxyrinchus* and the blacktip shark *Carcharhinus limbatus*. *J. Morphol.* 273, 1096–1110.
- Moura, R.S., Coutinho-Borges, J.P., Pacheco, A.P., Damota, P.O., Correia-Pinto, J., 2011. FGF signaling pathway in the developing chick lung: expression and inhibition studies. *PLoS One* 6, e17660.
- Moustakas-Verho, J.E., Zimm, R., Cebra-Thomas, J., Lempiainen, N.K., Kallonen, A., Mitchell, K.L., Hamalainen, K., Salazar-Ciudad, I., Jernvall, J., Gilbert, S.F., 2014. The origin and loss of periodic patterning in the turtle shell. *Dev.* 141, 3033–3039.
- Musser, J.M., Wagner, G.P., Liang, C., Stabile, F.A., Cloutier, A., Baker, A.J., Prum, R.O., 2018. Subdivision of ancestral scale genetic program underlies origin of feathers and avian scutate scales. *bioRxiv*.
- Musser, J.M., Wagner, G.P., Prum, R.O., 2015. Nuclear β -catenin localization supports homology of feathers, avian scutate scales, and alligator scales in early development. *Evol. Dev.* 17, 185–194.
- Mustonen, T., Ilmonen, M., Pummila, M., Kangas, A.T., Laurikkala, J., Jaatinen, R., Pispala, J., Gaide, O., Schneider, P., Thesleff, I., Mikkola, M.L., 2004. Ectodysplasin A1 promotes placodal cell fate during early morphogenesis of ectodermal

- appendages. *Development* 131, 4907–4919.
- Neumann, E., Schaefer-Ridder, M., Wang, Y., Hofschneider, P.H., 1982. Gene transfer into mouse lymphoma cells by electroporation in high electric fields. *EMBO J.* 1, 841–845.
- Nishimoto, S., Wilde, S.M., Wood, S., Logan, M.P.O., 2015. RA Acts in a Coherent Feed-Forward Mechanism with Tbx5 to Control Limb Bud Induction and Initiation. *Cell Rep.* 12, 879–891.
- Niswander, L., Jeffrey, S., Martin, G.R., Tickle, C., 1994. A positive feedback loop coordinates growth and patterning in the vertebrate limb. *Nature* 371, 609–612.
- Noramly, S., Freeman, A., Morgan, B.A., 1999. β -catenin signaling can initiate feather bud development. *Development* 126, 3509–3521.
- Noramly, S., Morgan, B.A., 1998. BMPs mediate lateral inhibition at successive stages in feather tract development. *Development* 125, 3775–87.
- O’Shaughnessy, K.L., Dahn, R.D., Cohn, M.J., 2015. Molecular development of chondrichthyan claspers and the evolution of copulatory organs. *Nat. Commun.* 6, 6698.
- Oeffner, J., Lauder, G. V., 2012. The hydrodynamic function of shark skin and two biomimetic applications. *J. Exp. Biol.* 215, 785–795.
- Ohuchi, H., Kimura, S., Watamoto, M., Itoh, N., 2000. Involvement of fibroblast growth factor (FGF)18-FGF8 signaling in specification of left-right asymmetry and brain and limb development of the chick embryo. *Mech. Dev.* 95, 55–66.
- Onimaru, K., Marcon, L., Musy, M., Tanaka, M., Sharpe, J., 2016. The fin-to-limb transition as the re-organization of a Turing pattern. *Nat. Commun.* 7, 11582.

- Ornitz, D.M., Itoh, N., 2015. The fibroblast growth factor signaling pathway. Wiley Interdiscip. Rev. Dev. Biol. 4, 215–266.
- Ornitz, D.M., Xu, J., Colvin, J.S., McEwen, D.G., MacArthur, C.A., Coulier, F., Gao, G., Goldfarb, M., 1996. Receptor Specificity of the Fibroblast Growth Factor Family. J. Biol. Chem. 271, 15292–15297.
- Ørvig, T., 1951. Histologic studies of ostracoderms, placoderms and fossil elasmobranchs 1. The endoskeleton, with remarks on the hard tissues of lower vertebrates in general. Ark. Zool. 2, 321–454.
- Ørvig, T., 1967. Phylogeny of tooth tissues: evolution of some calcified tissues in early vertebrates. In: Structural and Chemical Organisation of Teeth (Ed. AEW Miles). pp. 45–110.
- Ørvig, T., 1968. The dermal skeleton: General considerations. In: Wiksell, S.A. and (Ed.), Current Problems of Lower Vertebrate Phylogeny. pp. 374–397.
- Ørvig, T., 1977. A survey of odontodes (‘dermal teeth’) from developmental, structural, functional and phyletic points of view. In: Problems in Vertebrate Evolution. pp. 53–75.
- Oster, G.F., Murray, J.D., Harris, A.K., 1983. Mechanical aspects of mesenchymal morphogenesis. J. Embryol. Exp. Morphol. 78, 83–125.
- Pan, Y., Bai, C.B., Joyner, A.L., Wang, B., 2006. Sonic hedgehog Signaling Regulates Gli2 Transcriptional Activity by Suppressing Its Processing and Degradation Sonic hedgehog Signaling Regulates Gli2 Transcriptional Activity by Suppressing Its Processing and Degradation †. Mol. Cell. Biol. 26, 3365–3377.
- Panganiban, G., Rubenstein, J.L.R., 2002. Developmental functions of the Distal-less/Dlx

- homeobox genes. *Development* 129, 4371–4386.
- Park, H.B., Lam, Y.C., Gaffney, J.P., Weaver, J.C., Krivoschik, S.R., Hamchand, R., Pieribone, V., Gruber, D.F., Crawford, J.M., 2019. Bright Green Biofluorescence in Sharks Derives from Bromo-Kynurenine Metabolism. *iScience* 1–10.
- Paterson, J.L., Li, Z., Wen, X.-Y., Masih-Khan, E., Chang, H., Pollett, J.B., Trudel, S., Stewart, a K., 2004. Preclinical studies of fibroblast growth factor receptor 3 as a therapeutic target in multiple myeloma. *Br. J. Haematol.* 124, 595–603.
- Petit, F., Sears, K.E., Ahituv, N., 2017. Limb development: A paradigm of gene regulation. *Nat. Rev. Genet.* 18, 245–258.
- Pickering, J., Chinnaiya, K., Towers, M., 2019. An autoregulatory cell cycle timer integrates growth and specification in chick wing digit development. *Ecol. Lett.* 8, e47625.
- Pickering, J., Wali, N., Towers, M., 2017. Transcriptional changes in chick wing bud polarization induced by retinoic acid. *Dev. Dyn.* 246, 682–690.
- Pispa, J., Thesleff, I., 2003. Mechanisms of ectodermal organogenesis. *Dev. Biol.* 262, 195–205.
- Poss, K.D., Shen, J., Nechiporuk, A., McMahon, G., Thisse, B., Thisse, C., Keating, M.T., 2000. Roles for Fgf Signaling during Zebrafish Fin Regeneration. *Dev. Biol.* 222, 347–358.
- Prum, R.O., 1999. Development and Evolutionary Origin of Feathers. *J. Exp. Zool.* 285, 291–306.
- Pummila, M., Fliniaux, I., Jaatinen, R., James, M.J., Laurikkala, J., Schneider, P., Thesleff, I., Mikkola, M.L., 2007. Ectodysplasin has a dual role in ectodermal

- organogenesis: inhibition of Bmp activity and induction of Shh expression. *Development* 134, 117–125.
- Purnell, M.A., 1995. Microwear on conodont elements and macrophagy in the first vertebrates. *Nature* 374, 798–800.
- Quint, E., Smith, A., Avaron, F., Laforest, L., Miles, J., Gaffield, W., Akimenko, M.-A., 2002. Bone patterning is altered in the regenerating zebrafish caudal fin after ectopic expression of sonic hedgehog and *bmp2b* or exposure to cyclopamine. *Proc. Natl. Acad. Sci. U. S. A.* 99, 8713–8.
- Rasch, L.J., Martin, K.J., Cooper, R.L., Metscher, B.D., Underwood, C.J., Fraser, G.J., 2016. An ancient dental gene set governs development and continuous regeneration of teeth in sharks. *Dev. Biol.* 415, 347–370.
- Raschi, W., Tabit, C., 1992. Functional aspects of placoid scales: a review and update. *Mar. Freshw. Res.* 43, 123–147.
- Rasys, A.M., Park, S., Ball, R.E., Alcala, A.J., Lauderdale, J.D., Menke, D.B., 2019. CRISPR-Cas9 Gene Editing in Lizards through Microinjection of Unfertilized Oocytes. *Cell Rep.* 28, 2288–2292.
- Read, T.D., Petit, R.A., Joseph, S.J., Alam, M.T., Weil, M.R., Ahmad, M., Bhimani, R., Vuong, J.S., Haase, C.P., Webb, D.H., Tan, M., Dove, A.D.M., 2017. Draft sequencing and assembly of the genome of the world’s largest fish, the whale shark: *Rhincodon typus* Smith 1828. *BMC Genomics* 18, 1–10.
- Reif, W.-E., 1980. A model of morphogenetic processes in the dermal skeleton of elasmobranchs. *Neues Jahrb. für Geol. und Paläontologie, Abhandlungen* 159, 339–359.

- Reif, W.-E., 1982. Evolution of Dermal Skeleton and Dentition in Vertebrates: The Odontode Regulation Theory. *Evol. Biol.* 15, 287–368.
- Reif, W.-E., 1985a. Functions of Scales and Photophores in Mesopelagic Luminescent Sharks. *Acta Zool.* 66, 111–118.
- Reif, W.-E., 1985b. Morphology and hydrodynamic effects of the scales of fast swimming sharks. *Fortschr. Zool.* 30, 483–485.
- Reif, W.-E., 1985c. Squamation and ecology of sharks. *Cour. Forschungsinstitut Senckenb.* 78, 1–255.
- Reif, W.E., 1980. Development of dentition and dermal skeleton in embryonic *Scyliorhinus canicula*. *J. Morphol.* 166, 275–288.
- Riddle, R.D., Johnson, R.L., Laufer, E., Tabin, C., 1993. Sonic hedgehog mediates the polarizing activity of the ZPA. *Cell* 75, 1401–1416.
- Rivera-Rivera, C.J., Montoya-Burgos, J.I., 2017. Trunk dental tissue evolved independently from underlying dermal bony plates but is associated with surface bones in living odontode-bearing catfish. *Proc. R. Soc. B Biol. Sci.* 284.
- Rosenquist, T.A., Martin, G.R., 1996. Fibroblast growth factor signalling in the hair growth cycle: expression of the fibroblast growth factor receptor and ligand genes in the murine hair follicle. *Dev. Dyn.* 205, 379–386.
- Rouzankina, I., Abate-Shen, C., Niswander, L., 2004. *Dlx* genes integrate positive and negative signals during feather bud development. *Dev. Biol.* 265, 219–233.
- Ruxton, G.D., Wilkinson, D.M., 2011. Avoidance of overheating and selection for both hair loss and bipedality in hominins. *Proc. Natl. Acad. Sci.* 108, 20965–20969.

- Salomies, L., Eymann, J., Khan, I., Di-Poi, N., 2019. The alternative regenerative strategy of bearded dragon unveils the key processes underlying vertebrate tooth renewal. *Elife* 8, 1–26.
- Sansom, I.J., Smith, M.M., Smith, P., 1996. Scales of thelodont and shark-like fishes from the Ordovician of Colorado. *Nature* 379, 628–630.
- Sasaki, H., Nishizaki, Y., Hui, C., Nakafuku, M., Kondoh, H., 1999. Regulation of Gli2 and Gli3 activities by an amino-terminal repression domain: implication of Gli2 and Gli3 as primary mediators of Shh signaling. *Development* 126, 3915–3924.
- Sawyer, R.H., 1972. Avian scale development: Histogenesis and morphogenesis of the epidermis and dermis during formation of the scale ridge. *J. Exp. Zool.* 181, 365–384.
- Sawyer, R.H., Craig, K.F., 1977. Avian scale development. Absence of an “epidermal placode” in reticulate scale morphogenesis. *J. Morphol.* 154, 83–93.
- Sawyer, R.H., Knapp, L.W., O’Guin, W.M., 1986. Epidermis, Dermis and Appendages. In: Bereiter-Hahn, J., Matoltsy, A.G., Richards, K.S. (Eds.), *Biology of the Integument*. Vol. 2, Vertebrates. Springer, Berlin, Heidelberg, pp. 194–238.
- Schaefer, S.A., 1990. Anatomy and Relationships of the Scoloplacid Catfishes. *Proc. Acad. Nat. Sci. Philadelphia* 142, 167–210.
- Schindelin, J., Arganda-Carreras, I., Frise, E., Kaynig, V., Longair, M., Pietzsch, T., Preibisch, S., Rueden, C., Saalfeld, S., Schmid, B., Tinevez, J.Y., White, D.J., Hartenstein, V., Eliceiri, K., Tomancak, P., Cardona, A., 2012. Fiji: An open-source platform for biological-image analysis. *Nat. Methods* 9, 676–682.
- Schmidt-Ullrich, R., Tobin, D.J., Lenhard, D., Schneider, P., Paus, R., Scheidereit, C.,

2006. NF-kappaB transmits Eda A1/EdaR signalling to activate Shh and cyclin D1 expression, and controls post-initiation hair placode down growth. *Development* 133, 1045–1057.
- Scotland, R.W., 2010. Deep homology: a view from systematics. *Bioessays* 32, 438–49.
- Sengel, P., 1990. Pattern formation in skin development. *Int. J. Dev. Biol.* 34, 33–50.
- Sharpe, P.T., 2001. Fish scale development: Hair today, teeth and scales yesterday? *Curr. Biol.* 11, R751–R752.
- Shono, T., Thiery, A.P., Cooper, R.L., Kurokawa, D., Britz, R., Okabe, M., Fraser, G., 2019. From Scale to Spine: Evolution and Developmental Diversity of Skin Spines in Pufferfishes. *iScience* 19, 1–12.
- Shubin, N., Tabin, C., Carroll, S., 2009. Deep homology and the origins of evolutionary novelty. *Nature* 457, 818–23.
- Shyer, A.E., Rodrigues, A.R., Schroeder, G.G., Kassianidou, E., Kumar, S., Harland, R.M., 2017. Emergent cellular self-organization and mechanosensation initiate follicle pattern in the avian skin. *Science* 357, 811–815.
- Sick, S., Reinker, S., Timmer, J., Schlake, T., 2006. WNT and DKK Determine Hair Follicle Spacing Through a Reaction-Diffusion Mechanism. *Science* 314, 1447–1450.
- Sire, J.-Y., Donoghue, P.C.J., Vickaryous, M.K., 2009. Origin and evolution of the integumentary skeleton in non-tetrapod vertebrates. *J. Anat.* 214, 409–40.
- Smith, M.M., Coates, M., 1998. Evolutionary origins of the vertebrate dentition : phylogenetic patterns and developmental evolution. *Eur. J. Oral Sci.* 106, 482–500.

- Smith, M.M., Fraser, G.J., Chaplin, N., Hobbs, C., Graham, A., 2009. Reiterative pattern of sonic hedgehog expression in the catshark dentition reveals a phylogenetic template for jawed vertebrates. *Proc. Biol. Sci.* 276, 1225–33.
- Southall, E.J., Sims, D.W., 2003. Shark skin: a function in feeding. *Proc. R. Soc. B Biol. Sci.* 270, S47–S49.
- St-Jacques, B., Dassule, H.R., Karavanova, I., Botchkarev, V. a., Li, J., Danielian, P.S., McMahon, J. a., Lewis, P.M., Paus, R., McMahon, A.P., 1998. Sonic hedgehog signaling is essential for hair development. *Curr. Biol.* 8, 1058–1069.
- Stettenheim, P.R., 2000. The Integumentary Morphology of Modern Birds — An Overview. *Amer. Zool.* 40, 461–477.
- Stuart, E.S., Moscona, A.A., 1967. Embryonic Morphogenesis: Role of Fibrous Lattice in the Development of Feathers and Feather Patterns. *Science* 157, 947–948.
- Sullivan, T., Regan, F., 2011. The characterization, replication and testing of dermal denticles of *Scyliorhinus canicula* for physical mechanisms of biofouling prevention. *Bioinspir. Biomim.* 6, 046001.
- Sun, X., Meyers, E.N., Lewandoski, M., Martin, G.R., 1999. Targeted disruption of *Fgf8* causes failure of cell migration in the gastrulating mouse embryo. *Genes Dev.* 13, 1834–1846.
- Takamori, K., Hosokawa, R., Xu, X., Deng, X., Bringas, P., Chai, Y., 2008. Epithelial Fibroblast Growth Factor Receptor 1 Regulates Enamel Formation. *J. Dent. Res.* 87, 238–243.
- Tanaka, S., Kato, Y., 1983. Epigenesis in developing avian scales. II. Cell proliferation in relation to morphogenesis and differentiation in the epidermis. *J. Exp. Zool.* 225,

271–283.

- Tarazona, O.A., Lopez, D.H., Slota, L.A., Cohn, M.J., 2019. Evolution of limb development in cephalopod mollusks. *Elife* 8, e43828.
- Thesleff, I., Vaahtokari, A., Partanen, A.M., 1995. Regulation of organogenesis. Common molecular mechanisms regulating the development of teeth and other organs. *Int. J. Dev. Biol.* 39, 35–50.
- Thisse, B., Thisse, C., 2005. Functions and regulations of fibroblast growth factor signaling during embryonic development. *Dev. Biol.* 287, 390–402.
- Thomas, B.L., Liu, J.K., Rubenstein, J.L., Sharpe, P.T., 2000. Independent regulation of Dlx2 expression in the epithelium and mesenchyme of the first branchial arch. *Development* 127, 217–224.
- Tickle, C., Towers, M., 2017. Sonic Hedgehog Signaling in Limb Development. *Front. Cell Dev. Biol.* 5, 1–19.
- Ting-berreth, S.A., Chuong, C., 1996. Sonic Hedgehog in Feather Morphogenesis : Induction of Mesenchymal Condensation and Association With Cell Death. *Dev. Dyn.* 207, 157–170.
- Torii, K.U., 2012. Two-dimensional spatial patterning in developmental systems. *Trends Cell Biol.* 22, 438–446.
- Towers, M., Mahood, R., Yin, Y., Tickle, C., 2008. Integration of growth and specification in chick wing digit-patterning. *Nature* 452, 882–886.
- Trokovic, R., Jukkola, T., Saarimäki, J., Peltopuro, P., Naserke, T., Vogt Weisenhorn, D.M., Trokovic, N., Wurst, W., Partanen, J., 2005. Fgfr1-dependent boundary cells between developing mid- and hindbrain. *Dev. Biol.* 278, 428–439.

- Tucker, A.S., Headon, D.J., Schneider, P., Ferguson, B.M., Overbeek, P., Tschopp, J., Sharpe, P.T., 2000. Edar/Eda interactions regulate enamel knot formation in tooth morphogenesis. *Development* 127, 4691–4700.
- Turing, A.M., 1952. The chemical basis of morphogenesis. *Philos. Trans. R. Soc. Lond. B. Biol. Sci.* 237, 37–72.
- Vandebergh, W., Bossuyt, F., 2012. Radiation and functional diversification of alpha keratins during early vertebrate evolution. *Mol. Biol. Evol.* 29, 995–1004.
- Venkatesh, B., Lee, A.P., Ravi, V., Maurya, A.K., Lian, M.M., Swann, J.B., Ohta, Y., Flajnik, M.F., Sutoh, Y., Kasahara, M., Hoon, S., Gangu, V., Roy, S.W., Irimia, M., Korzh, V., Kondrychyn, I., Lim, Z.W., Tay, B.-H., Tohari, S., Kong, K.W., Ho, S., Lorente-Galdos, B., Quilez, J., Marques-Bonet, T., Raney, B.J., Ingham, P.W., Tay, A., Hillier, L.W., Minx, P., Boehm, T., Wilson, R.K., Brenner, S., Warren, W.C., 2014. Elephant shark genome provides unique insights into gnathostome evolution. *Nature* 505, 174–9.
- Vernerey, F.J., Barthelat, F., 2014. Skin and scales of teleost fish: Simple structure but high performance and multiple functions. *J. Mech. Phys. Solids* 68, 66–76.
- Wagner, G.P., 1989. The Biological Homology Concept. *Annu. Rev. Ecol. Syst.* 20, 51–69.
- Wagner, G.P., 2007. The developmental genetics of homology. *Nat. Rev. - Genet.* 8, 473–479.
- Wen, L., Weaver, J.C., Lauder, G. V., 2014. Biomimetic shark skin: design , fabrication and hydrodynamic function. *J. Exp. Biol.* 1656–1666.
- Wen, L., Weaver, J.C., Thornycroft, P.J.M., Lauder, G. V, 2015. Hydrodynamic function

- of biomimetic shark skin: effect of denticle pattern and spacing. *Bioinspir. Biomim.* 10, 066010.
- Wessells, N.K., 1965. Morphology and Proliferation during Early Feather Development. *Dev. Biol.* 12, 131–153.
- Widelitz, R.B., Jiang, T.X., Lu, J., Chuong, C.M., 2000. Beta-Catenin in Epithelial Morphogenesis: Conversion of Part of Avian Foot Scales Into Feather Buds With a Mutated Beta-Catenin. *Dev. Biol.* 219, 98–114.
- Widelitz, R.B., Ting-Xin, J., Noveen, A., Chen, C.-W.J., Chuong, C.-M., 1996. FGF Induces New Feather Buds From Developing Avian Skin. *J. Invest. Dermatol.* 107, 798–803.
- Wiens, J.J., Hutter, C.R., Mulcahy, D.G., Noonan, B.P., Townsend, T.M., Jr, J.W.S., Reeder, T.W., 2012. Resolving the phylogeny of lizards and snakes (Squamata) with extensive sampling of genes and species. *Biol. Lett.* 8, 1043–1046.
- Wu, P., Lai, Y.-C., Widelitz, R., Chuong, C.-M., 2018. Comprehensive molecular and cellular studies suggest avian scutate scales are secondarily derived from feathers, and more distant from reptilian scales. *Sci. Rep.* 8, 16766.
- Wyffels, J., L. King, B., Vincent, J., Chen, C., Wu, C.H., Polson, S.W., 2014. SkateBase, an elasmobranch genome project and collection of molecular resources for chondrichthyan fishes. *F1000Research* 3, 1–24.
- Xu, X., Weinstein, M., Li, C., Naski, M., Cohen, R.I., Ornitz, D.M., Leder, P., Deng, C., 1998. Fibroblast growth factor receptor 2 (FGFR2)-mediated reciprocal regulation loop between FGF8 and FGF10 is essential for limb induction. *Development* 125, 753–765.

- Yamaguchi, M., Yoshimoto, E., Kondo, S., 2007. Pattern regulation in the stripe of zebrafish suggests an underlying dynamic and autonomous mechanism. *Proc. Natl. Acad. Sci.* 104, 4790–4793.
- Yang, Z., Jiang, B., Mcnamara, M.E., Kearns, S.L., Pittman, M., Kaye, T.G., Orr, P.J., Xu, X., Benton, M.J., 2019. Pterosaur integumentary structures with complex feather-like branching. *Nat. Ecol. Evol.* 3, 24–30.
- Yokoi, H., Shimada, A., Carl, M., Takashima, S., Kobayashi, D., Narita, T., Jindo, T., Kimura, T., Kitagawa, T., Kage, T., Sawada, A., Naruse, K., Asakawa, S., Shimizu, N., Mitani, H., Shima, A., Tsutsumi, M., Hori, H., Wittbrodt, J., Saga, Y., Ishikawa, Y., Araki, K., Takeda, H., 2007. Mutant analyses reveal different functions of *fgfr1* in medaka and zebrafish despite conserved ligand-receptor relationships. *Dev. Biol.* 304, 326–337.
- Zhang, X., Ibrahimi, O.A., Olsen, S.K., Umemori, H., Mohammadi, M., Ornitz, D.M., 2006. Receptor specificity of the fibroblast growth factor family: The complete mammalian FGF family. *J. Biol. Chem.* 281, 15694–15700.
- Zhu, J., Nakamura, E., Nguyen, M.T., Bao, X., Akiyama, H., Mackem, S., 2008. Uncoupling Sonic Hedgehog Control of Pattern and Expansion of the Developing Limb Bud. *Dev. Cell* 14, 624–632.
- Zuniga, A., 2015. Next generation limb development and evolution: old questions, new perspectives. *Development* 142, 3810–3820.
- Zúñiga, A., Haramis, A.P., McMahon, A.P., Zeller, R., 1999. Signal relay by BMP antagonism controls the SHH/FGF4 feedback loop in vertebrate limb buds. *Nature* 401, 598–602.

